**UNIVERSITÀ DEGLI STUDI DI PADOVA**

DIPARTIMENTO DI INGEGNERIA INDUSTRIALE

CORSO DI LAUREA MAGISTRALE IN INGEGNERIA MECCANICA

**Tesi di Laurea in Ingegneria Meccanica**

# COMPARATIVE ANALYSIS OF TWO BIOFIDELIC INSTRUMENTED HUMAN HEAD SURROGATES FOR SPORT HELMETS EVALUATION

***Relatore: Prof. Nicola Petrone***
***Relatore estero: Prof. Andrey Koptyug***

***Laureando: EDOARDO MARZELLA***

ANNO ACCADEMICO 2017-2018

# Index

# Introduction

The project of which this thesis belongs was born as a collaboration of *Università degli Studi di Padova* and *Mittuniversitetet* (Mid Sweden University – Campus Östersund).

The purpose of the joint collaboration is to design, produce and test new instrumented models of human head surrogate through a formal Erasmus program. This head surrogate has to be characterized by an high level of biofidelity, unlike the standard dummy heads used in the laboratories and by companies all over the world.

The two models of head surrogates developed are called *Instrumented Human Head Surrogate 1* and *Instrumented Human Head Surrogate 2*, abbreviated in IHHS1 and IHHS2. These surrogates head have as their strengths the fact that they are easily reproducible with low cost material as silicon rubber or ABS plastic and easy-to-use tools as 3D printing and rapid prototyping. The most important point however is the high biofidelity reached through the shape of skull, obtained by real MRI scans, the presence of a surrogate brain in silicon rubber with the partition between right and left lobe and between main body and cerebellum, the possibility to fill the head with an oil resembling the cerebrospinal fluid. With both IHHS1 and IHHS2 can be collected a huge and complex amount of data concerning accelerations of chosen points of interest in the brain, angular velocity and angular acceleration of center of mass and also pressure sensors are placed in the inner surface of the skull. Besides these sensors inside the head, accelerometers and gyroscopes can be positioned on the skull or the helmet.

The project moved its first steps under the guide of Prof. Nicola Petrone and Prof. Andrey Koptyug in October 2015 with Giovanni Carraro [1] who designed and produced the skull and brain simplifying the complex and not producible geometries of the models and deleting the inconsistencies coming from the scans. After him the baton passed to Stefano Dal Castello [2] who produced the skin of IHHS1 and then Luca Broggio [3] closed the human surrogate, filled the head with a liquid resembling cerebrospinal fluid, calibrated the sensors and performed the first tests on IHHS1 and compared them with the results coming from *Hybrid III* head. Because of problems born from the interaction of the oil in the head with the silicon rubber of the brain, the swelling of it and dimensions of the head definitely above the $50^{th}$ percentile for adult male human head, Federico Uriati [4] designed and produced IHHS2. The aim of this thesis, instead, is to compare the results between data collected from IHHS1 and IHHS2 and to make the first studies on a method to calculate deformations inside the head.

# Chapter 1

# Head Trauma and Injury Mechanisms

It has been estimated that mild Traumatic Brain Injury (m-TBI) or concussion occurs in 42 milion people per year [5]. In particular, injuries related to sport have an high incidence, in fact, even if helmets are used widely in different disciplines as football, hockey and other recreation activities, they are the second most common cause of hospitalization for Traumatic Brain Injuries (TBI) [6].
This is the reason why TBIs from participation in sports and recreation activities have received increased public awareness, with different states considering or implementing laws directing the response to suspected brain injury [7].
In this period, Laboratory testing of helmets is shifting from only radial impact tests also towards the implementation of multidirectional impacts. The importance of multidirectional impact tests in the validation of helmets is underlined, for example, by Otte *et al.* [8]. In this work is shown that the average impact angle in motorcycle crashes, between the helmet and the horizontal direction, is 28 degrees. This permits to understand that in a typical fall, the horizontal velocity component is 3 times the vertical velocity component. Another proof of the revelance of multirectional impacts in laboratory testing is brought by Harrison *et al*. [9], who shows that, for a jockey falling from the horse in a steeplechase, the mean impact angle produces a horizontal velocity that is around 2 times the vertical one.
Understood the complexity and severity of TBI, in the next paragraphs, firstly the different kinds of TBI will be studied, and then the most important injury mechanisms that lead to it. The most important head traumas that bring to TBI are Diffuse Axonal Injury (DAI), as stated by Iwara *et al*. [10], and Subdural Hematoma (SDH). A complete survey of all the traumatic injury mechanisms will be given.

## 1.1 Traumatic Brain Injury

TBI has been defined as ‘injury to the head (arising from blunt or penetrating trauma or from acceleration-deceleration forces) that is associated with symptoms or signs attributable to the injury:

decreased level of consciousness, amnesia, other neurological or neuropsychological abnormalities, skull fracture, diagnosed intracranial lesions – or death' [11].

This definition means that TBI occurs whenever an external force applied to the head is strong enough to cause an alteration in consciousness or modify the normal neurological functioning for a period of time.

The Traumatic Brain Injury Task Force [12] identifies different kind of TBI, classified by their severity. Only when a penetrating brain injury occurs, for example an injury caused by the contact of the brain with an external body as a bullet, TBI is no more classified by severity. The severity of the injury is judged on the basis of 3 different indices: GCS, LOC and PTA.

GCS stands for Glasgow Coma Scale and was published for the first time in 1974. At the beginning, it was used to verify the level of consciousness after head injury, but, over the years, a strong correlation was found with severity and outcome of TBI [13].

GCS is a scale going from 3 to 15, with the highest part of the scale related to mild trauma and the lowest part related to a state in which the patient is not capable of following commands [14].

LOC means loss of consciousness and simply expresses the time during which the patient is not present to himself. However, questions regarding the accuracy of this indices has been moved [15].

The major part of patients hospitalized for TBI shows a period of altered consciousness called post-traumatic amnesia (PTA). Even if there is not a consistent definition for PTA, it is very often used as a construct in neurosurgical practice to guide decision-making and prognosis [16].

However, the Traumatic Brain Injury Task Force [12] divide TBI into 3 classes and they are mild, moderate and severe. Mild TBI is characterized by a LOC of 0-30 minutes, a period of PTA that disappears within 24 hours and a GCS index between 13 and 15. Moderate TBI is related to a LOC that lasts from 30 minutes to 24 hours, PTA contained between 24 hours and 7 days and a GCS index between 9 and 12. Severe TBI has a LOC that exceeds 24 hours, a PTA that exceeds 7 days and a GCS index between 3 and 8.

| Severity | GCS | LOC | PTA |
|---|---|---|---|
| mild | 13-15 | 0-30 minutes | 0-24 hours |
| moderate | 9-12 | 30 min-24 hours | 24 hours-7 days |
| severe | 3-8 | >24 hours | >7 days |

**Table 1.1** *Traumatic Brain Injury Description*

## 1.2 Diffuse Axonal Injury

Before studying Diffuse Axonal Injury (DAI), it is required to know the difference between focal and diffuse brain injury.

Focal brain injuries are typically caused by direct blows to the head and can vary from contusions to brain lacerations and haemorrhage that leads to the formation of hematoma in different compartments of the head, like the extradural, subarachnoid, subdural or intracerebral [17].

Instead, diffuse brain injuries can happen without the presence of impact forces, in fact they are only related to inertial forces, that are commonly produced during motor vehicle crashes, or for example falls and assaults [18].

The mechanism of DAI can be described as a deformation and stretching of the brain tissues leading to direct damage of axons, in particular, and blood vessels, secondly [19].

This means that shearing forces developed inside the brain during angular or rotational acceleration-deceleration on different axes can cause primary disconnections of axons [10].

Even if DAI is defined as diffuse brain injury, it would be better described by the word ‘multifocal’, because of the pattern of axonal damage present in the deep and subcortical white matter [18].

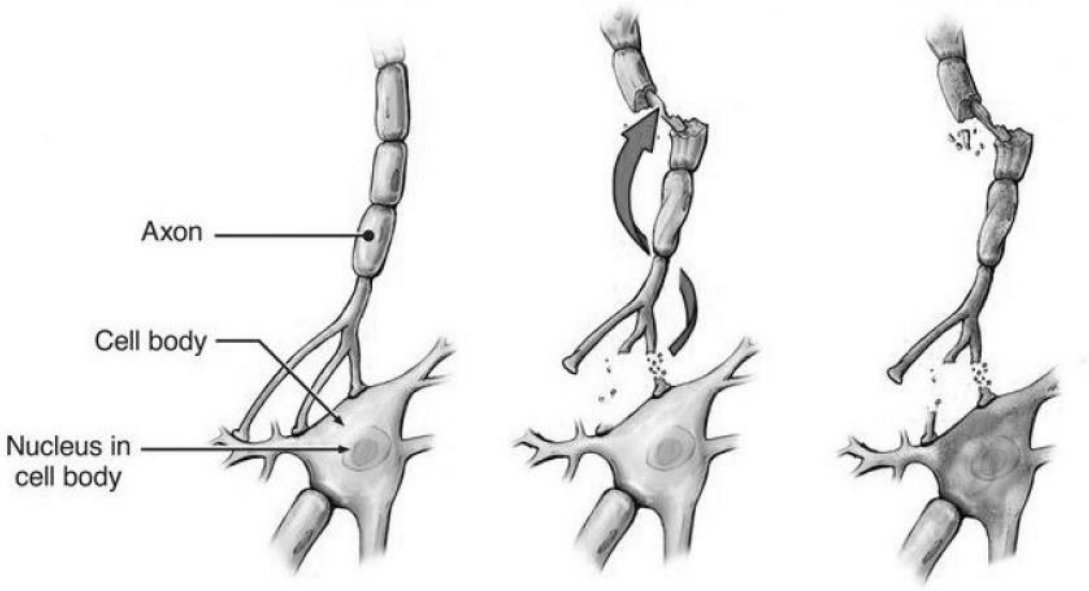


**Figure 1.1** *Scheme showing the event of DAI. (left) normal axon. (center) force applied to the axon. (right) post-trauma condition.*


**Figure 1.2** *CT of a trauma patient showing multiple petechial hemorrhages, that are the light grey spots, consistent with DAI. This image is a good representation of the reason why 'multifocal' would describe in a better way the characteristics of DAI.*

## 1.3 Subdural Hematoma

SDH is a common medical emergency through patients that are experiencing TBI [20]. Two different types of SDH can be identified, that are acute SDH and chronic SDH.

Acute SDH is characterized by the formation of a clot of blood between the surface of the brain and the dura mater [21]. There are three main causes that result in acute SDH, and they can be the direct lacerations of cortical arteries and veins because of penetrating injuries that also lacerate the brain, or closed injuries leading to large contusions with pulped frontal or temporal lobes [22].

Chronic SDH, instead, is due to the presence of an old clot of blood between the brain and the dura mater. The liquefied clots of blood occure more often in patients over 60 years who have brain atrophy. In this case, when brain shrinks in the skull over time, minor head trauma can lead to the tearing of blood vessels [23].

In the following images will be shown the evolution through time of an acute SDH and a CT scan showing a brain suffering chronic SDH.

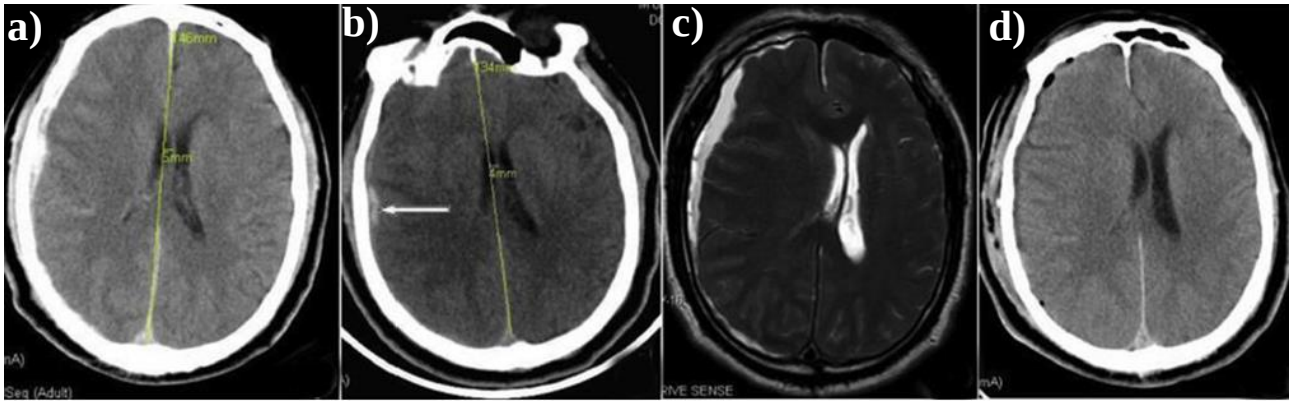


**Figure 1.3** *Progression of acute SDH. (a) Computed Tomography (CT) of acute SDH in right temporal region. (b) CT showing that most of hematoma was liquefied after 6 days from the previous CT. (c) Magnetic resonance imaging (MRI), performed on the 14$^{th}$ day after trauma, showing that hematoma has enlarged and shifted. In that time the acute SDH has become sub-acute. (d) CT of the brain after the removal of the hematoma.*

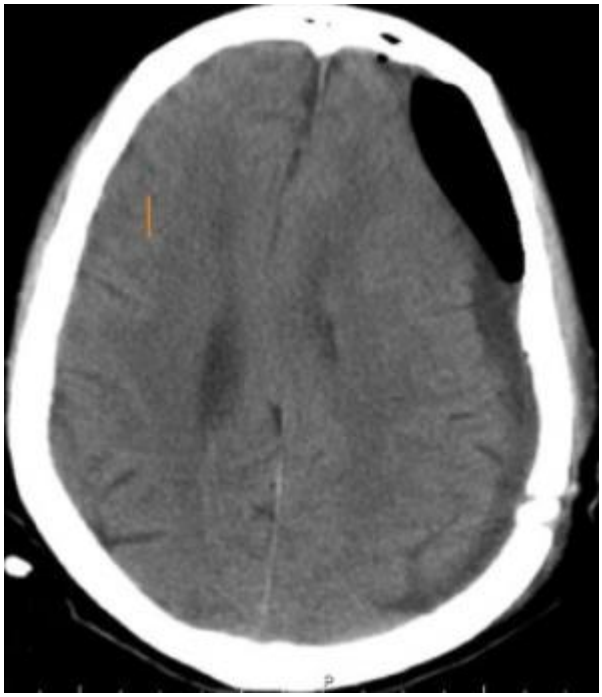

**Figure 1.4** *CT of brain suffering chronic SDH in the left frontal temporal region.*

## 1.4 Epidural Hematoma

Epidural hematoma (EDH) is characterzed by a traumatic accumulation of blood between the inner surface of the skull and the stripped-off dural membrane. EDH results from traumatic head injury, usually with arterial laceration and associated skull fracture. The cause often is a focused blow to the

head, such as that produced by a hammer or baseball bat. In 85-95% of patients, this type of trauma results in an overlying fracture of the skull. Blood vessels in close proximity to the fracture are the sources of the hemorrhage while the underlying brain has usually been minimally injured [24].

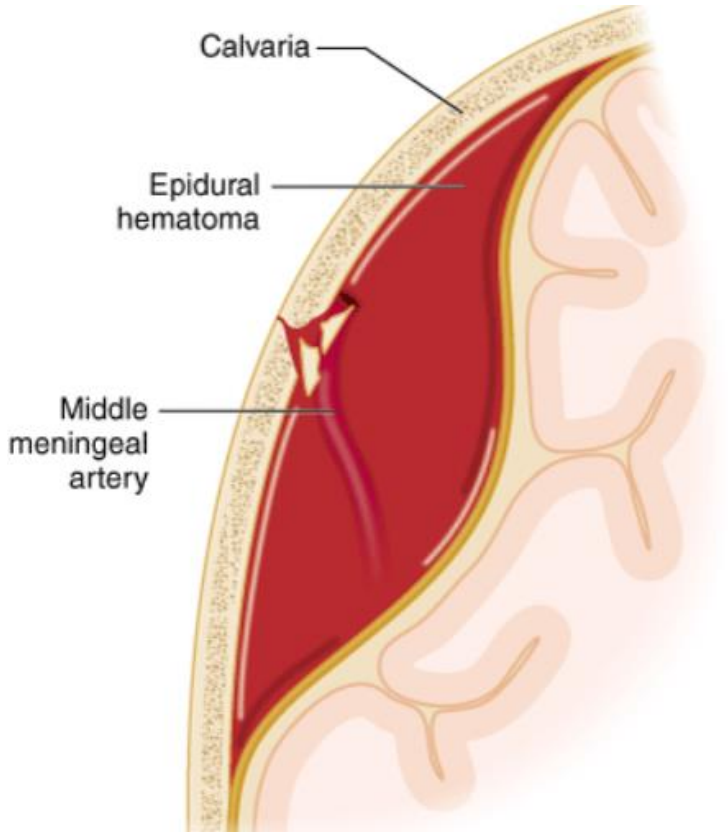


**Figure 1.5** *Scheme explaining Epidural hematoma (EDH).*

## 1.5 Intracerebral Hemorrhage

Intracerebral hemorrhage (ICH) can be traumatic or spontaneous as well. The spontaneous kind is defined as bleeding within the brain parenchyma. The hematoma locations are deep or ganglionic, lobar, cerebellar, and brain stem in descending order of frequency. Risk factors for ICH include hypertension, cerebral amyloid angiopathy, advanced age, antithrombotic therapy and history of cerebrovascular disease. The clinical presentation is similar to stroke with sudden onset of focal neurological deficits [25].

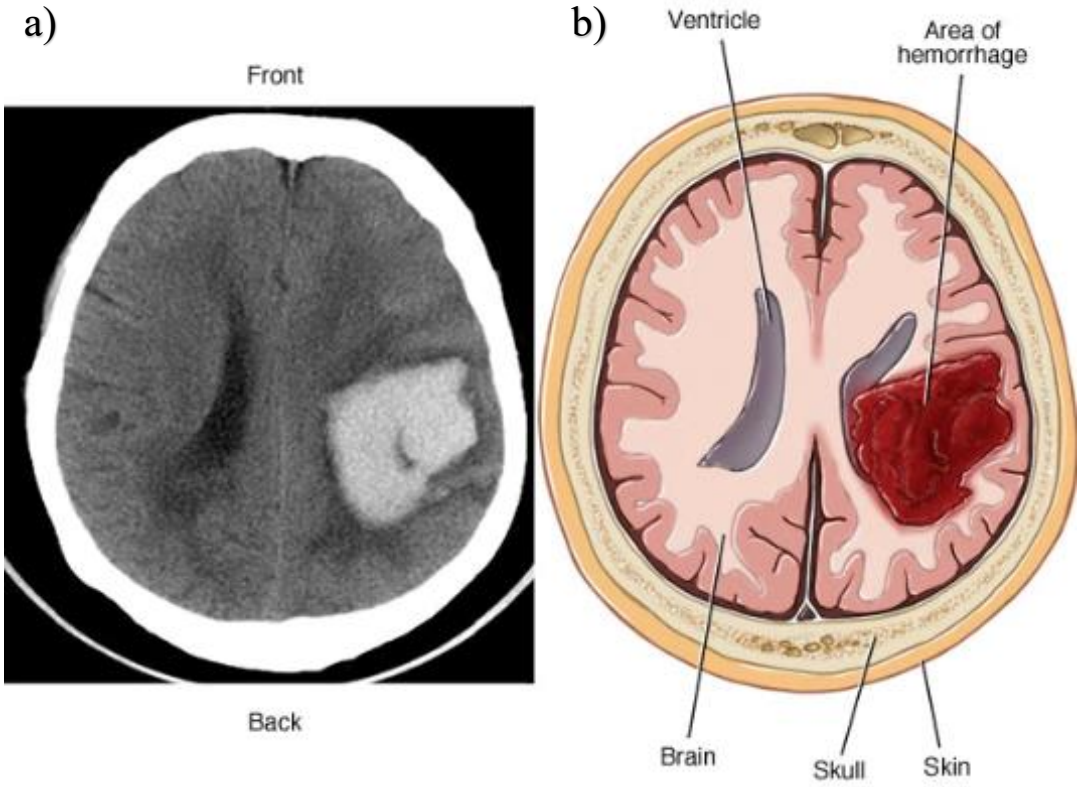


**Figure 1.6** *Intracerebral haemorrhage (ICH). (a) MRI scan (b) scheme*

## 1.6 Cerebral Contusion

Cerebral edema is a life-threatening condition that appears as a result of an inflammatory reaction. Most frequently, it is the consequence of cerebral trauma, massive cerebral infarction, hemorrhages, abscess, tumor, allergy, sepsis, hypoxia, and other toxic or metabolic factors. Cerebral edema is differentiated into different kinds: the vasogenic cerebral edema resulting from an increased permeability of the endothelium of cerebral capillaries to albumin and other plasma proteins; the cytotoxic cerebral edema resulting from the exhaustion of the energy potential of cell membranes without damage to the barrier; the hydrostatic cerebral edema resulting from disturbance of the autoregulation of cerebral blood circulation; the osmotic cerebral edema resulting from dilution of blood; the interstitial cerebral edema resulting from acute hydrocephaly; and ischemic cerebral edema [26].

# Chapter 2

# State of the Art of Laboratory Testing of Helmets

Through the years and in different countries, various regulations of the laboratory testing of helmets have been developed and used. There are different kind of tests required by regulations and law for motorcycle tests, ski and winter sports helmets, firemen helmets and every other type of helmets. One of the most interesting regulation that deserve to be analysed and that can be taken as example is the one published by United Nations Economic Commission for Europe in 2002, called '*Uniform Provisions Concerning the Approval of Protective Helmets and Their Visors for Drivers and Passangers of Motor Cycle and Mopeds*', known as ECE regulation 22-05.

There are two main reasons why it is interesting. Firstly, it is used in more than 50 countries and then is meant to comprehend the basis of most of the other regulation and standards.

The impact-absorption test is performed recording the acceleration imparted to a headform, wearing the helmet that has to be approved, during the guided free fall and the impact against a fixed steel anvil. The drop height must be adjusted in order to produce a velocity of the unit made by the headform and helmet just before the impact of 8.5 (-0.0/+0.15) m/s.The helmet passes the test if the following statement is respected: '*The absorption efficiency shall be considered sufficient where the resultant acceleration measured at the centre of gravity of the headform at no time exceeds 275 g, and the Head Injury Criterion does not exceed 2400.*' [27].

In the following figure the test machine and the drop assembly will be presented as reported in the regulation. In addition to this brief description, to have a full view of the standard tests performed by companies on their safety garments it is needed to study the most used headform or dummy head and the Head Injury Criterion (HIC), recalled in the previously reported statement. In the project ski helmets will be used during the tests on the instrumented human head surrogates, so it is right to show also the '*Standard Specifications for Helmet used for Recreational Snow Sport*' [28], approved by

ASTM. The impact test procedure is similar to the previously presented regulation for motorcycle helmets, with a different kind of anvil.

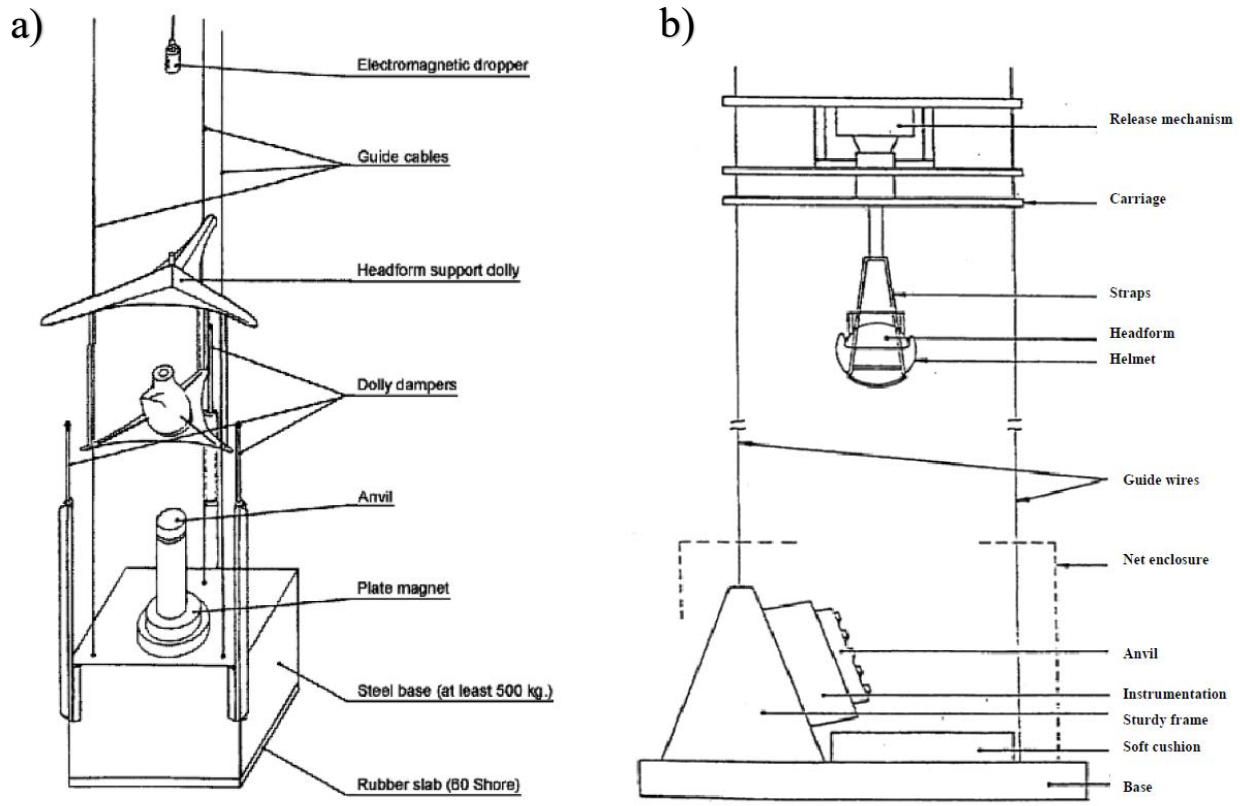


**Figure 2.1** *ECE Regulation 22-05 (a) setup of the impact-absorption test. (b) Example of a suitable test apparatus for projections and surface friction.*

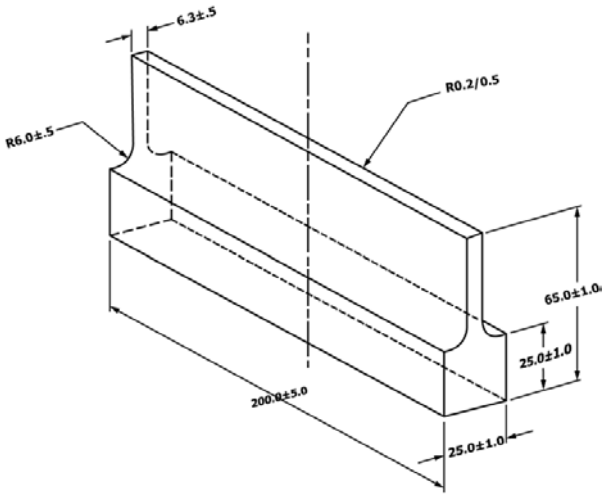


**Figure 2.2** *Edge anvil used in the: 'Standard Specifications for Helmet used for Recreational Snow Sport'.*

## 2.1 Cadaver and Animal Testing, Finite Element Models and Instrumented Dummy heads

The first studies related to biomechanics of brain injuries and characterization of human tissues were carried on performing tests on cadavers, for example as shown in the work of Donnelly *et al*. [29] in which 125 tissue samples of the brain taken from fresh cadavers are subject to shear tests. Another approach to study brain injury mechanics or to investigate the properties of tissue is animal testing. Animal testing is widely deployed in laboratories around the world, however there are some considerations to take into account: Concordance between key features of the animal model and the human disease or condition being modeled is required to confirm model biofidelity, experimental results observed in animals must be confirmed in human subjects for model validation and scaling the results from animal testing to human body [30]. Today studies, instead, prefer to utilize Finite Element (FE) models. Through the years, a certain number of FE models have been developed with a complexity that can vary from simple spherical and regular shapes for the description of the various layers present in the head [31,32] to complex geometry. Only to give some name, we can consider the EEVC WG17 adult headform FE model, *Wayne State University Head Injury* model (WSUHIM), TNO *Head Finite Element Model*, *Head-Brain* FE model, *University of Louis Pasteur Finite Element Model (*ULP FEM*), Politecnico di Torino University FEM* of the human head, *Harvard Medical School* FEM*, University College Dublin Brain Trauma Model* (UCDBTM), etc. [33].

Every FE model of the human head has different problems to address. One of the problem is the assumption of the mechanical characteristic and behaviour of the brain tissues, the Cerebrospinal fluid, the skull etc. The other problems are geometry and the level of discretization, in fact every single FE model differs for number of nodes, and the validation against experimental data. The characterization of human brain tissues and their mechanical behaviour is carried out using data from the literature works and the validation against experimental data often refers to the data obtained through human cadavers testing [33]. FE models are used widely because through human cadavers is difficult to reach the required repeatability and through animal testing there is the problem of data scaling and moral or ethical considerations about exploitation of animals. To reach the desired repeatability needed in a scientific project or research can be useful to resort to instrument crash test dummies.

The *Hybrid III* 50$^{th}$ Percentile male crash test dummy is the most used dummy in frontal crash tests and safety garment testing. At the beginning, the *Hybrid III* 50$^{th}$ Percentile male was developed by *General Motors* for vehicle safety purposes. It has been involved into the *Code of Federal*

*Regulations* under Title 49, Part 572 subpart E, in addition to the ECE Regulations, and is the required dummy in *National Highway Traffic Safety Administration's* (NHTSA) motor vehicle safety standards. The crash test dummy design is now maintained and developed by *Humanetics* in collaboration with the NHTSA and the *Society of Automotive Engineers*' (SAE) *Biomechanics Committees*. The dummy is produced to the Federal specifications and distributed by three companies; *Utama Engineering*, *First Technology Safety Systems* and *Applied Safety Technologies Corporation*. Since its first appearance in 1976, improvements have been made to the dummy in order to make it more biofidelic and suitable to represent the human body behaviour. [34]

The *Hybrid III* dummy is considered to have a high instrumentation capacity and biofidelity. This statement can be applied to the different parts of the dummy body, but it is not so correct for the head, in fact this part is composed of a skull and skull cap made by an aluminium hollow piece. Inside the cavity of the head there is nothing resembling a brain or the cerebrospinal fluid. The neck instead is a segmented rubber and aluminum construction with a center cable. The neck design, at least, simulates the human dynamic moment / rotation, flexion, and extension response characteristics [34].

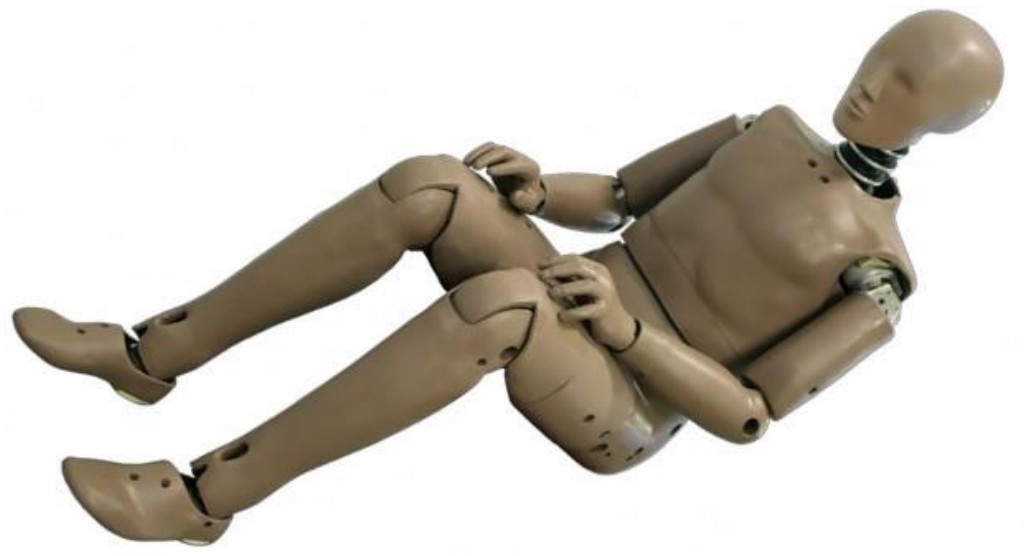

**Figure 2.3** *Hybrid III 50$^{th}$ Percentile crash test dummy.*


**Figure 2.4** *Hybrid III 50th Percentile dummy head composition.*

Besides the *Hybrid III* crash test dummy there are other dummies with a little more attention dedicated to the data coming from the head. An example can be *Test device for Human Occupant Restraint* (THOR) and it is an advanced frontal impact 50th percentile adult male crash test dummy. As well as *Hybrid III*, also THOR dummy is designed and produced by *Humanetics*. The difference between the two dummies is that THOR has an expanded instrumentation compared to the standard *Hybrid III*, in fact the latter is designed in order to have an only one triaxial accelerometer inside the cavity of the head, in correspondence of the center of gravity of it. THOR crash test dummy can contain not only accelerometers in different regions of the head, but also gyroscopes and loadcells [35]. In the next table the full list of the sensors that can be placed in the head and neck of THOR will be displayed.

| Sensor | Position |
|---|---|
| Accelerometer | Center of Gravity |
| Accelerometer | Top |
| Accelerometer | Side |
| Accelerometer | Rear |
| Head Angular Rate Sensor | Center of Gravity |
| Tilt Sensor | Head |
| Tilt Sensor | Neck |

| | |
|---|---|
| Face Load Cell | Left eye |
| Face Load Cell | Right eye |
| Face Load Cell | Left cheek |
| Face Load Cell | Right cheek |
| Face Load Cell | Chin |
| Neck Load Cell | Upper neck |
| Neck Load Cell | Lower neck |
| Skull Spring Load Cell | Front |
| Skull Spring Load Cell | Rear |
| O.C. Rotary Potentiometer | |

**Table 2.1** *Head channels of the Test device for Human Occupant Restraint (THOR).*

However, all the data recorded by the sensors are related to the outer part of the instrumented dummy head. Also the accelerometer placed on the center of gravity is related to the whole head kinematics and not the brain, in fact in the THOR dummy head there is nothing that can resemble it.

Another crash test dummy head, always designed and produced by *Humanetics*, is WorldSID, whose name means *Worldwide harmonized Side Impact Dummy*. Instead of being a dummy thought for frontal impact vehicle crash test, it is designed for side impacts. The head is characterized by two major parts: the skull-skin assembly and the instrumentation core. Sensors are included to measure the head center of gravity linear accelerations along the 3 directions, head center of gravity rotational accelerations around 3 axis, and head tilt, but only around 2 axis [36]. WorldSID is brainless, as well as *Hybrid III* and THOR.

Besides the development of the aforementioned crash test dummies produced by *Humanetics*, in literature can be found only some attempts to realize a biofidelic dummy head. In a research conducted by Zhang *et al*. [37] an ellipsoidal-shaped physical head model, made from 3-mm polycarbonate shell filled with *Sylgard 527* silicone gel, was used. The gel filling the head cavity is needed to represent the brain. Four pressure transducers were positioned outside the shell and four were distributed into the silicone gel. Results from the study are used to quantify intracranial biomechanical responses and external blast overpressures in order to understand the biomechanics of blast traumatic brain injury and to provide experimental data for computer simulation of blast-induced brain trauma. However, the limitation of this study is a lack of biofidelity.

Zhu *et al*. [38] used the same silicone gel by *Sylgard* to simulate Cerebrospinal fluid behaviour and an egg-shaped skull to create a head surrogate. The surrogate was exposed to blast overpressure in a shock tube. Not so much attention was given to the anatomical detail.
Taha *et al*. [39] performed a research trying to understand the effects of soccer heading on the brain. *Ultrasound gel 12* was used to fill a hollw ABS plastic skull. This solution did not care about the relative movement between brain, because there was no brain but only ultrasound gel, and skull. One triaxial accelerometer was placed inside the gel approximately at Center of Gravity assuming that these accelerations represented the brain acceleration.
In the work presented by Freitas *et al*. [40] *Human Head Surrogate* has been developed for use in behind helmet blunt trauma experiments. This human head surrogate fills the void between Post-Mortem Human Subject testing (with a high level of biofidelity but handling restrictions due to low repeatibility) and commercial ballistic head forms (with no biofidelity but ease of use). This human head surrogate is based on refreshed human craniums and surrogate materials representing human head soft tissues such as the skin, dura mater and brain. The methodology for refreshing the craniums is based in dehydrating human bone from donors and rehydrating by soaking for 30 minutes in a Shellac solution. The brain and external skin are manufactured from *Perma-gel*, a colorless, transparent petroleum-based thermoplastic material. Sensors embedded in the human head surrogates allow for direct measurement of intracranial pressure, cranial strain, and head and helmet acceleration. The human head surrogate presented in this work is the most advanced found in the literature.

## 2.2 Head Injury Criterion and Brain Injury Criterion

The most used injury criterion in crash tests is HIC, also present in the ECE regulation 22-05 [27]. HIC is developed as a further study of the *Wayne State Tolerance Curve* (WSTC) [41]. The WSTC tries to describe the correlation between linear head acceleration on the anterior-posterior direction, duration of acceleration and risks of concussion. The WSTC shows that the head can withstand very high acceleration for a very short duration. Conversely, any increase in the duration of impact for the same intensity of acceleration is likely to cause head injury. Points that are placed above the line defining the tolerance level in the following graph can lead to death [42].

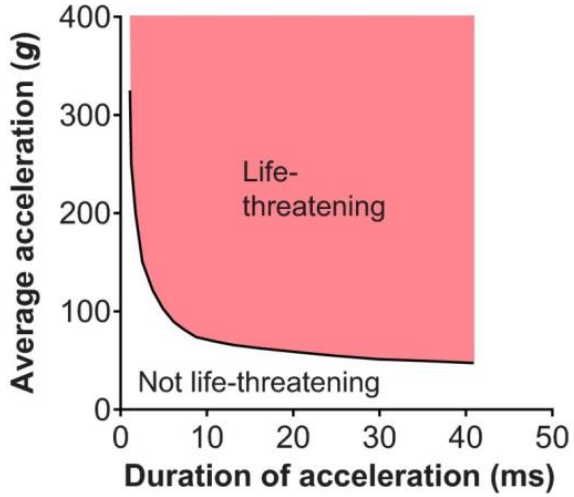


**Figure 2.5** *Wayne State Tolerance Curve*

HIC is an index that tries to put in correlation both the time of impact and the acceleration, similarly to the WSTC.

$$HIC = \left\{\left[\frac{1}{t_2 - t_1}\int_{t_1}^{t_2} a(t)dt\right]^{2.5}(t_2 - t_1)\right\}_{\max\{\Delta T\}}$$

In the formula, *a(t)* stands for the resultant of the acceleration in the center of gravity of the head measured in *g* along the 3 axes X, Y and Z, $t_2$ and $t_1$ are the boundaries of an arbitrary time interval within the acceleration impulse. For the head the chosen index is 2.5, value based on experiments. The duration of HIC is included between ΔT of 3ms and 36ms at maximum. Usually a time interval of 15ms is chosen [43]. There are different studies and researches that proposed correlations between different values of HIC and risk of injuries. One of the most famous correlation is the *Abbreviate Injury Scale* (AIS) proposed by NHTSA. The categories of injury severity in AIS, related to head and neck, are subdivided into 6 levels, shown in *Table 2.2* [44]. In the following image will be given the correlation between HIC and head injury probability belonging to the different AIS categories as presented by ASME [45].

| AIS | Categories | Injuries |
|---|---|---|
| 1 | Minor | Light brain injuries with headache, vertigo, no loss of consciousness, light cervical injuries, whiplash, abrasion, contusion. |
| 2 | Moderate | Concussion with or without skull fracture, less than 15 minutes unconsciousness, corneal tiny cracks, detachment of retina, face or nose fracture without shifting. |
| 3 | Serious | Concussion with or without skull fracture, more than 15 minutes unconsciousness without severe neurological damages, closed and shifted or impressed skull fracture without unconsciousness or other injury indications in skull, loss of vision, shifted and/or open face bone fracture with antral or orbital implications, cervical fracture without damage of spinal cord. |
| 4 | Severe | Closed and shifted or impressed skull fracture with severe neurological injuries. |
| 5 | Critical | Concussion with or without Skull fracture with more than 12 hours unconsciousness with hemorrhage in skull and/or critical neurological indications. |
| 6 | Survival not Sure | Death, partly or fully damage of brainstem or upper part of cervical due to pressure or disruption, Fracture and/or wrench of upper part of cervical with injuries of spinal cord. |

**Table 2.2** *Abbreviate Injury Scale related to head and neck injuries.*

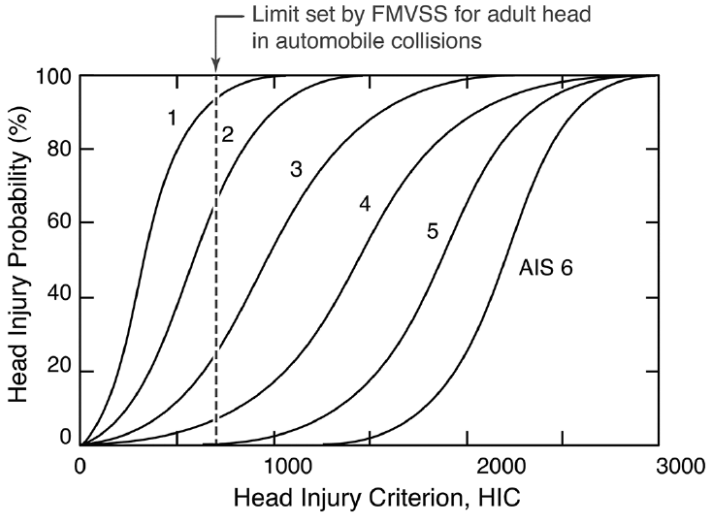


**Figure 2.6** *Correlation between HIC and probability of injuries belonging to different AIS categories.*

A category 6 of AIS corresponds to death. For example, as can be seen from the Figure 2.5, a value of HIC equal to 2000 bring to a probability of death around 30%. Even if HIC is the most used index related to brain injuries, it received some criticism. In fact, HIC is a measure of linear impulse of the head's motion during a crash, so studies continue to reiterate that HIC was not developed as a comprehensive predictor of all head injuries, but rather an indication of translational-based skull fracture injuries involving impacts and not rotational-based injury mechanisms [46]. The NHTSA

decided also to develop a Brain Injury Criterion (BrIC) based on head rotational velocity that could be used in addition to HIC for a more complete evaluation of TBI risk [47]. To evaluate BrIC, it is needed to record the angular velocities $\omega_x$, $\omega_y$, and $\omega_z$.

$$BrIC = \sqrt{\left(\frac{\omega_x}{\omega_{xCr}}\right)^2 + \left(\frac{\omega_y}{\omega_{yCr}}\right)^2 + \left(\frac{\omega_z}{\omega_{zCr}}\right)^2}$$

In the formula, the axes X, Y and Z are respectively posterior-anterior, laterally to the right and superior-inferior direction, instead $\omega_{xCr}$, $\omega_{yCr}$ and $\omega_{zCr}$ are critical values equal to 66.25rad/s, 56.45rad/s and 42.87rad/s [46].

However, it is needed to say that both HIC and BrIC treat head as a whole, solid entity in order to evaluate brain injury risks, neglecting the influence of relative cinematics between different parts of the head [1].

# Chapter 3

# Technologies and Instrumentation

In this section, firstly, the tools and machines to produce the molds and the different parts of the surrogate heads and then the hardware, that is the sensors, used both for *Instrumented Human Head Surrogate 1* (IHHS1) and for *Instrumented Human Head Surrogate 2* (IHHS2) will be presented. Secondly the software involved in the project will be described.

## 3.1 Additive Manufacturing Technology

### *3.1.1 uPrint SE PLUS*

*uPrint SE PLUS* is an additive manufacturing machine distributed by *Stratasys* (*Stratasys Ltd., Eden Prairie, MN, USA*). In the project this machine has been used for producing both the molds of the 2 brains, the molds for the mockup cube needed to study the possibility of calculating the deformations inside the silicone rubber brains and the skulls of the instrumented head surrogates.

*uPrint SE PLUS* uses *Fused Deposition Modeling* (FDM) to produce the parts. FDM is a technique that exploits a plastic filament that is unwound as the machine supplies material to the extrusion nozzle. The nozzle is heated so, when the plastic filament pass through it, the material begins to melt. The movement of the nozzle is managed by a *Computer Aided Manufacturing* (CAM) software, in this case called *CatalystEX*, and during its moving the plastic material is deposed on the precedent layer. The material hardens immediately after it is extruded and released in contact with the air [48]. With this technology is possible to prototype or create pieces and parts that cannot be produced with traditional manufacturing techniques. To build complex geometries support parts are needed. The support is created using a different extruding nozzle that deposes a soluble material; when the *uPrint SE Plus* finish its work, the part needs to be separated by the supporting structures and this is performed by immersing the unit composed by both in a specific washing machine sold with the 3D printer itself and called *WaveWash* support removal system. After leaving the unit in the washing

machine, the support is dissolved in a bath of water-based solution and the desired part can be collected. In the case of the machine present in the Sport Technology Laboratory of *Mid Sweden University*, the principal part is made of ABSplus, instead the support is composed by a soluble acrylic copolymer called *SR-30*. The build size of *uPrint SE PLUS* is 203x203x152mm and the two thickness for the layer are 0.330mm and 0.254mm [49].

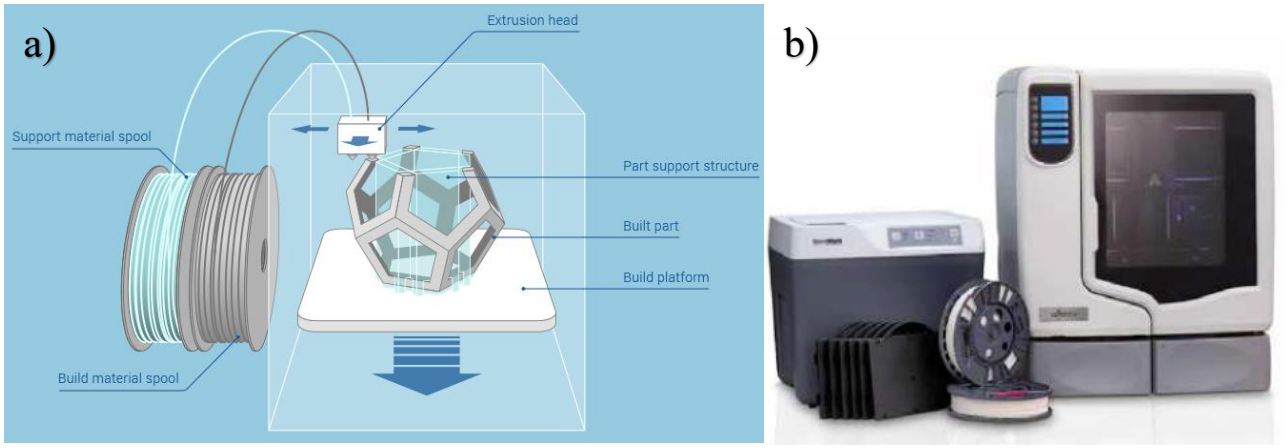


**Figure 3.1** *(a) scheme representing the functioning of FDM machine. (b) uPrint SE Plus.*

### 3.1.2 Arcam Q10 plus

*Arcam Q10 plus* is the machine used to produce the base that connects the *Hybrid III* neck with the structure on the force platform and the piece connecting the neck with the head.

*Arcam Q10 plus* is an *Electron Beam Melting* (EBM) machine. EMB is a technique that works distributing a layer of metal powder onto a building platform. The electron beam melts the only parts of the layer that are indicated in the sliced .stl file of the desired part. As in every *Additive Manufacturing* (AM) process, the file is firstly designed with a 3D parametric modelling software like *Solidworks*, then is converted to .stl format and lastly is sliced in order to have the different sections of the part needed to guide the electron beam. After the melting of the precedent layer, the building platform is lowered and the next layer of metal powder will be coated on top. The process of coating and melting where needed is repeated until the part is completely formed. EBM needs supporting structures to anchor the part to produce and to enable the heat transfer away from where the powder is melted, so thermal stresses are reduced and wrapping prevented. The parts are built up in a vacuum chamber. Vacuum is needed so the electrons will be able to travel along a clear path to the metal. EBM produces pieces with very high density and mechanical properties better than sintering, but is a very slow process, is expensive and is applicable to only a few standard materials [48].

The built size of *Arcam Q10 plus* is 200x200x180 mm and its metal powder layer thickness is 0,05 mm. The material worked by this machine is a powder of T6Al4V [50].

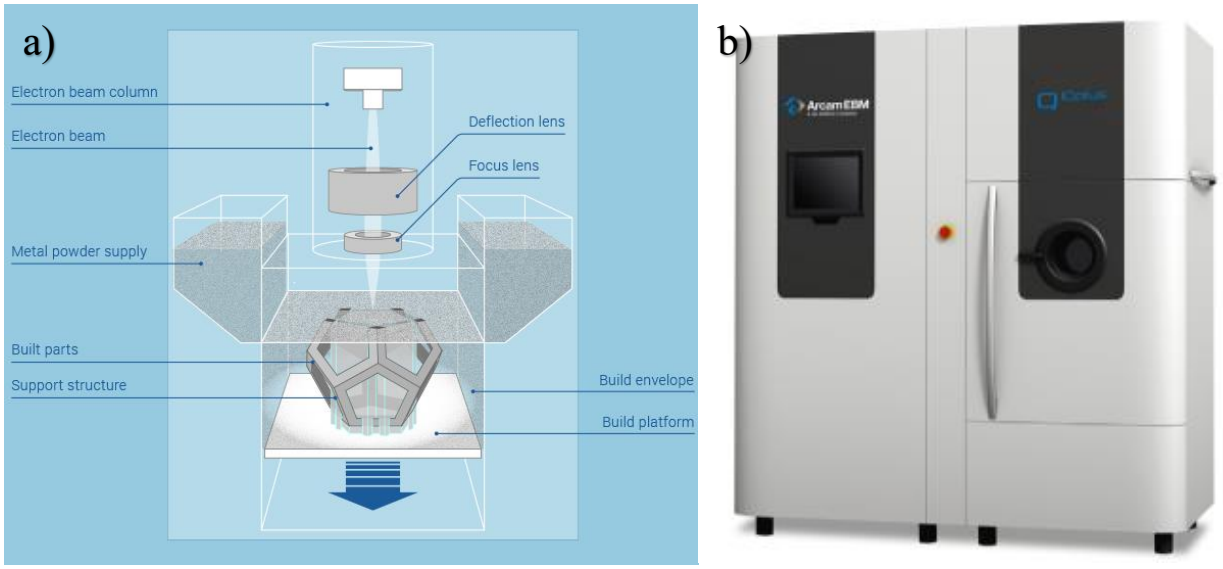


**Figure 3.2** *(a) scheme representing the functioning of an EBM machine. (b) Arcam Q10 plus.*

## 3.2 Sensors and Hardware used in the Project

For tests on both IHHS1 and IHHS2 accelerations in different part of the brain, on the skull and on the helmet has been recorded, as well as angular velocity of the skull and in the center of gravity of the brain, through which calculating the angular acceleration has become possible by time-derivating, forces transmitted through the basis of the neck, speed of the impactor hitting the two instrumented head, pressure only inside the cerebrospinal fluid substitute of IHHS2 and slow motion videos of the impacts.

### *3.2.1 Accelerometers*

As explained by Giovanni Carraro [1], the major part of impact events that can lead to brain injuries produce peak accelerations that are lower than 200 g. Because of the that, the accelerometers chosen to be used in the project are set at the range of ± 200 g.

The model of all the accelerometers for both the heads is *ADXL377* 3-Axes accelerometer, produced by *Analog Devices Inc.*, whose datasheet specifically communicate that these devices where designed to detect concussion and head trauma. The sensors are very small (3x3x1.45 mm), so they don't influence so much with their weight and dimensions the system.


**Figure 3.3** *ADXL337 accelerometer produced by Analog Devices Inc.*

### *3.2.2 Gyroscopes*

For the gyroscopes, the models chosen were already owned by the *Mid Sweden University*. The two used models are *LPY4150AL* and *LPR4150AL*. Both have a full scale of ±1500dps, in case the signal is amplified, or a range of ±6000dps, if the signal is not amplified, and are capable of detecting rates with a -3dB bandwidth up to 140 Hz. That means that the full scale for signal amplified and not amplified is respectively 26.2 rad/s and 104.7 rad/s. They are 2-axes gyroscopes, so to detect angular velocity around 3 axes, it was required to mount 2 different gyroscopes on the same board (pitch & yaw and pitch & roll). As well as accelerometers, these gyroscopes have very limited dimensions (4x5x1 mm) [1,3].

### *3.2.3 Pressure Sensors*

In the first and the second head surrogate two different kind of pressure sensors have been placed. In IHHS1 for pressure sensors have been used piezoelectric transducers from *STD* series produced by *Sensera Co, L* [3]. However, in this part of the project, they were not used because the liquid chosen to represent the cerebrospinal fluid in IHHS1, that is *SilOil M40*, a low-viscosity silicone fluid, reacted with the brain making it to swell and enlarge. So, it was decided to remove the oil from the skull and without a fluid inside the pressure sensors could not work properly. Instead for the second head surrogate, Miniature *SMD Pressure Sensors MS5401* have been applied. These devices are made of a silicon micromachined pressure sensor die mounted on ceramic carrier of 6.2x6.4 mm of dimensions. *MS5401* have a full scale of ±1 bar that is ±760 mmHG.

During the impacts the brain can move and hit the sensors because they are not covered. The fact that the brain can come in touch with the piezo electric transducers can lead to skewed data.

**Figure 3.4** *SMD Pressure sensor MS5401.*

### 3.2.4 Force Platform

The form platform on which IHHS1 and IHHS2 have been mounted is a *Kistler* multi-component force plate *Type 9281 EA*. It is composed of a 600x400 mm aluminum sandwich top plate of lightweight construction and four piezoelectric 3-component force sensors. Measurements are allowed over a very wide frequency range. The measuring range can go from –10 to 20 kN [51].

**Figure 3.5** *Kistler multi-component force plate Type 9281 EA*

### 3.2.5 Video Cameras

The impacts performed on the heads have been recorded using two *GoPro Hero 5 Black*. Two *GoPro* where needed to record the video of the impact both from a lateral point of view and from the top. These devices have been chosen because can be operated remotely by using smartphones. That

possibility made the performing of the test far way easier and without the help of another human assistant. *Hero 5 Black* are characterized by a maximum resolution for videos of 4K for a recording speed of 30 fps, instead photos are performed at 12 MP [52]. In the project, settings were a resolution of 1920x1080p, 120 fps of recording speed and a Field of View (FOV) called narrow in order to reduce the fish eye effect of the *GoPro* lenses. It was chosen to record with a lower resolution with the purpose of increasing the frame per second of recording, without increasing to much the dimensions of the files that could lead to problems with transfer and storage of information. It is important to have a high number of frames because impact happen in a very little time interval (no more than 25 ms). Recording at 120 fps means that the time between two images is of 8.33 ms, and so only a few frames of the videos could really depict the moment of contact between the impactor and the helmet mounted on the head. However, the videos have been used to check if the testing routine was followed in the correct way in order to increase repeatability. In case the routine was not respected or something not expected happened, the test was repeated. The videos were also used to verify approximately the concordance between the real displacement of the head and the displacement calculated by time integrating two times the acceleration.


**Figure 3.6** *GoPro Hero 5 Black*

### *3.2.6 Laser Trigger System*

Through the hardware system also the laser system needed as trigger for the data acquisition has to be presented. This system is made up of two lasers and two optical sensors. The optical sensors and lasers are placed in order to have them coaxial in pairs, with the optical sensors collecting the laser

beams. When the hammer used as impactor on the surrogate head passes between the laser and optical sensor of the first pair, blocking the laser beam, the optical sensor does not receive anymore the signal and so the system makes the acquisition start. The second pair of laser and optical sensor is needed in order to calculate the speed of hammer. The system counts how much time passes between the interruption of the first and second laser beam, and knowing the distance between the two pairs is possible to arrive to the speed value by dividing distance by time.

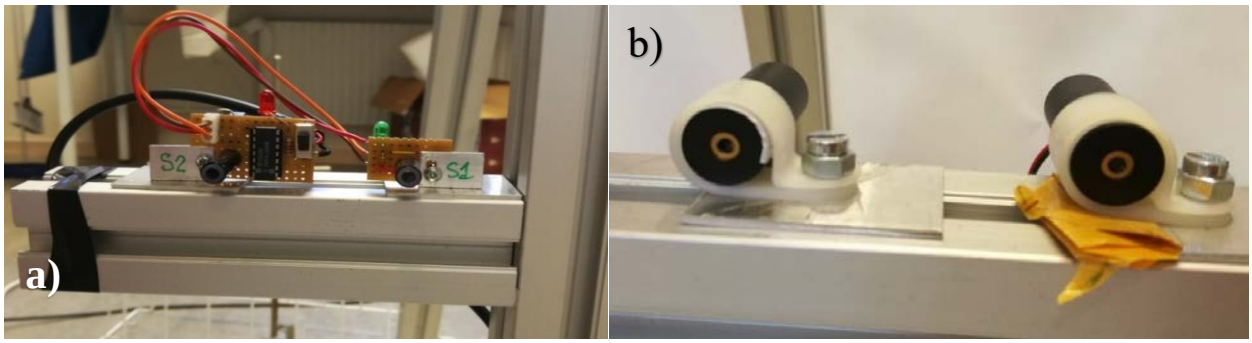


**Figure 3.7** *Laser trigger system (a) Optical sensors (b) Lasers*

## 3.3 Software used in the Project

In this section, the different software involved in the project will be presented. These softwares have been used for a wide range of operation that can go from the design of the molds, the creation of the STL files needed for the AM machines to the elaboration and presentation of the data.

### *3.3.1 LabView*

*Labview*, meaning *'Laboratory Virtual Instrument Engineering Workbench'*, is a programming environment published by *National Instruments* that exploits a graphical language of programming, unlike other traditional programming languages like *Java* or *C++*. A *LabVIEW* program is designed in a section called block diagram through different virtual instruments (VIs). Virtual instruments are called such because in the block diagram the program is built by the user connecting different VIs, working as functions, using virtual wires. VIs in the block diagram have an appearance and functioning that often imitate physical instruments. The program is organized in the block diagram but is managed by the user in the front panel. The front panel is the interactive user interface, whose name depends on the fact that it simulates the front panel of a physical instrument, containing knobs, push buttons, graphs, and other controls, used as inputs, and indicators as graphs that are outputs [53].

In the project, *LabView* has been used to design the program through which all the sensors were started, from the laser beams and optical sensors, working as triggers for the data acquisition when the impactor passes between them, to the *Kistler* force platform, the accelerometers and gyroscopes in the head etc. The program used was capable of writing down the data acquired.

### 3.3.2 Bioware

*Bioware* is a software designed to work with the *Kistler* multi-component forceplate. It is a software designed for data acquisition and signal processing in the sport environment of research and biomechanics [3,54]. This software was the one recording the ground reaction forces that were transmitted from the hit head surrogate to the force platform.

### 3.3.3 Matlab

*Matlab* is a programming language widely used in different environment that can vary from engineering to finance or robotics for example. *Matlab* stands for *'Matrix Laboratory'* in fact is a matrix-base language [55].

Even if *Matlab* is populated by different pre-built toolboxes, it leaves a great freedom of programming to the user through the creation of functions and scripts.

It has been widely used during the project for different activities that can go, in order, from extracting the vectors of data acquired by the *LabView* program, cutting the files where needed, design filter to clean the different signals, zeroing the vectors defining the different acceleration-time history, angular velocity-time history, pressure-time history etc., calibrate the great number of sensors involved in the project in order to pass from mV of the signals to the correct unit of measure, calculate complex functions as HIC that requires routines and sub-routines or iterative processes or simpler functions as BrIC and present the elaborated data in graphs highly organized by the user concerning the limits of the axis, colour of the signals, legend, title, unit of measure and so on.

### 3.3.4 Solidworks

*Solidworks* is a *Computer Aided Design* (CAD) and a *Computer Aided Engineering* (CAE) program published by *Dassault Systèmes*. This means that the program accompanies the user through the phase of design until the phase of production of the desired part with tools helping to define the machine tool path during working. This software follows a 3D parametric feature based-approach. Parameters can be both numeric and geometric. Numeric parameters are, for example, length of lines or diameters

instead geometric parameters can be tangent, parallel and so on. With *Solidworks* both single parts and multiple part assemblies and projects can be assessed [56].

*Solidworks* has been particularly used during the project in the designing part of the molds. After the part was designed, *Meshmixer* was needed to prepare the .stl file for the AM machine whose software is *CatalystEX*.

# Chapter 4

# Experimental Setup and Test Method

In this section the structure used to perform the test and the procedure followed to mount in the right position the two instrumented human heads surrogate will be presented and explained.

## 4.1 Structure Supporting the Pendulum

To make the tests both on the IHHS1 and IHHS2, the structure and pendulum system, built buy Luca Broggio [3], has been deployed.
The structure is made of aluminium profiles. The length of the pendulum arm, from the axis of the pin around which the pendulum rotates to the center of gravity of the weight used as impactor, is of 1035 mm. At the end of the pendulum arm, that is the moving part of the structure, there is an impactor of circular section. The dimensions of the impactor are 60 mm for diameter and 255 mm for height. The impactor is made of common steel whose density $\rho$ is 7749.5 kg/m$^3$, meaning that it weights 5.59kg. The part of the impactor that comes in touch with the helmet mounted on the instrumented human heads is padded with foam to not spoil too much the helmet, in fact with the foam the edges are less sharp. To make easier the action of moving the pendulum arm for the operator a rope and a pulley are needed. The rope is attached to the pendulum arm near the impactor and pass through the pulley that is attached to the upper part of the whole structure. A manual trigger is used to make fall the hammer and start the acquisition of data. This trigger is a metal pin with an L-shape, positioned in a hole in the center of a horizontal beam. The pin is inserted in the hole and the rope needed to make easier the movement of the impactor is bound to the pin. The pin is removed quickly from its position inside the hole, so the rope is no more bound to the pin and the hammer falls passing between the laser beams and the optical sensors that make the acquisition start. After the release of the hammer and its passing in front of the digital trigger system the instrumented head is hit. In the following pictures the structure will be shown.


**Figura 4.1** *(a) Structure. (b) Hammer, rope, pulley and manual trigger. (c) L-shaped manual trigger.*

## 4.2 Setup and Mounting of IHHS1 and IHHS2

The placement and preparation for IHHS1 and IHHS2 are very similar, there is only a little difference in the first step.

The skulls of both have an accelerometer attached. IHHS1 has a little piece of ABS, produced with *uPrint SE PLUS*, positioned under the hard palate needed to make flat the surface on which the accelerometer is placed. Instead IHHS2 has the accelerometer in a different position, in fact, after the session of tests on the first head surrogate, it was decided that the accelerometer measuring the acceleration of the skull have to be at the same height of the one in the center of mass of the brain, in order to have comparable values of HIC for both the skull and the brain. In fact, for IHHS1 the value of HIC calculated with the data coming from the accelerometer of the skull are a lot lower than the HIC evaluated in the brain, in fact the accelerometer on the skull is in a lower position. IHHS2 has

the accelerometer of skull placed on the forehead exactly at the reference level of center of mass (CoM). Another difference is that IHHS2 has also a gyroscope positioned on the skull in order to evaluate the differences between rotation of the brain and rotation of the skull. This gyroscope is placed exactly above the CoM of IHHS2. IHHS1 did not have that sensor.

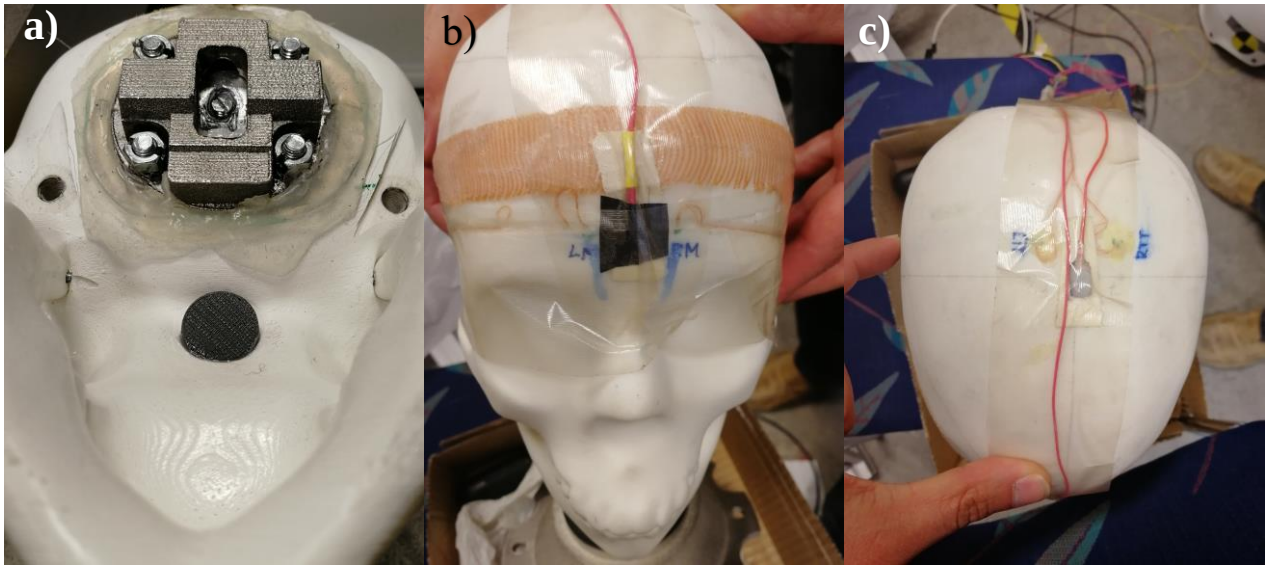


**Figura 4.2** *(a) ABS flat piece used as basis for placing accelerometer on IHHS1 skull. (b) accelerometer of IHHS2 at the same level of the one at the center of gravity of the brain. (c) gyroscope used to measure angular velocity of IHHS2.*

After the positioning of the additional sensors of the skull, the step followed to mount the head are the same. Before the head is attached to the *Hybrid III* neck, the neck is fixed on a structure of aluminium profiles positioned on the force platform. This structure between the neck and the force platform is needed to change the position of the head in the horizontal plane. It is useful to adjust the position of the head in order to perform radial impacts, so the direction of the hammer is always directed towards the CoM.

In vivo measurement has been taken to be used as reference during the positioning of the head, so the orientation of the brain was known. As reference line was chosen the one connecting the external acoustic meatus, placed on the temporal bone, with the root of nose. In vivo, this line resulted inclined of 17° in respect of the horizontal line in the sagittal plane. To obtain the same inclination on IHHS1 and IHHS2 of this line, a basement for the neck has been designed. This basement gives an inclination of 7° to the neck in respect of the vertical line in the sagittal plane. The basement was initially printed in ABS, then it was printed in titanium with the EBM machine, to make it more adapt to sustain

intense impacts. In the next image will be shown the process only for IHHS1 because for IHHS2 is the same exactly.

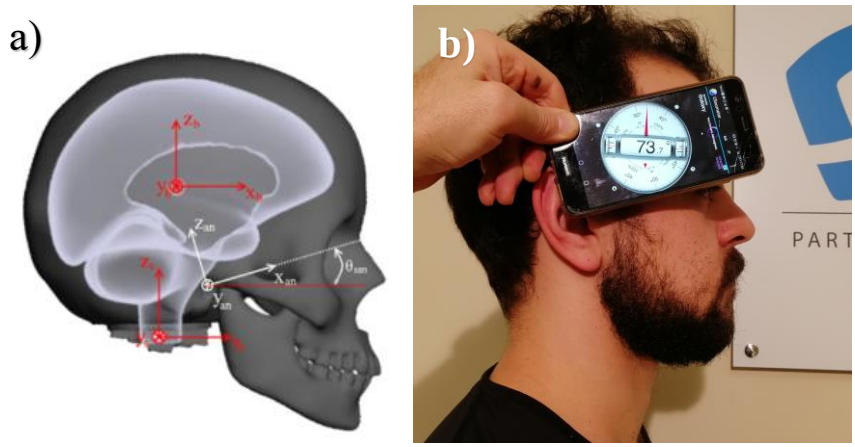


**Figure 4.3** *(a) individuation of external acoustic meatus and root of nose. (b) In vivo measurement of inclination of the line connecting external acoustic meatus with root of the nose.*

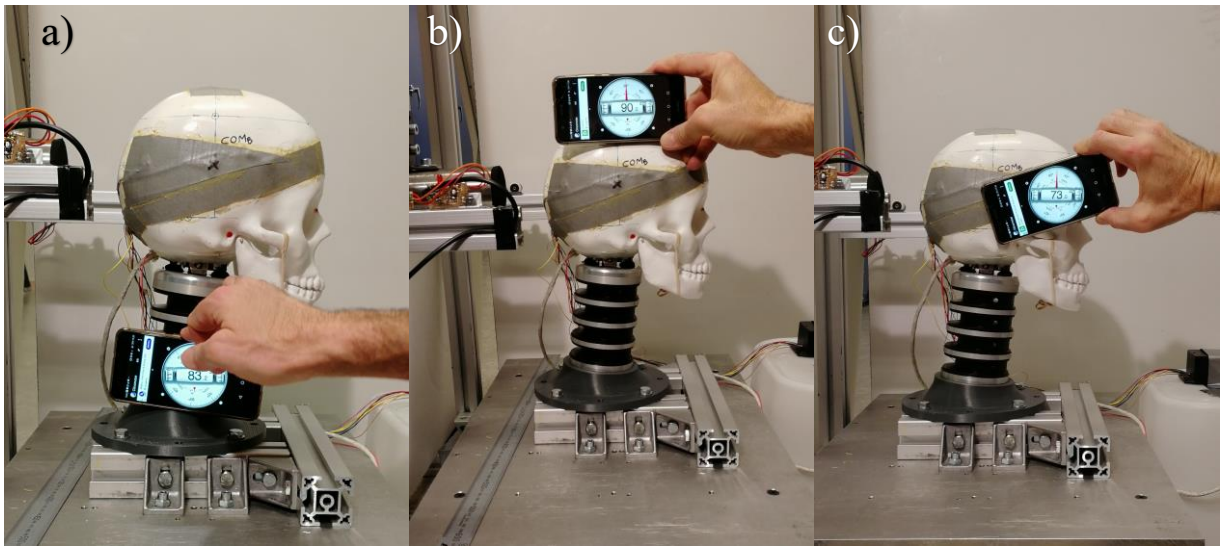


**Figure 4.4** *(a) inclination of the basement. (b) horizontal reference line. (c) line connecting the external acoustic meatus with root of nose inclined of 17°.*

After the right positioning of the skull, the skin of silicone rubber can be added. Because of contact between the silicone rubber and the internal layer of the helmet, a thin cap is then put on the head to reduce friction. In the end the head can wear the helmet and on it, both for IHHS1 and IHHS2, an accelerometer is attached right above the CoM.

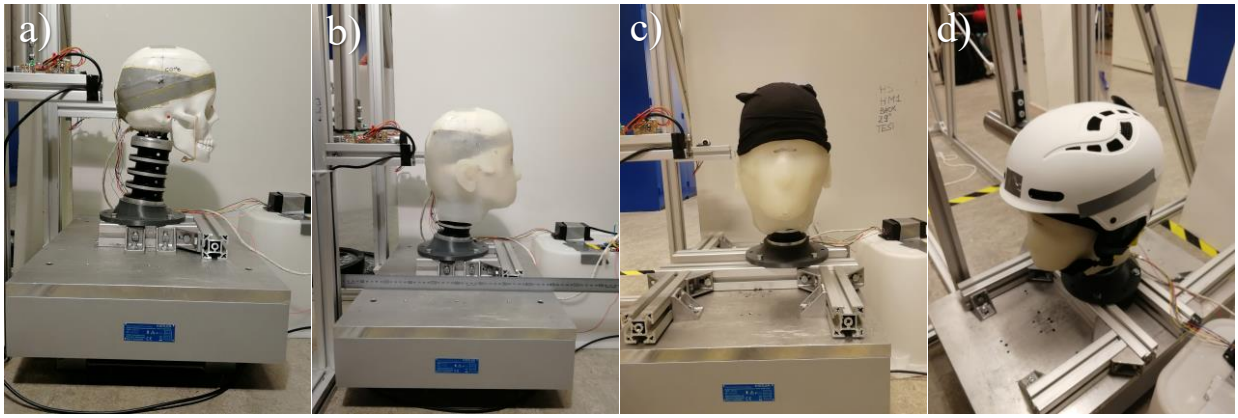


**Figure 4.5** *(a) Positioning of the head. (b) Application of skin. (c) Application of cap. (d) application of helmet.*

## 4.3 Protocol

After the positioning of the head, there is a precise protocol to follow in order to perform the tests.

1. Turn on *National Instruments* board
2. Turn on lasers and optical sensors
3. Turn on the board connected to the extra sensors mounted on the skull (for IHHS2 this board is also connected to the pressure sensors)
4. Check if the optical sensors collect the signal from the laser beams
5. Open the *LabView* VI project related to the instrumented head to be tested
6. Write the name of the file of data to record
7. Choose the folder where the file will be saved
8. Choose the sample rating (10 ksps for IHHS1 and 4 ksps for IHHS2)
9. Choose the time of acquisition (500 ms)
10. Position the hammer
11. Position the 2 *GoPro* cameras
12. Connect the smartphone to the *GoPros*
13. Make the videos start through the smartphone
14. Press 'Run' in the *LabView* VI project (now the system waits for the digital trigger, that is composed by the laser beams and optical sensors)
15. Release the hammer (acquisition starts when the hammer passes through the first pair composed by laser and optical)
16. Block the hammer before hitting the head for the second time because of rebound
17. Stop the videos

18. Save the file

These are the steps needed for the first test of the session. After the first one, only step 6, 7, 10 and from 13 to 18 are needed.

## 4.4 Type of Impacts

To describe the positions of the head during impacts, defining the reference system of the head is mandatory. The origin of this system is the CoM of the brain, the X-axis is the one going from the CoM in direction of the nose horizontally, the Y-axis goes from the CoM toward the left side of the face and z-axis is the one going from CoM vertically to the top.

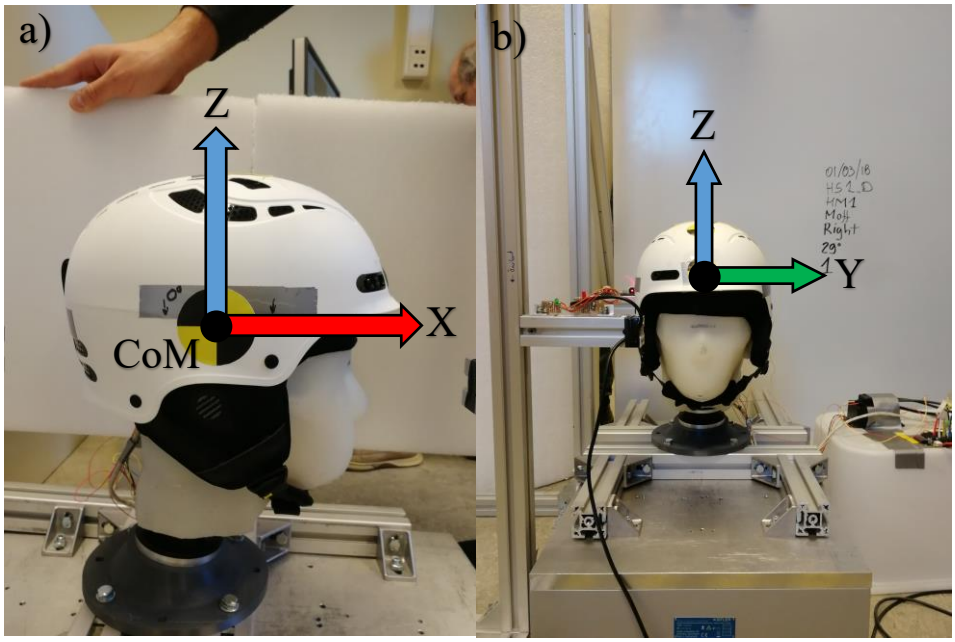


**Figure 4.6** *Representation of the reference system. Red is X, green is Y, blue is Z. (a) lateral view. (b) frontal view.*

The principal type of impacts performed are the radial ones, with the direction of movement of the hammer passing through the CoM, called Back, Back-Right, Right or Front-Right, from the direction the hammer comes from. Back hits the nape of the head, Right hits the right side of the head, Back-Right is exactly the middle way between them, hitting the right part of the nape, instead Front-Right is a middle way between a Front impact, not performed because the impactor would have hit the helmet on its edge, and the Right direction. The opposite test, i.e. Back-Left, Left, Front-Left and Front have been discarded because they would have been a repetition with different signs of the

acceleration peaks found with the other tests. In the project, the different type of impacts will be also indicated with the smaller angle formed between the direction of impact and the X-axis of the reference system.

| **Name** | **Angle [degrees]** |
|---|---|
| Back | 0 |
| Back-Right | 45 |
| Right | 90 |
| Front-Right | 135 |

**Table 4.1** *Correspondence between name of the impact and the angle between the direction of movement of the hammer and the X direction.*

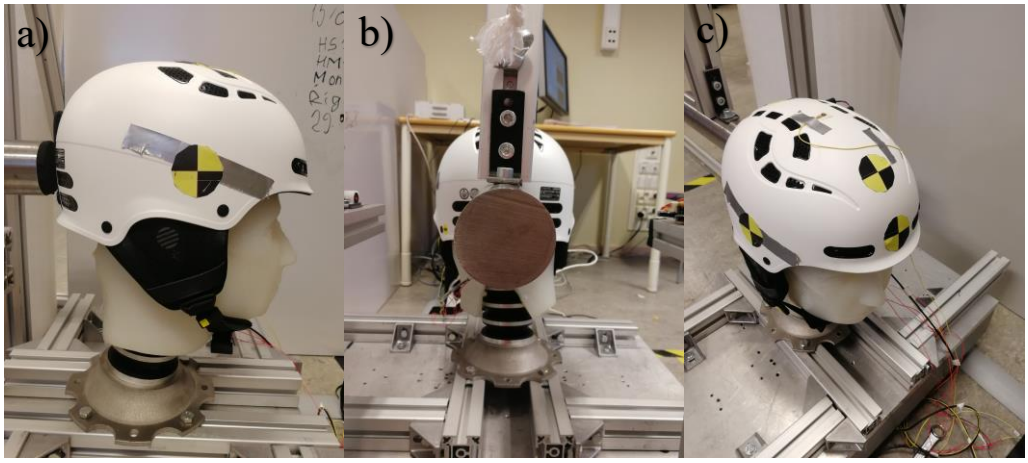


**Figure 4.7** *Back Impact. (a) lateral view. (b) back view. (c) prospective view*

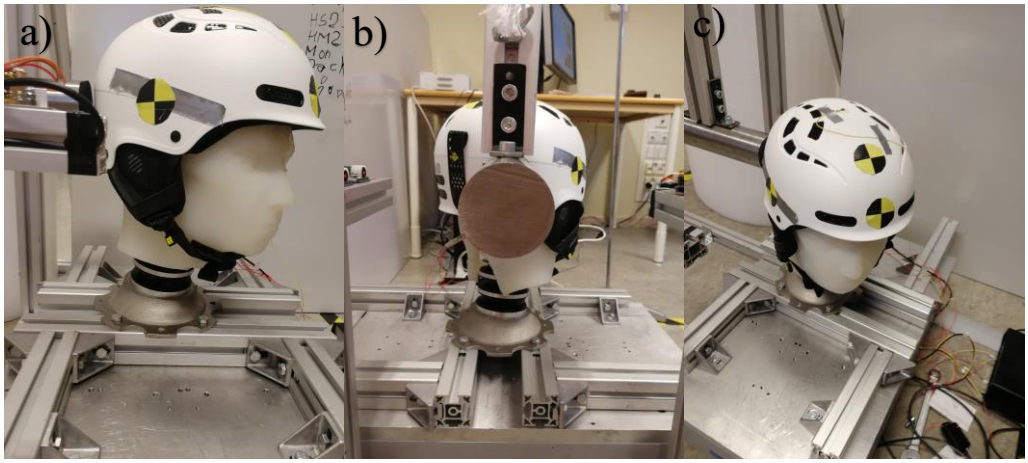


**Figure 4.8** *Right-Back Impact. (a) lateral view. (b) back view. (c) prospective view*

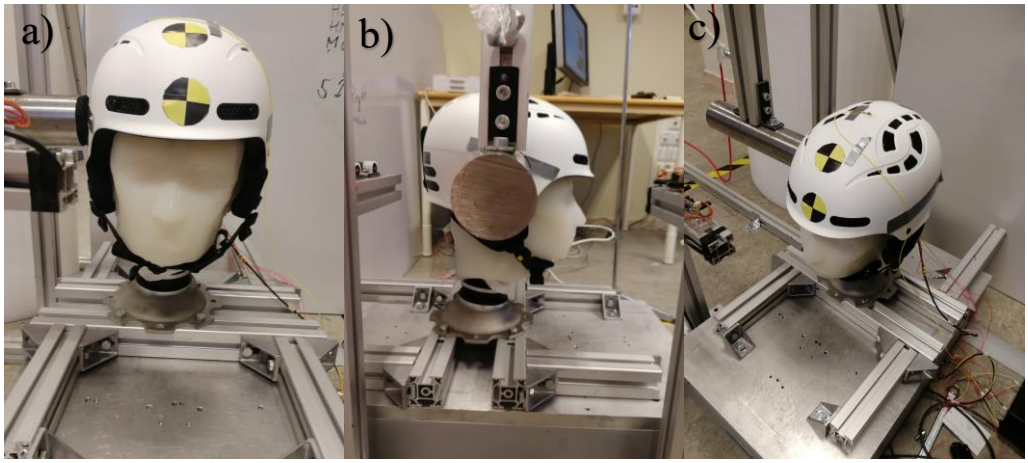


**Figure 4.9** *Right Impact. (a) lateral view. (b) back view. (c) prospective view*

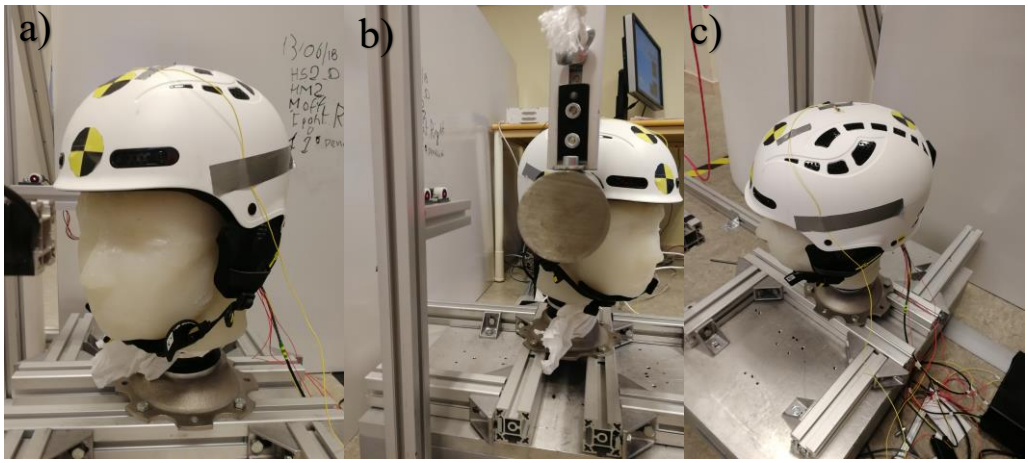


**Figure 4.10** *Front-Right Impact. (a) lateral view. (b) back view. (c) prospective view*

# Chapter 5

# Instrumented Human Head Surrogate 1: Description and Test Results

Now it is time to describe the first surrogate head in detail, called *Instrumented Human Head Surrogate 1*.

The project begins with the modification and simplification of a 3D model of the skull based on MRI scans. The aim of the simplification was to close every single hole of the model, except for the foramen magnum, to be sure that every single part was attached to the main body, to create a possible connection between the jaw and the rest of the skull and to flatten the lower part of the object in order to make easier the connection with the *Hybrid III* head. The material in which the skull has been printed is *ABS plus*, and to obtain similar mechanical properties for the surrogate skull, the model was subjected to a phase of thickening. The 3D model was also scaled to have the length of the head, the horizontal distance from the most anterior point of the forehead between the brow-ridges to the back of the head, of 200 mm. At the end of this steps, the skull has been printed in 3 different parts. They are the jaw and the principal body divided into two pieces through a diagonal jigsaw cut [1].

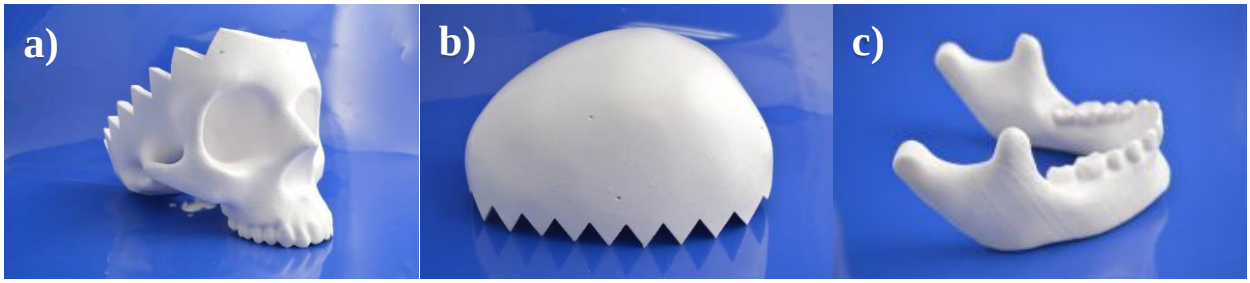


**Figure 5.1** *(a) lower part of the skull (b) upper part of the skull (c) jaw*

The brain was subjected to a similar initial phase. In fact, it was also based on a 3D model built thanks to MRI scans, and then was simplified and scaled. The simplification consists in the smoothing of the

outer surfaces of the brain, instead the scaling was needed in order to place it inside the two parts of the main body of the printed skull. The silicon rubber used to mould the brain is Plastil Gel 01-30.

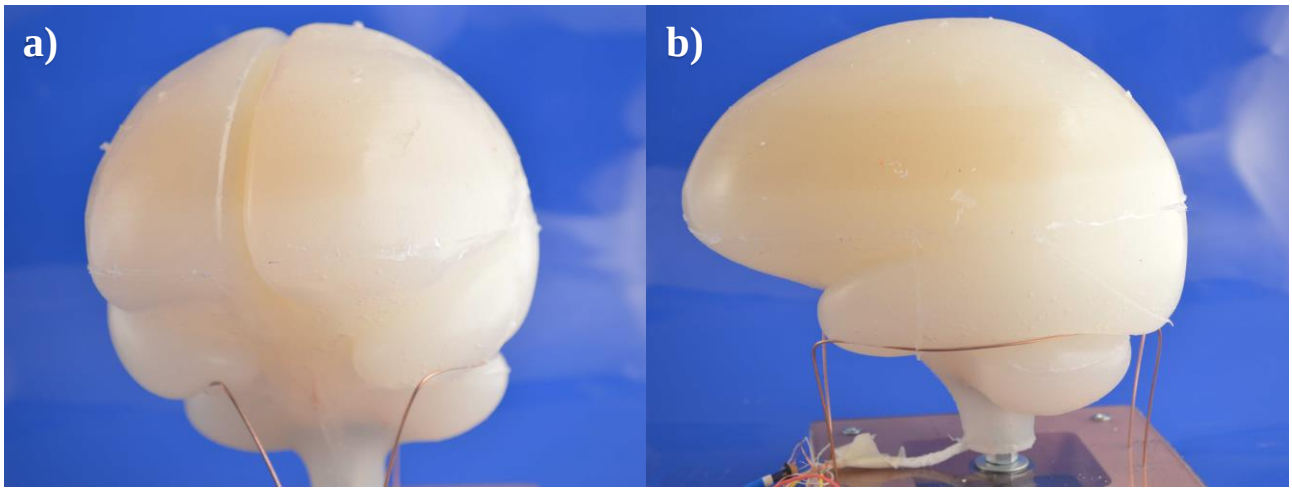


**Figure 5.2** *(a) frontal view of the brain, in which can be seen the division between the right and left lobes (b) lateral view of the brain in which can be seen the separation between the brain itself and the cerebellum.*

To simulate the presence of dura mater and arachnoid trabeculae, different pieces of templates, made of Silicone coated *Nylon Denier 31*, were wrapped around the brain.


**Figure 5.3** *Two different views of the wrapped brain.*

For the cerebrospinal fluid, an oil was chosen. The fluid has to be the more similar possible to water, so must have a low viscosity, both cinematic and kinetic, and a low degree of friction. Even if the

electric cables of the sensors positioned inside the brain were insulated, for their safety, water was not chosen because of the danger of electric short circuit. Besides that, the fluid does not have to react with the silicone rubber of the brain. In the end, the low-viscosity silicone oil *SilOil M4.165/220.10* was utilized to fill the head.

IHHS1 is also equipped with a layer of skin. The skin is composed by only one piece of silicone rubber that have to be placed with the opening of the neck in front of the skull and pulled back until the head is correctly inserted inside it. The layer of skin was moulded using as silicone rubber *Plastil Gel 00-25.*

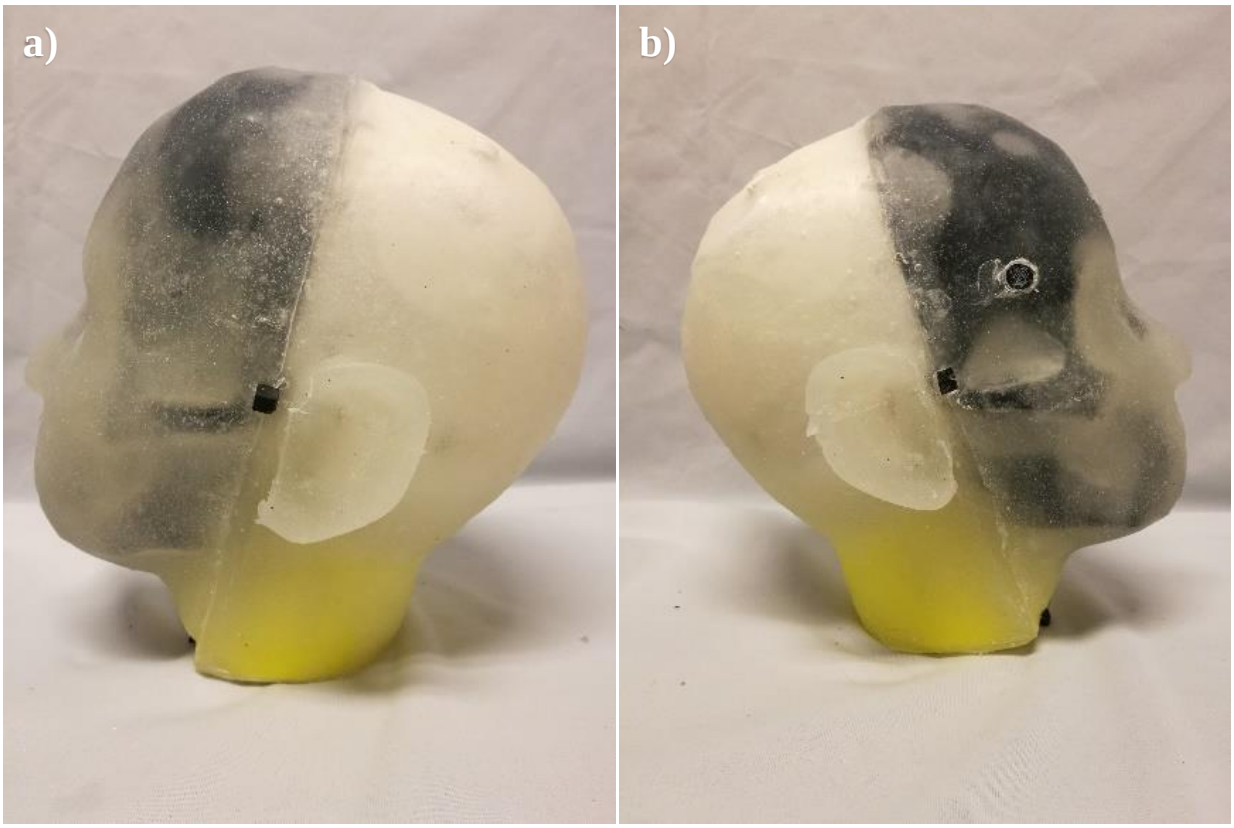


**Figure 5.4** *(a) Left view of the skin (b) Right view of the skin*

## 5.1 Sensors Position and Problems with IHHS1

In this section the position of the different sensors inside the head will be presented.

Inside the brain 8 accelerometers are located and two biaxial gyroscopes (two gyroscopes are necessary to record the angular velocity around the 3 reference axes). One accelerometer is placed in the CoM of the brain and the two gyroscopes too. Besides them, the other seven accelerometers inside the brain are located around it in areas of interests. A couple of them, called Top-Left (TL) and Top-

Right (TR), are placed on the same coronal plane of the CoM in the top part of left lobe and right lobe respectively, 15 mm from the surface. Another couple is also in the same coronal plane but by the side of CoM. They are called Mid-Left and Mid-Right and both are positioned at 40 mm from CoM. The last 3 accelerometers, instead of being placed in the brain, are used to analyse the behaviour of cerebellum during impacts. One, called Cerebellum-Center, is placed in the center of mass of this part, instead the other 2 are at its side. There is also an additional accelerometer positioned on the skull, under the hard palate, as shown in *Par. 4.2*. In the next figure and table the exact position of the sensors will be described.

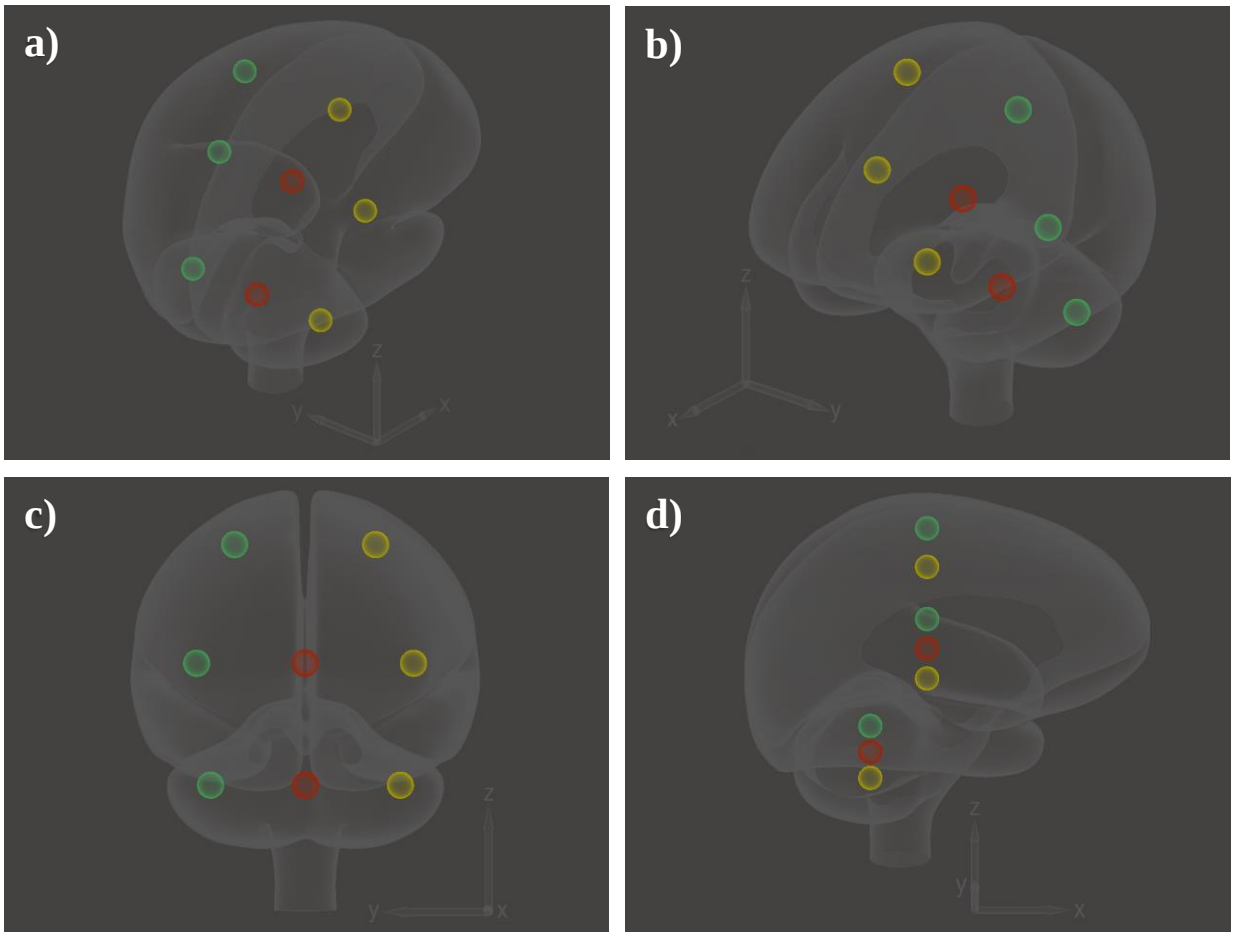


**Figure 5.5** *(a) Back-Right view of the brain with highlighted sensor position. (b) Front-Right view. (c) Back view (d) Right view.*

| Sensor Name | Abbreviation | X [mm] | Y [mm] | Z [mm] |
|---|---|---|---|---|
| Top-Left | TL | 0.0 | +26.0 | +43.6 |
| Top-Right | TR | 0.0 | -26.0 | +43.6 |
| Mid-Left | ML | 0.0 | +40.0 | 0.0 |
| Center of Mass | CoM | 0.0 | 0.0 | 0.0 |
| Mid-Right | MR | 0.0 | -40.0 | 0.0 |

| | | | | |
|---|---|---|---|---|
| Cerebellum-Left | CL | -23.4 | +35.0 | -44.4 |
| Cerebellum-Center | CC | -23.4 | 0.0 | -44.4 |
| Cerebellum-Right | CR | -23.4 | -35.0 | -44.4 |
| Gyroscopes | Gyr-CoM | 0.0 | 0.0 | 0.0 |

**Table 5.1** *Position of the sensors.*

In the presentation of data recorded during tests the results from CC will not be displayed because this accelerometer does not function properly.

Besides the aforementioned sensors, In the head, in the inner surface of the upper part of the skull, 10 pressure sensors are located. The pressure sensors are placed inside little holes drilled in the skull.

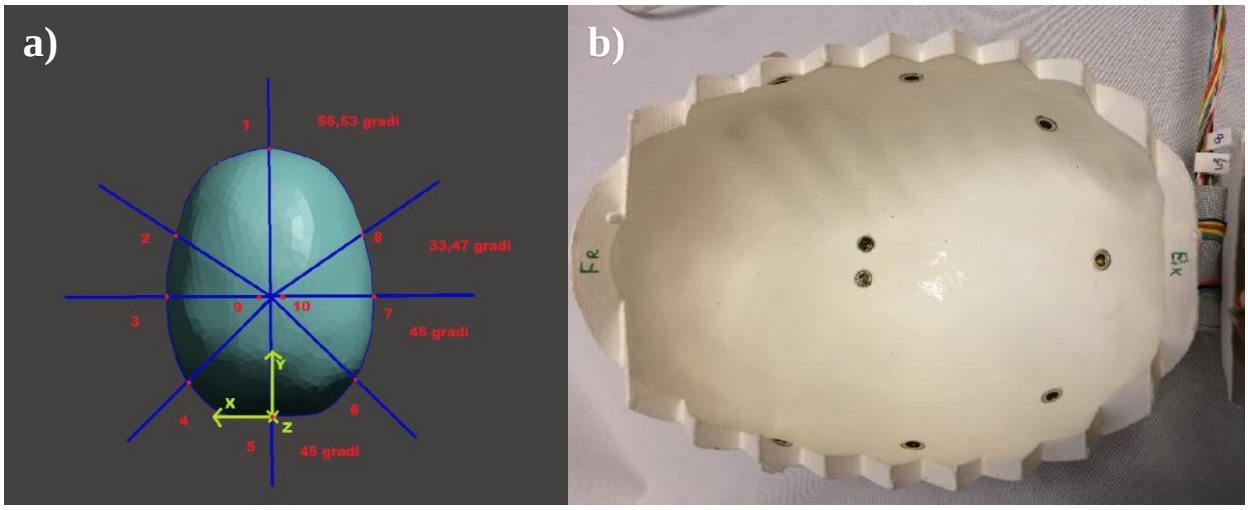


**Figure 5.6** *(a) Digital representation of the pressure sensors in the inner surface of the skull. (b) Pressure sensors placed in the skull.*

During the tests, data from them were not recorded because of some problems with the oil resembling the cerebrospinal fluid.

There are two problems related to the oil filling the space left between the brain and the inner part of skull. The first one is that, after the first tests to check the right functioning of all the sensors, the oil began to leak outside. This could be caused by the not perfect sealing of the metal adaptor under the skull used to connect the head with the *Hybrid III* neck. The other problem is that the silicone oil used to fill the head reacted somehow with the silicon rubber of the brain. The brain probably absorbed the liquid and so expanded and swelled. With the brain increasing its dimensions, parts of its possible moving during impacts are limited. Because of the swelling of the brain and the leakage of the oil, it has been decided to remove the liquid from inside the head. Without the silicone oil there was no sense in using the pressure sensors.

Besides the oil and pressure sensors, there is a last problem related to the dimensions of the head. In fact, the final size of the completely mounted head is not comparable to a $50^{th}$ percentile adult male. This was caused by the thickening of the skull for obtaining mechanical properties similar to the real bones and the layer of skin used was also to much thick. The circumference of IHHS1 is 63 cm, and so an XXL size helmet was needed to perform the tests.

## 5.2 Data Analysis of IHHS1

Now that the IHHS1 has been presented and described in detail, giving attention to all the sensors placed inside the brain and on the skull, with all the problems found during this first part of the project, and the structure and experimental setup analysed as well, it is time to present the data recorded during impact tests.

Firstly, will be presented an example of Back impact, then Back-Right and Right impact and in the end a Front-Right impact, respectively indicated with a θ angle of 0°, 45°, 90° and 135°, angle formed between the direction of movement of the hammer and the X axis of the reference system of the head. The performed tests are characterized by an impact energy that can be 8J, 16J, 24J and 44J. The different impact energies are obtained through positioning the hammer at a specific angle α. An impact occurring at 8J needs an angle formed by the pendulum arm with the vertical direction of 29°, an impact of 16° is performed by positioning the hammer at an angle of 41°, 24J is bound to 51° and 44J is related to 72°.

With IHHS1 has been performed 48 tests (4 position of the head tested at 4 different energy levels of the impact with 3 repetitions) for the head wearing a normal sky helmet and 48 tests for the head wearing the same helmet with multi-direction impact protection system (MIPS) activated, that means a total of 96 tests performed.

In the following table will be shown the test program.

| Position | | Impact | |
|---|---|---|---|
| Name | θ [deg] | Energy [J] | α [deg] |
| Back | 0 | 8 | 29 |
| | | 16 | 41 |
| | | 24 | 51 |
| | | 44 | 72 |
| Back-Right | 45 | 8 | 29 |
| | | 16 | 41 |
| | | 24 | 51 |
| | | 44 | 72 |
| Right | 90 | 8 | 29 |
| | | 16 | 41 |
| | | 24 | 51 |
| | | 44 | 72 |
| Front-Right | 135 | 8 | 29 |
| | | 16 | 41 |
| | | 24 | 51 |
| | | 44 | 72 |

**Table 5.2** *Test program to repeat 3 times and both for MIPS helmet and no-MIPS helmet. In the table is also presented the correlation between the name defining the position with the angle between direction of movement of the hammer and the X axis direction of the head reference system and the correlation between the level of energy and the angle between the pendulum arm and the vertical direction.*

In the following paragraph, only one impact per position will be presented. In fact, the data analysis shows that, for example, the shape of the signals from both accelerometers and gyroscopes for a Back impact is the same for every level of energy. The only differences between the levels of energy are the values of the peaks in the graphs, but the phenomenon is the same exactly. So, a Back, a Back-Right, a Right and a Front-Right impact all occurring at 24J will be shown in every detail. The rest of the impacts will be presented via tables. The efficacy of MIPS helmets will be assessed during the tables presentation. However, before going on with the analysis, it is right to study the MIPS protection system.

Common helmets contain an energy-absorbing polymer foam liner, that can be attached at a single point, or be an interference fit to a stiff thermoplastic, or fiber composite external protection layer. In an oblique impact, the helmet shell will transfer the tangential force component to the foam liner and

that one can partly transfer it to the head. Some helmet manufacturers believe that head protections can be improved by interposing a low friction layer between the shell and the liner. MIPS helmet are thought to mimic the natural protection of the brain inside the skull, permitting to the head to slide inside the helmet in the same way the brain floating in the cerebrospinal fluid can slide inside the skull [57].

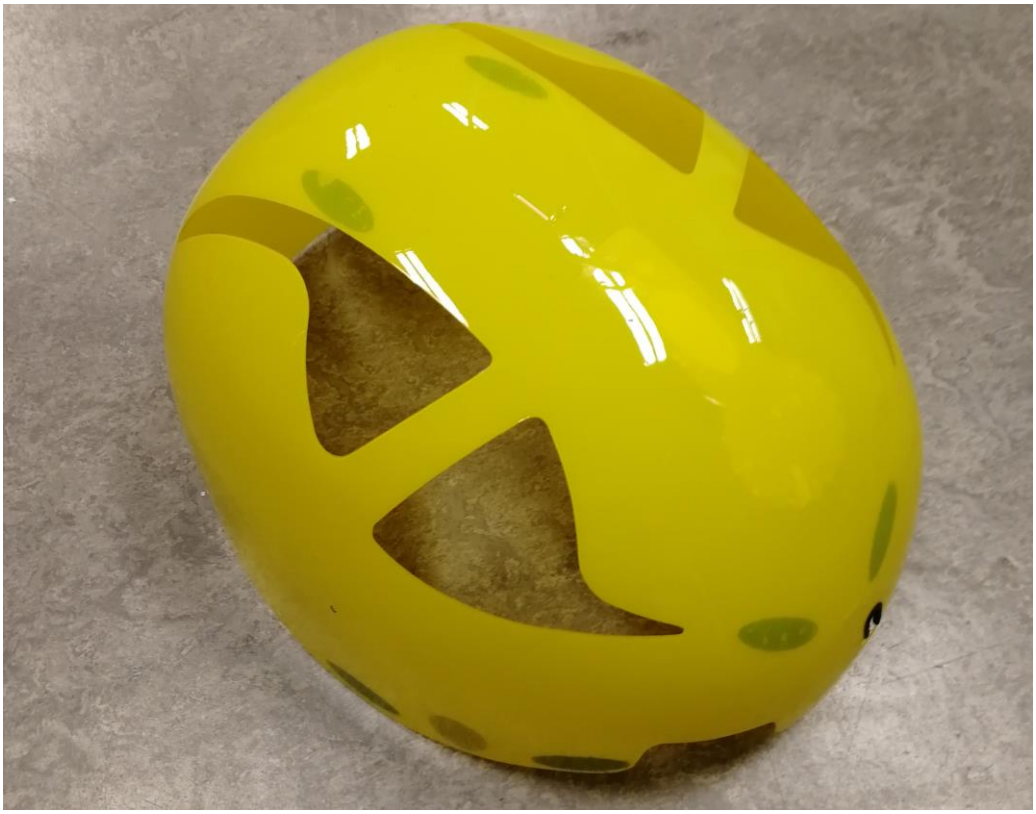

**Figure 5.7** *Low friction layer posed between the external protection shell and the internal energy-absorbing polymer foam liner of the MIPS helmet used during tests.*

### 5.2.1 Back Impact

In this section, a Back Impact with MIPS not activated on IHHS1 occurring at the energy level of 24J will be shown. For what concerns other energy levels, 8J, 16J and 44J, the shape of the signal is identical, only with different values of the peaks. In the following figures, the graphs will be presented from the top layer, composed by the signals of Top-Left and Top-Right, to the middle layer characterized by the graphs recorded through accelerometers Mid-Left and Mid-Right and what concerns the Center of Mass, both accelerometer CoM and gyroscope Gyr-CoM, and finally the lower part composed by Cerebellum, Cereb-Left and Cereb-Right. Cereb-Center will not be shown because

is damaged. In addition, also the signals from the accelerometers mounted on the helmet and the skull have to be shown.

**a)**

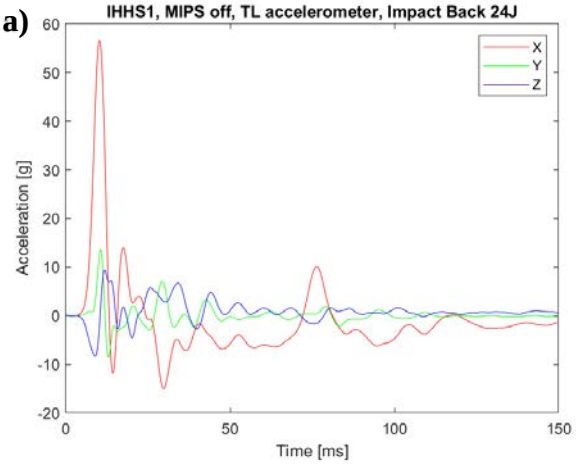


**b)**

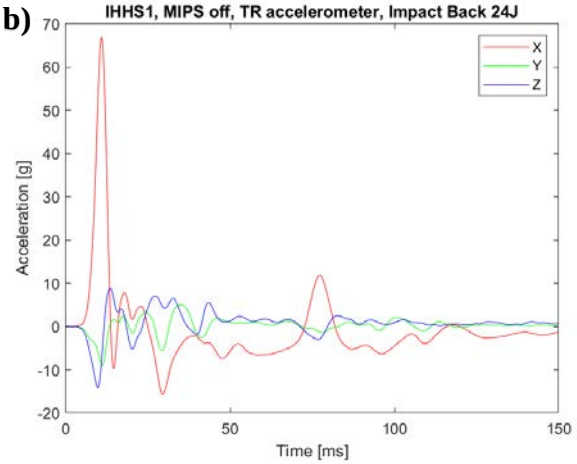


**c)**

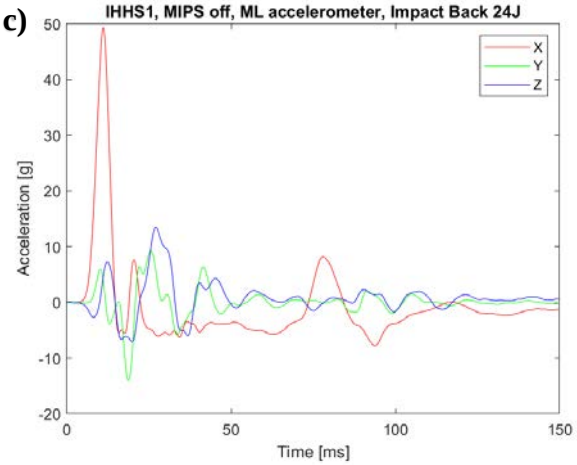


**d)**

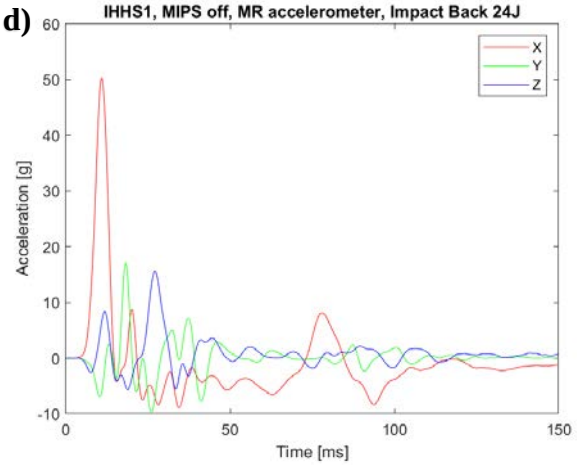


**e)**

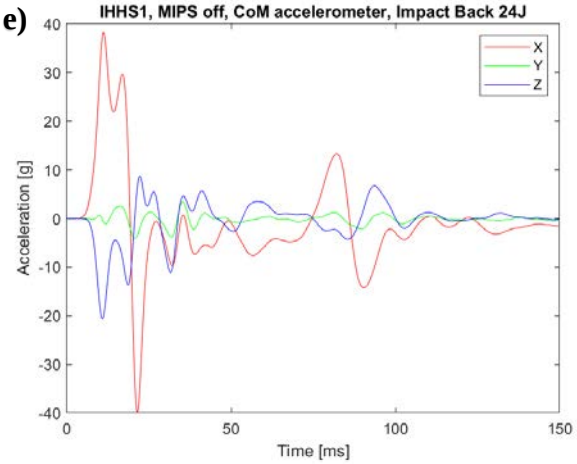


**f)**

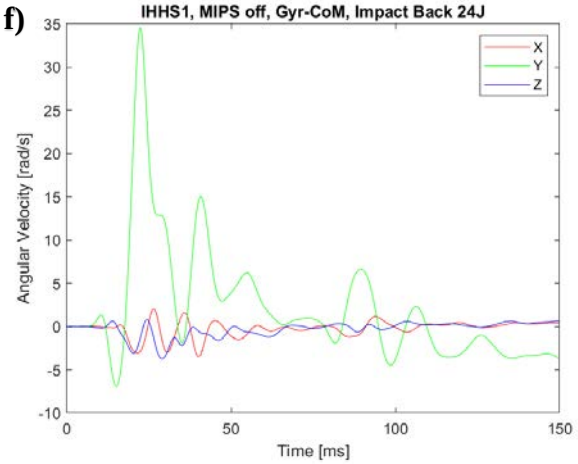

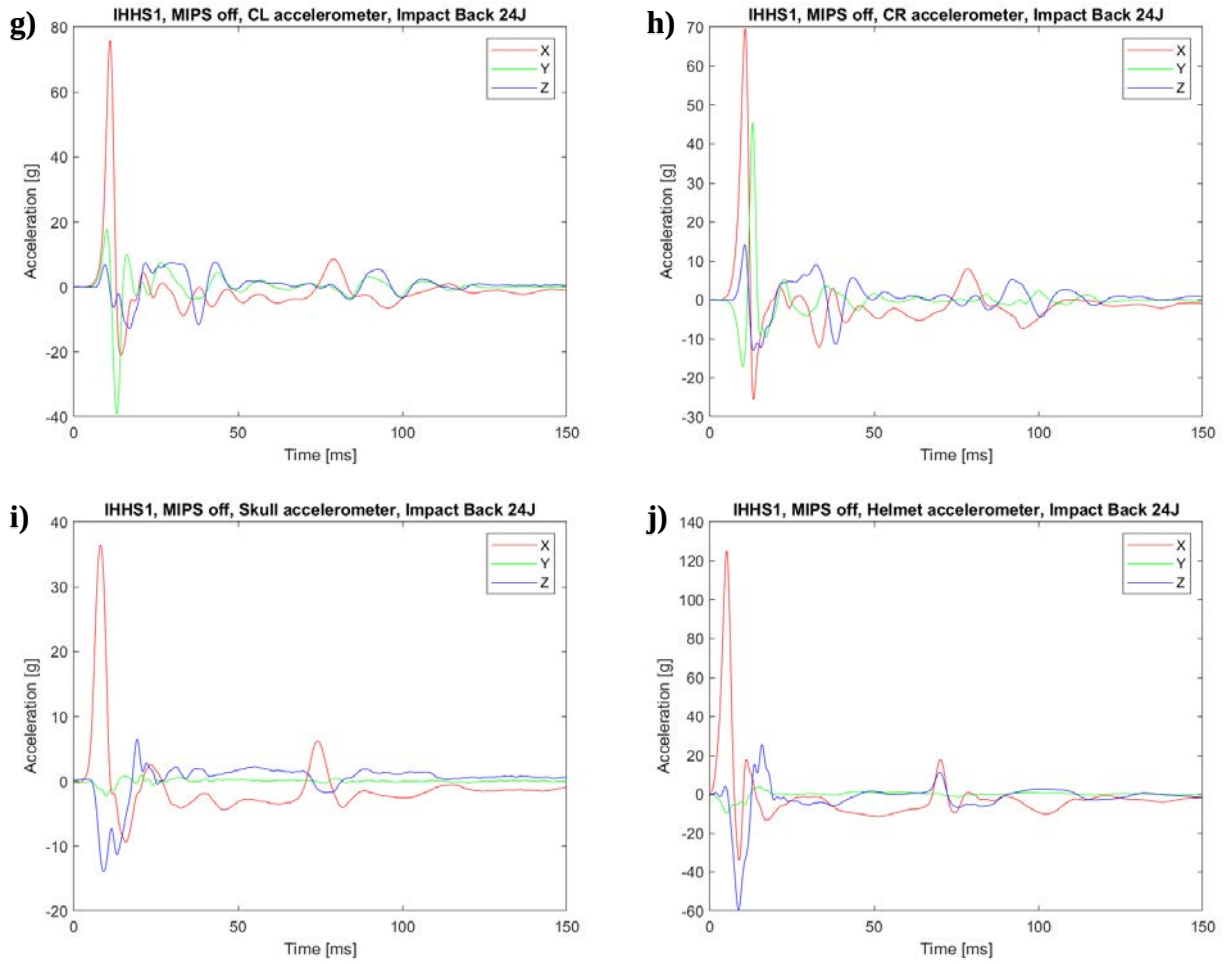


**Figure 5.8** *Signals recorded by IHHS1 with MIPS off during Impact Back 24J. (a) TL (b) TR (c) ML (d) MR (e) CoM (f) Gyr-CoM (g) CL (h) CR (i) Skull (j) Helmet.*

As can be seen in every single graph of *Figure 5.8*, Accelerometers record a great positive peak in the X direction, corresponding to the instant in which the accelerometer is moved because of the impactor hitting the helmet. Besides this first peak in X direction, the following waving of the signal is due to the fact that the head is connected to the *Hybrid III* neck acting as a spring that brings back the head and makes it to move around the initial position until the motion is ended. The head is hit by the impactor from behind and so is pushed along the direction going from the CoM to the forehead. However the development of the impact will be explained with photograms taken from the recorded videos in *Figure 5.9*. For what concerns the other directions, in Y cannot be seen huge peaks, in fact the signal only waves around values near 0 g, instead in Z direction can be detected a not negligible peak. Z direction is the one going from CoM to the top of the head vertically. The peaks in the Z signals are firstly negative, in fact the hit approximately makes the head rotate around the pin connecting itself with the neck, while the neck is flexing so that the distance between the aforementioned pin to the ground. Only in *Figure 5.8 (g)* and *(h)*, corresponding to CL and CR

accelerometers, the first peak of Z signal is positive, and it is why the Cerebellum is positioned behind and in a lower position in respect of the CoM. When the head rotates, all the accelerometers positioned in the same coronal plane of CoM are pushed down, instead the accelerometers placed in the cerebellum are behind this plane and so are pushed towards the top.

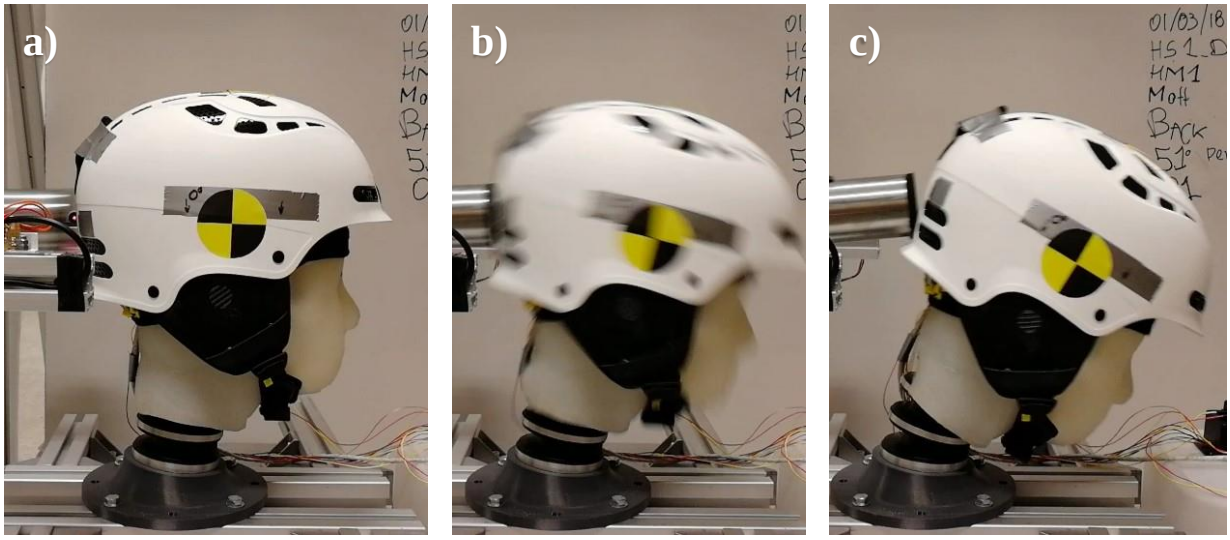


**Figure 5.9** *Photograms taken from the recorded video of the Impact. (a) Photogram before the contact between impactor and IHHS1. (b) Head is touched by the hammer and pushed forward. (c) Maximum displacement of the head in X direction. After the photogram begins the phase of waving around the initial position.*

*Figure 5.8 (f)* represent the signals recorded through the gyroscopes positioned in the CoM. In this graph a huge peak is visible in the Y direction, describing the angular velocity developed during impact around the axis going from the CoM towards the left side of the head. Rotation around the other 2 axes is not interesting. It is easy to notice that the values of the peaks tends to decrease going from the top layer towards the middle one, in fact both TL and TR present peaks near 60 g in the X direction, instead ML, MR and CoM, which are positioned in a lower position, show peaks near 50 g. That is because ML, MR and CoM are near the center of rotation of the head instead the top ones are far from it. Strangely the peaks in X direction of accelerometers in cerebellum are around 70 g, and so are even bigger than the ones found in the top layer. Considering the fact that cerebellum accelerometers are the sensors in the lower position, this does not even make sense. These strange values could be caused by the fact that IHHS1 had problems with the silicon oil used to fill the space between the skull and the floating brain, in fact the oil made the brain to swell. Probably the swelling of the brain produced compression for the accelerometers causing some kind of damage, in particular it is supposed to be in the cerebellum region, so that signals recorded by CC are not even presented.

The compression suffered by CL and CR could have probably caused a change in the sensibility of the accelerometers. From the graphs can also be seen that the impact happens in a very short temporal window, in fact the huge peaks are located in the first 0.03 s after the beginning of recording.
Other interesting considerations can be deducted by making comparisons of the different signals. In particular the signals from Helmet, Skull and CoM in the principal direction of impact, that for a Back test is X, are to be analysed to comprehend the evolution of the hit.

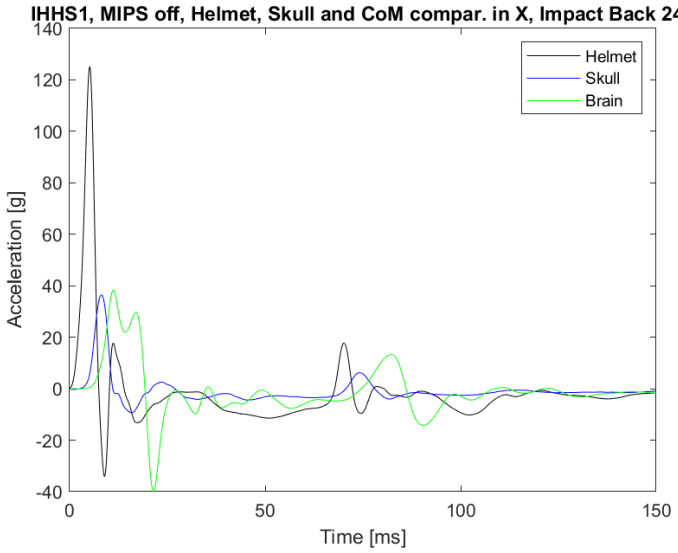


**Figure 5.10** *Comparison of accelerations of Helmet, Skull and CoM in the X direction.*

In *Figure 5.10* it is easy to notice that the first peak to appear is the one of the Helmet, the second peak developed is the Skull, instead the brain is the last one. This temporal displacement of the different peaks respects the position of the different layers, in fact the hammer firstly touches the helmet, under the helmet and the skin the movement is transmitted to the skull and so the skull begins to move, instead the brain that is free to move inside the cranial box, because there is not even the oil resembling the cerebrospinal fluid and it is attached to the skull only through the brain stem , stays firstly still. The brain is pushed only after that the skull has moved and the rear part of it, that is the occipital region, transmit the motion to the silicon rubber. The helmet is characterized by the highest peak of more than 120 g because it is both the first object to be touched and it is placed in the highest point of IHHS1, i.e. the apex of the helmet, exactly above the CoM. The skull and CoM are characterized by modest peaks in comparison, only around 35 g.
Now it is time to compare the signals belonging to the same level. In particular it is interesting to put in the same graph signals of the Y direction from sensors of the same layer, top, middle and cerebellum, in order to understand a possible kind of deformation suffered by the brain.

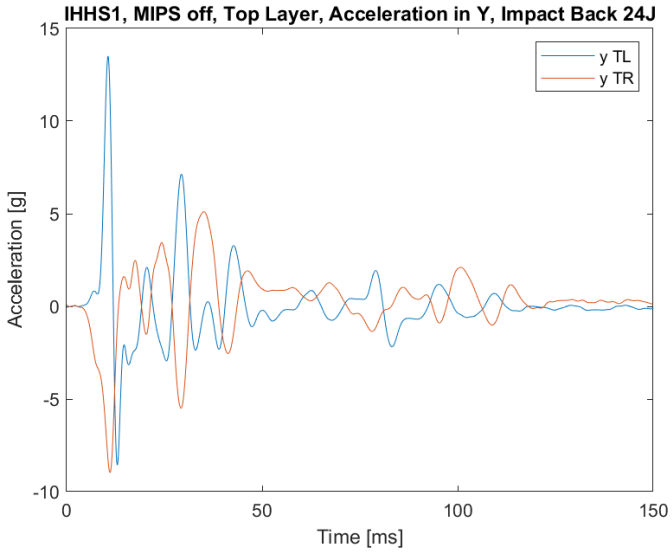


**Figure 5.11** *Comparison of Y signals from TL and TR accelerometers, belonging to the top layer.*

In *Figure 5.11* The Y signals of TL and TR and juxtaposed. Both signals are characterized by low levels of acceleration, less than 15 g, in fact Y is transverse in respect of the principal direction of Impact and so it is not solicited. But what is really interesting is the fact that the first peaks of TL and TR present different signs. TL has a positive first peak, instead TR has a negative one. A positive peak in Y direction means that the accelerometer is moving towards the left part of the face, instead a negative one means that it is moving towards right, so TL and TR are moving away from each other when the hit is transmitted to the brain. Because of that the brain has a positive deformation at the beginning of the impact, then the signs of the peaks of both TL and TR change, in fact the second peak of TL is negative and the second of TR is positive, so TL and TR are now coming back and the brain has a phase of compression. This alternation of positive deformation in Y direction firstly and compression continues until the head is still. This exact explanation can be applied to both middle layer and cerebellum layer as shown in *Figures 5.12* and *5.13.*

For what concerns the differences of MIPS and no MIPS test, it is necessary to make a comparison of the angular acceleration, obtained by deriving from time the angular velocity recorded through the gyroscopes positioned in CoM. As stated by Halldin *et al*. [53], a MIPS helmet should reduce the angular acceleration by 30%, in a near tangential impact. However the Back impact performed during this project hits IHHS1 in correspondence of the occipital region, in a place of the helmet that is quite flat, so the rotation impressed to the helmet could be not so significant to show the MIPS protection effect. In *Figure 5.14* will be shown the comparison of angular accelerations.

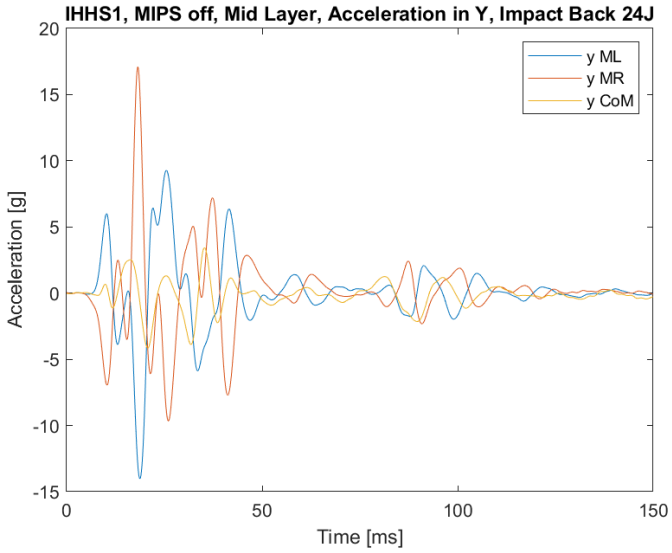


**Figure 5.12** *Comparison of Y signals from ML, MR and CoM accelerometers, belonging to the top layer. ML and MR show the alternation of positive and negative peaks that characterize the extension-compression phase of the brain in Y direction, instead CoM is defined only by a smooth waving of the signal that never surpass 5g of acceleration, in fact it is placed in between of ML and MR.*

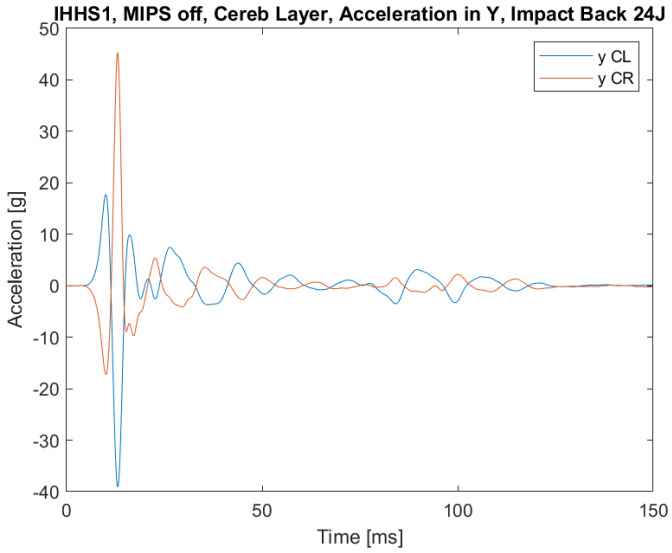


**Figure 5.13** *Comparison of Y signals from CL and CR, belonging to the cerebellum or lower layer. As stated before, CL and CR accelerometers does not present realistic values of the peaks, in fact the second peak for both stays near 40 g, even if Y is the less solicited direction during the test.*

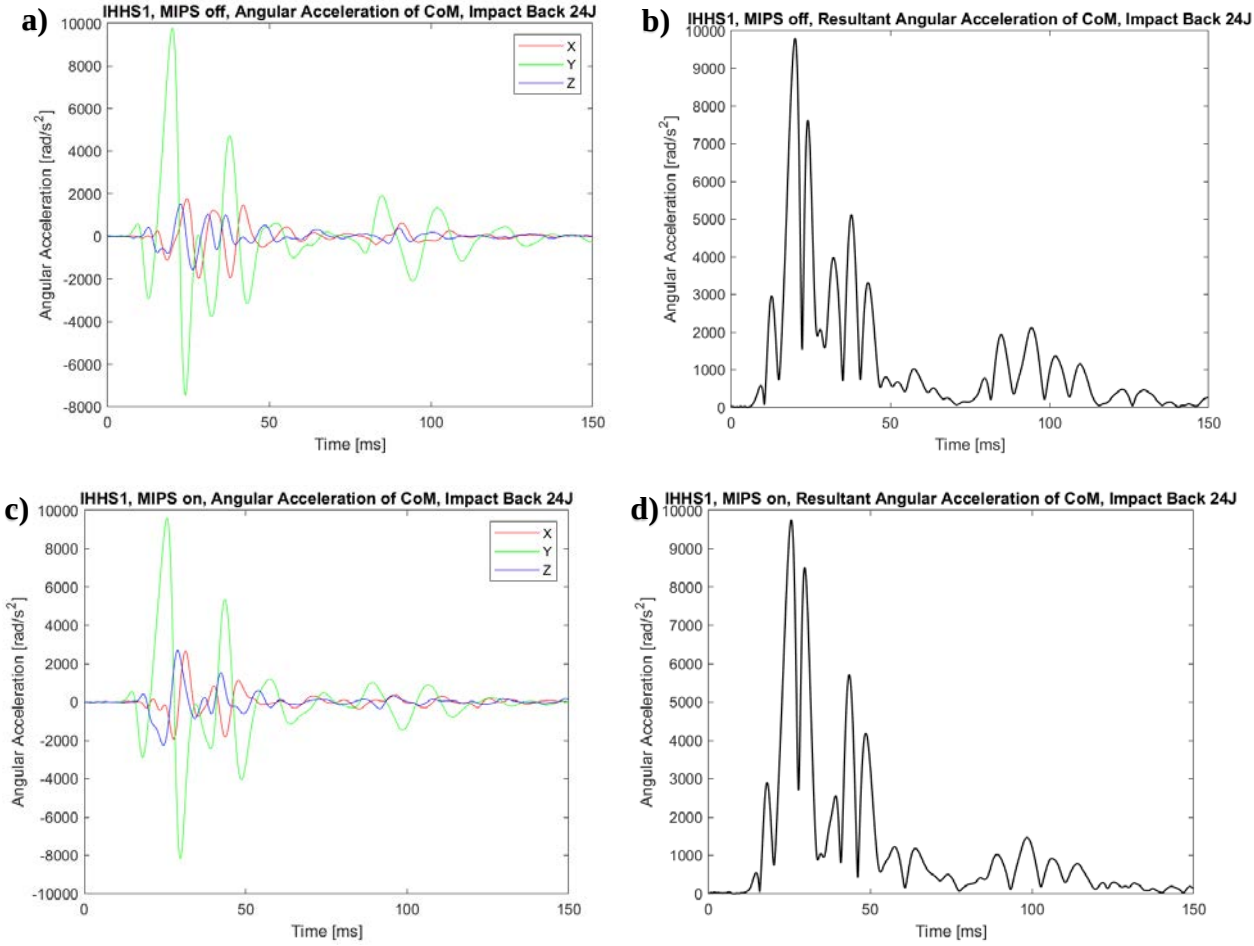


**Figure 5.14** *Comparison of angular accelerations for impact Back 24J performed on IHHS 1 with MIPS not activated and then activated. (a) Angular acceleration of CoM with no MIPS. (b) Resultant angular acceleration of CoM with no MIPS. (c) Angular acceleration of CoM with MIPS activated. (d) Resultant angular acceleration of CoM with MIPS activated.*

As can be seen by the graphs, there is no significant differences between impacts with MIPS activated and MIPS not activated, neither between the graphs representing the angular acceleration nor the graphs with its resultant. For both tests can be individuated a first huge positive peak of angular acceleration around the Y axis near the value of 10000 rad/s$^2$, while angular accelerations around X and Z axis are modest, slightly surpassing the level of 2000 rad/s$^2$. Even if no differences are detected, it cannot be said that MIPS is not effective, because it is right to remember that a central hit has been performed. In the following paragraph will be presented a Back-Right impact, and the comparison between MIPS on and MIPS off will be done another time, in fact even if Back-Right is another central impact, as all the tests realized during the project , IHHS1 is hit in a different portion of the head producing different angular velocities and accelerations.

### 5.2.2 Back-Right Impact

In this paragraph a Back-Right impact performed at an energy level of 24J with MIPS not active will be presented reporting the signals recorded by every single sensor mounted on IHHS1 and then an analysis and explanation will be given. This time the principal direction of impact is not only one, as in a Back test, but IHHS1 will be strongly pushed both in the X direction and in the Y direction, in fact the θ angle formed between the direction of movement of the hammer and the X axis is 45°, so X and Y should be solicited in the same way.

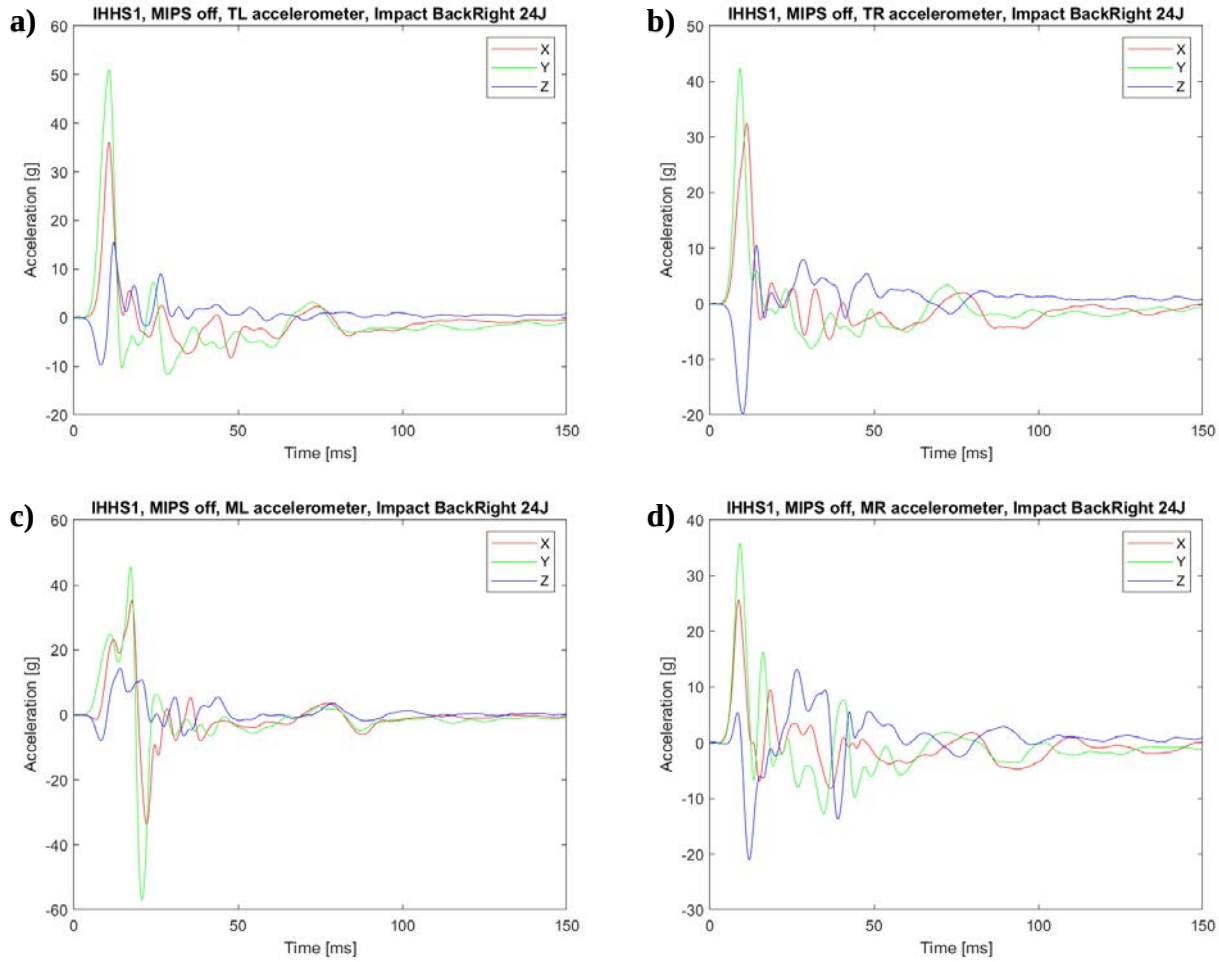

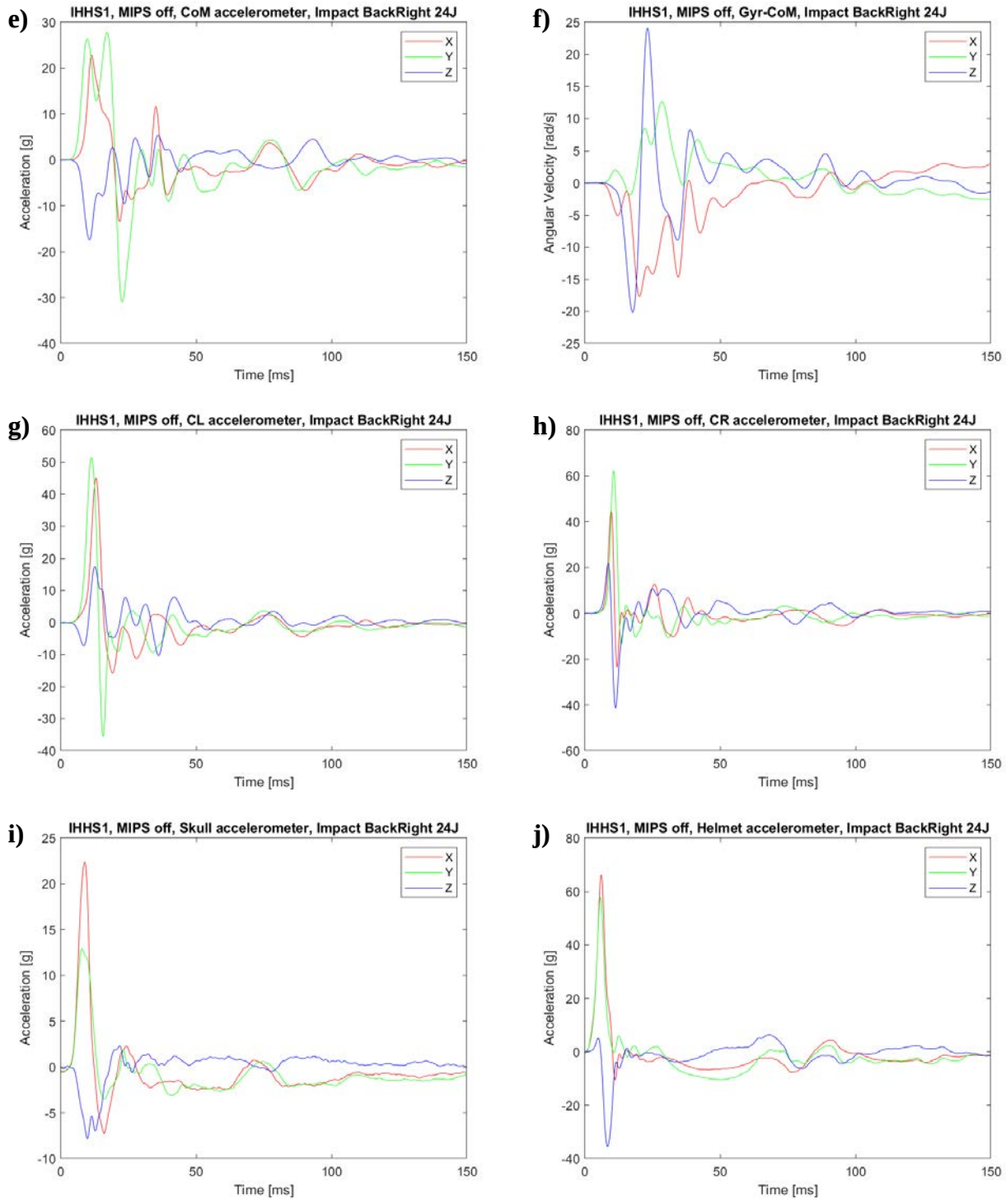


**Figure 5.15** *Signals recorded by IHHS1 with MIPS off during Impact Back-Right 24J. (a) TL (b) TR (c) ML (d) MR (e) CoM (f) Gyr-CoM (g) CL (h) CR (i) Skull (j) Helmet.*

From the different graphs of *Figure 5.15* can be seen that both X and Y direction records huge peaks of acceleration during impacts. In this case, instead of having an only one big peak in X as in Back test previously presented, the two peaks are characterized by slightly smaller values. If in Back impact TL and TR, sensors belonging to the top layer, recorded a huge peak in X direction around 60 g, in

Back-Right Impact there are two peaks, X and Y, both around 40 g. For the middle layer, Back Impact has one peak near 45 g for every accelerometer, instead in Back-Right there are two peaks near 35 g. It is the same thing for the cerebellum layer. As the accelerations present two principal direction of impact, also the angular velocity has two principal direction of rotation. This two directions around which the head rotate are X and Y, in particular around X there is a negative rotation and around Y there is a positive one. Both in Back and Back-Right impact the rotation around Y presents a positive peak. In Back test the rotation around X was negligible. From *Figure 5.15 (f)*, accounting the angular velocities recorded by gyroscopes in CoM, can be seen two peaks of the Z signal, even if Z is not one of the principal direction of rotation predicted, that are higher than X and Y. Firstly there is a negative peak in Z and then became positive, that means that a Back-Right impact tends to produce a rotation of IHHS1 around the neck, in particular the head tends to watch towards right and then to rotate towards the left side. Even if these peaks are high, they are also very sharp, instead the peaks of X and Y are wide and large, meaning that, integrating the angular velocity by the time, the angle produced around X and Y should be bigger than the angles around the vertical direction. In fact while the rotation produced by the hammer around X and Y direction can be easily detected in the video, the angle of rotation around the neck is difficult to see. In *Figure 5.16* will be shown three photograms from the video, the first one depicting the head the instant before the hammer touches the helmet, the second one showing the hammer pushing the head and the third one characterized by IHHS1 at the end of the push, that is a photogram before the head beginning to come back towards the initial position. In the third photogram can be seen that the nose of IHHS1 seems to be observed from a profile point of view, instead the second photogram show the nose from a three-quarter view, meaning that a little rotation has happened, even if little.

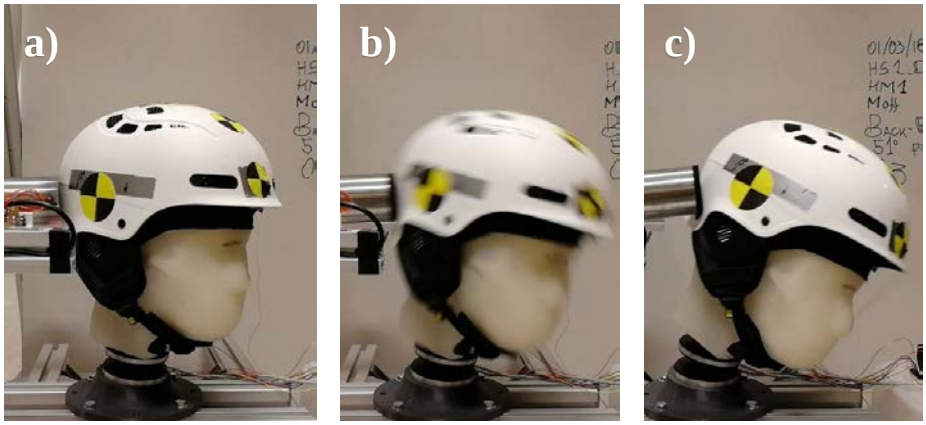


**Figure 5.16** *Photograms taken from the recorded video of Impact Back-Right 24J. (a) Photogram before the contact between impactor and IHHS1. (b) Head is touched by the hammer and pushed forward. (c) Maximum displacement of the head both in X direction and Y direction. After the photogram begins the phase of waving around the initial position.*

In this test, all of the accelerometer tends to have, at least little, a first negative peak in the Z direction, besides CR and MR. In the Back impact only CL and CR where characterized by a first peak in Z positive, instead the others were pushed down, and it was due to the position of the cerebellum, behind the coronal plane passing through the CoM. This time instead the IHHS1 is rotated of 45° and the accelerometers in the right part tends to be pushed up instead the left part tends to be pushed down. This phenomenon is easy to see comparing the signal in Z direction of ML with MR and CL with CR, instead in the top layer characterized by the presence of TL and TR is not visible, in fact these two accelerometers seems to move together.

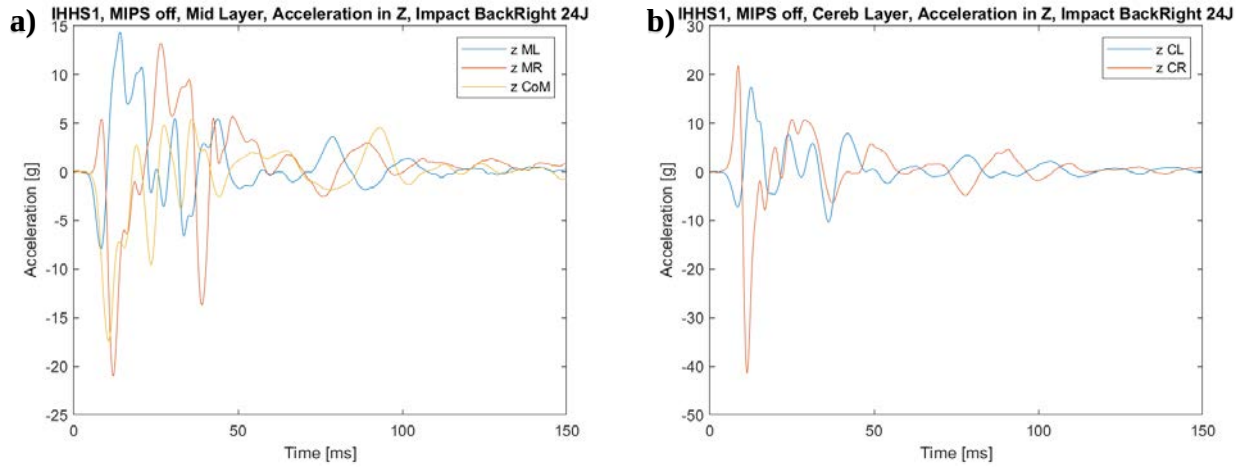


**Figure 5.17** *Comparison of Z signals in different layer (a) Middle layer (b) Cerebellum or lower layer.*

For the Back-Right Impact is particularly interesting to perform a comparative analysis of the signals from helmet, skull and CoM in the principal directions of impact, as shown in *Figure 5.18.*

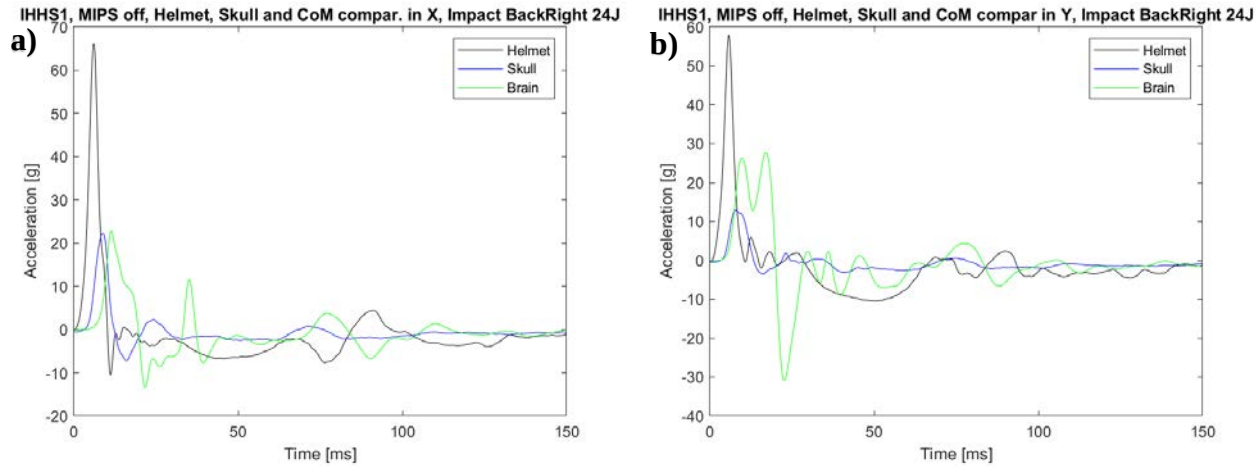


**Figure 5.18** *Comparison of accelerations of Helmet, Skull and CoM (a) X direction (b) Y direction.*

The first and the sharpest peak to be developed during impact is from the helmet, both in X direction and in Y direction. After this one, in X direction the second peak is skull and the third one in CoM, exactly as in the Back impact. For the Y direction there is a little difference, in fact both peaks from skull and CoM seem to begin in the same instant, even if the skull should receive the push before the brain. Another thing that can be seen by observing these graphs, as well as the ones presented in *Figure 5.15*, is that all the signals tend to have a first high and sharp peak in the principal direction of impact, instead the CoM presents both in X and Y a large peak or even a double peak, with the second one beginning before the fading of the first, and this is particularly evident in the Y direction for Back-Right, more than the X direction, and in the Back test previously discussed. To understand the origins of this phenomenon it is necessary to compare the signals from ML and MR, the accelerometers belonging to the same layer of CoM, placed at its sides. As can be seen in *Figure 5.19*, both in X direction and in Y direction, ML and MR have the first peak in different instants of time, in particular MR, near the point of contact between the hammer and the helmet, happens first and then ML, far from the point of impact, is the second to appear. The first peak of CoM is influenced by MR peak, instead the second peak, developed before the fading of the first one, is due to the peak of ML. It is like the right lobe of the brain begins to move dragging behind it CoM, placed in the region of connection between the lobes, and then the left lobe moves while the acceleration of the other one is diminishing, dragging another time the CoM with itself.

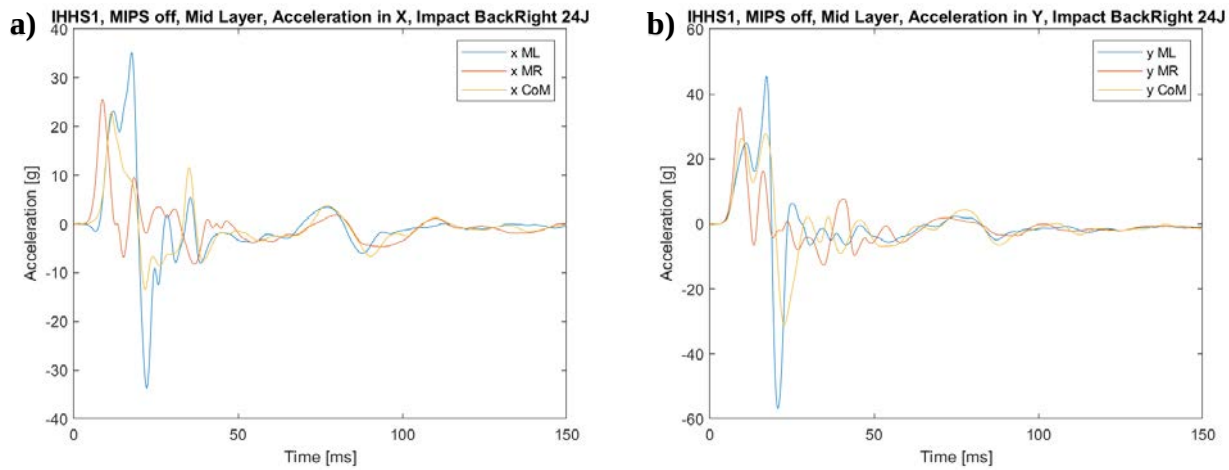


**Figure 5.19** *Comparison of signals from the middle layer in the principal directions of impact. (a) X direction. (b) Y direction.*

As for the Back impact, in order to verify the effectiveness of the MIPS protection it is necessary to compare the angular acceleration obtained in an impact with MIPS not activated and an impact with MIPS activated, and it will be done in *Figure 5.20*.

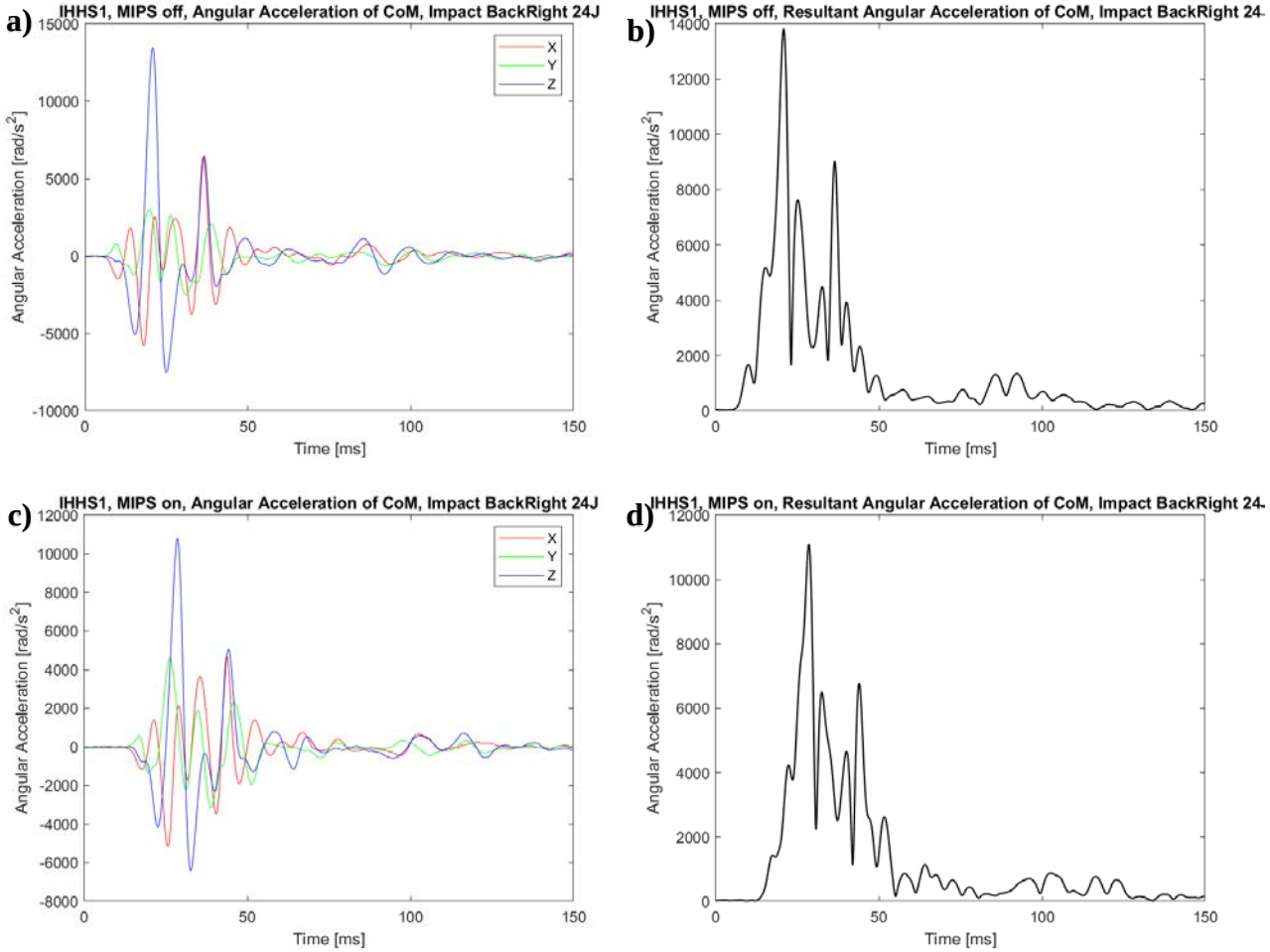


**Figure 5.20** *Comparison of angular accelerations for impact BackRight 24J performed on IHHS 1 with MIPS not activated and then activated. (a) Angular acceleration of CoM with no MIPS. (b) Resultant angular acceleration of CoM with no MIPS. (c) Angular acceleration of CoM with MIPS activated. (d) Resultant angular acceleration of CoM with MIPS activated.*

Differently from the Back impact, in this Back-Right Impact the MIPS protection seems to be effective, in fact the resultant angular acceleration for the no MIPS test almost touches 14000 rad/s$^2$, while the MIPS test have a resultant angular acceleration that stay under 12000 rad/s$^2$, near 11000 rad/s$^2$. That means that there is a difference almost of 3000 rad/s$^2$, with a reduction of the angular acceleration of nearly 20%. This difference between Back and Back-Right impact can be caused by the different place in which the contact between the hammer and the helmet happens, in fact in a Back test the impactor touches the helmet in an almost flat region, instead the Back-Right impact happens between the occipital region and the lateral face of the helmet producing a different angular acceleration.

### 5.2.3 Right Impact

In this paragraph a Right impact with MIPS not activated, occurring at an energy level of 24J will be analysed by showing the signals recorded by the sensors mounted in IHHS1.
The Right impact will be very similar to the Back one, because both are characterized by an only one principal direction of impact, X for the Back test and Y for the Right test.

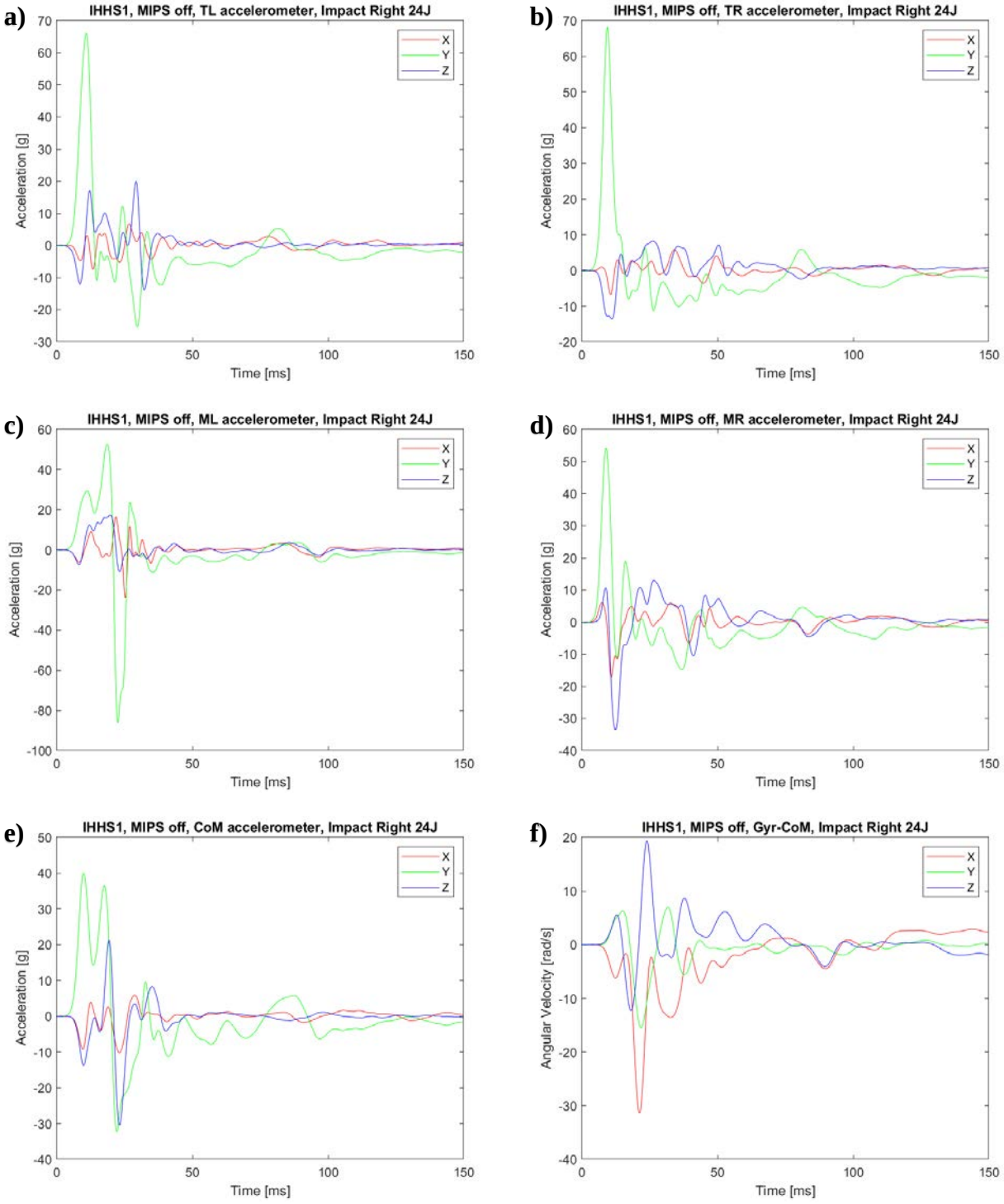

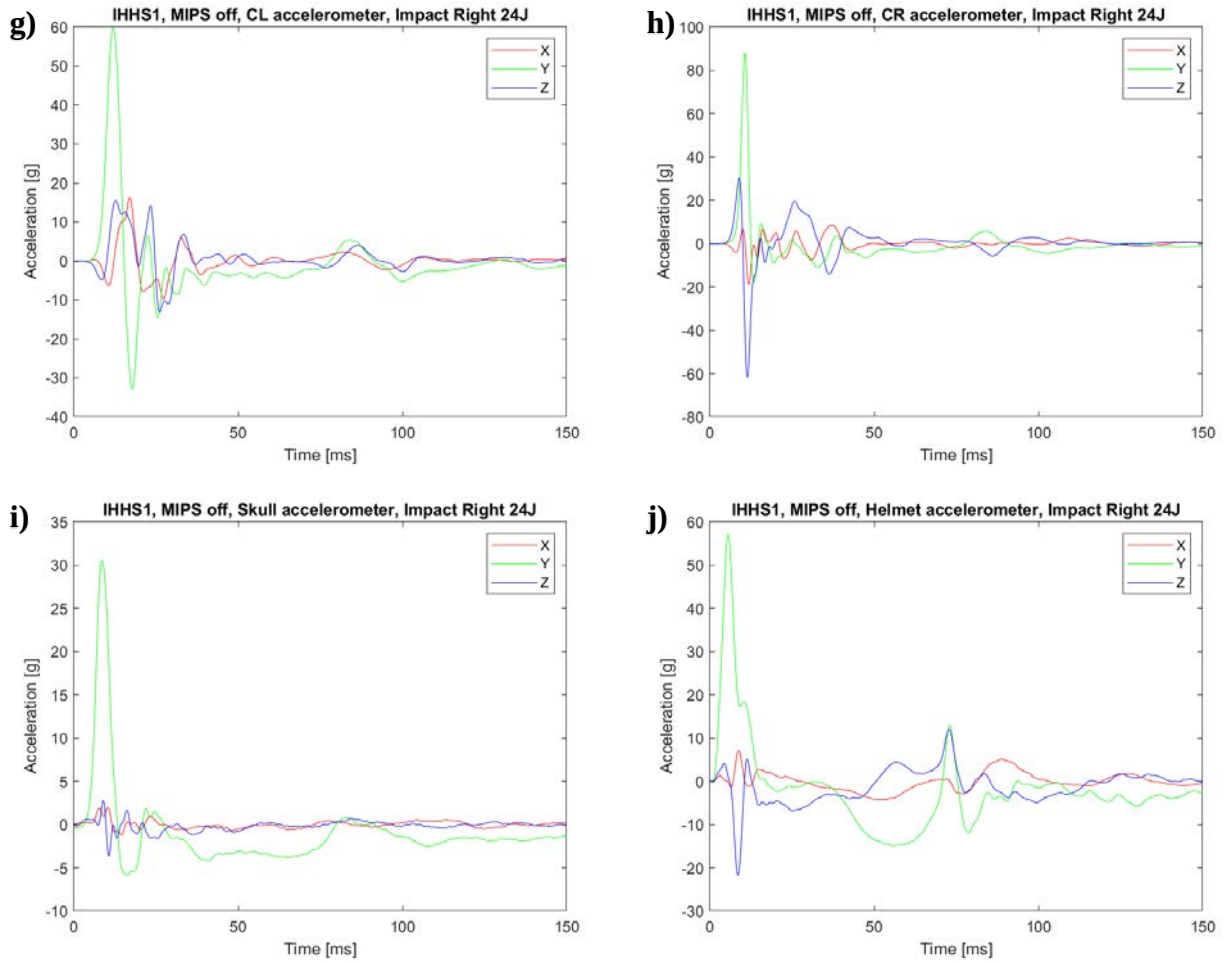


**Figure 5.21** *Signals recorded by IHHS1 with MIPS off during Impact Right 24J. (a) TL (b) TR (c) ML (d) MR (e) CoM (f) Gyr-CoM (g) CL (h) CR (i) Skull (j) Helmet.*

From the graphs of Figure 5.21 it is easy to see that the direction more solicited by the hammer is the Y direction for the accelerations, instead for the angular velocity is X. In particular can be seen in the angular velocities that the rotation is negative around X, but there is also another signal with a high value of the first peak, and it is Z, characterized by a trend predominantly positive, and so the head tends also to rotate around the vertical direction in order to watch towards left. In the following figure some significative photograms taken from the video of the test will be shown.

From the signals of the accelerometers no abnormalities can be seen, besides in Y signal of ML sensors. In fact this accelerometer recorded a wide acceleration in Y characterized by two peaks, in a similar way to CoM, and then a very strong negative peak surpassing the level of -80 g. Probably this peak is due to an electrical phenomenon inside the system of acquisition of data.

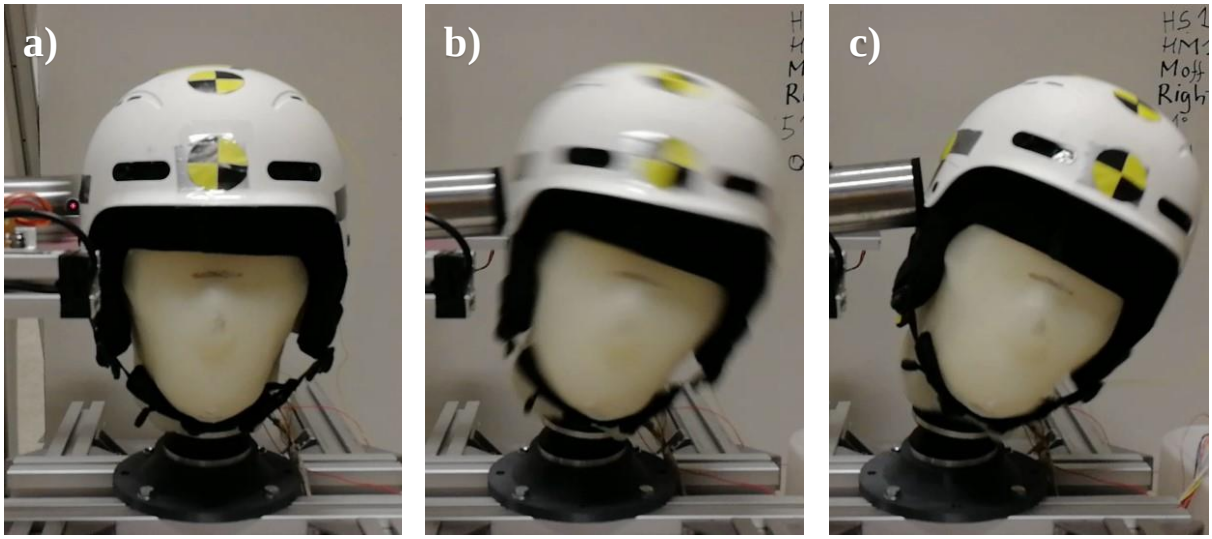


**Figure 5.22** *Photograms taken from the recorded video of Impact Right 24J. (a) Photogram before the contact between impactor and IHHS1. (b) Head is touched by the hammer and pushed forward. (c) Maximum displacement of the head both in Y direction. After the photogram begins the phase of waving around the initial position.*

It is interesting to observe the comparison of different signals in the X direction, not the principal one, for accelerometers from the same layer.

Making this confront in the Back impact, the fact that the brain in the transverse direction was subjected to alternate phases of elongation and compression was discovered. In the Back impact the transverse direction was Y and the principal was X, instead now in the Right impact it is the opposite. In this case we can a similar phenomenon. In fact, when ML has a positive peak in X direction, MR is characterized by a negative one and the other way round. This fact is particularly evident in the middle layer, instead in the top layer and the cerebellum or lower one the trend is more difficult to be individuated. An alternation of signs of the peaks can be seen but is more confused in respect of the middle layer. However, the middle layer seems to suggest that the brain tends to rotate around the brain stem or the vertical direction, in fact in the first peak the right lobe tends to be pushed towards the face instead the left lobe seems to be thrown towards the occipital region. After the first peaks the roles are inverted.

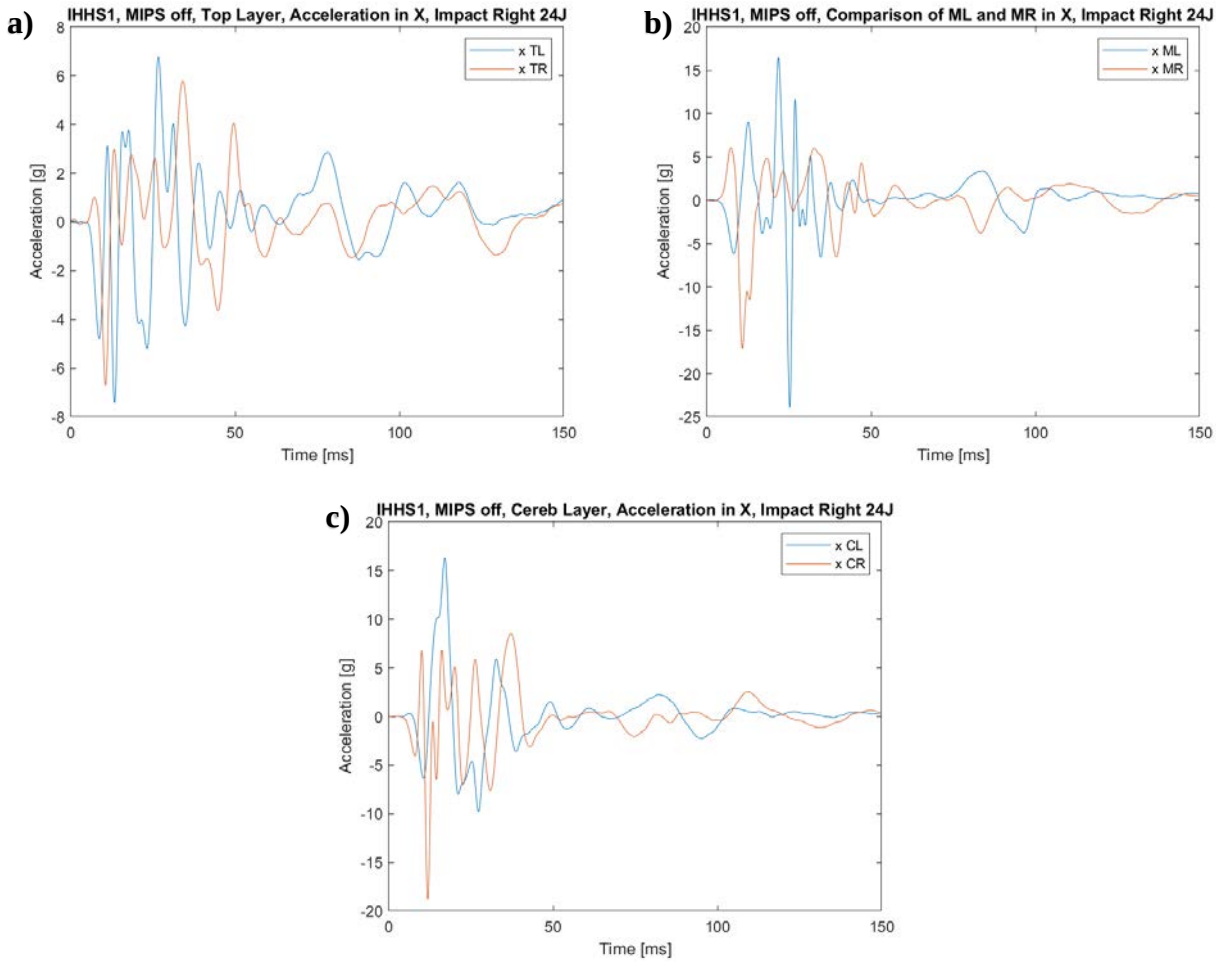


**Figure 5.23** *Comparison of X signals in different layer (a) Top layer (b) Middle layer (c) Cerebellum or lower layer.*

As in the previously shown impact, it is right to present a comparation of the signals from helmet, skull and CoM in the principal direction of impact, that is Y.

What is interesting in this case is that CoM and skull seem to have their first peak developing at the same time, even if the theory should suggest the order: 1) helmet 2) skull 3) brain. This phenomenon is similar to the one analysed in the Back-Right impact, in fact in that test the order was respected in the X direction, instead in the Y direction the two peaks of skull and CoM happened at the same time. There are two possible explanation to this particularity. One is that the instrumented human head is more deep than wide, so in the X direction there is more space left between the occipital region of the skull and the brain, so it takes more time for the hit to be transmitted, instead the space left between the temporal region and the brain is little and it is required less time for the propagation of the hit. The second and more simple explanation is that the brain remained deformed after the removal of the silicone oil that made the brain to swell, so there is no space left between the skull and the brain and when the first one receives the hit, also the brain at the same time is pushed.

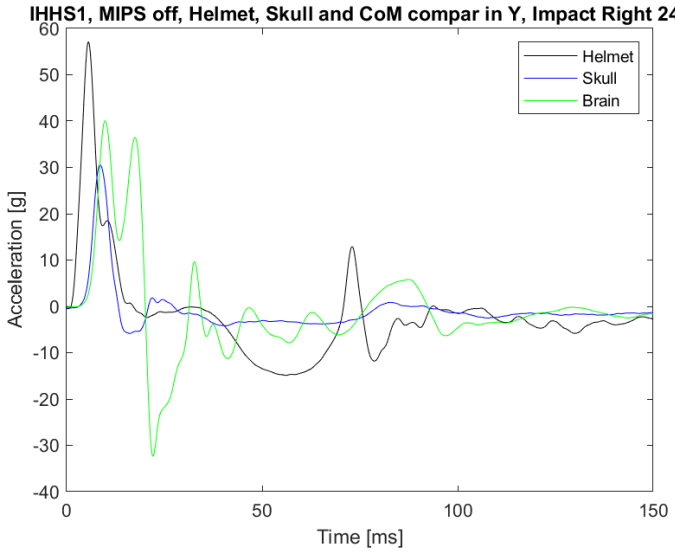


**Figure 5.24** *Comparison of accelerations of Helmet, Skull and CoM in the Y direction.*

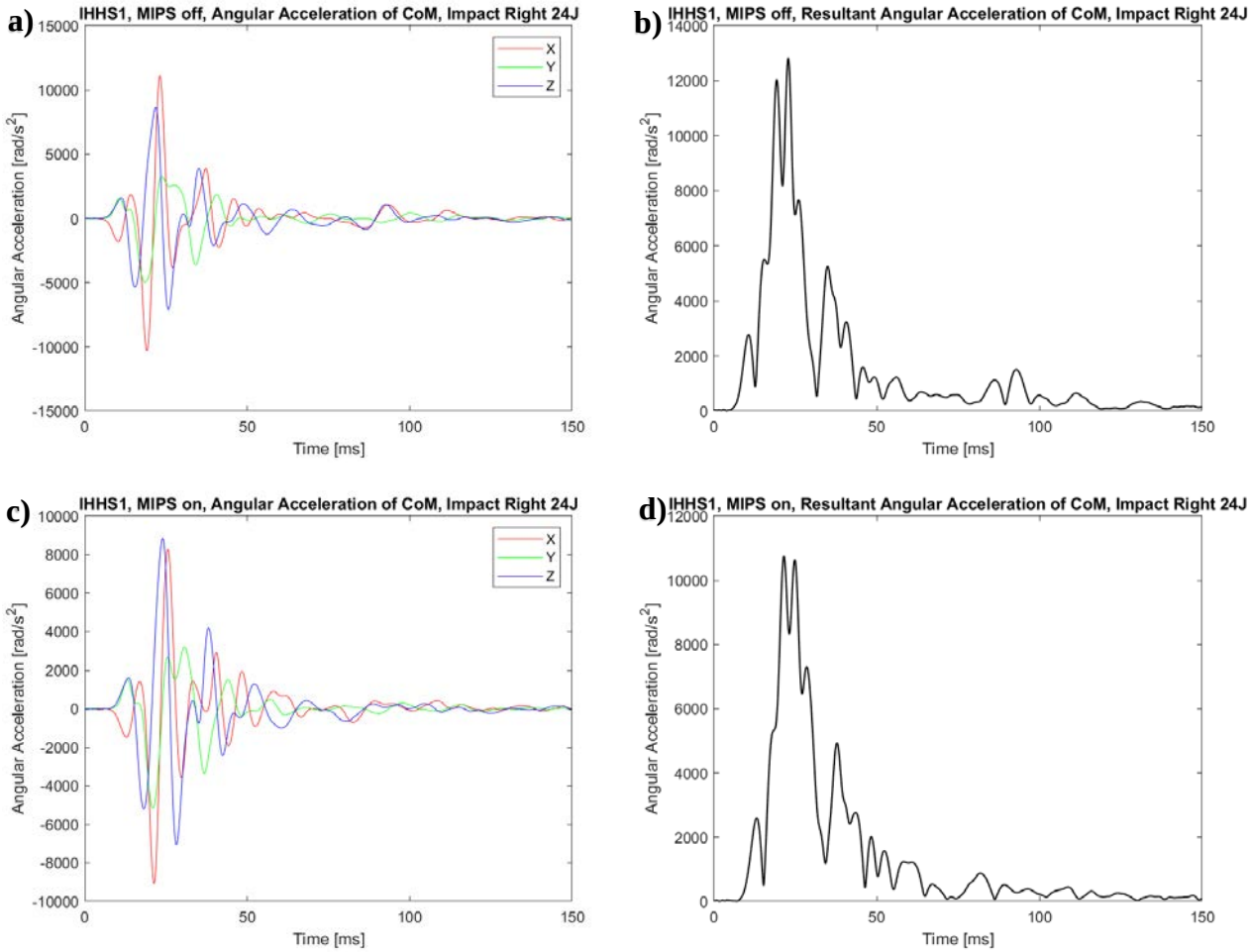


**Figure 5.25** *Comparison of angular accelerations for impact BackRight 24J performed on IHHS 1 with MIPS not activated and then activated. (a) Angular acceleration of CoM with no MIPS. (b) Resultant angular acceleration of CoM with no MIPS. (c) Angular acceleration of CoM with MIPS activated. (d) Resultant angular acceleration of CoM with MIPS activated.*

### 5.2.4 Front-Right Impact

The last impact to be shown is the Front-Right impact with MIPS not activated occurring at 24J. This impact is similar to the Back-Right one, in fact both have two principal direction of impact, the X and Y direction. In this test the head is pushed backward, so the first peak of the X direction will be negative, instead the first peak in the Y direction for the accelerometers will be positive because if the impact arrive from right, the head will be pushed toward left. Also the angular velocity will be characterized by two principal direction around the head rotates, in fact IHHS1 will have a negative rotation both around the X and around the Y direction. However in the following figure will be shown every single signal recorded by the 7 functioning accelerometers placed inside the brain and the gyroscopes, and the by the 2 accelerometers outside IHHS1, that are mounted on helmet and skull.

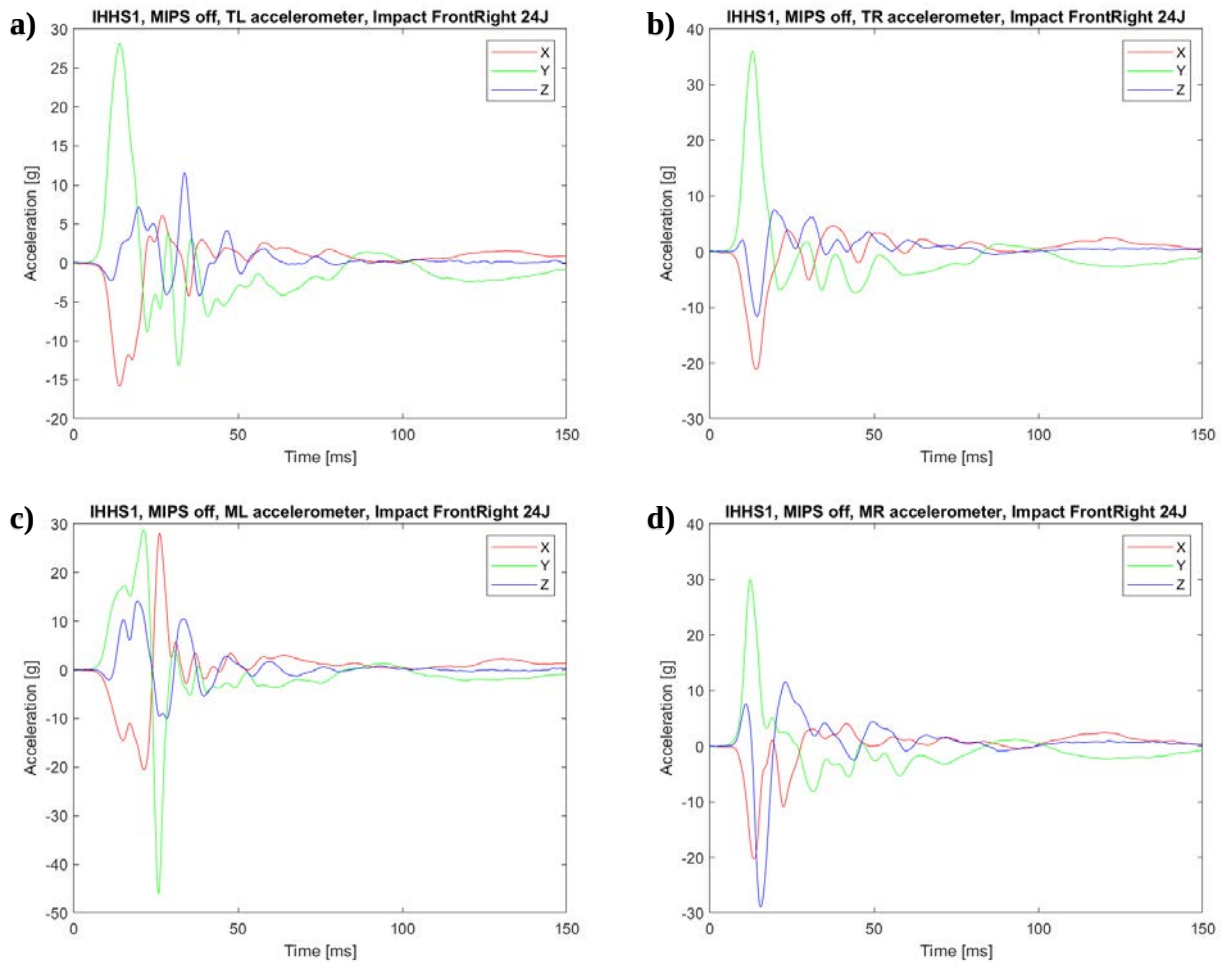

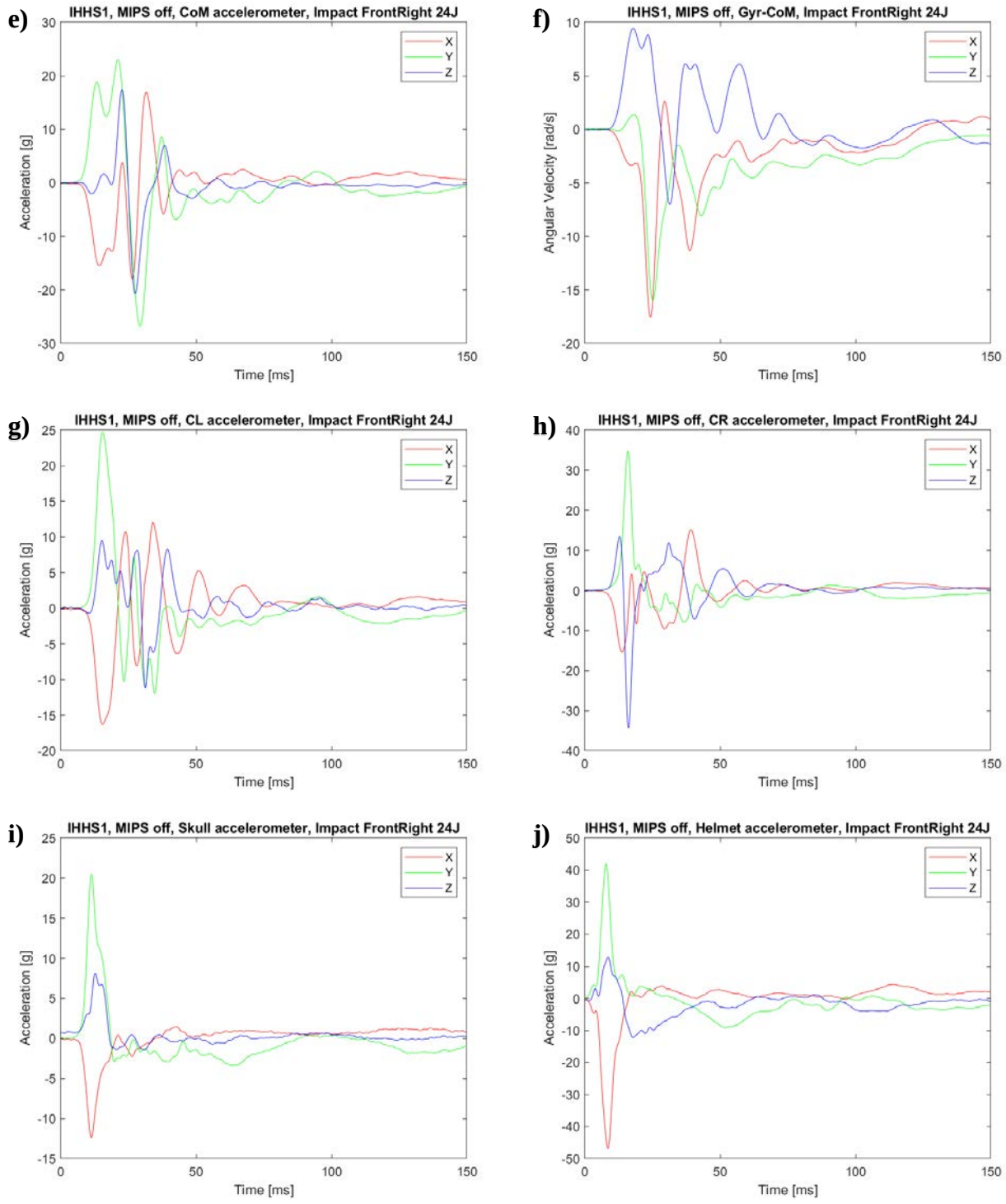


**Figure 5.26** *Signals recorded by IHHS1 with MIPS off during Impact Front.Right 24J. (a) TL (b) TR (c) ML (d) MR (e) CoM (f) Gyr-CoM (g) CL (h) CR (i) Skull (j) Helmet.*

From *Figure 5.26 (f)*, besides what has been said before about the principal direction of rotation, the Z signal of Gyr-CoM shows a different number of peaks with positive sign. The first peak is in the order of 10 rad/s, not so much smaller than the principal direction of rotation X and Y that stay around -15 rad/s. A positive rotation around Z means that the head tends to watch towards left during the

test, however this rotation is difficult to be detected in the video recorded of the test, even if some significant photograms of the head before the contact with the hammer, during the displacement of the head and at the maximum distance from the initial position, as in the following figure.

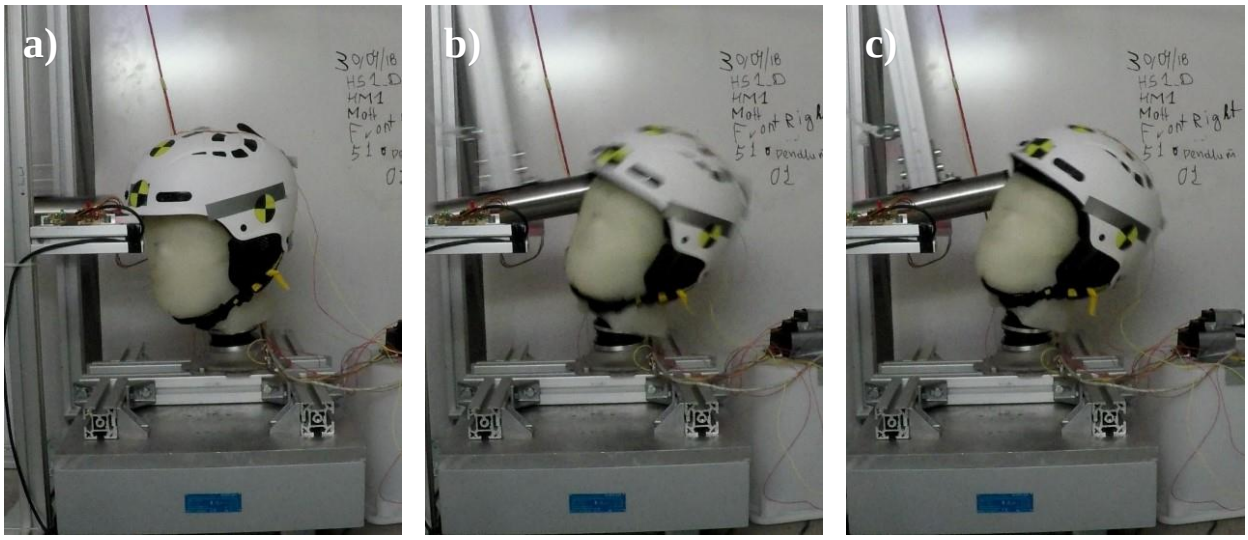


**Figure 5.27** *Photograms taken from the recorded video of Impact Front-Right 24J. (a) Photogram before the hit (b) Head is touched by the hammer and pushed forward. (c) Maximum displacement.*

As for every other impact, it is needed to comment the comparison of the signals in the principal directions, that are X and Y, for helmet, skull and brain. As can be seen from the following graphs, both in the X direction and in the Y direction, the order of development of peaks is respected, meaning that the first peak is helmet, then there is skull and finally CoM. However the signal of skull tends to be contained, for the X direction, inside the peak of helmet, in fact skull has a peak that begins after the one of helmet, but they fade at the same time practically.

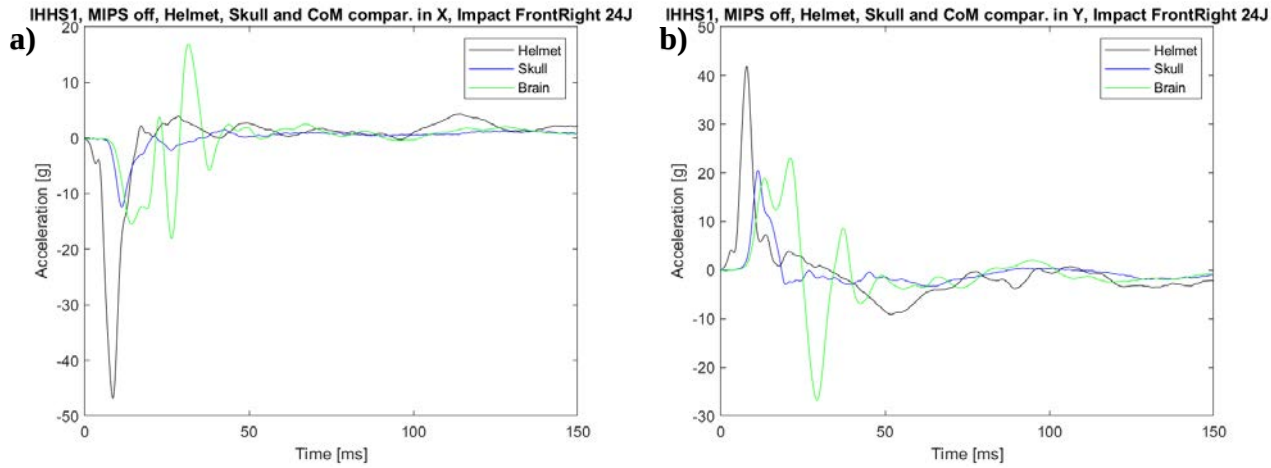


**Figure 5.28** *Comparison of accelerations of Helmet, Skull and CoM (a) X direction (b) Y direction.*

The Front-Right impact is similar to a Back-Right one, and in the latter was present a discrete reduction of the resultant angular acceleration of the CoM, around 20%, between the impact performed with MIPS not activated and MIPS activated. Knowing that, it is right to suppose that in a Front-Right impact there are differences between MIPS on and MIPS off. As exhibited in the following graphs, it can be seen that the resultant angular acceleration with no MIPS stays around 7000 rad/s$^2$ while with MIPS on is about 6000 rad/s$^2$, with a difference of no more than 1000 rad/s$^2$, but a reduction of 15%. It can be said that, in this case, MIPS is effective in both Back-Right and Front-Right impact, but not in Back and Right impact. However it is right to remember that MIPS is declared to be effective for near tangential impacts, and none of the performed test was like that. A future development of this project can be to modify the structure of the pendulum arm in order to have near tangential impacts.

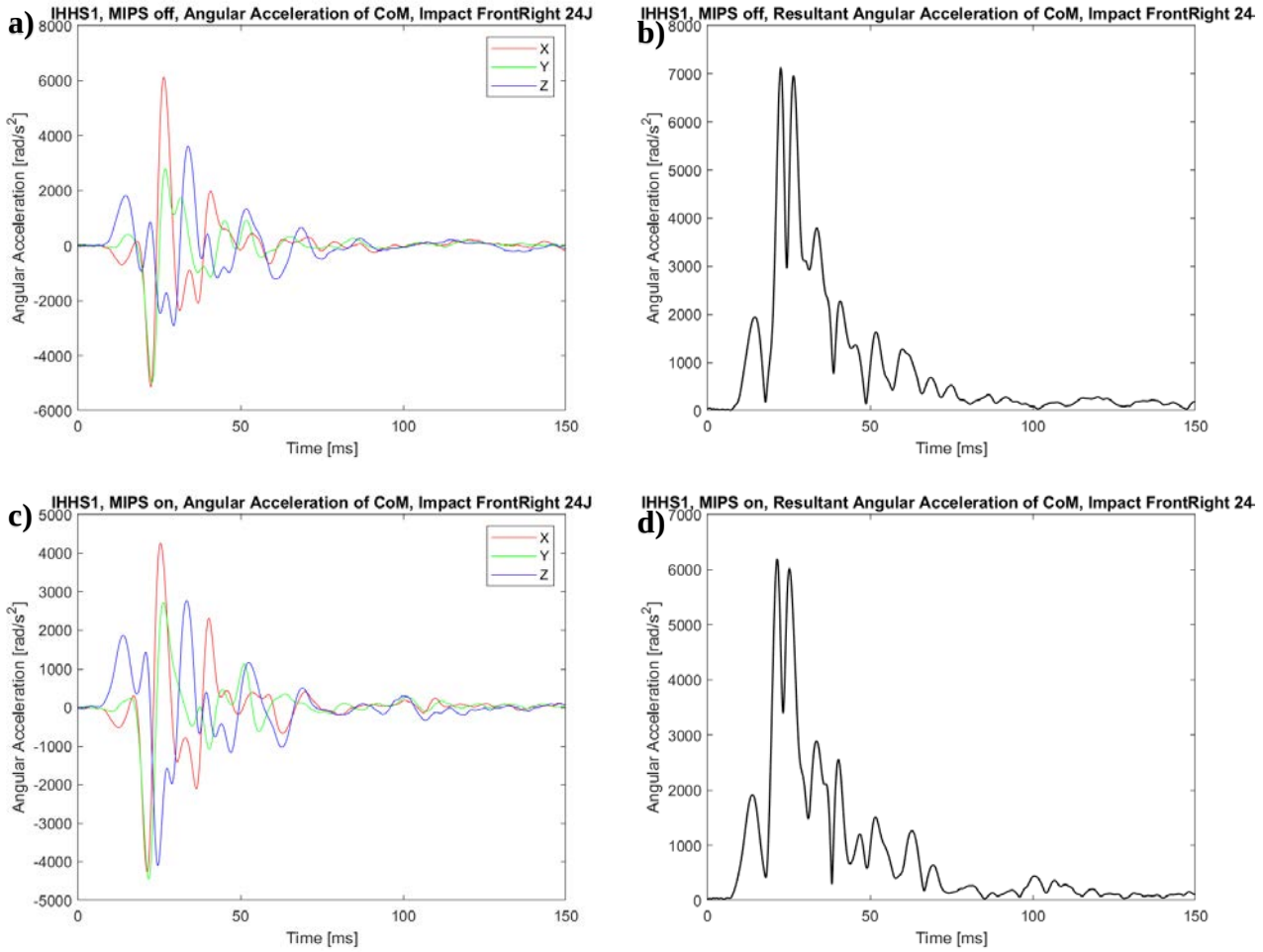


**Figure 5.29** *Comparison of angular accelerations for impact Front-Right 24J performed on IHHS 1 with MIPS not activated and then activated. (a) Angular acceleration of CoM with no MIPS. (b) Resultant angular acceleration of CoM with no MIPS. (c) Angular acceleration of CoM with MIPS activated. (d) Resultant angular acceleration of CoM with MIPS activated.*

## 5.3 Tables

In this section will be presented the summary tables of all the tests performed on IHHS1.
Every table contains the results of 12 tests: 3 Back impacts, 3 Back-Right, 3 Right, 3 Front-Right. To build the tables was needed to find the maximum value in mathematical form of X, Y and Z signals recorded by the accelerometers of helmet, skull, CoM and gyroscope Gyr-CoM, while the other accelerometers were not considered interesting for the purpose of a summary. Of the 3 impacts of each kind is presented the mean value and the standard deviation of the previously mentioned signals. In the tables HIC and BrIC are also presented. The 12 test needed to complete a table are performed at the same energy level, that can be 8J, 16J, 24J or 44J and have to be all the same or MIPS on or MIPS off. So 8 tables are necessary to describe the 96 tests performed on IHHS1.

| Energy | 8J | BACK | | BACKRIGHT | | RIGHT | | FRONTRIGHT | |
|---|---|---|---|---|---|---|---|---|---|
| MIPS | off | Theta = 0 deg | | Theta = 45 deg | | Theta = 90 deg | | Theta = 135 deg | |
| | | MEAN | STD Dev | MEAN | STD Dev | MEAN | STD Dev | MEAN | STD Dev |
| Helmet | acc_x [g] | 44,02 | 6,85 | 32,00 | 0,66 | 4,09 | 0,04 | -19,04 | 1,56 |
| | acc_y [g] | -0,84 | 4,60 | 26,37 | 0,32 | 28,23 | 0,13 | 18,83 | 2,05 |
| | acc_z [g] | -24,37 | 0,54 | -16,25 | 0,13 | -5,60 | 0,12 | -1,78 | 7,31 |
| | acc_R [g] | 44,18 | 6,93 | 41,32 | 0,72 | 28,24 | 0,13 | 27,24 | 2,46 |
| Skull | acc_x [g] | 14,23 | 2,40 | 9,73 | 0,25 | 0,79 | 0,05 | -5,14 | 0,91 |
| | acc_y [g] | -0,91 | 0,12 | 6,24 | 0,17 | 12,78 | 0,10 | 7,43 | 1,02 |
| | acc_z [g] | -7,28 | 0,69 | -4,30 | 0,09 | -1,24 | 0,07 | 3,91 | 0,19 |
| | acc_R [g] | 15,33 | 2,66 | 12,14 | 0,35 | 12,80 | 0,10 | 9,61 | 1,39 |
| | HIC* | 1,63 | 0,60 | 1,42 | 0,05 | 1,30 | 0,01 | 1,20 | 0,19 |
| Brain | acc_x [g] | 20,50 | 0,85 | 11,49 | 0,08 | -3,94 | 0,09 | -10,11 | 0,50 |
| | acc_y [g] | -0,71 | 2,25 | 16,94 | 0,19 | 21,02 | 0,13 | -12,67 | 0,80 |
| | acc_z [g] | -8,03 | 1,70 | -7,28 | 0,15 | -10,29 | 0,11 | -8,54 | 1,20 |
| | acc_R [g] | 20,90 | 0,78 | 19,79 | 0,17 | 23,18 | 0,07 | 15,29 | 1,06 |
| | HIC | 13,59 | 4,76 | 13,41 | 0,10 | 15,94 | 0,08 | 7,50 | 1,11 |
| | ω_x [rad/s] | -1,83 | 0,02 | -10,59 | 0,02 | -13,83 | 0,12 | -8,02 | 0,31 |
| | ω_y [rad/s] | 17,45 | 3,60 | 7,03 | 0,11 | -7,97 | 0,11 | -8,08 | 0,51 |
| | ω_z [rad/s] | -2,02 | 0,12 | 12,62 | 0,48 | 9,10 | 0,03 | 5,76 | 0,49 |
| | ω_R [rad/s] | 17,46 | 3,60 | 15,85 | 0,42 | 15,78 | 0,11 | 11,85 | 0,47 |
| | ω_R [dps] | 1000,65 | 206,15 | 908,30 | 23,97 | 903,84 | 6,29 | 678,78 | 26,87 |
| | BrIC | 0,31 | 0,06 | 0,36 | 0,01 | 0,33 | 0,00 | 0,23 | 0,01 |
| | α_R [rad/s^2] | 3988,13 | 856,38 | 6652,27 | 199,18 | 3931,60 | 61,39 | 3173,30 | 219,73 |

**Table 5.3** *Energy level: 8J. MIPS off*

| Energy | 16J | BACK | | BACKRIGHT | | RIGHT | | FRONTRIGHT | |
|---|---|---|---|---|---|---|---|---|---|
| MIPS | off | Theta = 0 deg | | Theta = 45 deg | | Theta = 90 deg | | Theta = 135 deg | |
| | | MEAN | STD Dev | MEAN | STD Dev | MEAN | STD Dev | MEAN | STD Dev |
| Helmet | acc_x [g] | 73,95 | 7,96 | 50,24 | 2,09 | 2,22 | 6,38 | -31,11 | 2,79 |
| | acc_y [g] | -5,97 | 0,35 | 41,99 | 1,66 | 42,80 | 2,18 | 26,37 | 1,63 |
| | acc_z [g] | -39,31 | 5,65 | -25,15 | 0,53 | -11,05 | 4,67 | -10,68 | 0,42 |
| | acc_R [g] | 74,27 | 7,96 | 65,11 | 2,65 | 42,84 | 2,12 | 41,45 | 3,36 |
| Skull | acc_x [g] | 32,32 | 4,25 | 17,21 | 0,47 | 4320,33 | 7480,44 | -6,89 | 0,59 |
| | acc_y [g] | -1,72 | 0,22 | 9,88 | 0,29 | 23,11 | 0,49 | 10,19 | 1,55 |
| | acc_z [g] | -12,68 | 0,98 | -6,60 | 0,02 | -2,51 | 0,22 | 5,32 | 0,35 |
| | acc_R [g] | 34,18 | 4,26 | 20,69 | 0,44 | 23,17 | 0,48 | 12,91 | 1,54 |
| | HIC* | 9,15 | 1,67 | 4,18 | 0,09 | 3,84 | 0,19 | 1,94 | 0,15 |
| Brain | acc_x [g] | -36,44 | 5,47 | 17,85 | 0,35 | -7,83 | 0,25 | -11,09 | 0,18 |
| | acc_y [g] | -4,01 | 0,31 | -26,39 | 0,31 | 31,72 | 0,52 | -17,87 | 1,10 |
| | acc_z [g] | -17,93 | 2,07 | -12,76 | 0,32 | -22,59 | 0,21 | -13,67 | 1,31 |
| | acc_R [g] | 37,67 | 4,70 | 29,43 | 0,36 | 37,15 | 0,55 | 21,31 | 1,47 |
| | HIC | 49,63 | 7,49 | 32,66 | 0,19 | 44,61 | 0,54 | 16,22 | 2,11 |
| | ω_x [rad/s] | -2,83 | 0,32 | -15,56 | 0,27 | -24,37 | 0,32 | -13,69 | 0,79 |
| | ω_y [rad/s] | 31,95 | 2,21 | 9,91 | 0,22 | -13,15 | 0,18 | -11,54 | 0,55 |
| | ω_z [rad/s] | -3,21 | 0,28 | 21,14 | 0,21 | 16,17 | 0,22 | 6,96 | 0,52 |
| | ω_R [rad/s] | 32,06 | 2,24 | 25,30 | 0,15 | 27,43 | 0,33 | 18,11 | 0,74 |
| | ω_R [dps] | 1837,13 | 128,21 | 1449,37 | 8,69 | 1571,47 | 19,12 | 1037,69 | 42,62 |
| | BrIC | 0,57 | 0,04 | 0,57 | 0,00 | 0,58 | 0,01 | 0,33 | 0,01 |
| | α_R [rad/s^2] | 8758,47 | 833,37 | 11401,00 | 114,53 | 8962,07 | 142,71 | 5626,27 | 280,68 |

**Table 5.4** *Energy level: 16J. MIPS off*

| Energy | 24J | BACK | | BACKRIGHT | | RIGHT | | FRONTRIGHT | |
|---|---|---|---|---|---|---|---|---|---|
| MIPS | off | Theta = 0 deg | | Theta = 45 deg | | Theta = 90 deg | | Theta = 135 deg | |
| | | MEAN | STD Dev | MEAN | STD Dev | MEAN | STD Dev | MEAN | STD Dev |
| Helmet | acc_x [g] | 120,90 | 7,81 | 69,53 | 8,90 | 2,65 | 7,32 | -46,87 | 0,65 |
| | acc_y [g] | -9,36 | 0,65 | 60,76 | 8,43 | 56,63 | 2,04 | 41,81 | 1,54 |
| | acc_z [g] | -57,58 | 3,89 | -35,14 | 5,83 | -20,81 | 3,08 | 12,71 | 0,60 |
| | acc_R [g] | 121,33 | 7,80 | 91,92 | 12,19 | 56,70 | 1,94 | 62,86 | 1,49 |
| Skull | acc_x [g] | 39,88 | 4,41 | 21,50 | 1,16 | 2,08 | 0,13 | -12,47 | 0,93 |
| | acc_y [g] | -2,30 | 0,40 | 12,82 | 0,23 | 30,18 | 0,63 | 20,68 | 1,26 |
| | acc_z [g] | -14,39 | 0,88 | -7,92 | 0,12 | -3,49 | 0,16 | 8,14 | 0,41 |
| | acc_R [g] | 41,73 | 4,40 | 25,63 | 0,70 | 30,30 | 0,61 | 24,61 | 1,55 |
| | HIC* | 15,00 | 1,77 | 6,80 | 0,54 | 6,50 | 0,45 | 5,01 | 0,49 |
| Brain | acc_x [g] | -43,76 | 4,87 | 22,17 | 1,20 | -9,67 | 0,55 | -17,97 | 0,95 |
| | acc_y [g] | -4,66 | 0,52 | -30,27 | 1,73 | 39,30 | 0,77 | -26,88 | 0,20 |
| | acc_z [g] | -21,67 | 1,81 | -16,85 | 0,78 | -30,23 | 0,56 | -20,81 | 0,17 |
| | acc_R [g] | 46,12 | 3,61 | 35,19 | 1,74 | 43,97 | 0,60 | 32,45 | 0,58 |
| | HIC | 71,58 | 7,06 | 48,99 | 5,67 | 73,14 | 0,38 | 41,21 | 1,84 |
| | ω_x [rad/s] | -3,58 | 0,16 | -17,31 | 1,13 | -31,51 | 0,10 | -17,62 | 0,19 |
| | ω_y [rad/s] | 35,73 | 1,89 | 12,39 | 0,22 | -15,79 | 0,33 | -16,00 | 0,25 |
| | ω_z [rad/s] | -3,88 | 0,14 | 23,78 | 1,61 | 19,59 | 0,24 | 9,48 | 0,44 |
| | ω_R [rad/s] | 35,89 | 1,91 | 28,18 | 1,65 | 35,06 | 0,06 | 24,55 | 0,13 |
| | ω_R [dps] | 2056,03 | 109,29 | 1614,57 | 94,49 | 2008,57 | 3,50 | 1406,40 | 7,24 |
| | BrIC | 0,64 | 0,03 | 0,65 | 0,04 | 0,72 | 0,01 | 0,45 | 0,01 |
| | α_R [rad/s^2] | 10369,63 | 898,73 | 13457,00 | 1142,12 | 12707,00 | 137,29 | 7197,17 | 245,12 |

**Table 5.5** *Energy level: 24J. MIPS off*

| Energy | 44J | BACK | | BACKRIGHT | | RIGHT | | FRONTRIGHT | |
|---|---|---|---|---|---|---|---|---|---|
| MIPS | off | Theta = 0 deg | | Theta = 45 deg | | Theta = 90 deg | | Theta = 135 deg | |
| | | MEAN | STD Dev | MEAN | STD Dev | MEAN | STD Dev | MEAN | STD Dev |
| Helmet | acc_x [g] | 170,74 | 11,90 | 97,52 | 16,01 | 4,09 | 10,78 | -74,94 | 2,63 |
| | acc_y [g] | -16,50 | 0,52 | 81,97 | 12,17 | 92,69 | 3,97 | 64,80 | 2,35 |
| | acc_z [g] | -55,22 | 2,38 | -58,11 | 10,02 | -38,80 | 5,16 | 19,04 | 0,96 |
| | acc_R [g] | 171,65 | 11,82 | 127,21 | 20,23 | 93,23 | 3,24 | 100,60 | 2,40 |
| Skull | acc_x [g] | 58,68 | 3,13 | 38,83 | 1,08 | -0,45 | 3,05 | -20,99 | 0,99 |
| | acc_y [g] | -6,58 | 0,33 | 19,77 | 0,65 | 46,70 | 1,26 | 37,79 | 4,07 |
| | acc_z [g] | -20,46 | 1,61 | -13,76 | 0,75 | 6,80 | 0,27 | 12,09 | 0,73 |
| | acc_R [g] | 61,02 | 3,46 | 44,28 | 1,40 | 47,07 | 1,20 | 43,68 | 3,89 |
| | HIC* | 28,11 | 3,52 | 16,00 | 0,40 | 15,35 | 0,85 | 12,26 | 1,75 |
| Brain | acc_x [g] | 67,06 | 4,04 | 39,91 | 2,24 | -14,71 | 0,35 | -36,94 | 3,51 |
| | acc_y [g] | 2,82 | 9,60 | -38,28 | 1,02 | 62,55 | 1,85 | -35,17 | 1,32 |
| | acc_z [g] | -32,98 | 2,01 | -30,48 | 1,11 | -46,86 | 2,36 | 28,09 | 0,88 |
| | acc_R [g] | 74,71 | 4,52 | 59,05 | 3,25 | 67,10 | 2,07 | 47,35 | 2,71 |
| | HIC | 139,63 | 4,76 | 113,40 | 2,61 | 140,61 | 4,63 | 100,99 | 9,16 |
| | ω_x [rad/s] | -9,00 | 0,41 | -25,33 | 1,57 | -40,25 | 0,12 | -25,17 | 0,50 |
| | ω_y [rad/s] | 44,34 | 0,05 | 18,28 | 0,37 | -16,37 | 0,38 | -20,32 | 0,71 |
| | ω_z [rad/s] | -9,76 | 1,69 | 25,74 | 0,55 | 24,52 | 1,93 | 14,46 | 0,59 |
| | ω_R [rad/s] | 45,87 | 0,32 | 35,48 | 0,85 | 43,49 | 0,15 | 33,77 | 0,76 |
| | ω_R [dps] | 2628,33 | 18,24 | 2032,70 | 48,70 | 2491,73 | 8,63 | 1934,57 | 43,39 |
| | BrIC | 0,83 | 0,01 | 0,78 | 0,01 | 0,89 | 0,03 | 0,62 | 0,01 |
| | α_R [rad/s^2] | 13754,00 | 417,61 | 16175,67 | 357,09 | 16903,67 | 94,39 | 12954,00 | 335,64 |

**Table 5.6** *Energy level: 44J. MIPS off*

| Energy | 8J | BACK | | BACKRIGHT | | RIGHT | | FRONTRIGHT | |
|---|---|---|---|---|---|---|---|---|---|
| MIPS | on | Theta = 0 deg | | Theta = 45 deg | | Theta = 90 deg | | Theta = 135 deg | |
| | | MEAN | STD Dev | MEAN | STD Dev | MEAN | STD Dev | MEAN | STD Dev |
| Helmet | acc_x [g] | 37,21 | 5,25 | 19,69 | 0,26 | -2,53 | 0,09 | -18,72 | 0,17 |
| | acc_y [g] | -2,92 | 0,26 | 18,34 | 0,51 | 23,35 | 0,07 | 15,84 | 0,15 |
| | acc_z [g] | -16,35 | 2,94 | -14,97 | 1,06 | -6,97 | 0,03 | -5,56 | 0,12 |
| | acc_R [g] | 37,29 | 5,27 | 27,36 | 0,47 | 23,45 | 0,07 | 24,30 | 0,13 |
| Skull | acc_x [g] | 10,80 | 0,30 | 8,00 | 0,62 | -0,54 | 0,05 | -6,08 | 0,13 |
| | acc_y [g] | -1,88 | 0,14 | 3,59 | 0,12 | 11,12 | 0,06 | 8,11 | 0,13 |
| | acc_z [g] | -5,72 | 0,13 | -4,17 | 0,23 | 1,29 | 0,07 | 4,42 | 0,11 |
| | acc_R [g] | 11,71 | 0,50 | 9,31 | 0,49 | 11,20 | 0,07 | 10,98 | 0,19 |
| | HIC* | 1,22 | 0,20 | 0,88 | 0,03 | 1,10 | 0,01 | 1,13 | 0,04 |
| Brain | acc_x [g] | 21,39 | 0,50 | 12,75 | 0,24 | -4,94 | 0,15 | -10,23 | 0,12 |
| | acc_y [g] | -1,05 | 0,19 | 11,55 | 0,02 | 17,56 | 0,11 | -12,32 | 0,09 |
| | acc_z [g] | -6,82 | 0,58 | -6,61 | 0,19 | -8,92 | 0,12 | -9,25 | 0,11 |
| | acc_R [g] | 21,78 | 0,50 | 17,75 | 0,12 | 18,07 | 0,01 | 14,82 | 0,10 |
| | HIC | 11,62 | 2,51 | 7,68 | 0,24 | 10,60 | 0,08 | 6,59 | 0,18 |
| | ω_x [rad/s] | -2,62 | 0,41 | -8,38 | 0,12 | -12,70 | 0,08 | -6,57 | 0,09 |
| | ω_y [rad/s] | 14,43 | 0,86 | 7,40 | 0,35 | -5,91 | 0,03 | -8,64 | 0,09 |
| | ω_z [rad/s] | -4,29 | 1,14 | -7,34 | 0,38 | 7,52 | 0,14 | 8,49 | 0,13 |
| | ω_R [rad/s] | 14,83 | 0,92 | 11,75 | 0,53 | 13,56 | 0,08 | 12,63 | 0,16 |
| | ω_R [dps] | 849,72 | 52,80 | 673,25 | 30,36 | 777,18 | 4,68 | 723,37 | 9,12 |
| | BrIC | 0,28 | 0,02 | 0,25 | 0,01 | 0,28 | 0,00 | 0,27 | 0,00 |
| | α_R [rad/s^2] | 3299,60 | 165,40 | 3479,77 | 283,24 | 3089,30 | 54,83 | 2795,70 | 36,06 |

**Table 5.7** *Energy level: 8J. MIPS on*

| Energy | 16J | BACK | | BACKRIGHT | | RIGHT | | FRONTRIGHT | |
|---|---|---|---|---|---|---|---|---|---|
| MIPS | on | Theta = 0 deg | | Theta = 45 deg | | Theta = 90 deg | | Theta = 135 deg | |
| | | MEAN | STD Dev | MEAN | STD Dev | MEAN | STD Dev | MEAN | STD Dev |
| Helmet | acc_x [g] | 77,82 | 12,43 | 37,29 | 0,15 | -3,03 | 0,03 | -35,70 | 0,42 |
| | acc_y [g] | -6,47 | 0,63 | 34,20 | 0,10 | 36,62 | 0,50 | 30,75 | 0,64 |
| | acc_z [g] | -24,39 | 0,69 | -26,39 | 0,43 | -10,70 | 0,22 | 10,11 | 0,43 |
| | acc_R [g] | 78,06 | 12,43 | 50,53 | 0,14 | 36,67 | 0,52 | 47,71 | 0,81 |
| Skull | acc_x [g] | 21,64 | 1,47 | 16,37 | 0,27 | -0,95 | 0,09 | -11,06 | 0,75 |
| | acc_y [g] | -3,82 | 0,52 | 6,50 | 0,22 | 21,58 | 0,06 | 15,38 | 0,95 |
| | acc_z [g] | -9,96 | 0,44 | -8,07 | 0,13 | 2,46 | 0,09 | 7,97 | 0,42 |
| | acc_R [g] | 23,41 | 1,73 | 18,70 | 0,33 | 21,73 | 0,07 | 20,08 | 1,19 |
| | HIC* | 4,75 | 0,74 | 3,49 | 0,07 | 3,71 | 0,02 | 3,13 | 0,13 |
| Brain | acc_x [g] | 27,90 | 0,75 | 20,05 | 0,04 | -10,31 | 0,35 | -13,57 | 0,27 |
| | acc_y [g] | -2,72 | 0,29 | -19,09 | 0,08 | 27,05 | 0,41 | -20,28 | 0,21 |
| | acc_z [g] | -13,23 | 1,26 | -13,11 | 0,03 | -21,15 | 0,22 | -15,25 | 0,23 |
| | acc_R [g] | 29,86 | 1,65 | 27,40 | 0,06 | 30,85 | 0,22 | 23,99 | 0,40 |
| | HIC | 36,17 | 5,14 | 28,07 | 0,62 | 34,56 | 0,56 | 20,66 | 0,56 |
| | ω_x [rad/s] | -4,33 | 0,39 | -13,20 | 0,25 | -21,74 | 0,38 | -11,29 | 0,36 |
| | ω_y [rad/s] | 25,36 | 2,21 | 11,81 | 0,20 | -11,14 | 0,07 | -13,47 | 0,17 |
| | ω_z [rad/s] | -5,97 | 1,39 | 15,36 | 0,11 | 16,02 | 0,43 | 12,62 | 0,04 |
| | ω_R [rad/s] | 25,98 | 2,42 | 21,07 | 0,17 | 24,22 | 0,30 | 20,19 | 0,26 |
| | ω_R [dps] | 1488,27 | 138,43 | 1207,40 | 9,63 | 1387,97 | 17,11 | 1156,93 | 14,78 |
| | BrIC | 0,48 | 0,05 | 0,46 | 0,00 | 0,54 | 0,01 | 0,42 | 0,00 |
| | α_R [rad/s^2] | 6560,93 | 605,12 | 8404,27 | 68,34 | 7481,80 | 206,57 | 5051,90 | 125,37 |

**Table 5.8** *Energy level: 16J. MIPS on*

| Energy | 24J | BACK | | BACKRIGHT | | RIGHT | | FRONTRIGHT | |
|---|---|---|---|---|---|---|---|---|---|
| MIPS | on | Theta = 0 deg | | Theta = 45 deg | | Theta = 90 deg | | Theta = 135 deg | |
| | | MEAN | STD Dev | MEAN | STD Dev | MEAN | STD Dev | MEAN | STD Dev |
| Helmet | acc_x [g] | 97,83 | 8,41 | 52,17 | 0,38 | 3,86 | 0,60 | -44,81 | 3,74 |
| | acc_y [g] | -10,22 | 0,44 | 46,46 | 0,60 | 50,37 | 0,73 | 38,99 | 3,19 |
| | acc_z [g] | -32,29 | 1,37 | -35,82 | 0,34 | -18,09 | 1,59 | 13,46 | 0,95 |
| | acc_R [g] | 98,36 | 8,37 | 69,42 | 0,66 | 50,46 | 0,65 | 60,08 | 5,39 |
| Skull | acc_x [g] | 34,47 | 1,23 | 23,65 | 0,79 | -1,22 | 0,05 | -14,69 | 1,59 |
| | acc_y [g] | -5,93 | 0,03 | 9,86 | 0,65 | 29,11 | 0,24 | 19,93 | 1,79 |
| | acc_z [g] | -15,55 | 0,34 | -10,43 | 0,03 | 3,65 | 0,07 | 10,17 | 0,98 |
| | acc_R [g] | 37,09 | 1,22 | 26,81 | 0,80 | 29,35 | 0,23 | 26,03 | 2,43 |
| | HIC* | 10,79 | 0,75 | 6,76 | 0,39 | 6,47 | 0,09 | 4,61 | 0,06 |
| Brain | acc_x [g] | -41,19 | 1,45 | 28,25 | 0,18 | -11,87 | 0,28 | -17,73 | 1,15 |
| | acc_y [g] | 4,75 | 0,58 | -25,19 | 0,01 | 37,55 | 0,15 | -23,63 | 0,09 |
| | acc_z [g] | -20,89 | 0,64 | -19,76 | 0,18 | -30,33 | 0,08 | 17,16 | 0,38 |
| | acc_R [g] | 45,19 | 1,48 | 39,57 | 0,31 | 40,27 | 0,14 | 28,85 | 0,37 |
| | HIC | 71,18 | 2,90 | 49,88 | 0,08 | 61,44 | 0,75 | 32,86 | 1,77 |
| | ω_x [rad/s] | -5,85 | 0,05 | -16,24 | 0,24 | -28,38 | 0,49 | -13,98 | 0,34 |
| | ω_y [rad/s] | 35,41 | 0,47 | 14,26 | 0,04 | -14,06 | 0,32 | -15,49 | 0,25 |
| | ω_z [rad/s] | -9,16 | 0,68 | 19,14 | 0,01 | 20,01 | 0,55 | 14,42 | 0,19 |
| | ω_R [rad/s] | 36,56 | 0,60 | 26,32 | 0,01 | 31,67 | 0,53 | 23,96 | 0,12 |
| | ω_R [dps] | 2094,83 | 34,36 | 1508,15 | 0,92 | 1814,47 | 30,63 | 1366,60 | 10,48 |
| | BrIC | 0,67 | 0,01 | 0,57 | 0,01 | 0,68 | 0,02 | 0,48 | 0,01 |
| | α_R [rad/s^2] | 9792,27 | 228,35 | 11133,50 | 47,38 | 10852,00 | 228,35 | 6473,00 | 243,34 |

**Table 5.9** *Energy level: 24J. MIPS on*

| Energy | 44J | BACK | | BACKRIGHT | | RIGHT | | FRONTRIGHT | |
|---|---|---|---|---|---|---|---|---|---|
| MIPS | on | Theta = 0 deg | | Theta = 45 deg | | Theta = 90 deg | | Theta = 135 deg | |
| | | MEAN | STD Dev | MEAN | STD Dev | MEAN | STD Dev | MEAN | STD Dev |
| Helmet | acc_x [g] | 146,80 | 5,75 | 80,76 | 19,77 | 5,13 | 0,07 | -77,89 | 1,75 |
| | acc_y [g] | -16,22 | 1,02 | 70,09 | 11,79 | 84,25 | 0,97 | 66,73 | 1,45 |
| | acc_z [g] | -47,19 | 5,02 | -47,54 | 14,14 | -37,53 | 1,28 | 27,16 | 0,35 |
| | acc_R [g] | 147,67 | 5,79 | 106,45 | 22,52 | 84,39 | 0,84 | 105,74 | 2,42 |
| Skull | acc_x [g] | 62,94 | 2,09 | 39,02 | 5,01 | -3,30 | 0,75 | -25,30 | 1,12 |
| | acc_y [g] | -7,60 | 0,43 | 18,51 | 2,16 | 49,38 | 0,19 | 35,14 | 1,64 |
| | acc_z [g] | -26,27 | 0,92 | -13,44 | 1,12 | 9,38 | 0,11 | 17,46 | 0,79 |
| | acc_R [g] | 66,37 | 2,29 | 44,04 | 5,72 | 49,91 | 0,12 | 45,06 | 1,98 |
| | HIC* | 34,34 | 4,92 | 15,88 | 4,83 | 13,12 | 0,26 | 9,41 | 0,35 |
| Brain | acc_x [g] | 72,67 | 2,98 | 42,04 | 4,53 | -16,18 | 0,19 | -37,82 | 1,10 |
| | acc_y [g] | 9,64 | 0,22 | 35,66 | 4,88 | 64,30 | 0,48 | -33,65 | 0,48 |
| | acc_z [g] | -38,37 | 2,14 | -30,23 | 4,59 | -47,86 | 0,57 | 27,20 | 0,55 |
| | acc_R [g] | 82,19 | 3,68 | 60,06 | 7,74 | 69,08 | 0,44 | 43,63 | 0,74 |
| | HIC | 158,56 | 5,42 | 105,99 | 13,19 | 142,87 | 1,50 | 83,86 | 2,06 |
| | ω_x [rad/s] | -6,85 | 0,14 | -22,80 | 0,75 | -41,75 | 0,76 | -21,12 | 0,36 |
| | ω_y [rad/s] | 49,19 | 0,75 | 19,14 | 1,31 | -17,03 | 0,24 | -19,93 | 0,19 |
| | ω_z [rad/s] | -14,37 | 0,11 | 8,93 | 25,23 | 26,47 | 1,07 | 15,32 | 0,72 |
| | ω_R [rad/s] | 51,36 | 0,74 | 33,59 | 1,61 | 45,29 | 0,81 | 32,18 | 0,11 |
| | ω_R [dps] | 2942,80 | 42,08 | 1924,83 | 92,52 | 2594,83 | 46,43 | 1843,63 | 6,47 |
| | BrIC | 0,94 | 0,01 | 0,71 | 0,05 | 0,93 | 0,03 | 0,60 | 0,01 |
| | α_R [rad/s^2] | 15899,67 | 196,88 | 14341,00 | 1175,86 | 17755,67 | 384,23 | 11851,67 | 169,33 |

**Table 5.9** *Energy level: 44J. MIPS on*

The tables, even if necessary to comprehend all the huge numbers of data, are difficult to read, so they will be commented and explained using different histograms. The first one will be a graph comparing the resultant acceleration of the CoM for every position of impact and every level of energy for MIPS off and then for MIPS on.

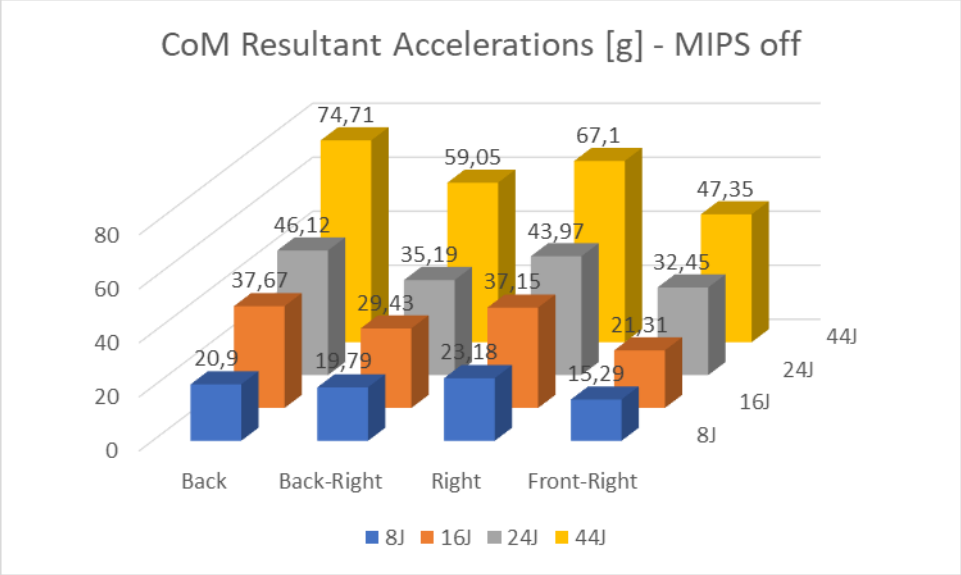


**Figure 5.30** *CoM Resultant Accelerations from every energy level, 8J, 16J, 24J and 44J, and from every different type of impact, Back. Back-Right, Right, Front-Right. MIPS off*

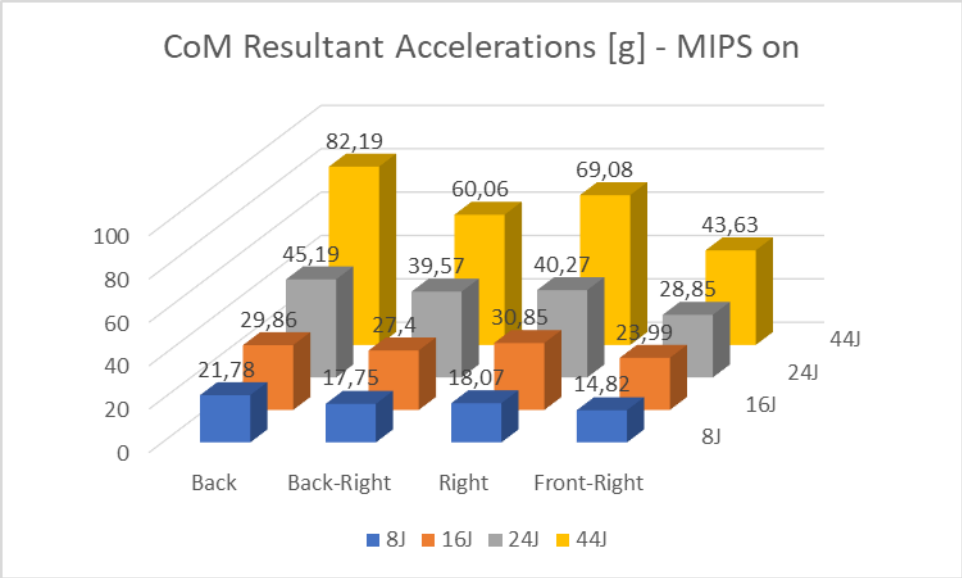


**Figure 5.31** *CoM Resultant Accelerations from every energy level, 8J, 16J, 24J and 44J, and from every different type of impact, Back. Back-Right, Right, Front-Right. MIPS on.*

From both of the previous image can be easily seen that passing from a level of energy to an higher one means an increase in the resultant angular acceleration always. Instead, staying at the same level of energy but passing from a position of the head to another presents some particularities, in fact its easy to see a tendency for Back and Right impacts, that have only one principal direction of impact, to have higher values in respect of Back-Right and Front-Right. Between the two graphs, the first representing MIPS off impacts and the second one representing MIPS on, great differences can't be seen in the values of the peaks, meaning that the little layer posed in the helmets to activate MIPS protection does not influence accelerations, in fact some time a peak is higher in the MIPS off case while another kind of peak, different per position or energy level, is higher in the MIPS on case, without a particular rule behind it.

In the following image, representing the HIC values for MIPS off, the same tendency found in the resultant angular accelerations can be seen and it is so because HIC is calculated on the resultant angular acceleration. HIC of Back and Right impacts are always higher than HIC of Back-Right and Front-Right. To make easier to see that a graph for the selected energy level of 24J with HIC values both from MIPS on and MIPS off cases will be given.

In the table is also presented a row for HIC* that has been calculated on the resultant angular acceleration of the skull. Its values, however, are not comparable with the HIC calculated with the CoM signals because the accelerometer on skull is in a lower position that the accelerometer in the brain, so it recorded a lower value of accelerations.

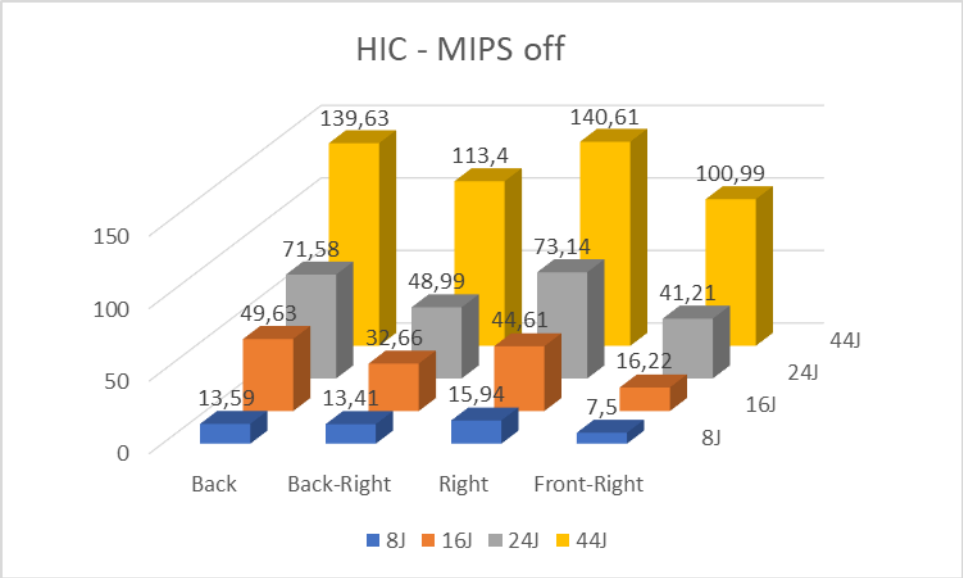


**Figure 5.32** *HIC from every energy level, 8J, 16J, 24J and 44J, and from every different type of impact, Back. Back-Right, Right, Front-Right. MIPS off.*

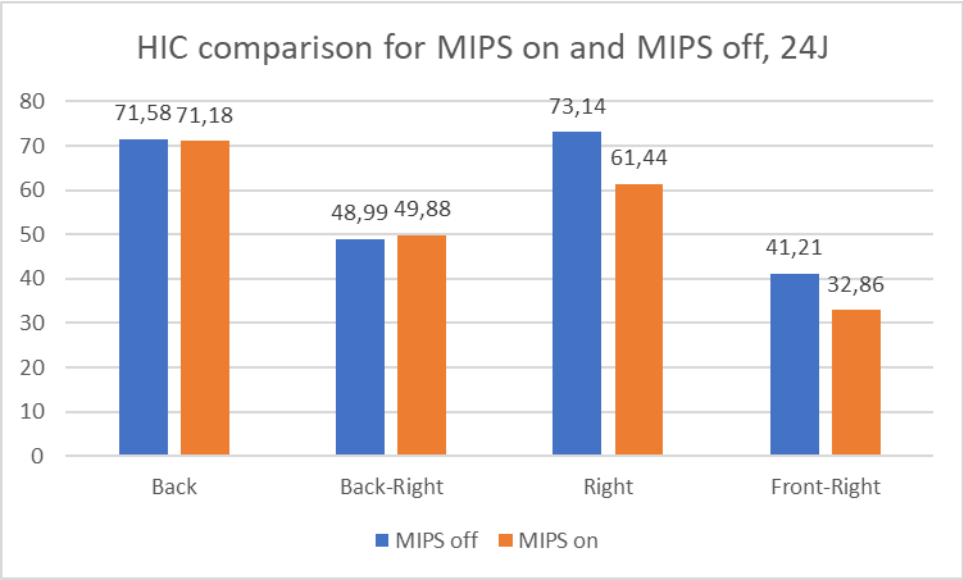


**Figure 5.33** *Comparison of HIC for Helmet for MIPS on and MIPS off, 24J.*

It is now time to analyse and comment the results from the BrIC calculation both from MIPS off and MIPS on.

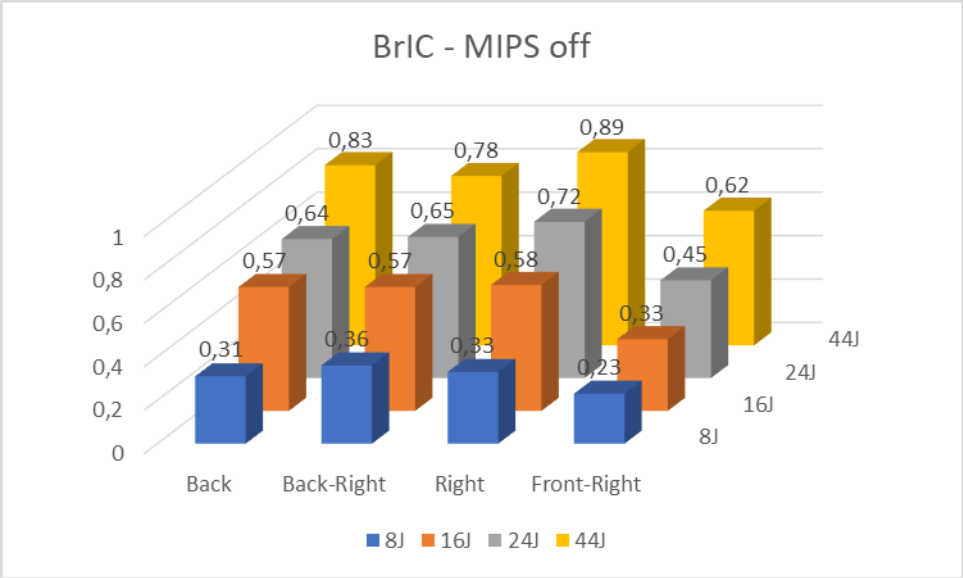


**Figure 5.34** *BrIC from every energy level, 8J, 16J, 24J and 44J, and from every different type of impact, Back. Back-Right, Right, Front-Right. MIPS off.*

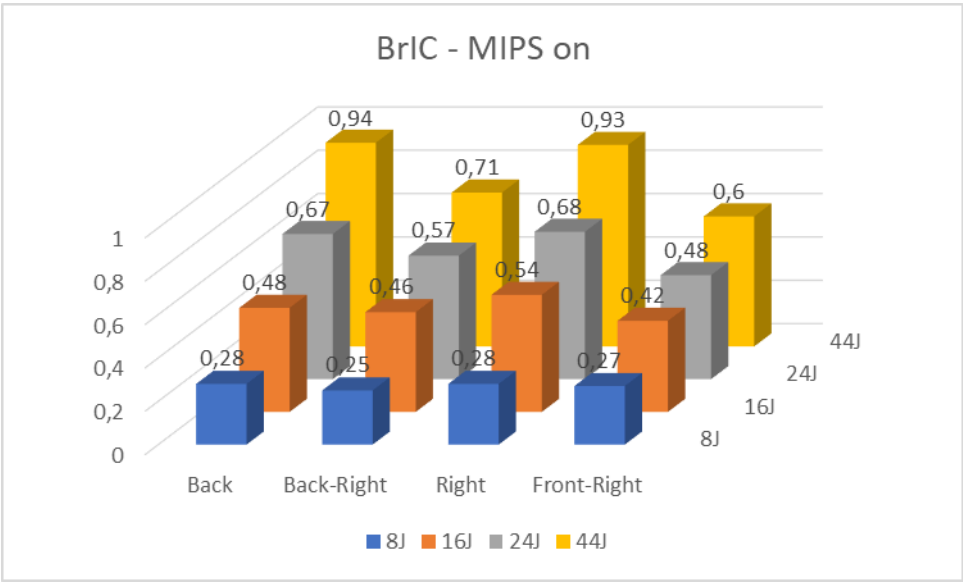


**Figure 5.35** *HIC from every energy level, 8J, 16J, 24J and 44J, and from every different type of impact, Back. Back-Right, Right, Front-Right. MIPS on.*

From the two previous graphs can be seen that there are no meaningful differences between MIPS on and MIPS off. It is not strange, in fact MIPS is created to protect the head from angular accelerations, while BrIC is calculated using the maximum values in mathematical form of the angular velocities signals. The fact that BrIC has very similar values both for MIPS on and MIPS off cases does not mean that MIPS is not effective, in fact even if the peaks of angular velocities have the same value, they can have different temporal extension and so when the signals are derived to obtain the angular

accelerations, differences in the values of the derived function can be found. However the tendency that Back and Right impacts present higher values in respect of Back-Right and front-Right impacts is more difficult to see than in the accelerations or HIC graphs, in fact for BrICit is really evident only for the highest level of energy, 44J.

It is now time to describe in a more detailed way a level of energy and take it as example for every other level. The level chosen is 24J.

In the following image a comparison of resultant angular acceleration for helmet, skull and brain will be assessed. An intersting thing about this graph is that both skull and CoM have higher peaks values in Back and Right impact, instead the helmet has the lowest values of accelerations in the Right tests and this tendency is visible in every table. However as expected the helmet values are always the highest peaks in respect of Skull and brain, second there is CoM and last one is Skull.

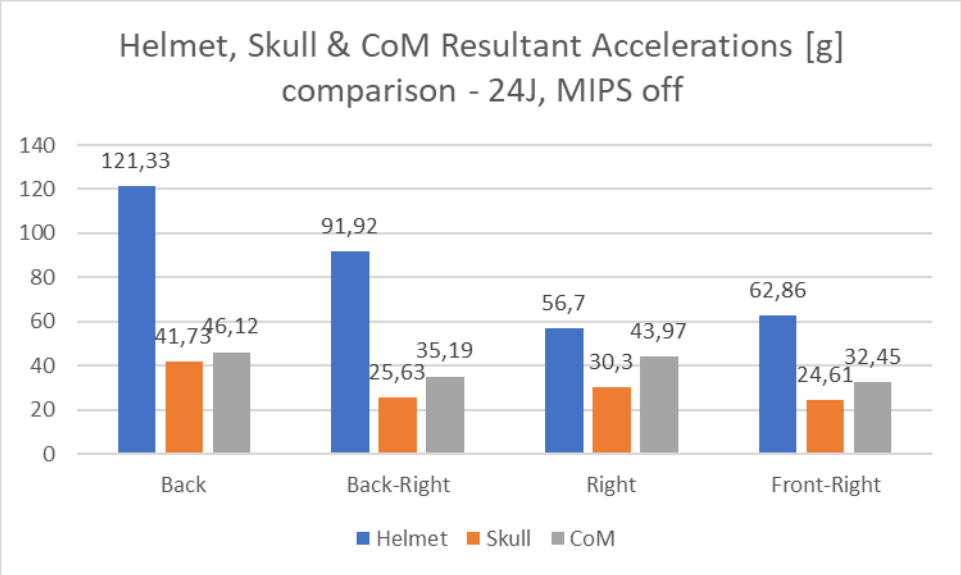


**Figure 5.36** *Comparison of resultant accelerations for Helmet, Skull and CoM, 24J.*

What is now interesting to analyse is the correlation between BrIC and resultant angular accelerations both for MIPS on and MIPS off.

For the calculation of BrIC there is absolutely no differences between MIPS on and MIPS off, even for the Back tests the mean value of BrIC for MIPS on is higher than the one for MIPS off. The other values are however very similar.

For the angular accelerations is different. For every position MIPS on tests have lower values than MIPS off. For the Back impact however the difference is difficult to notice, instead for the other positions the effect is visible, in particular for the Back-Right position were the decrease between the two cases is near 20%.

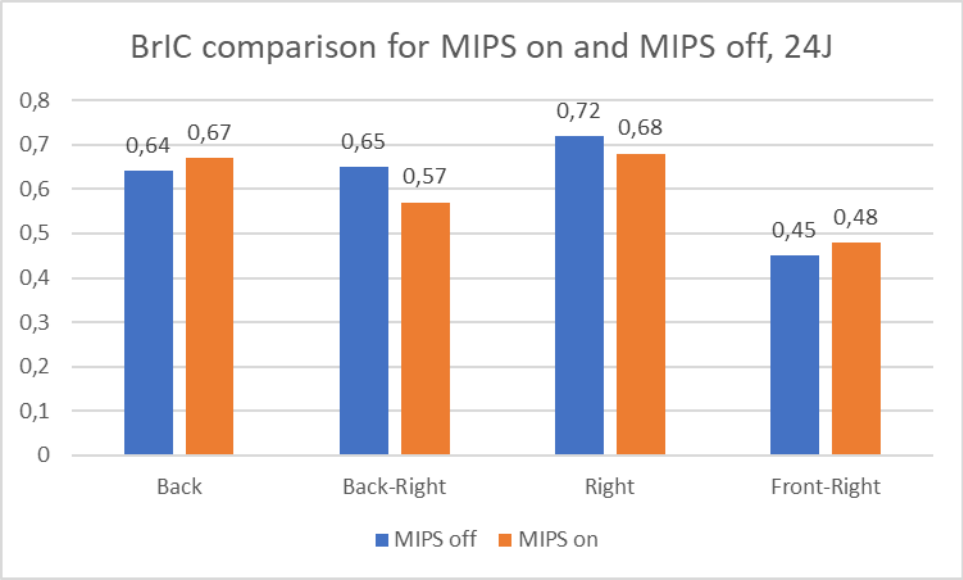


**Figure 5.37** *Comparison of BrIC for MIPS on and MIPS off, 24J.*

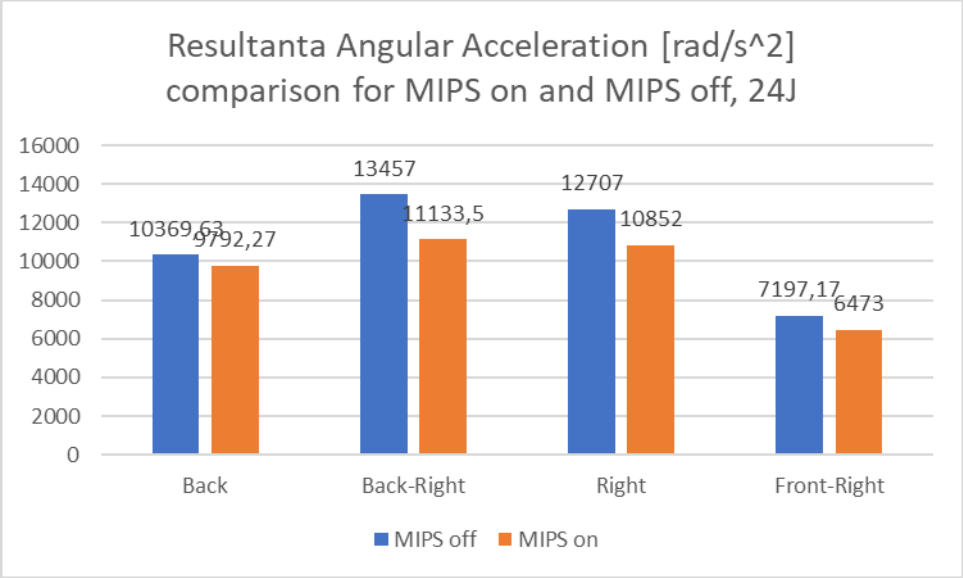


**Figure 5.38** *Comparison of resultant angular accelerations for MIPS on and MIPS on, 24J.*

In conclusion it can be said that IHHS1, even if it does not have the cerebrospinal fluid, is capable of showing a difference between the MIPS on and MIPS off tests for the rotational quantities. It is important this result because MIPS is an already tested and functioning technology and the fact that the head model recognise the difference is a proof of its good functioning, it has a validation meaning.

# Chapter 6

# Instrumented Human Head Surrogate 2: Description and Test Results

In this chapter will be described the IHHS2, the new and improved version of the previously analysed IHHS1. After the first description of the new head surrogate, the data analysis of impacts will be assessed.

IHHS2 has been designed, produced and built by Uriati Federico [4], with the goal of correct some problems that appeared in the first version.

The first problem that was assessed is the head size, in fact IHHS1 needed a XXL size helmet, not the size of a $50^{th}$ percentile human head. To solve this error a scaling of the 3D models used to print the skull, in order to have an head 10% smaller than before. However, the 3D models were also modified in order to have a different way of sealing, in fact the jigsaw cut between the upper and lower pieces of the skull used in the first sensorized head is changed with the one showed in the figure.

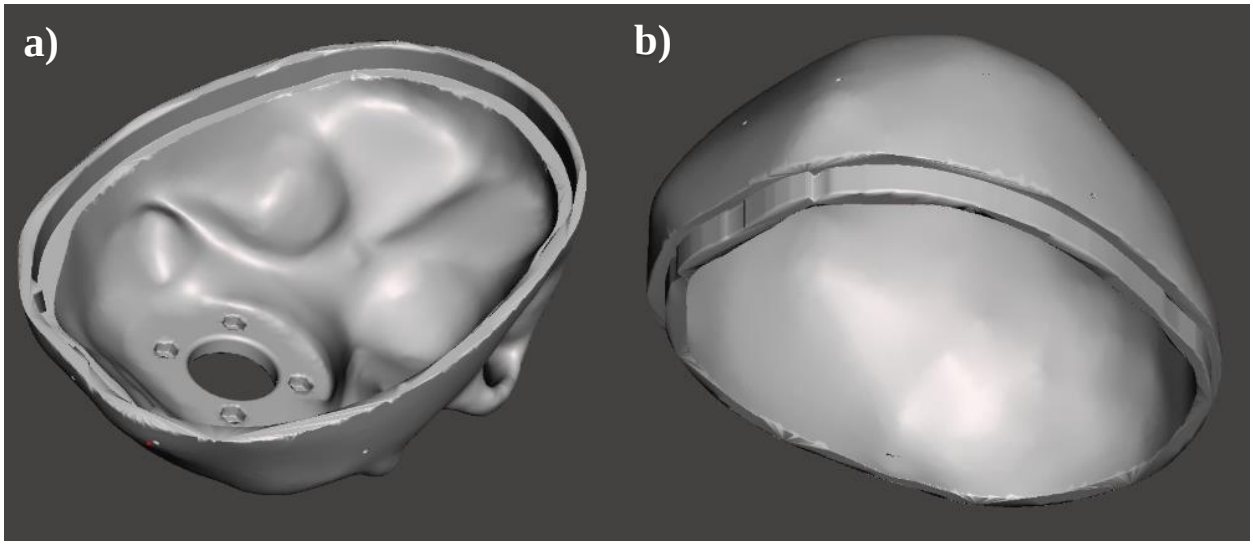


**Figure 6.1** *Upper and lower part of the skull (a) Lower (b) Upper.*

Besides the changing in dimensions, the jaw did not received any variations in shape.
As well as skull, also the dimensions of the layer of skin were scaled. This process lead the new skin to have dimensions decreased of 10% in respect of the original one. The skin needed also a changing in the material, in fact the first instrumented head was realized in *Plastil Gel 00-25*, instead now the silicon rubber used is *Plastil Gel 01-30*.

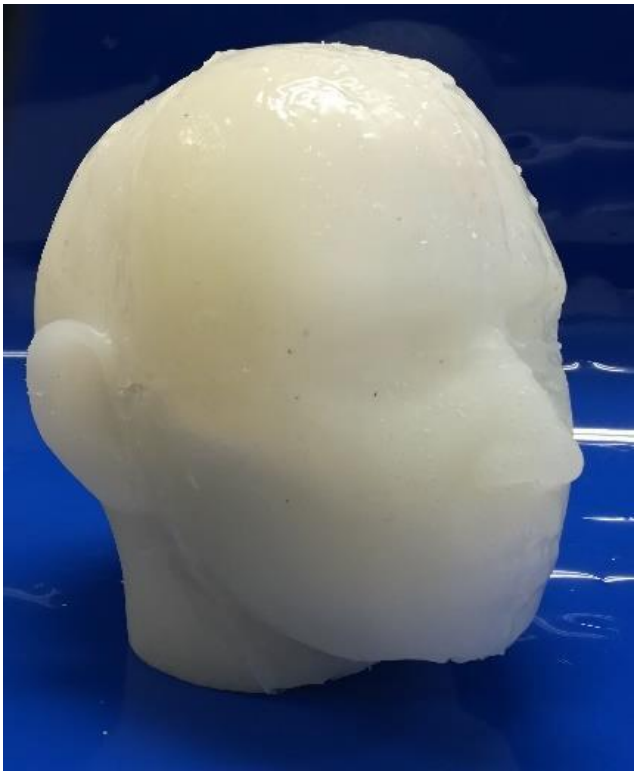

**Figure 6.2** *Skin of IHHS2.*

For what concerns the brain, it was decided to use a softer rubber than before, that is *Plastil Gel 00-20*, instead of *Plastil Gel 01-30*. The brain too was reduced in its dimensions to the 90% of the initial model, that means that all the parts used to assemble the head were reduced of 10%.
Inside the brain are placed different types of sensors, both accelerometers and gyroscopes. In the disposition of the sensors some changes has been done. Instead having 8 accelerometers as in IHHS1, there is one less in IHHS2. The accelerometer eliminated is Cerebellum-Center, CC. As before there are 2 accelerometers in the top layer, always called TL and TR, in the middle layer there are ML, MR and obviously CoM, and in the end there is the lower or cerebellum layer with CL and CR. The accelerometers of the top and middle layer are part of the same coronal plane of CoM. In the following table will be given the complete name of the sensors, and their coordinates in order to locate them in a precise way.

| Sensor Name | Abbreviation | X [mm] | Y [mm] | Z [mm] |
|---|---|---|---|---|
| Top-Left | TL | 0.0 | +20 | +42 |
| Top-Right | TR | 0.0 | -20 | +42 |
| Mid-Left | ML | 0.0 | +37 | 0.0 |
| Center of Mass | CoM | 0.0 | 0.0 | 0.0 |
| Mid-Right | MR | 0.0 | -37 | 0.0 |
| Cerebellum-Left | CL | -26 | +32 | -45 |
| Cerebellum-Right | CR | -26 | -32 | -45 |

**Table 6.1** *Position of the accelerometers.*

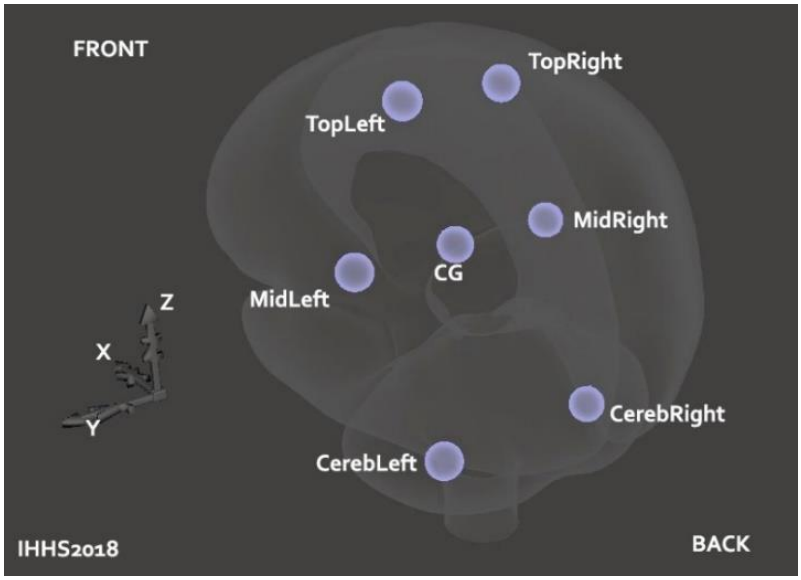


**Figure 6.3** *Back-Left view of the accelerometers placed inside the brain.*

This time in the head is placed an additional gyroscope, beside the one placed in CoM. Even if the Gyr-CoM is called gyroscope, it is made up of two biaxial gyroscopes mounted on the same plate in order to obtain the signals in all the directions. The additional gyroscope is a substitute of the accelerometer of IHHS1 placed in the center of cerebellum. This accelerometer, differently from Gyr-CoM, is only a biaxial gyroscope recording angular velocities around X and Y direction.

| Sensor Name | Abbreviation | X [mm] | Y [mm] | Z [mm] |
|---|---|---|---|---|
| Center of Mass | Gyr-CoM | 0 | 0 | 0 |
| Cerebellum Center | Gyr-CC | -26 | 0 | 45 |

**Table 6.2** *Position of the gyroscopes.*

As already explained and shown through figures in Chapter 4 in the section about the experimental setup, IHHS2 also have two other accelerometer and one gyroscope. One accelerometer is placed on the forehead of the skull in correspondence with CoM and the other is placed on the helmet exactly above CoM in the vertical direction. The additional gyroscope is used to measure the angular velocity of the skull and is placed on the top of it exactly above CoM.
It is now time to describe the pressure sensors position. In IHHS2 there are 10 pressure sensors placed in small sockets carved on the inner surface of the skull, both in the lower and upper pieces of it.

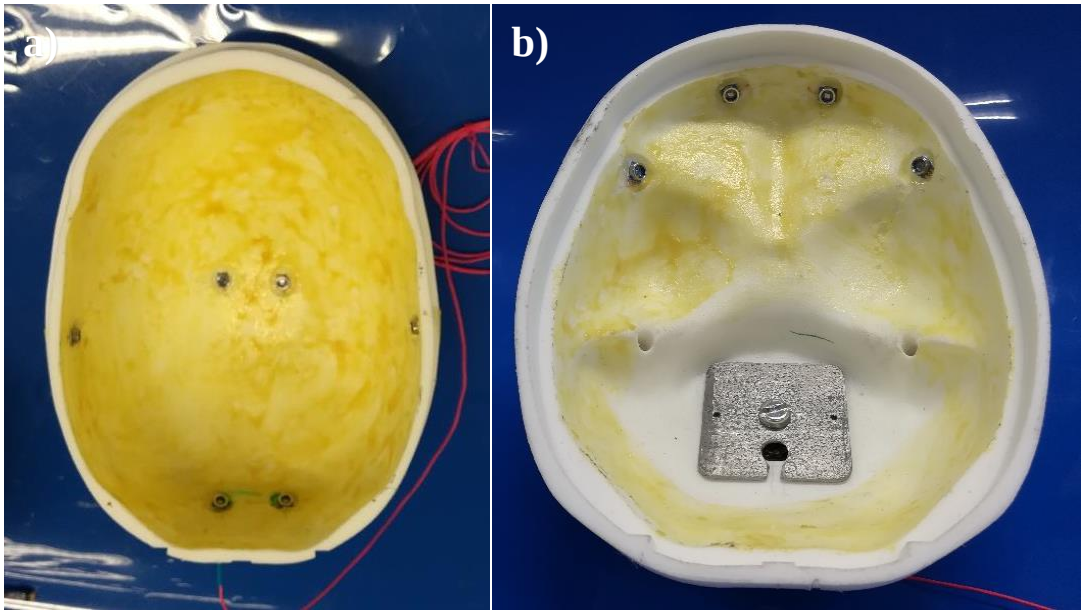


**Figure 6.4** *Internal surface of skull (a) Upper piece of skull (b) Lower piece of skull.*

Pressure sensors are typically called with the name on which they are placed. In the following table their name, abbreviation and coordinates in respect of the CoM will be shown.

| Sensor Name | X [mm] | Y [mm] | Z [mm] |
|---|---|---|---|
| Occipital Left | -80 | 15 | 0 |
| Occipital Right | -80 | -15 | 0 |
| Frontal Left | 95 | 15 | 0 |
| Frontal Right | 95 | -15 | 0 |
| Parietal Left | 0 | 15 | 68,5 |
| Parietal Right | 0 | -15 | 68,5 |
| Temporal Left | 0 | 70 | 0 |
| Temporal Right | 0 | -70 | 0 |
| Sphenoid Left | 57,5 | 55 | -4,5 |
| Sphenoid Right | 57,5 | -55 | -4,5 |

**Table 6.3** *Position of the pressure sensors.*

As last thing to remember about IHHS2 is the silicon oil used in place of the cerebrospinal fluid. It was chosen *Q8 Formula Ultra V 0W-20*, characterized by a density of 0.845 g/cm$^3$, a dynamic viscosity of 41,15 mPas and a kinetic viscosity of 48,7 cSt at the temperature of 40°C.

## 6.1 Data Analysis of IHHS2

In this section a description of the tests performed on IHHS2 will be given. In the first place, the program of impact tests is necessary. In this case, differently from IHHS1, only the energy levels of 16J and 24J were performed. 8J level was not useful because not too much strong, instead in 44J level the hammer is so fast that the time taken by the laser beam trigger system to start the acquisition is long enough to have the signals of the accelerometers not fully recorded, meaning that there was no horizontal plateau of the accelerations before the first peak and also a little piece of the same peak is not saved. The performed tests are 48, in fact 4 different positions are analysed, Back, Back-Right, Right and Front-Right, for only 2 energy levels, for both MIPS on and MIPS off and for 3 repetitions of each impact.

| Position | | Impact | |
|---|---|---|---|
| Name | θ [deg] | Energy [J] | α [deg] |
| Back | 0 | 16 | 41 |
| | | 24 | 51 |
| Back-Right | 45 | 16 | 41 |
| | | 24 | 51 |
| Right | 90 | 16 | 41 |
| | | 24 | 51 |
| Front-Right | 135 | 16 | 41 |
| | | 24 | 51 |

**Table 6.4** *Test program to repeat 3 times and both for MIPS helmet and no-MIPS helmet. In the table is also presented the correlation between the name defining the position with the angle between direction of movement of the hammer and the X axis direction of the head reference system and the correlation between the level of energy and the angle between the pendulum arm and the vertical direction.*

In the following paragraphs will be described in detail 4 tests, Back, Back-Right, Right and Front-Right impact at energy level of 24J with MIPS not activated. The whole number of tests will be analysed via tables.

### 6.1.1 Back Impact

In this section, before will be presented the signal recorded during a Back Impact, at 24J of energy level with no MIPS, by the sensors in or mounted on IHHS2, then they will be explained and commented and some meaningful comparisons with the results from IHHS1 will be done.

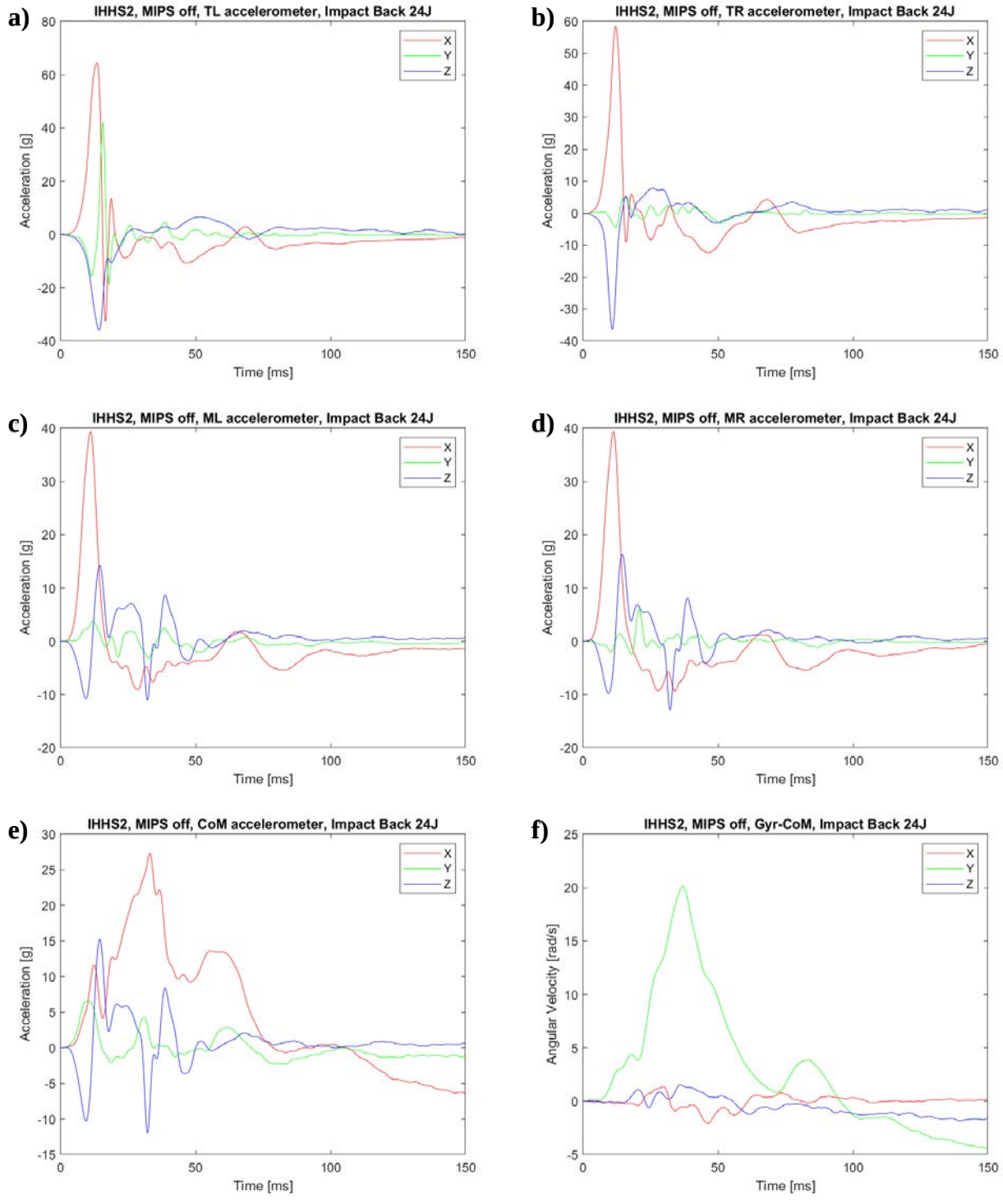

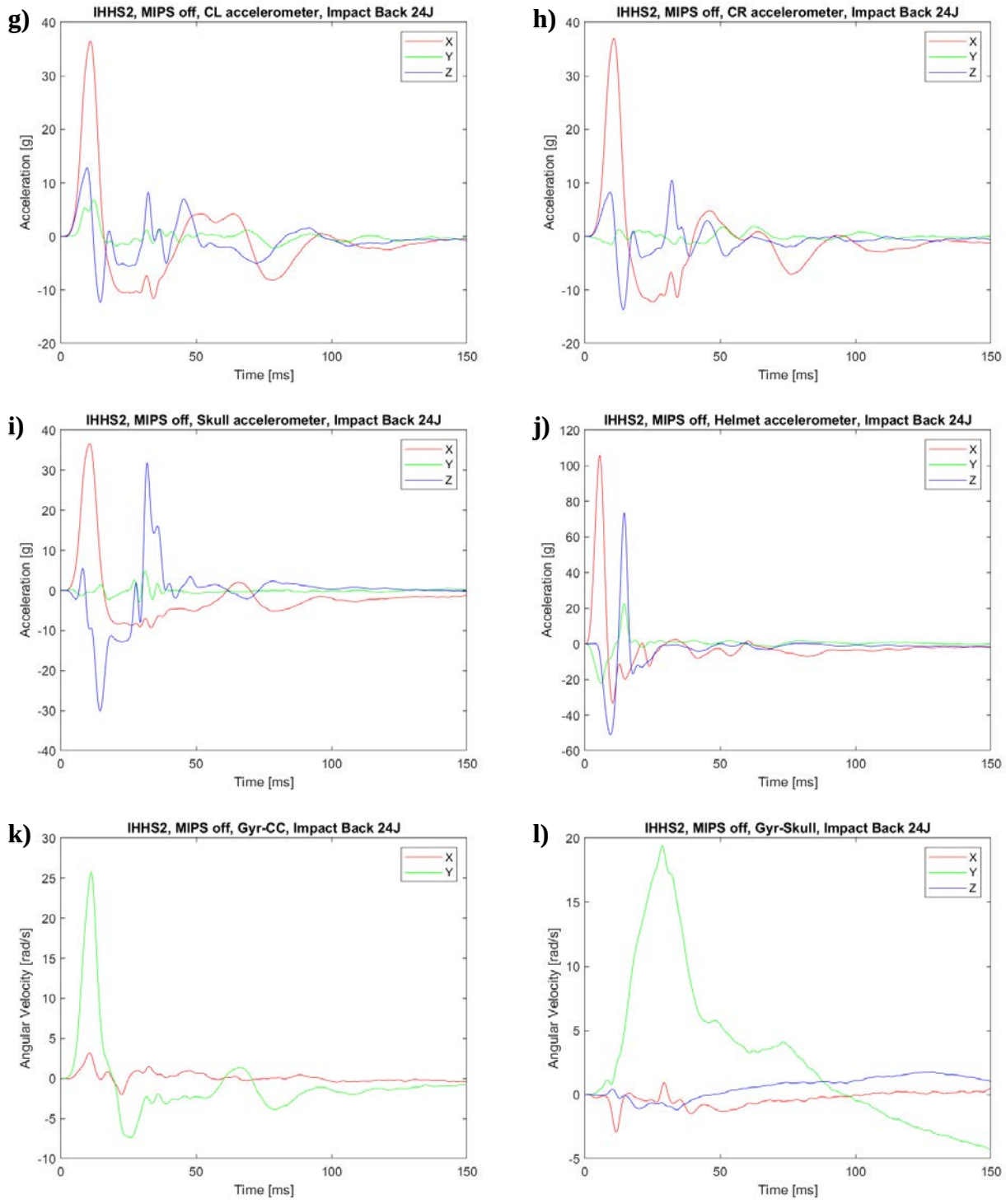


**Figure 6.5** *Signals recorded by IHHS2 with MIPS off during Impact Back 24J. (a) TL (b) TR (c) ML (d) MR (e) CoM (f) Gyr-CoM (g) CL (h) CR (i) Skull (j) Helmet (k) Gyr-CC (l) Gyr-Skull.*

This is a Back Impact so it is easy to see that the principal direction of impact is X, in fact all the accelerometer have the very high peak in that direction. In the Y direction the values of the signal is not high, instead in the Z direction, as for IHHS1, it can be seen that all the accelerometers belonging to the same coronal plane of CoM are pushed down, while CL and CR, which are placed behind, have

the first peak that is positive. The helmet and skull accelerometer also recorded a second positive peak in the Z direction. This peak is even higher of the first negative peak and it is difficult to interpret. In fact all the other accelerometers have a second peak in Z with a different sign in respect of the first one, but it is not so strong, it is lower or at least as the same values of the first one without surpassing it. The fact that every accelerometer has this kind of behaviour suggests that the second peak in Z is the rebound that brings back the head toward the initial position. IHHS2 has two more sensors than IHHS1, and they are Gyr-CC and Gyr-Skull. As expected both present a high and positive angular velocity around the Y direction, that is transverse in respect of the direction of impact. It is interesting to see the differences between the signals of the various gyroscopes, in fact the sensors in CoM and Skull have a very similar peak both for shape and value in the Y direction, instead Gyr-CC is characterized by a higher angular velocity. This could be caused by the fact that cerebellum rotates with the principal body because is connected to the brain, but it is also an appendix, so it has its own freedom of rotating around itself. The angular velocity recorded by Gyr-CC around Y axis is near the value of 25 rad/s, instead both Gyr-CoM and Gyr-Skull stays at about 20 rad/s.
The presented graphs are similar however to what has already been explained about IHHS1, but there is an accelerometer in particular that has a different shape of the signals and so a different behaviour. It is therefore needed to make a comparison between the CoM of IHHS2 and IHHS1 to see how the fluid inside the head influences the sensors.

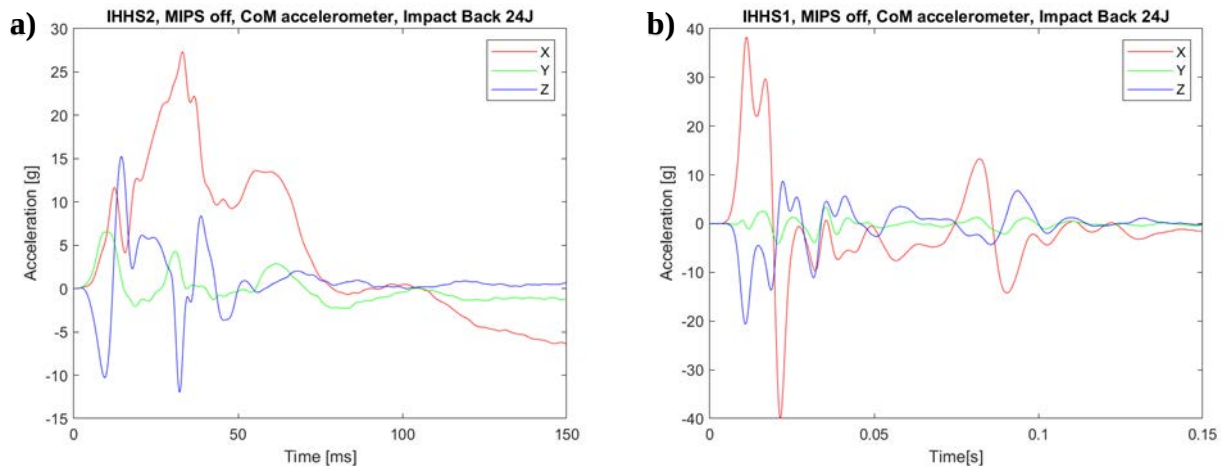


**Figure 6.6** *Comparison of signals recorded by CoM of the two instrumented human head surrogate models during impact Back, 24J, MIPS off. (a) CoM of IHHS2 (b) CoM of IHHS1.*

The shape of the X direction for CoM are very different in the two head models. In IHHS1 the X direction is characterized by two positive peaks, with the second one appearing before the fading of the first one, and a third negative peak very strong, in fact the third peak has a value in mathematical

forma that is higher than the first two peaks. Instead in IHHS2 the X direction of the accelerometer as a very large peak both lower. Both the augmented time window in which the peak is developed and its lower value in respect of the peaks of IHHS1 are due to the presence of the cerebrospinal fluid that acts as a dumper.

Because of the effect of the liquid inside the head, a comparison of the helmet, skull and CoM signal is needed.

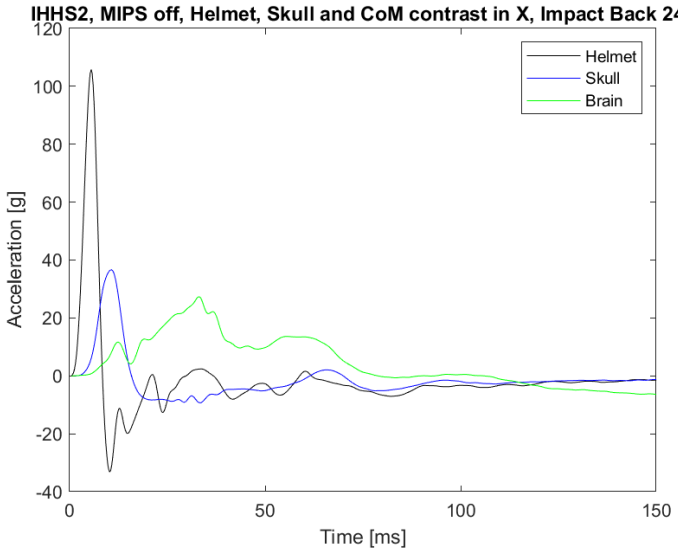


**Figure 6.7** *Comparison of accelerations of Helmet, Skull and CoM in the X direction.*

What can be seen by the superior graph is that the order of the peaks is respected. The first peak to appear is always the one from the helmet, then there is the skull and last is the CoM. This order is easier to detect than in IHHS1 because the dumper effect of the liquid makes the brain to begin it movement with a major delay in time. In IHHS1 a lot of times the skull in the principal direction of impact had a lower peak than CoM, this time instead is the opposite. This is caused by two reasons, in fact the accelerometer of skull in IHHS2 is at the same height of CoM instead in IHHS1 was under the hard palate, while the second cause is the presence of the silicon oil, that produces in CoM a shape of the peak less sharp and with lower values.

About the Z signal of CoM IHHS2, there is one thing to notice. In fact it was not able to record informations, because the accelerometer is damaged. So a fictional Z signal was created by calculating the mean values of the Z signals from the ML and MR sensors.

It is also needed to comment the differences between the angular velocities and accelerations of CoM in IHHS1 and IHHS2.

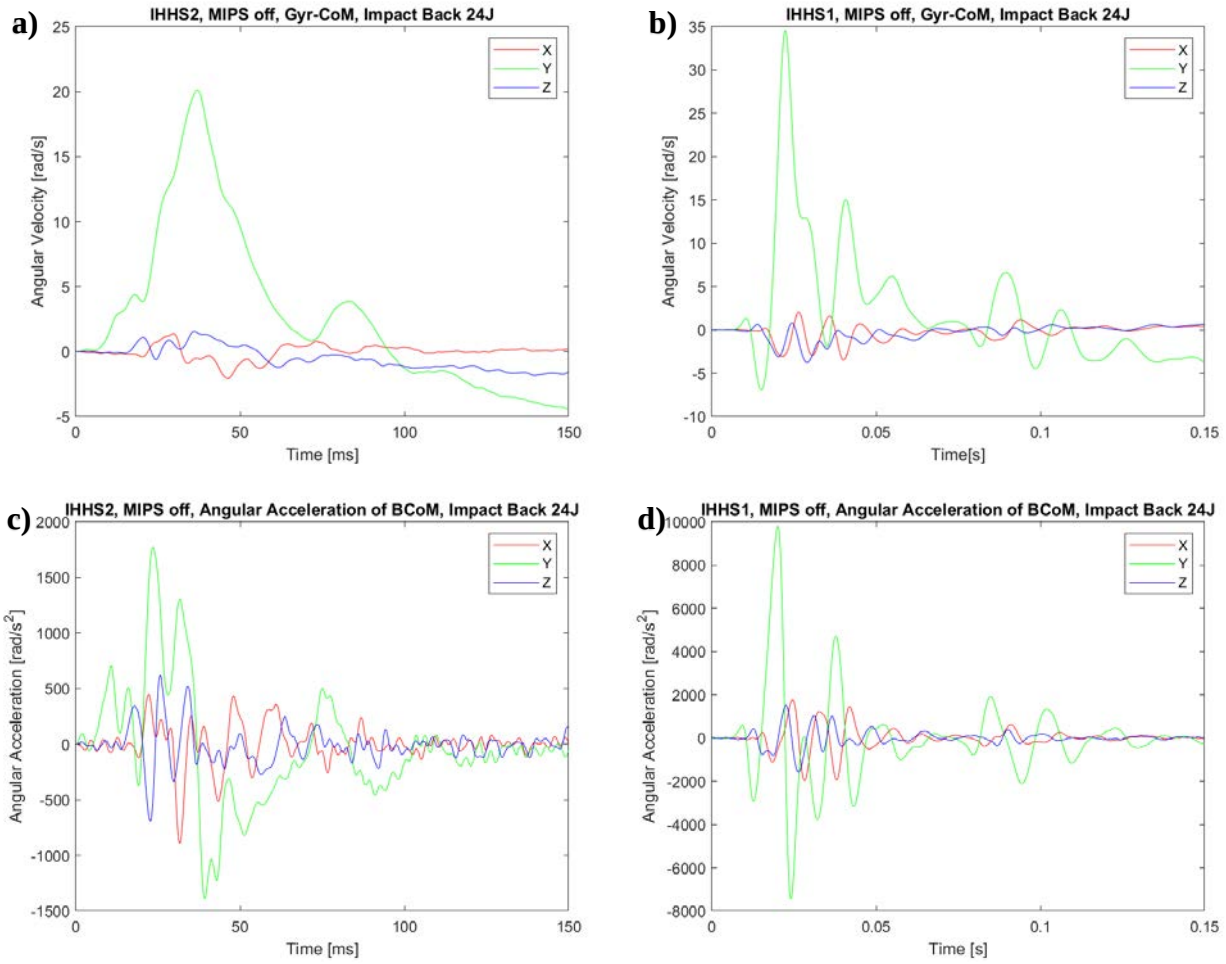


**Figure 6.8** *Comparison of angular velocities and accelerations in CoM between IHHS1 and IHHS2 in impact Back, 24J, MIPS off. (a) angular velocity, IHHS2 (b) angular velocity, IHHS1 (c) angular acceleration, IHHS2 (d) angular acceleration, IHHS1.*

The differences between Gyr-CoM of IHHS2 and IHHS1 are in shape and peaks value. The angular velocity in IHHS2 is large but has a low peak, instead the peak in IHHS1 is very sharp and lasts a shorter time. IHHS2 is characterized by a peak that touches 20 rad/s instead IHHS1 has the angular velocity peak about 35 rad/s. The fact that the peak of the first head model is a lot higher and has a sharp shape influences the angular accelerations bringing it to values around 10000 rad/s$^2$ in the Y direction, while IHHS2 that has a lower and wider peak is characterized by an angular acceleration under 2000 rad/s$^2$. This great difference in values is completely due to the presence of the silicon oil used to simulate the cerebrospinal fluid.

It is now time to describe the behaviour of pressure sensors, thing that was not possible for IHHS1. In IHHS2 the pressure sensors are placed in order to understand the different movements between the right and the left lobe. In fact, in the frontal, in the occipital and in the parietal regions are placed 2 sensors per bone, instead of only one. The frontal bone has attached to it 2 pressure sensors called

Frontal left and Frontal Right at a very low distance, 3 cm only, in order to detect differences in pressure near the extremities of the lobes, instead of having one in a central position, corresponding to the space left between lobes. The same is for the Occipital region with Occipital Left and Occipital Right and the Parietal region with Parietal Left and Parietal Right, also with 3 cm for distance.

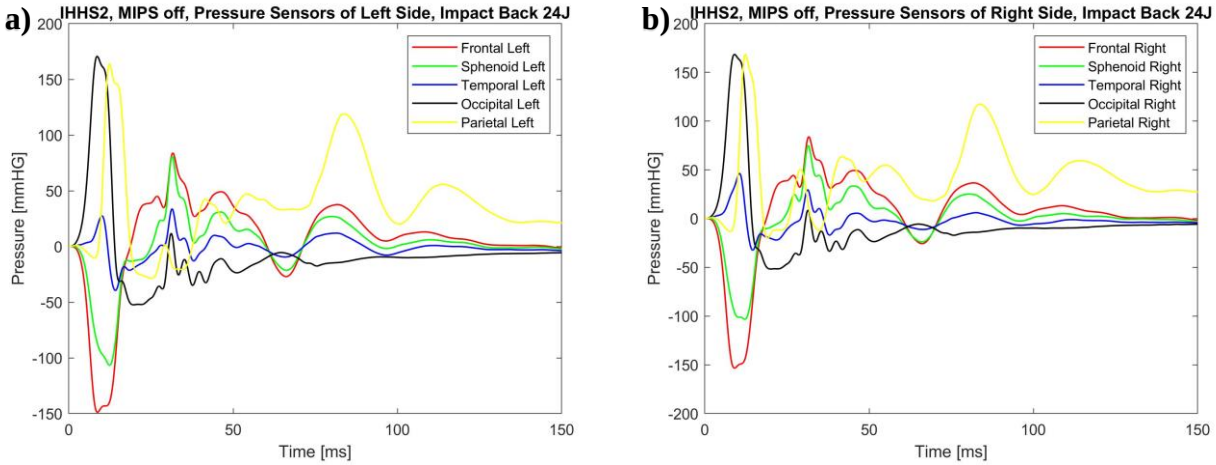


**Figure 6.9** *Pressure sensors (a) Left side of the head (b) Right side of the head.*

From both the graph of the right side and the left side, the same behaviour in right and left lobe can be detected. Both Occipital left and Occipital Right present a high pressure, in fact they are the nearest sensors to the region of impact and the skull begins its motion before the brain, so there is this period of time in which the skull is moving in the X positive direction while the brain is still unmoved or is moving slowly and the distance between the two objects is decreasing. The decreasing distance between skull and brain means that the cerebrospinal fluid is compressed and obliged to slide around the brain going toward the frontal part of IHHS2, where the distance between skull and brain is instead increasing. That's the reason why both Frontal Left and Frontal Right are in depression, and the same is for Sphenoid Left and Sphenoid Right. Interesting is the behaviour of Parietal sensors, both placed on top of the skull. They have a high and positive pressure. This could be caused by the fact that while the head is pushed forward by the hammer, it also rotates around the Y axis and at the same time the brain is moving in the positive direction of X. For what concerns the Temporal sensors, that are placed in lateral positions, the pression firstly increase and then decrease, always at low values. This is a confirmation of the fact that during a Back impact the brain has alternate phases of firstly positive deformation and then compression and so on.

The signal recorded by the pressure sensors can be used to understand the behaviour and movements of the brain, but no considerations on the value of the peaks can be done because the signals often saturate. The row and no filtered signals presents in correspondence of the highest point of peaks a

plateau region. This plateau region is not visible because of the 7$^{th}$ order low-pass filter at 200 Hz. The signal saturates not because of the sensors, but because of the board used to record the signals.

### 6.1.2 Back-Right Impact

In this section a Back-Right impact occurring at 24J energy level with MIPS off will be discussed.

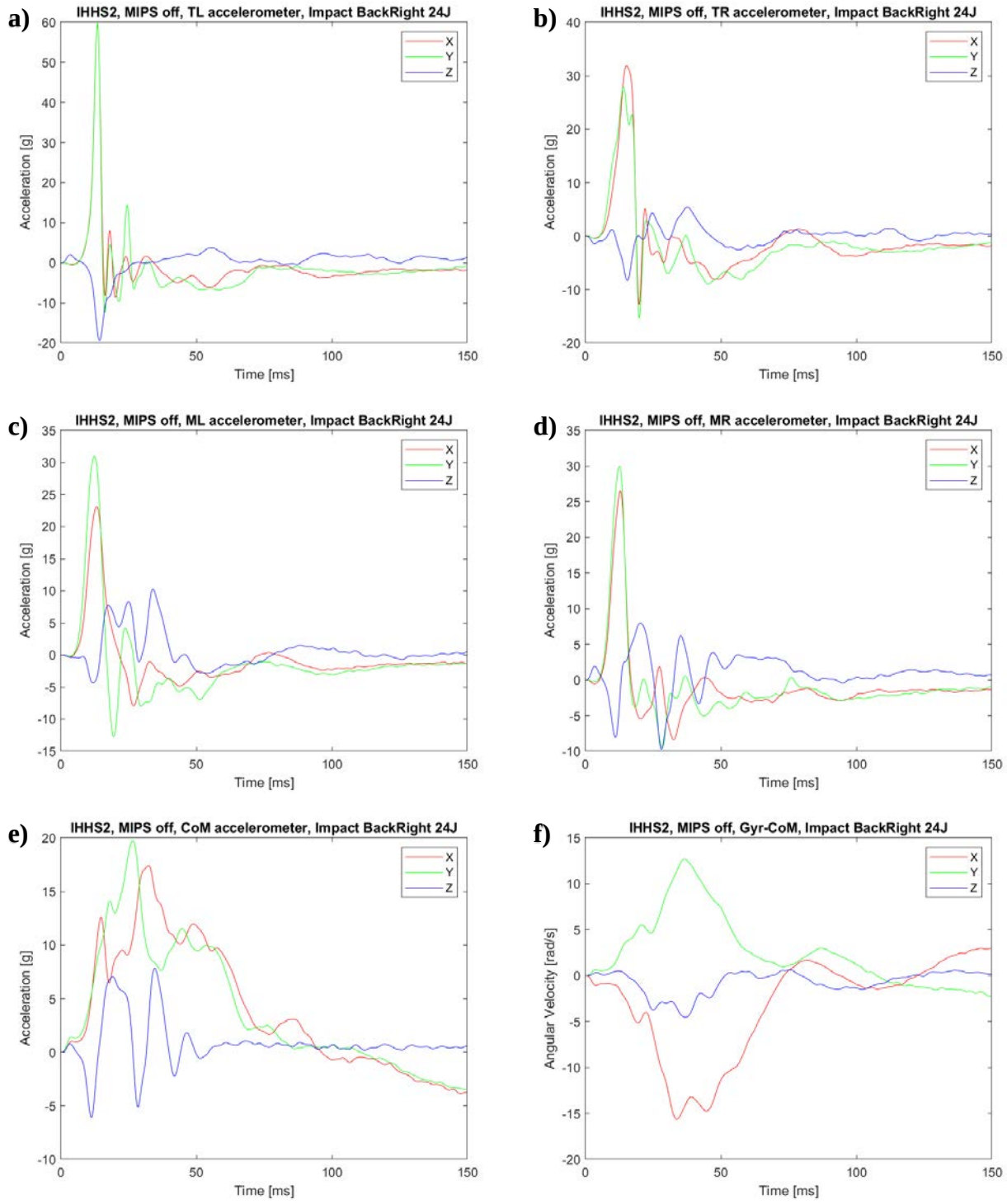

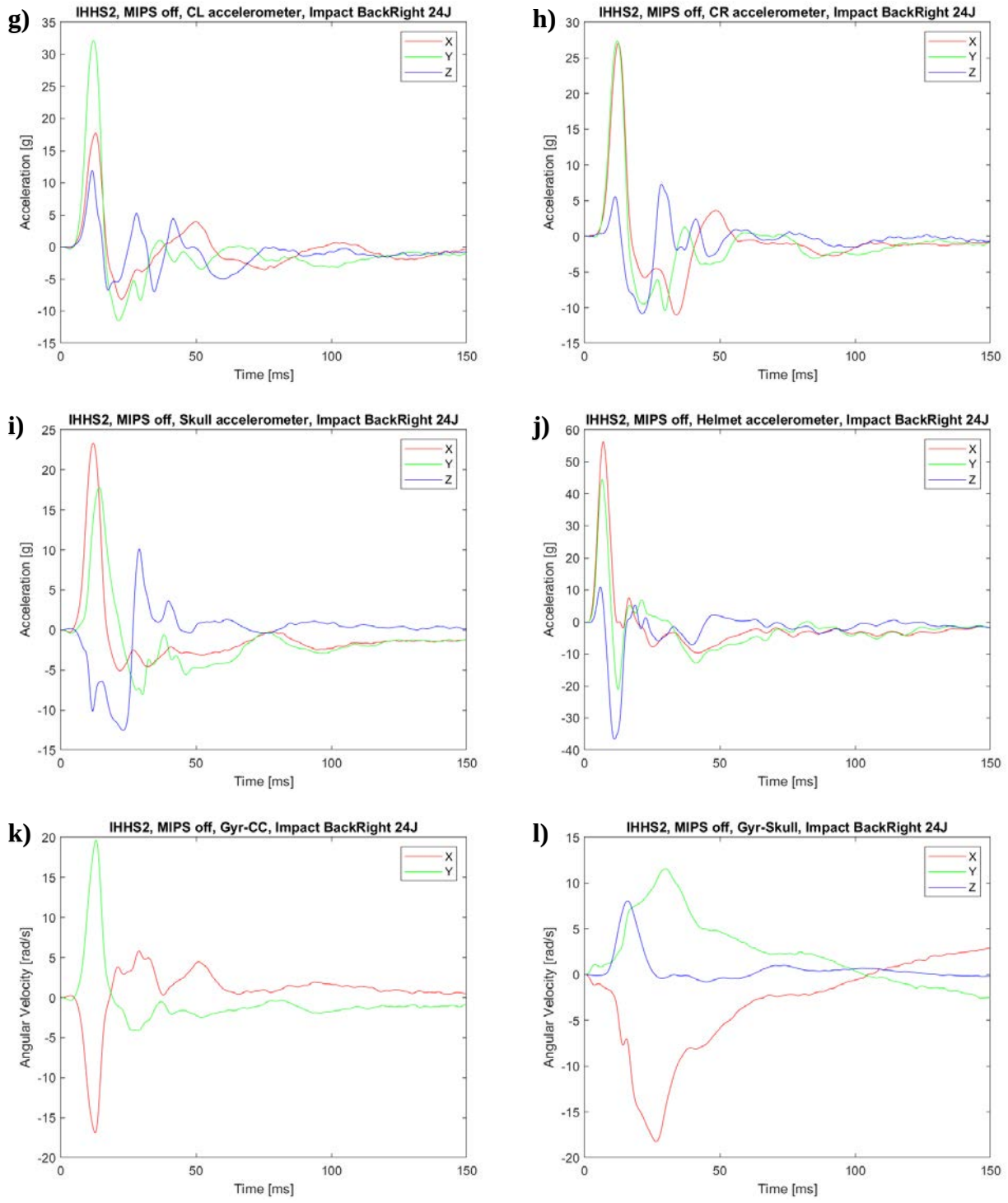


**Figure 6.10** *Signals recorded by IHHS2 with MIPS off during Impact Back-Right 24J. (a) TL (b) TR (c) ML (d) MR (e) CoM (f) Gyr-CoM (g) CL (h) CR (i) Skull (j) Helmet (k) Gyr-CC (l) Gyr-Skull.*

It is a Back-Right impact, so there must be 2 principal directions of impact, X and Y. In fact every accelerometers are characterized by a first positive peak both in the X and the Y direction, instead the gyroscopes measure a first positive angular velocity around Y and a first negative angular velocity around X axis. Watching *Figure 6.10 (f), (k)* and *(l)* a comparison between brain, cerebellum and

skull can be done regarding the angular velocities. It can be seen that the angular velocity around the X axis for each sensors has very similar values near 15 rad/s, instead what is different in values are the angular velocities around the Y axis with a peak for cerebellum that is higher the peaks of CoM and Skull. It could suggest that the cerebellum has more freedom in movement around the Y axis, while for the X axis is strongly related to the movement of the whole head. However must be noticed that the peaks of cerebellum are much sharper that CoM and Skull and that means that integrating in respect of time the signals, the angles of rotation travelled by the sensor in cerebellum are smaller than the ones travelled by skull and CoM.

In order to highlight the differences between IHHS1 and IHHS2 the signals recorded by accelerometer in CoM need to be commented.

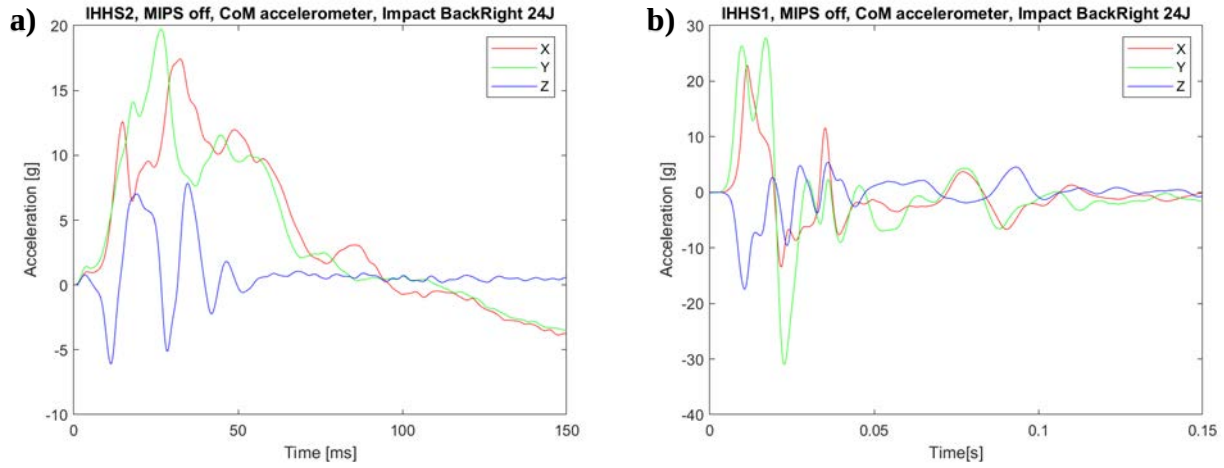


**Figure 6.11** *Comparison of signals recorded by CoM of the two instrumented human head surrogate models during impact Back-Right, 24J, MIPS off. (a) CoM of IHHS2 (b) CoM of IHHS1.*

As in Back impact, also in Back-Right impact the peaks of acceleration of CoM in IHHS2 are wide and with lowest values of peaks compared to what is recorded by IHHS1. The peak in CoM of IHHS1 is sharper, higher and with two tips. The fact that the peak of CoM in IHHS1 is really composed by two overlapping peaks was described with the different time of motion of the two lobes as explained through *Figure 5.19 (b).* Instead in IHHS2 this phenomenon is not visible neither in the X nor in the Y direction of accelerations. It can be seen that the peaks both in X and in Y for IHHS2 have different tips, they are jagged, and the first tip in the X direction of CoM happens in the same temporal window of the peaks from ML and MR. It is like the motion of the two lobes, where ML and MR are placed influences and make the motion of CoM to begin, but there are a various number of following tips caused by different phenomenon. Probably the whole peak of acceleration in CoM is made by different peaks from other causes that could be shock waves travelling through the silicon oil.

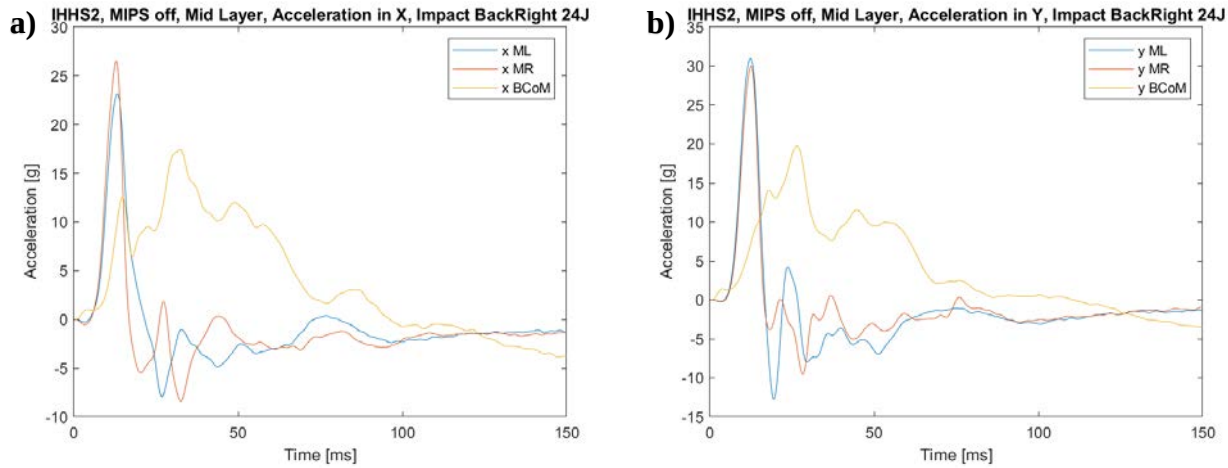


**Figure 6.12** *Comparison of signals from the middle layer in the principal directions of impact. (a) X direction. (b) Y direction.*

As in the previous described impact, is really easy to see the delay in time of CoM compared to helmet and skull. This time, instead of being identified only in X direction, also in Y direction can be found.

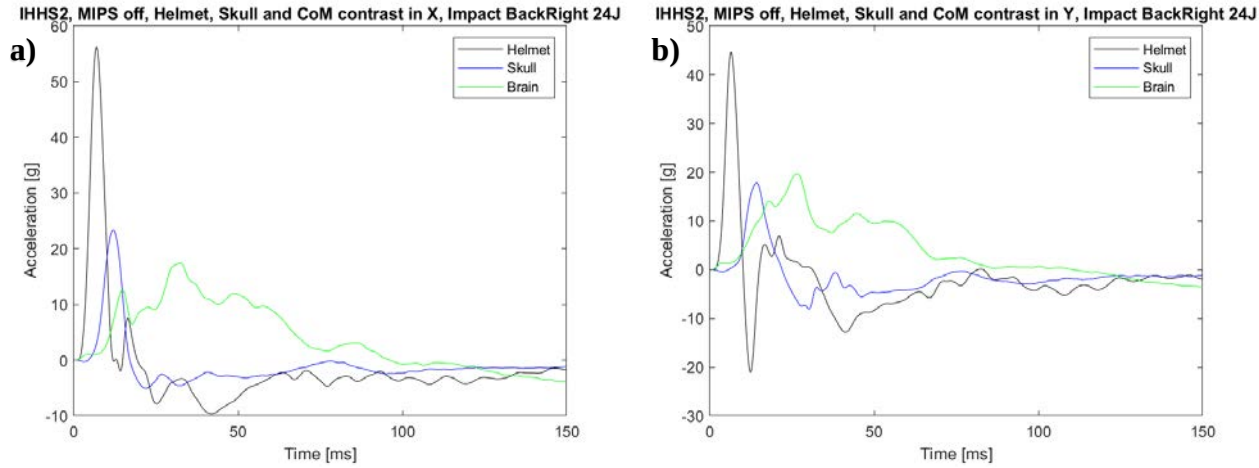


**Figure 6.13** *Comparison of accelerations of Helmet, Skull and CoM (a) X direction (b) Y direction.*

In the following figure the differences of angular velocities and accelerations between CoM of IHHS2 and IHHS1 will be assessed. In this type of impact the shape, temporal length and height of the peaks of angular velocity around X and Y are very similar. The greatest difference in angular velocity is the Z signal. In IHHS2 seems that there is no rotation around the axis passing through the neck, instead in IHHS1 the peak in Z is the highest. This could be caused by the presence of the cerebrospinal fluid. The strong peak in Z of IHHS1 is more similar to a vibration around the vertical direction, in fact, if an integration will be done, it should be easy to see that the angle travelled by the brain is small. Instead the fluid, acting like a dumper, eliminates this kind of vibrations and only the major movement

of the whole head is remained. For what concerns the angular acceleration can be seen that the peaks have an order of magnitude as difference. IHHS1 have much greater peaks in angular acceleration than IHHS2.

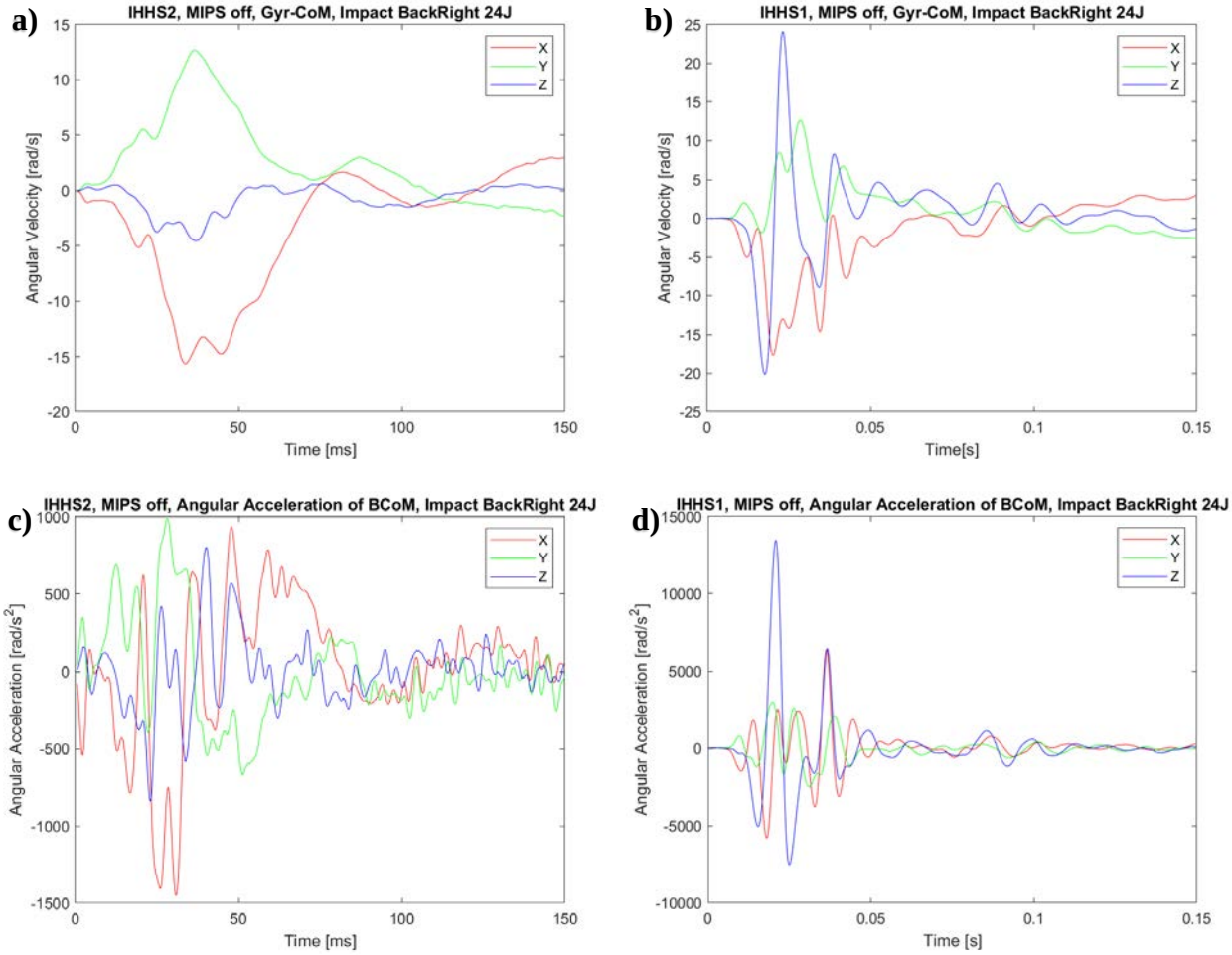


**Figure 6.14** *Comparison of angular velocities and accelerations in CoM between IHHS1 and IHHS2 in impact Back-Right, 24J, MIPS off. (a) angular velocity, IHHS2 (b) angular velocity, IHHS1 (c) angular acceleration, IHHS2 (d) angular acceleration, IHHS1.*

It is now time to describe the behaviour of brain as recorded by the pressure sensors. From the pressure sensors is understandable that the sensors near the point of contact between impactor and helmet are characterized by a first positive peak of pressure, instead the sensors far away from the impact have a first negative pression, because the delay in time of movement between skull and brain causes variations in the distance between the two of them. Near the impact the distance between skull and brain decrease because the skull is moving towards the brain, instead far from the impact the distance increase. Both Occipital Left and Right have a positive pressure firstly that arrives to saturate. From the Temporal sensors, only the right one has a positive pressure and the same is for the Sphenoid

sensors. Frontal sensors have a first peak of depression, in fact they are far from the Back-Right region. For what concerns the Parietal sensors, is interesting to notice the fact that both have a positive peak but only the Left one saturates. This is caused by the fact that the head rotates while the brain is moving forward, so the Left sensors in a Back-Right impact is more solicited.

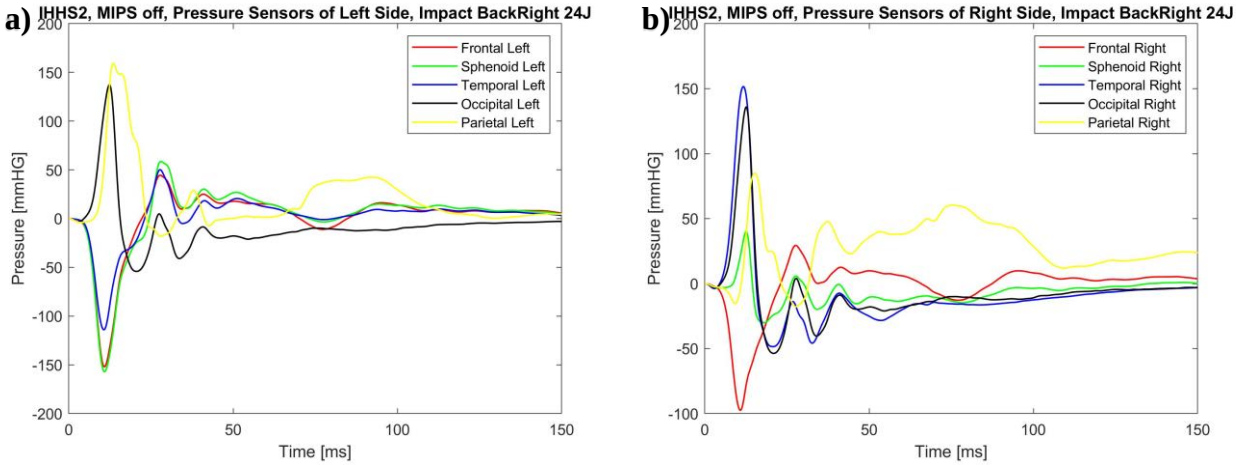


**Figure 6.15** *Pressure sensors (a) Left side of the head (b) Right side of the head.*

## 6.1.3 Right Impact

The Right impact will be now assessed. It is a kind of impact similar to the Back one because both are characterized by only one principal direction of impact, X for Back and Y for Right, while the principal direction for angular acceleration and velocities is Y for Back and X for Right.

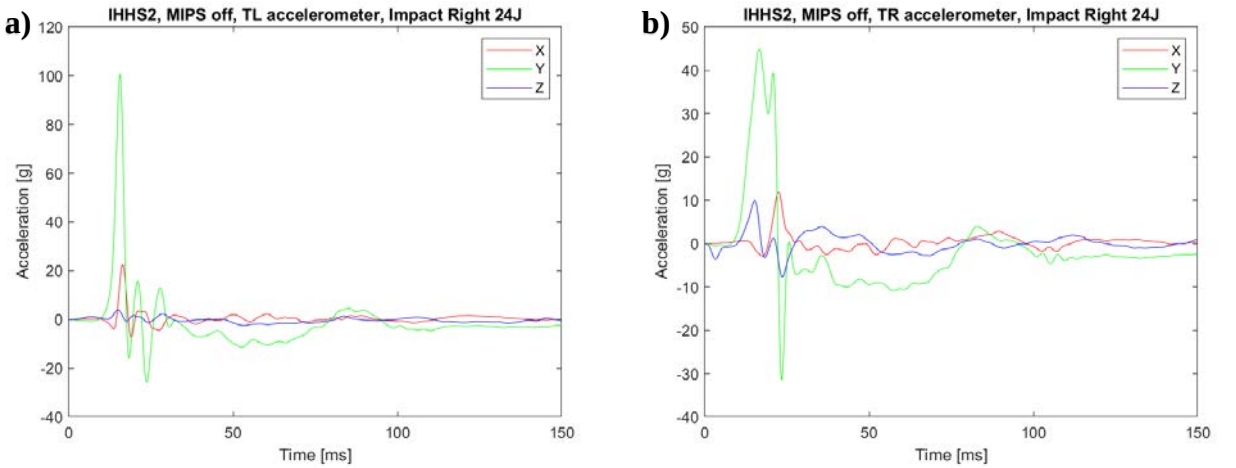

**c)**

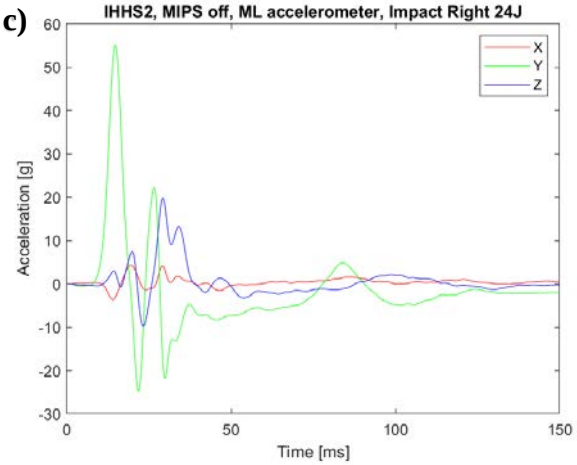
IHHS2, MIPS off, ML accelerometer, Impact Right 24J
X
Y
Z
Acceleration [g]
Time [ms]

**d)**

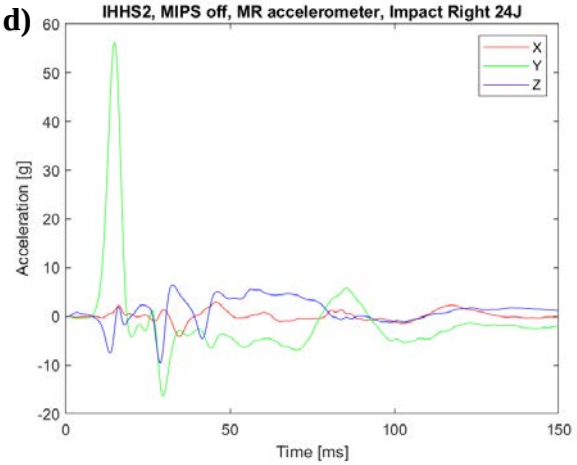
IHHS2, MIPS off, MR accelerometer, Impact Right 24J
X
Y
Z
Acceleration [g]
Time [ms]

**e)**

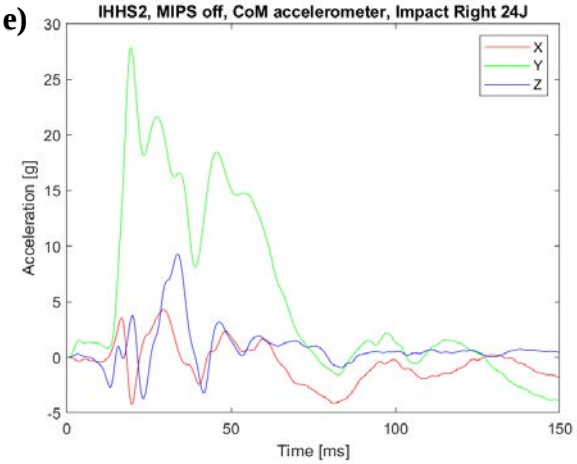
IHHS2, MIPS off, CoM accelerometer, Impact Right 24J
X
Y
Z
Acceleration [g]
Time [ms]

**f)**

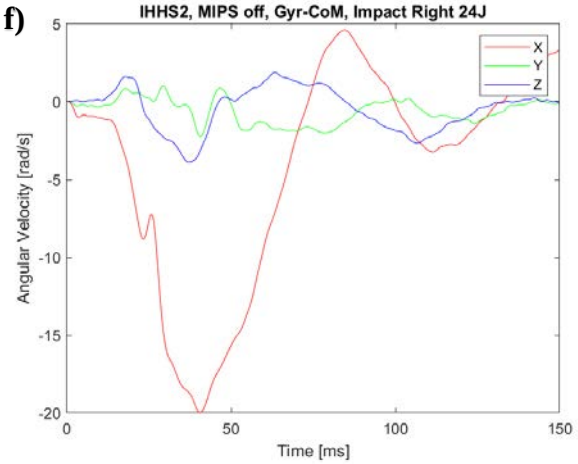
IHHS2, MIPS off, Gyr-CoM, Impact Right 24J
X
Y
Z
Angular Velocity [rad/s]
Time [ms]

**g)**

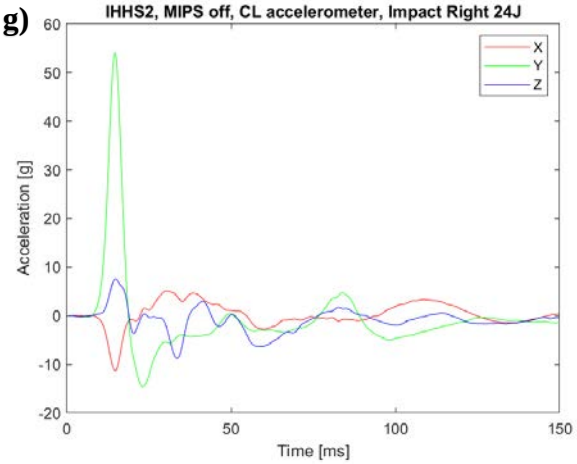
IHHS2, MIPS off, CL accelerometer, Impact Right 24J
X
Y
Z
Acceleration [g]
Time [ms]

**h)**

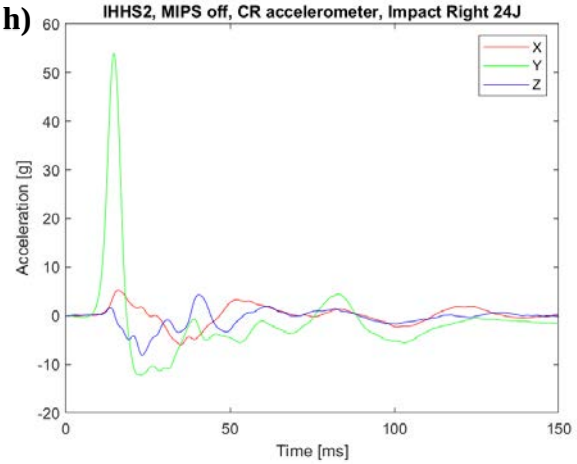
IHHS2, MIPS off, CR accelerometer, Impact Right 24J
X
Y
Z
Acceleration [g]
Time [ms]

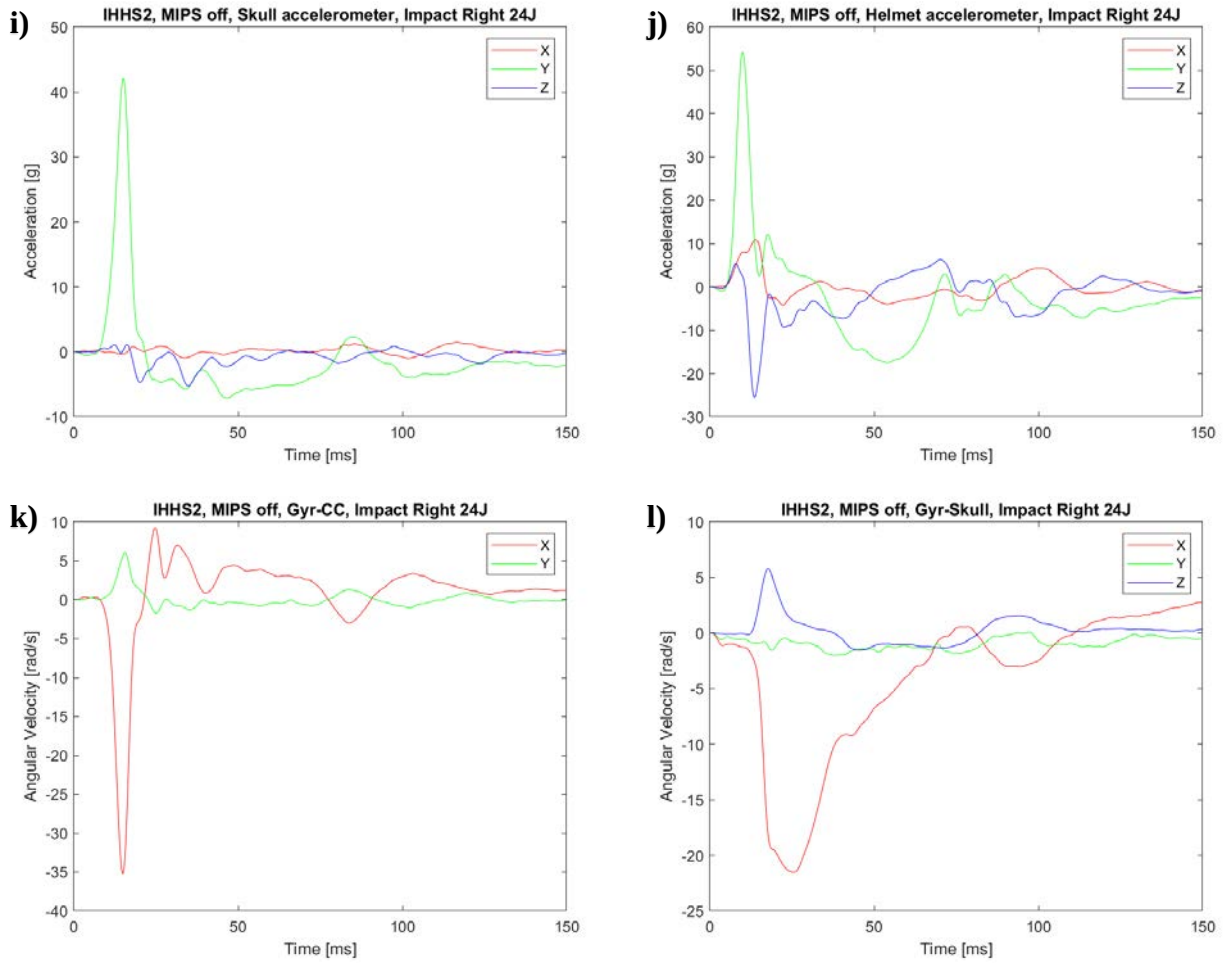


**Figure 6.16** *Signals recorded by IHHS2 with MIPS off during Impact Right 24J. (a) TL (b) TR (c) ML (d) MR (e) CoM (f) Gyr-CoM (g) CL (h) CR (i) Skull (j) Helmet (k) Gyr-CC (l) Gyr-Skull.*

As always, also in X direction the same kind of differences between CoM of IHHS1 and IHHS2 can be found.

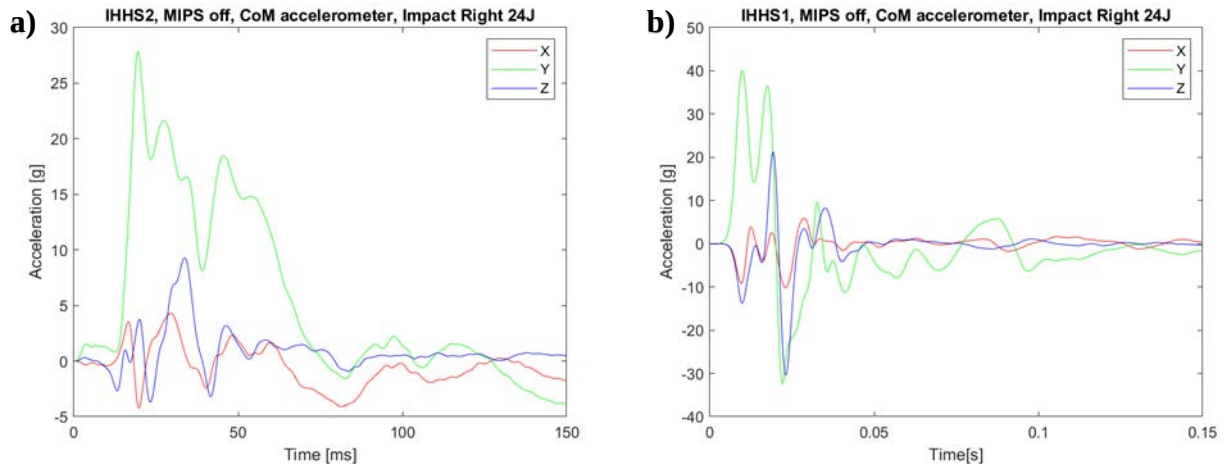


**Figure 6.17** *Comparison of signals recorded by CoM of the two instrumented human head surrogate models during impact Right, 24J, MIPS off. (a) CoM of IHHS2 (b) CoM of IHHS1.*

The peaks order in time from the signals of helmet, skull and CoM is always the same, both for IHHS1 and IHHS2.

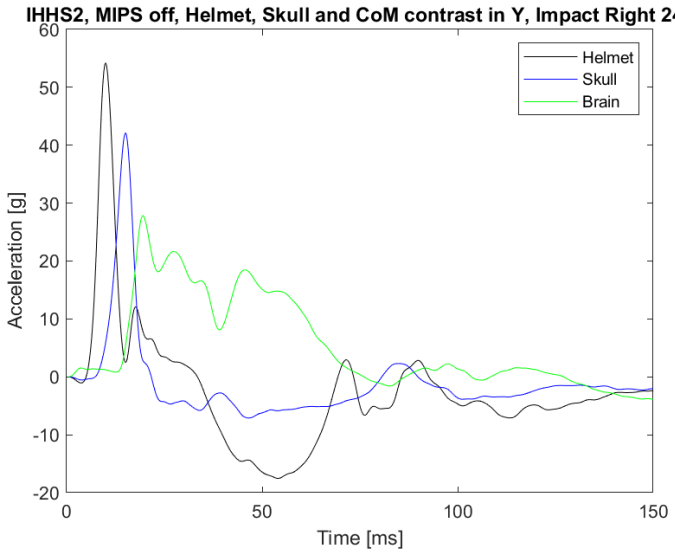


**Figure 6.18** *Comparison of accelerations of Helmet, Skull and CoM in Y direction.*

As in every impact type the differences in angular velocity and accelerations between the two instrumented human head surrogates are very marked, in contrast with the differences between the accelerometers. The differences in the accelerometers are typically located in the CoM that presents a particular and unique behaviour in the different head models. Accelerometers as TL, TR, ML or MR and others seem not to be affected by the presence of the liquid simulating the cerebrospinal fluid. The shape is exactly the same and the temporal window during which the peaks are developed is quite the same, as can be seen in almost every graph from *Chapter 5* or *Chapter 6*.

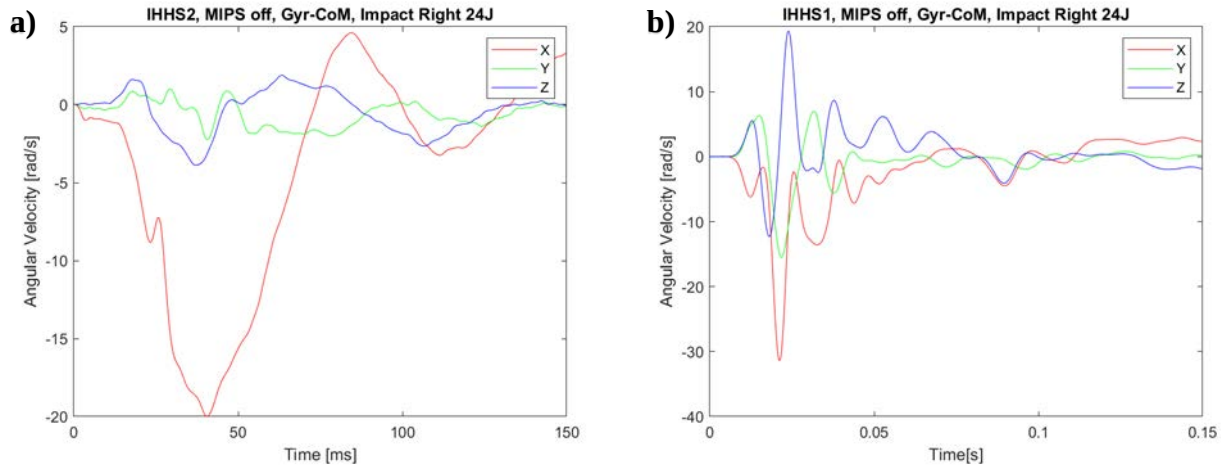

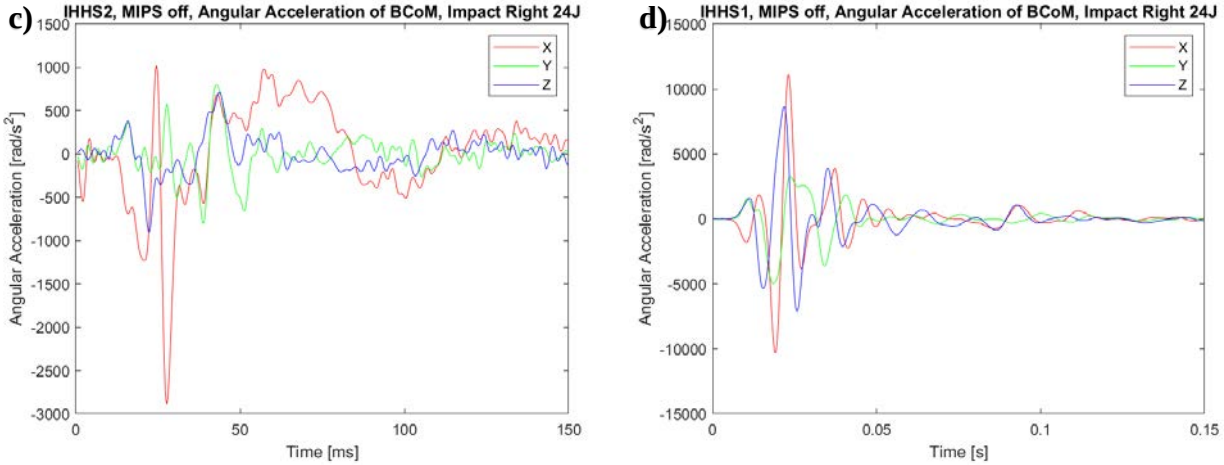


**Figure 6.19** *Comparison of angular velocities and accelerations in CoM between IHHS1 and IHHS2 in impact Right, 24J, MIPS off. (a) angular velocity, IHHS2 (b) angular velocity, IHHS1 (c) angular acceleration, IHHS2 (d) angular acceleration, IHHS1.*

The greatest differences between tests on IHHS1 and IHHS2 are always seen in the angular dimensions. Both for angular velocities and accelerations the law followed by CoM in IHHS1 and IHHS2 are completely different. This time is no different, the angular velocity of CoM in IHHS2 is wider and less sharp than IHHS1 and the highest values of angular accelerations in IHHS1 are at least 3 times the values of peaks in IHHS2.

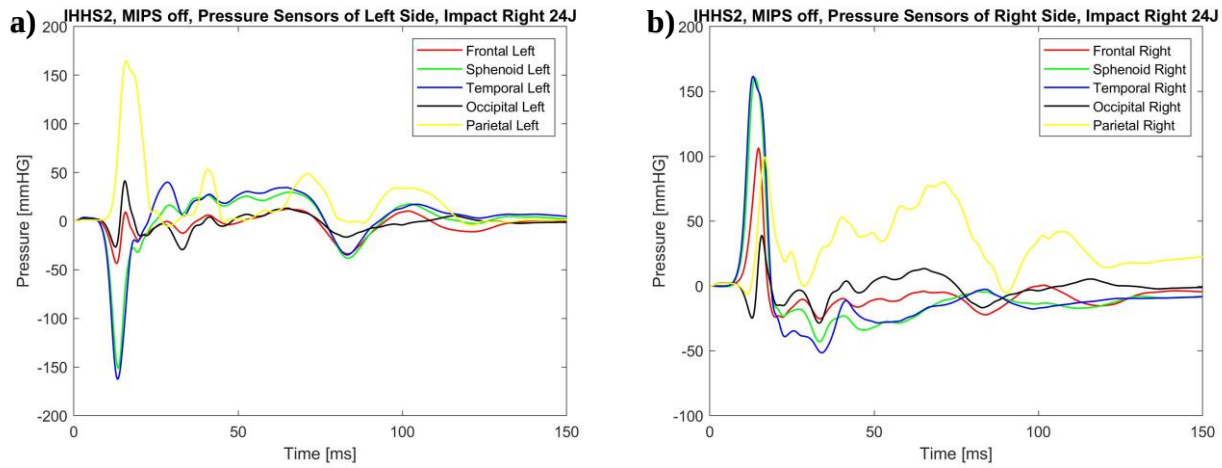


**Figure 6.20** *Pressure sensors (a) Left side of the head (b) Right side of the head.*

Pressure sensor analysis is the last thing needed to complete the description of Right impact. It is easy to understand that all the sensors in the left side of the head go in depression, besides Parietal Left that is placed on top of the skull and have a positive pressure in the first peak. Parietal Right instead has a positive pression but does not arrive to saturate the signal, because in a Right impact, as well as

in Back-Right, the rotation of the head brings the Parietal Left sensor in a lower position compared to the right side, so the effect of movement of the brain inside the head is more evident for the lower one. Both the Occipital sensors go in a little depression as the brain is going away from that region, while for what concerns the Frontal region, Right sensor have a first peak of positive pression and the Left one has a first peak of depression, as the brain is rotating around the vertical direction with positive sign, even if this behaviour is not detected from the gyroscope. Both in Frontal and in Occipital sensors the maximum value of the peaks are low because they are placed along the X direction and in a right impact the X axis is not the principal direction of impact.

### 6.1.4 Front-Right Impact

The last impact left to analyse is Front-Right at 24J of energy level and with MIPS not activated.

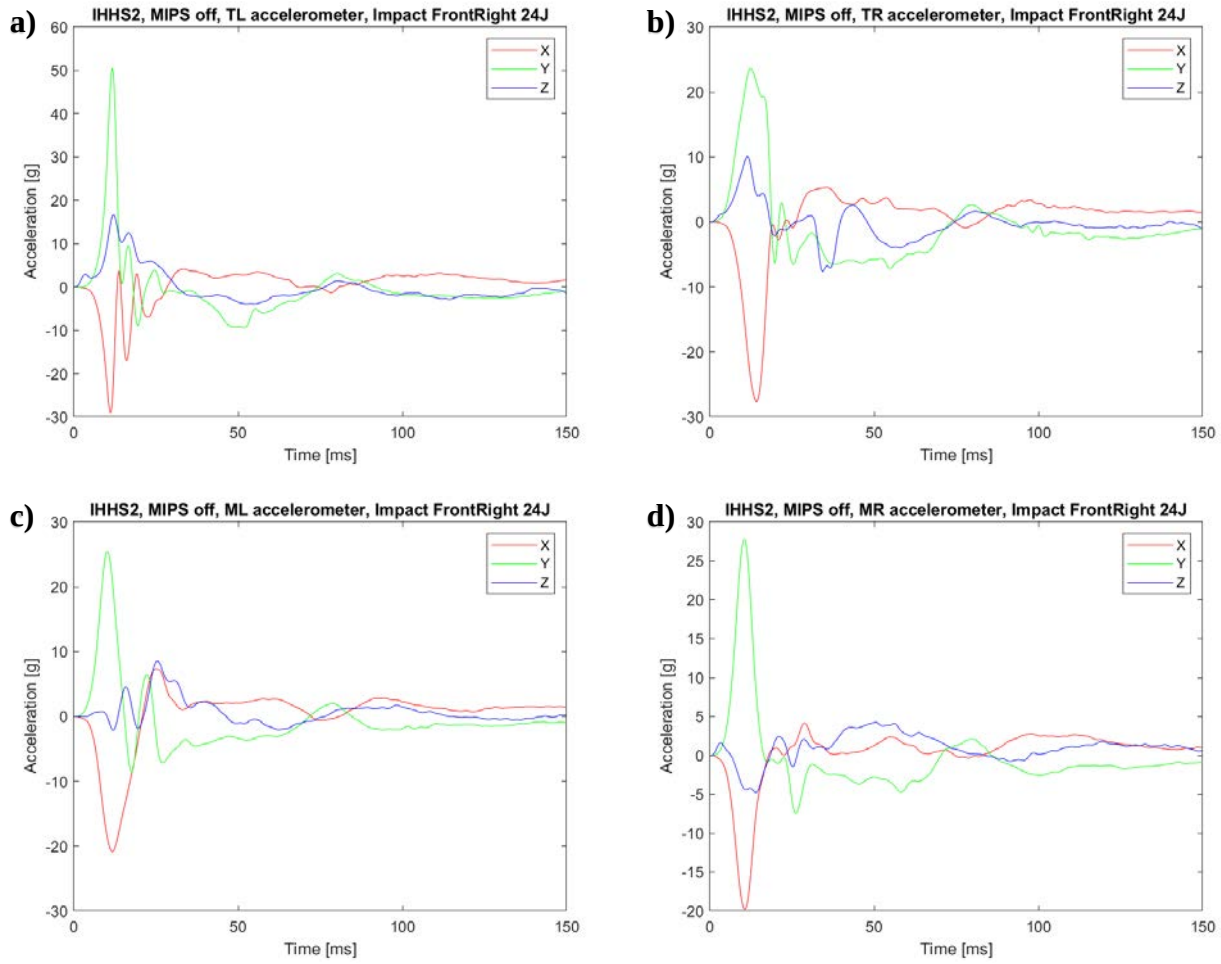

**e)**

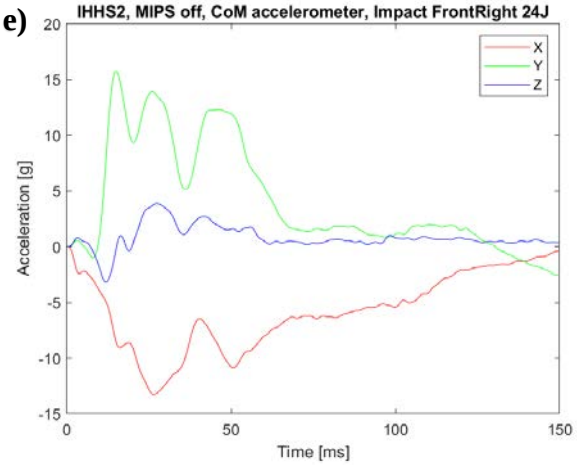
IHHS2, MIPS off, CoM accelerometer, Impact FrontRight 24J
X
Y
Z
Acceleration [g]
Time [ms]

**f)**

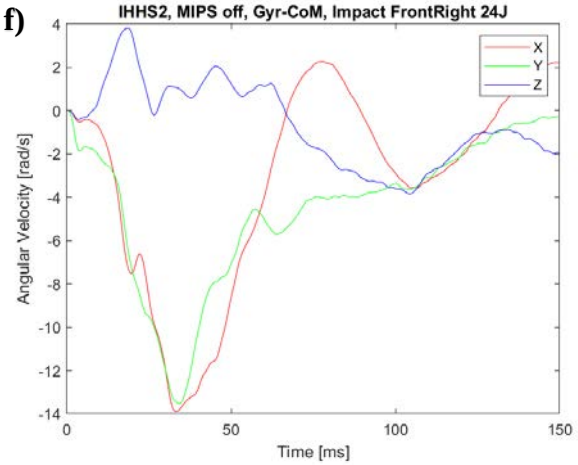
IHHS2, MIPS off, Gyr-CoM, Impact FrontRight 24J
X
Y
Z
Angular Velocity [rad/s]
Time [ms]

**g)**

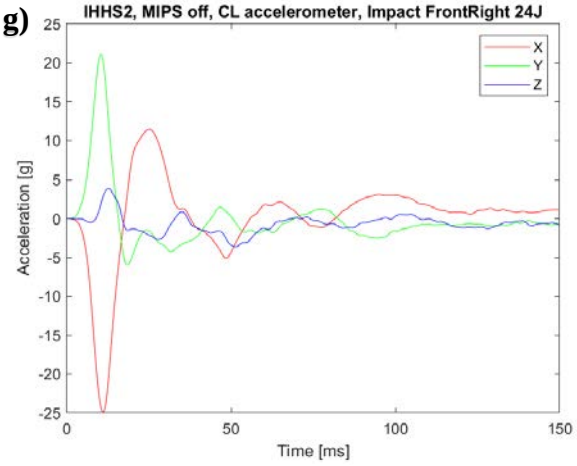
IHHS2, MIPS off, CL accelerometer, Impact FrontRight 24J
X
Y
Z
Acceleration [g]
Time [ms]

**h)**

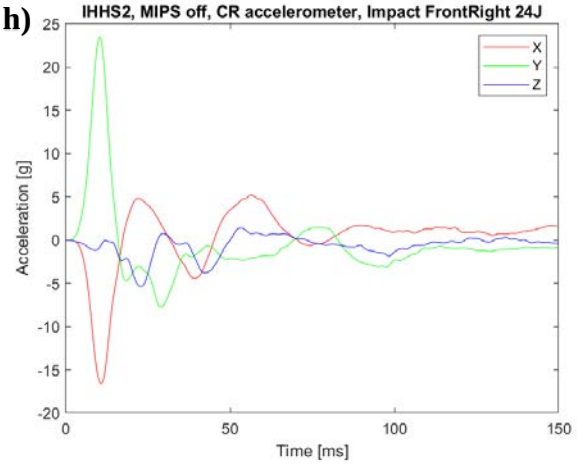
IHHS2, MIPS off, CR accelerometer, Impact FrontRight 24J
X
Y
Z
Acceleration [g]
Time [ms]

**i)**

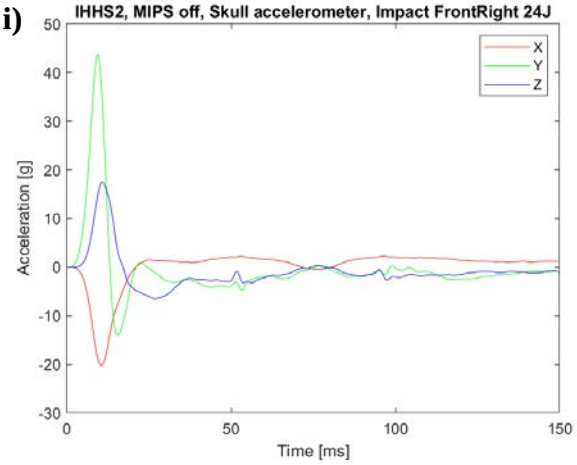
IHHS2, MIPS off, Skull accelerometer, Impact FrontRight 24J
X
Y
Z
Acceleration [g]
Time [ms]

**j)**

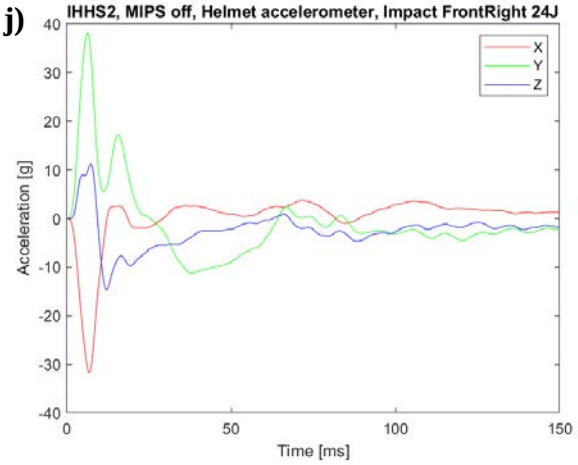
IHHS2, MIPS off, Helmet accelerometer, Impact FrontRight 24J
X
Y
Z
Acceleration [g]
Time [ms]

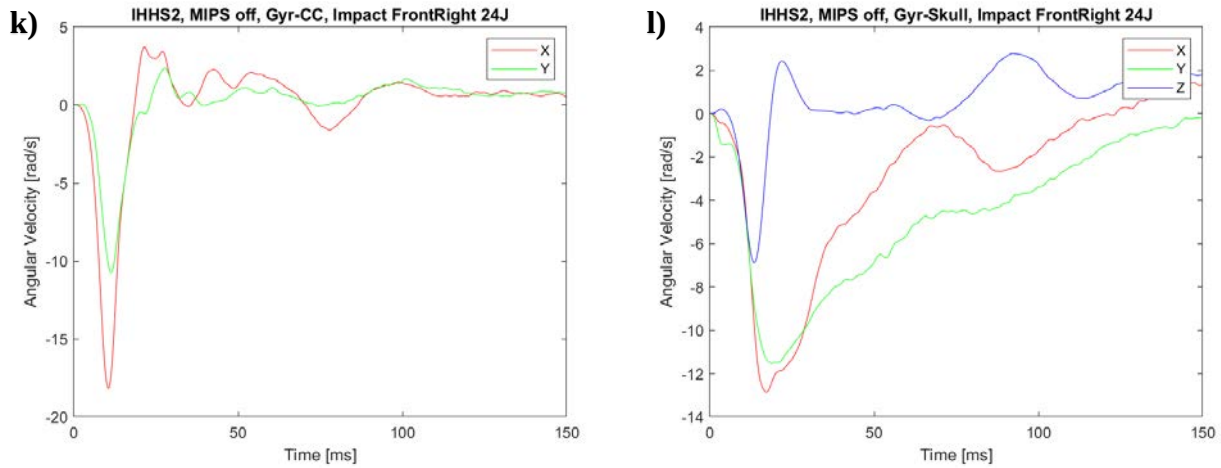


**Figure 6.21** *Signals recorded by IHHS2 with MIPS off during Impact Front-Right 24J. (a) TL (b) TR (c) ML (d) MR (e) CoM (f) Gyr-CoM (g) CL (h) CR (i) Skull (j) Helmet (k) Gyr-CC (l) Gyr-Skull.*

It is a typical Front-Right impact characterized by two principal direction of impact. For the accelerometers the first peak in X direction is negative while the first peak in the Y direction is positive. For the gyroscopes the first peaks both in X and Y direction are negative.

It is interesting to notice that during this impact the gyroscope in CoM records a positive first peak, while the gyroscope on the skull records a negative one, meaning that the skull and its content rotate in different directions, with the brain rotating towards left part of the face and the skull toward right side. Because of this it is needed to make a comparison between the graphs of angular velocity and accelerations of Gyr-CoM and Gyr-Skull. This phenomenon of the opposite rotation of brain and skull was also visible in the graphs of the Back-Right impact.

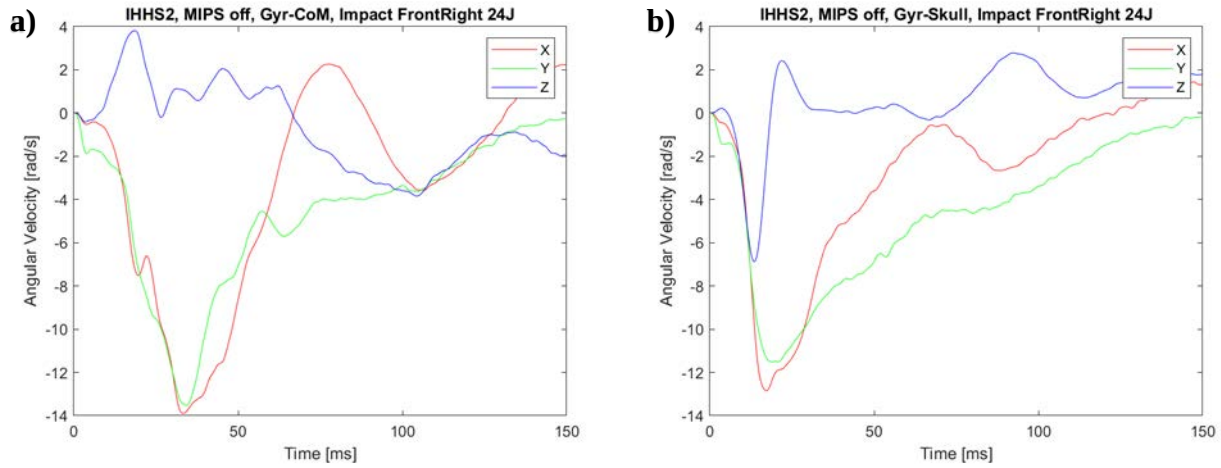

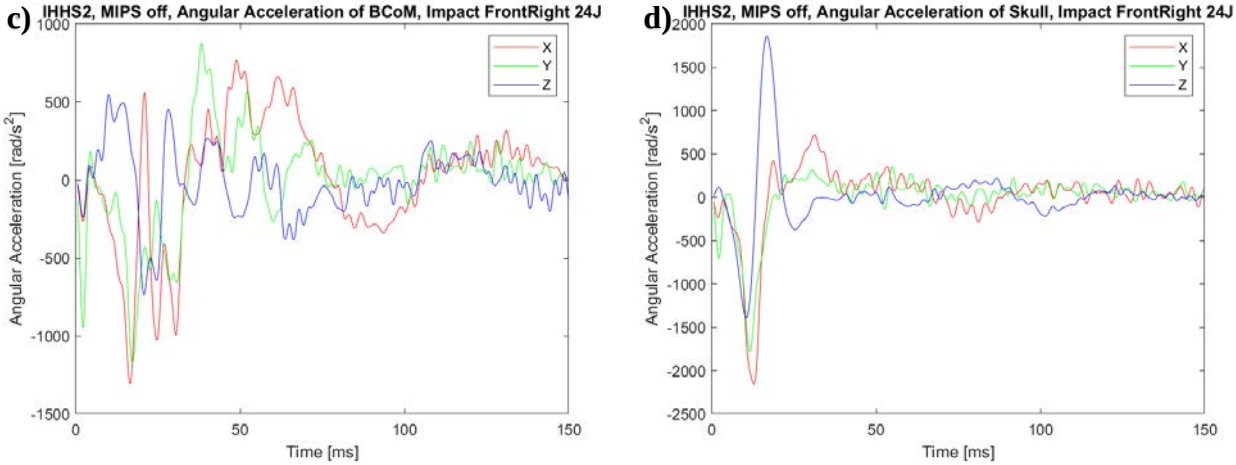


**Figure 6.22** *Comparison of angular velocities and accelerations in CoM and Skull Front-Right, 24J, MIPS off. (a) angular velocity, CoM (b) angular velocity, Skull (c) angular acceleration, CoM (d) angular acceleration, Skull.*

For what concerns the angular accelerations of brain and skull, it can be seen that the signals from CoM are simile to noise, with no particular trend that can be detected, while in Skull can be found clear peaks in each direction.

It is now time to show the comparison between the accelerometers in helmet, skull and brain in the two principal direction of impact.

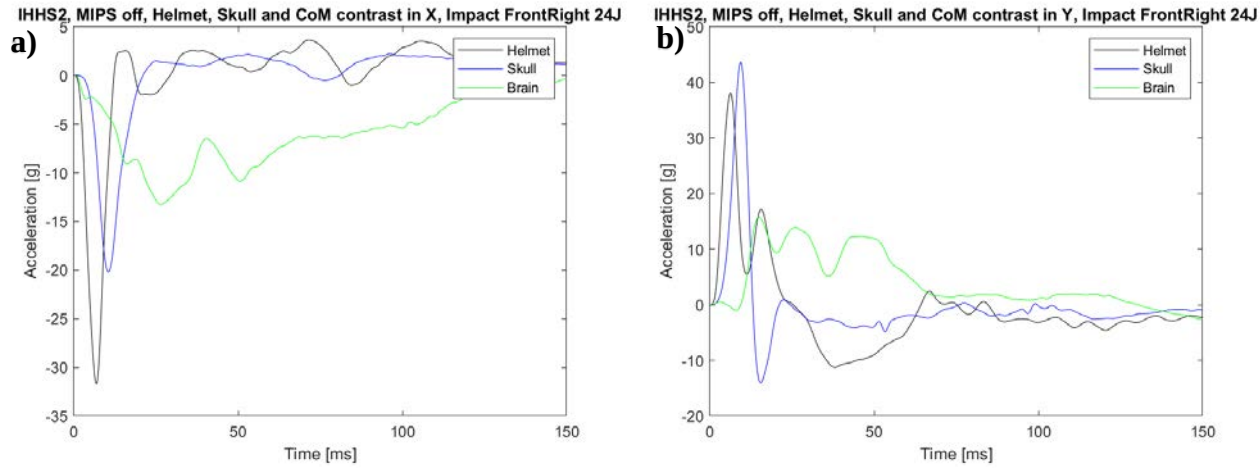


**Figure 6.23** *Comparison of accelerations of Helmet, Skull and CoM (a) X direction (b) Y direction.*

From the previous graphs a particular thing can be noticed. The peak of helmet accelerometer in X direction has a higher value in mathematical form than the one from skull, and it is normal because the accelerometer on helmet is in a higher position, instead in the Y direction the opposite is true, that is the peak of skull is higher than helmet. Probably it is caused by the fact that the accelerometer on

skull is positioned in the forehead of the skull, so it is sensible to different kinds of accelerations in this impact, in fact the point of contact between hammer and IHHS2 are really near. From the comparison in Y direction, it is also visible that the peak of helmet is characterized by two tips and the second one is in coincidence with the first tip of the CoM acceleration.
As last thing the pressure has to be analysed.

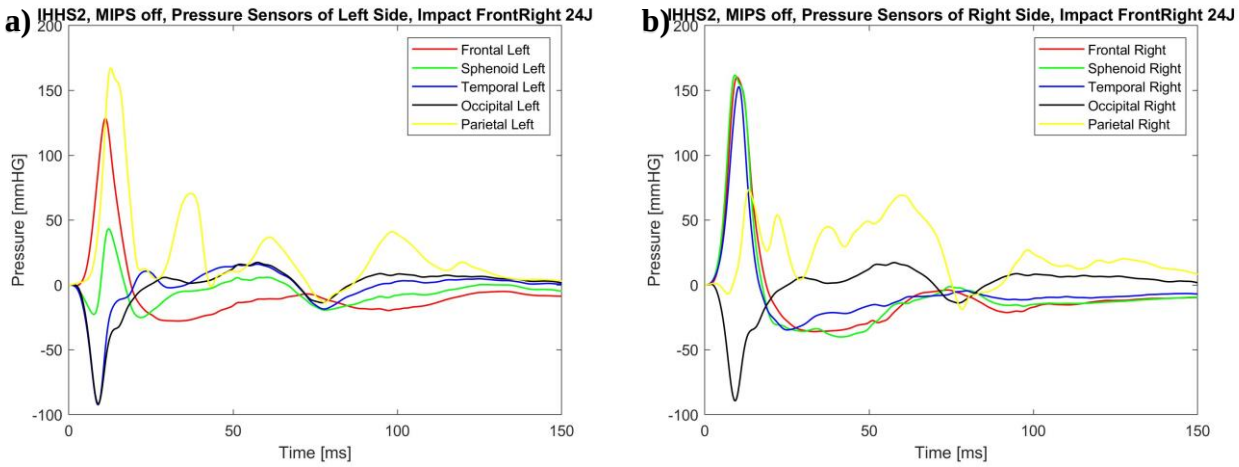


**Figure 6.24** *Pressure sensors (a) Left side of the head (b) Right side of the head.*

Sphenoid Right is the nearest pressure sensor to the point of impact, so it is characterized by a positive first peak that arrives to saturate. Also Frontal Right and Temporal Right arrive to saturation, however, their real peak value would be not has high as the Sphenoid Right one. Both the Occipital sensors have a first peak of depression, while the Parietal, on top on the skull, have positive pression, even if only the left one arrives to saturation.

## 6.2 Tables

Tests performed on IHHS2 will be presented through tables. Each table sums up 12 tests: 3 Back impacts, 3 Back-Right, 3 Right, 3 Front-Right. These tables are built and organized in the same way of the tables from the previous chapter, with the difference that also data from the extra gyroscope mounted on the skull are hosted.
The 12 test needed to complete a table are performed at the same energy level, 16J or 24J and have to be all the same or MIPS on or MIPS off. So 4 tables are necessary to describe the 48 tests performed on IHHS1.

| Energy | 16J | BACK | | BACKRIGHT | | RIGHT | | FRONTRIGHT | |
|---|---|---|---|---|---|---|---|---|---|
| MIPS | off | Theta = 0 deg | | Theta = 45 deg | | Theta = 90 deg | | Theta = 135 deg | |
| | | Mean | STD Dev | Mean | STD Dev | Mean | STD Dev | Mean | STD Dev |
| Helmet | acc_x [g] | 64,04 | 4,81 | 35,21 | 7,48 | 9,02 | 2,27 | -29,59 | 6,07 |
| | acc_y [g] | -13,43 | 0,76 | 28,10 | 5,76 | 38,06 | 3,17 | 38,64 | 9,52 |
| | acc_z [g] | 34,61 | 10,13 | -17,50 | 8,41 | -12,25 | 2,88 | -11,41 | 1,30 |
| | acc_R [g] | 65,19 | 4,83 | 45,28 | 8,76 | 38,89 | 3,12 | 48,72 | 11,29 |
| Skull | acc_x [g] | 32,10 | 3,25 | 22,92 | 2,00 | 1,10 | 0,17 | -17,26 | 4,54 |
| | acc_y [g] | 6,65 | 0,47 | 17,44 | 0,37 | 26,36 | 3,60 | 32,38 | 11,34 |
| | acc_z [g] | 35,25 | 4,50 | 3,99 | 12,34 | -3,02 | 0,12 | 14,23 | 1,82 |
| | acc_R [g] | 35,69 | 4,06 | 26,17 | 1,12 | 26,38 | 3,59 | 38,09 | 12,26 |
| | HIC* | 31,23 | 4,29 | 14,55 | 0,19 | 7,73 | 0,65 | 21,84 | 7,93 |
| | ω_x [rad/s] | -2,94 | 1,11 | -9,00 | 11,89 | -16,34 | 0,54 | -11,06 | 0,53 |
| | ω_y [rad/s] | 18,27 | 0,84 | 10,14 | 0,08 | -1,51 | 0,24 | -9,56 | 0,71 |
| | ω_z [rad/s] | 0,47 | 1,98 | 8,42 | 0,07 | 4,48 | 0,97 | -2,60 | 5,39 |
| | ω_R [rad/s] | 18,29 | 0,84 | 18,42 | 0,51 | 16,47 | 0,51 | 14,40 | 0,80 |
| | ω_R [dps] | 1048,06 | 48,13 | 1055,30 | 29,42 | 943,43 | 29,29 | 824,94 | 45,68 |
| | BRiC* | 0,33 | 0,01 | 0,36 | 0,00 | 0,26 | 0,01 | 0,27 | 0,02 |
| | α_R [rad/s^2] | 2223,20 | 111,93 | 3101,90 | 689,52 | 3229,27 | 690,45 | 2116,17 | 377,47 |
| Brain | acc_x [g] | 23,26 | 1,39 | 16,31 | 0,44 | 1,57 | 4,67 | -10,34 | 0,65 |
| | acc_y [g] | 6,30 | 0,38 | 16,08 | 0,89 | 20,19 | 1,72 | 13,33 | 1,74 |
| | acc_z [g] | 10,40 | 0,33 | 9,87 | 0,60 | 4,84 | 0,44 | 3,09 | 0,82 |
| | acc_R [g] | 24,25 | 0,57 | 23,15 | 0,88 | 20,33 | 1,67 | 16,42 | 1,40 |
| | HIC | 24,75 | 4,53 | 24,84 | 0,63 | 17,00 | 1,09 | 12,26 | 2,38 |
| | ω_x [rad/s] | 1,81 | 0,08 | -12,76 | 0,55 | -15,88 | 0,02 | -12,61 | 1,16 |
| | ω_y [rad/s] | 17,70 | 0,67 | 11,73 | 0,36 | -1,60 | 0,05 | -10,74 | 0,47 |
| | ω_z [rad/s] | 1,95 | 0,28 | -4,95 | 0,15 | -3,35 | 0,24 | 0,93 | 4,08 |
| | ω_R [rad/s] | 17,71 | 0,67 | 17,34 | 0,11 | 16,07 | 0,05 | 16,58 | 0,84 |
| | ω_R [dps] | 1014,91 | 38,48 | 993,31 | 6,53 | 920,83 | 2,93 | 950,10 | 48,36 |
| | BRiC | 0,32 | 0,01 | 0,31 | 0,00 | 0,25 | 0,00 | 0,28 | 0,02 |
| | α_R [rad/s^2] | 1686,93 | 29,19 | 1648,13 | 108,26 | 2374,17 | 55,29 | 1200,67 | 161,35 |

**Table 6.5** *Energy level: 16J. MIPS off*

| Energy | 24J | BACK | | BACKRIGHT | | RIGHT | | FRONTRIGHT | |
|---|---|---|---|---|---|---|---|---|---|
| MIPS | off | Theta = 0 deg | | Theta = 45 deg | | Theta = 90 deg | | Theta = 135 deg | |
| | | Mean | STD Dev | Mean | STD Dev | Mean | STD Dev | Mean | STD Dev |
| Helmet | acc_x [g] | 100,98 | 24,61 | 54,50 | 11,47 | 12,34 | 3,36 | -33,41 | 2,11 |
| | acc_y [g] | -23,67 | 6,96 | 42,03 | 7,45 | 57,06 | 7,39 | 38,16 | 0,19 |
| | acc_z [g] | -42,66 | 12,92 | -32,61 | 13,37 | -29,81 | 10,37 | -17,39 | 2,41 |
| | acc_R [g] | 103,58 | 25,94 | 68,91 | 12,84 | 58,29 | 8,35 | 50,76 | 0,46 |
| Skull | acc_x [g] | 38,87 | 6,18 | 26,90 | 5,38 | 0,31 | 2,00 | -18,42 | 1,64 |
| | acc_y [g] | 6,47 | 2,13 | 20,48 | 3,85 | 41,53 | 2,44 | 37,86 | 5,62 |
| | acc_z [g] | -27,65 | 5,40 | -14,95 | 2,27 | -5,43 | 0,48 | 18,15 | 0,57 |
| | acc_R [g] | 40,33 | 5,54 | 31,57 | 3,99 | 41,55 | 2,41 | 44,14 | 5,69 |
| | HIC* | 47,59 | 11,96 | 23,93 | 3,54 | 15,67 | 1,54 | 33,39 | 7,11 |
| | ω_x [rad/s] | -0,48 | 3,24 | -18,35 | 0,32 | -20,63 | 1,42 | -13,01 | 0,26 |
| | ω_y [rad/s] | 19,26 | 0,74 | 12,34 | 0,70 | -3,21 | 1,70 | -11,85 | 0,34 |
| | ω_z [rad/s] | 2,10 | 0,42 | 9,18 | 1,83 | 4,77 | 1,51 | -2,52 | 6,11 |
| | ω_R [rad/s] | 19,30 | 0,72 | 21,73 | 0,67 | 20,68 | 1,42 | 17,48 | 0,19 |
| | ω_R [dps] | 1105,73 | 41,41 | 1245,07 | 38,56 | 1184,90 | 81,40 | 1001,81 | 10,62 |
| | BRiC* | 0,35 | 0,02 | 0,41 | 0,03 | 0,34 | 0,02 | 0,31 | 0,01 |
| | α_R [rad/s^2] | 2486,90 | 791,13 | 3028,33 | 367,25 | 5559,13 | 1257,63 | 2725,37 | 189,87 |
| Brain | acc_x [g] | 28,29 | 2,07 | 18,64 | 2,09 | 4,30 | 0,42 | -13,50 | 0,23 |
| | acc_y [g] | 6,43 | 0,29 | 20,45 | 0,92 | 26,01 | 3,54 | 15,47 | 0,25 |
| | acc_z [g] | 0,10 | 0,35 | 0,44 | 0,06 | 0,41 | 0,02 | 0,46 | 0,02 |
| | acc_R [g] | 29,49 | 2,06 | 25,95 | 2,47 | 26,63 | 3,18 | 19,05 | 0,55 |
| | HIC | 37,86 | 3,73 | 35,39 | 6,58 | 30,82 | 2,72 | 16,53 | 1,04 |
| | ω_x [rad/s] | 0,67 | 2,37 | -15,00 | 0,81 | -20,00 | 0,10 | -13,56 | 0,31 |
| | ω_y [rad/s] | 20,50 | 0,90 | 13,50 | 0,70 | -2,21 | 0,10 | -13,47 | 0,07 |
| | ω_z [rad/s] | -0,30 | 2,70 | -5,01 | 0,59 | -3,69 | 0,74 | 1,00 | 4,19 |
| | ω_R [rad/s] | 20,55 | 0,89 | 20,24 | 0,82 | 20,31 | 0,07 | 19,11 | 0,25 |
| | ω_R [dps] | 1177,60 | 51,14 | 1164,67 | 42,51 | 1163,53 | 3,75 | 1095,00 | 14,23 |
| | BRiC | 0,37 | 0,02 | 0,35 | 0,01 | 0,32 | 0,01 | 0,32 | 0,01 |
| | α_R [rad/s^2] | 1956,60 | 352,54 | 1897,10 | 287,51 | 3059,57 | 274,60 | 1676,13 | 106,73 |

**Table 6.6** *Energy level: 24J. MIPS off*

| Energy | 16J | BACK | | BACKRIGHT | | RIGHT | | FRONTRIGHT | |
|---|---|---|---|---|---|---|---|---|---|
| MIPS | on | Theta = 0 deg | | Theta = 45 deg | | Theta = 90 deg | | Theta = 135 deg | |
| | | Mean | STD Dev | Mean | STD Dev | Mean | STD Dev | Mean | STD Dev |
| Helmet | acc_x [g] | 77,28 | 2,35 | 53,36 | 2,33 | -1,37 | 8,26 | -30,33 | 2,19 |
| | acc_y [g] | -5,37 | 0,81 | 37,12 | 0,57 | 39,01 | 2,18 | 27,58 | 1,04 |
| | acc_z [g] | -44,92 | 3,25 | -39,70 | 2,94 | -14,00 | 1,73 | -15,37 | 9,59 |
| | acc_R [g] | 77,44 | 2,33 | 65,36 | 2,10 | 39,45 | 2,00 | 41,62 | 0,95 |
| Skull | acc_x [g] | 32,77 | 3,53 | 17,90 | 3,98 | -2,87 | 0,06 | -17,67 | 0,89 |
| | acc_y [g] | 1,63 | 4,62 | 17,93 | 2,75 | 37,93 | 0,83 | 34,37 | 4,52 |
| | acc_z [g] | -26,92 | 1,25 | -16,15 | 1,47 | -3,65 | 0,06 | 11,76 | 0,44 |
| | acc_R [g] | 34,56 | 3,77 | 27,24 | 5,21 | 38,06 | 0,84 | 39,68 | 4,32 |
| | HIC* | 30,17 | 3,12 | 14,62 | 0,96 | 15,22 | 0,22 | 23,93 | 1,64 |
| | ω_x [rad/s] | -2,63 | 1,87 | -9,82 | 0,90 | -15,77 | 0,48 | -10,23 | 0,31 |
| | ω_y [rad/s] | 13,85 | 0,13 | 8,08 | 0,53 | -3,24 | 2,00 | -8,33 | 0,43 |
| | ω_z [rad/s] | -1,74 | 0,08 | 1,42 | 2,90 | 0,55 | 2,12 | -5,82 | 0,19 |
| | ω_R [rad/s] | 13,98 | 0,12 | 12,71 | 1,01 | 16,07 | 0,89 | 13,14 | 0,36 |
| | ω_R [dps] | 800,92 | 7,01 | 728,38 | 58,00 | 920,66 | 50,79 | 752,76 | 20,89 |
| | BRiC* | 0,25 | 0,01 | 0,22 | 0,02 | 0,25 | 0,02 | 0,25 | 0,00 |
| | α_R [rad/s^2] | 2218,20 | 170,61 | 2218,20 | 657,91 | 3958,43 | 1424,89 | 1962,50 | 159,79 |
| Brain | acc_x [g] | 17,77 | 0,18 | 12,69 | 1,01 | -0,98 | 4,19 | -9,47 | 0,27 |
| | acc_y [g] | 5,05 | 0,31 | 12,02 | 0,15 | 20,56 | 0,30 | 13,51 | 0,59 |
| | acc_z [g] | 9,89 | 1,44 | 9,07 | 0,60 | 6,56 | 1,04 | 2,84 | 0,40 |
| | acc_R [g] | 18,03 | 0,11 | 16,67 | 0,29 | 20,81 | 0,23 | 16,44 | 0,39 |
| | HIC | 12,46 | 0,43 | 12,91 | 1,19 | 16,29 | 0,11 | 12,28 | 0,33 |
| | ω_x [rad/s] | -1,34 | 0,17 | -2,08 | 13,42 | -15,17 | 0,19 | -12,11 | 0,27 |
| | ω_y [rad/s] | 6,92 | 10,11 | 4,70 | 8,04 | -1,94 | 0,12 | -10,49 | 1,38 |
| | ω_z [rad/s] | 0,54 | 1,29 | 2,24 | 0,03 | 2,41 | 0,06 | -1,20 | 4,35 |
| | ω_R [rad/s] | 12,69 | 0,21 | 12,84 | 0,38 | 15,27 | 0,17 | 15,67 | 0,09 |
| | ω_R [dps] | 727,13 | 12,30 | 735,69 | 21,71 | 874,81 | 9,65 | 897,85 | 5,21 |
| | BRiC | 0,23 | 0,00 | 0,23 | 0,01 | 0,24 | 0,00 | 0,27 | 0,00 |
| | α_R [rad/s^2] | 1740,30 | 158,27 | 1416,60 | 51,72 | 2551,27 | 42,19 | 1258,53 | 68,24 |

**Table 6.7** *Energy level: 16J. MIPS on*

| Energy | 24J | BACK | | BACKRIGHT | | RIGHT | | FRONTRIGHT | |
|---|---|---|---|---|---|---|---|---|---|
| MIPS | on | Theta = 0 deg | | Theta = 45 deg | | Theta = 90 deg | | Theta = 135 deg | |
| | | Mean | STD Dev | Mean | STD Dev | Mean | STD Dev | Mean | STD Dev |
| Helmet | acc_x [g] | 101,03 | 0,07 | 48,80 | 4,37 | 8,71 | 1,98 | -39,94 | 1,54 |
| | acc_y [g] | -8,68 | 0,94 | 53,38 | 5,41 | 30,33 | 15,07 | 34,07 | 2,17 |
| | acc_z [g] | -54,58 | 1,40 | -34,91 | 4,94 | -22,01 | 7,41 | 11,74 | 0,99 |
| | acc_R [g] | 101,42 | 0,02 | 72,33 | 6,84 | 36,75 | 9,62 | 52,89 | 2,82 |
| Skull | acc_x [g] | 50,50 | 0,81 | 31,01 | 1,78 | -3,78 | 0,38 | -21,66 | 1,28 |
| | acc_y [g] | 4,67 | 0,20 | 25,34 | 2,21 | 52,31 | 1,23 | 48,40 | 1,80 |
| | acc_z [g] | -31,96 | 0,55 | -15,54 | 0,19 | -5,25 | 0,58 | 17,07 | 0,18 |
| | acc_R [g] | 51,99 | 0,73 | 36,03 | 2,41 | 52,47 | 1,25 | 54,48 | 2,10 |
| | HIC* | 61,63 | 1,30 | 32,83 | 1,96 | 22,08 | 4,97 | 43,11 | 0,94 |
| | ω_x [rad/s] | -3,86 | 1,73 | -15,85 | 0,51 | -18,67 | 0,39 | -12,86 | 0,14 |
| | ω_y [rad/s] | 16,44 | 0,26 | 10,81 | 0,41 | -3,94 | 2,83 | -11,20 | 0,20 |
| | ω_z [rad/s] | -2,26 | 0,13 | 9,30 | 0,33 | -2,28 | 0,10 | -7,52 | 0,21 |
| | ω_R [rad/s] | 16,60 | 0,30 | 18,89 | 0,68 | 19,13 | 0,33 | 17,24 | 0,23 |
| | ω_R [dps] | 950,87 | 17,28 | 1082,40 | 38,96 | 1096,27 | 19,09 | 987,67 | 12,98 |
| | BRiC* | 0,30 | 0,01 | 0,38 | 0,01 | 0,30 | 0,01 | 0,33 | 0,01 |
| | α_R [rad/s^2] | 3038,30 | 136,83 | 3777,30 | 712,53 | 5875,50 | 880,06 | 2824,17 | 63,36 |
| Brain | acc_x [g] | 20,80 | 0,09 | 16,49 | 0,35 | -4,58 | 0,27 | -12,57 | 0,43 |
| | acc_y [g] | 5,40 | 0,07 | 16,50 | 0,43 | 25,72 | 1,22 | 16,56 | 0,10 |
| | acc_z [g] | 15,72 | 1,18 | 8,53 | 0,96 | 8,12 | 0,63 | 4,30 | 0,28 |
| | acc_R [g] | 20,82 | 0,10 | 19,73 | 0,84 | 26,27 | 1,10 | 19,52 | 0,14 |
| | HIC | 18,89 | 0,41 | 20,87 | 1,72 | 25,32 | 1,55 | 18,39 | 0,35 |
| | ω_x [rad/s] | -1,01 | 0,01 | -13,54 | 0,32 | -17,75 | 0,52 | -13,83 | 0,37 |
| | ω_y [rad/s] | 16,26 | 0,37 | 12,71 | 0,36 | -2,55 | 0,46 | -12,82 | 0,27 |
| | ω_z [rad/s] | 1,98 | 0,21 | -4,35 | 0,28 | 2,69 | 0,13 | -4,86 | 0,12 |
| | ω_R [rad/s] | 16,38 | 0,40 | 18,11 | 0,39 | 17,91 | 0,59 | 18,91 | 0,22 |
| | ω_R [dps] | 938,69 | 22,89 | 1037,43 | 22,56 | 1026,08 | 33,71 | 1083,67 | 12,49 |
| | BRiC | 0,29 | 0,01 | 0,32 | 0,01 | 0,28 | 0,01 | 0,33 | 0,00 |
| | α_R [rad/s^2] | 2005,37 | 1,15 | 2089,47 | 63,95 | 2837,93 | 322,42 | 1665,60 | 133,01 |

**Table 6.8** *Energy level: 24J. MIPS on*

To take a first glance of the trends found changing the type of impact and the energy level a first graph comparing the resultant accelerations for MIPS off will be shown. MIPS on is not necessary because no differences are expected between its activation or not for the linear accelerations. After that it is more interesting to select an energy level, that will 24J, and make comparison graphs about HIC, BrIC, resultant angular accelerations and so on between what is recorded in CoM and in Skull and between IHHS1 and IHHS2.

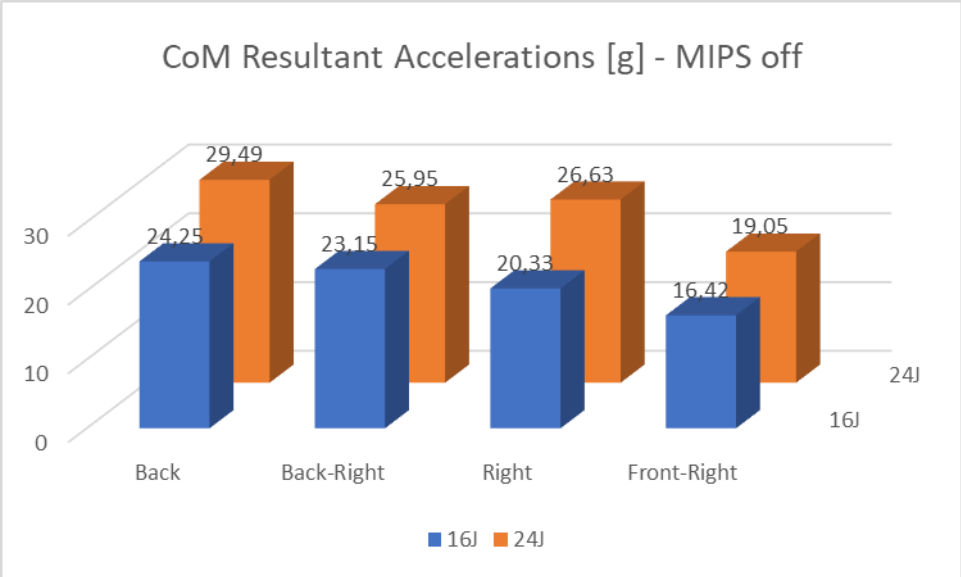


**Figure 6.25** *CoM Resultant Accelerations from every energy level, 16J and 24J, and from every different type of impact, Back. Back-Right, Right, Front-Right. MIPS on.*

The CoM resultants obviously increase passing from energy level 16J to 24J, instead passing from Back to Back-Right, Right or Front-Right the values of the resultants' peaks show the trend of decreasing, that is more the angle θ, describing the position of the head compared to the direction of movement of the hammer, increases, lower is the value of resultant acceleration.

In the following figure the comparison between the values of resultant angular acceleration for helmet, skull and CoM will be assessed. This time, differently from IHHS1, the accelerometer on the skull is positioned on the same level of CoM, so the values between skull and CoM are really comparable. It is easy to see that skull has always values that are a little bigger than CoM and it makes sense because CoM is the last part of the head to be solicited by the hammer, and so is protected by the previous layers, helmet and the skull itsel. In IHHS2 is also present the liquid filling the head, producing a dumping effect that should reduce the values of peak accelerations of the brain.

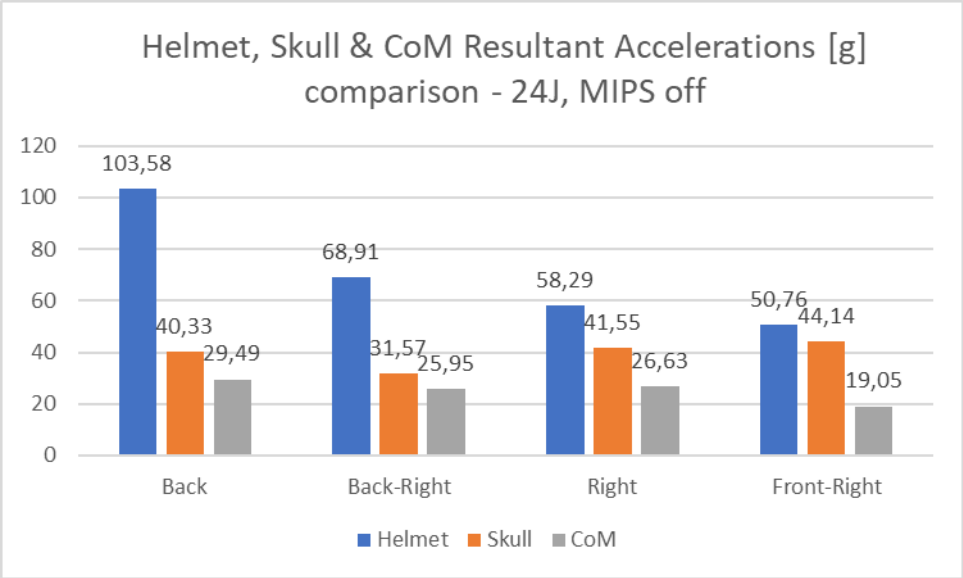


**Figure 6.26** *Comparison of resultant accelerations for Helmet, Skull and CoM, 24J.*

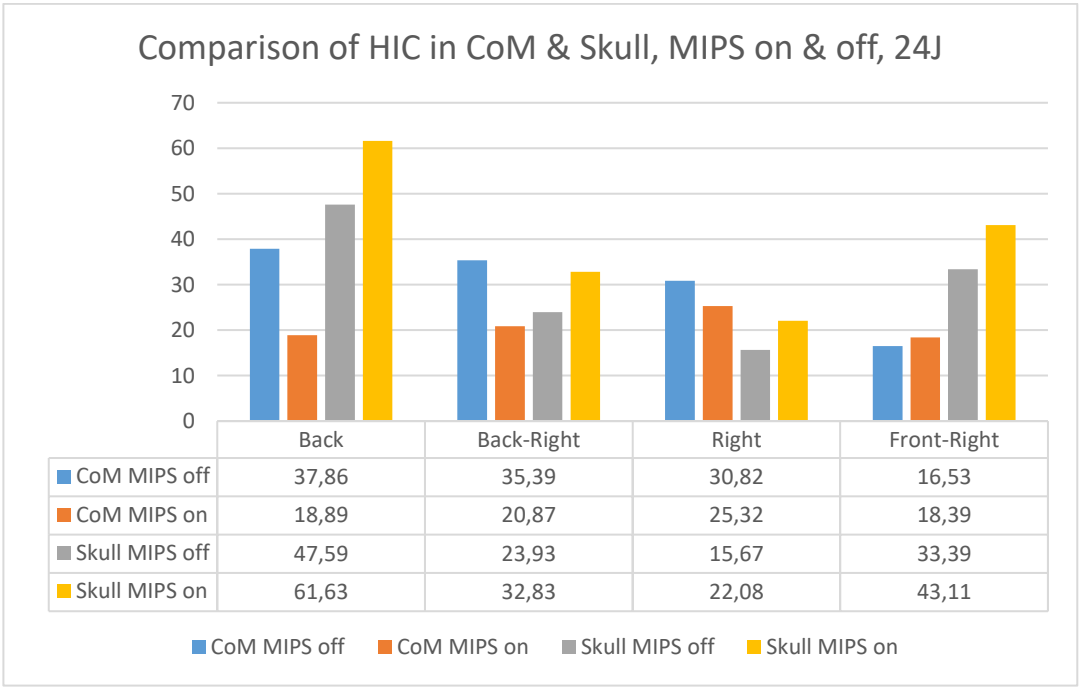


**Figure 6.27** *Comparison of HIC between CoM and Skull and between MIPS on and MIPS off tests.*

In *Figure 6.27* a trend of changing in the HIC values between CoM and skull and between MIPS on and MIPS off is difficult to understand. It is true the fact that CoM is more protected and Skull receive the hit before the brain, and it should make the HIC values of CoM lower that skull, but it is also true that HIC is calculated considering the temporal window in which the impact happens, and CoM has a larger peak than skull, so, for this cause, the HIC of CoM should be higher than skull. However, it can be seen that with θ increasing, the values of HIC for skull tends to become lower than CoM,

besides in Front-Right impact where the point of contact between head and hammer is near the accelerometer of skull.

In the following graph will be discussed the differences in BrIC between CoM and Skull and between MIPS on and MIPS off for energy level of 24J. It is easy to notice that the values of BrIC are very similar, both for different positions and for the part of the head analysed or the type of protection. Differences in values between MIPS on and MIPS off are not expected in fact MIPS is created to reduce the angular accelerations. The only thing that can be seen is that BrIC for skull tends to be a little higher than CoM, but not always.

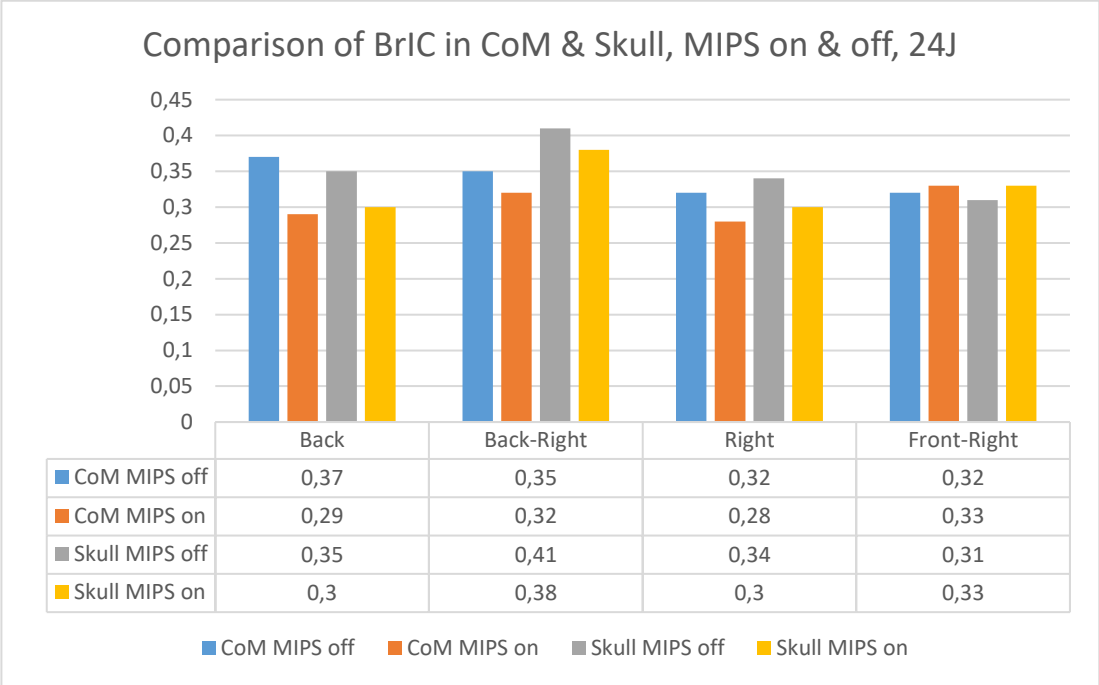


| | Back | Back-Right | Right | Front-Right |
|---|---|---|---|---|
| CoM MIPS off | 0,37 | 0,35 | 0,32 | 0,32 |
| CoM MIPS on | 0,29 | 0,32 | 0,28 | 0,33 |
| Skull MIPS off | 0,35 | 0,41 | 0,34 | 0,31 |
| Skull MIPS on | 0,3 | 0,38 | 0,3 | 0,33 |

**Figure 6.28** *Comparison of BrIC between CoM and Skull and between MIPS on and MIPS off tests.*

The effect of MIPS should be seen in the comparison of angular accelerations, not for forsake in angular velocities or BrIC. So, In figure 6.29 will be shown a histogram about angular accelerations in CoM and skull, both for MIPS and no MIPS activated.

From the graph, the fact that resultant angular accelerations for skull are higher than the ones from brain is easy to see, and it is normal because the brain is floating inside the cerebrospinal fluid. Instead in IHHS2 the MIPS seems to be ineffective compared to the results obtained in IHHS1. The values of angular accelerations in the CoM between MIPS on and MIPS off does not show significant differences, in fact some time accelerations in tests with MIPS are higher, other time lower or at same values. The fact that MIPS is effective on IHHS1 is a proof of good working because it shows that the sensorized human head is capable to react as predicted. Doing impact tests on the head with MIPS

activated or not is a way to validate IHHS1 or IHHS2. The fact that IHHS2 does not show the behaviour of MIPS as predicted could be caused by complication in the process of inserting and removing the MIPS layer inside the helmet.

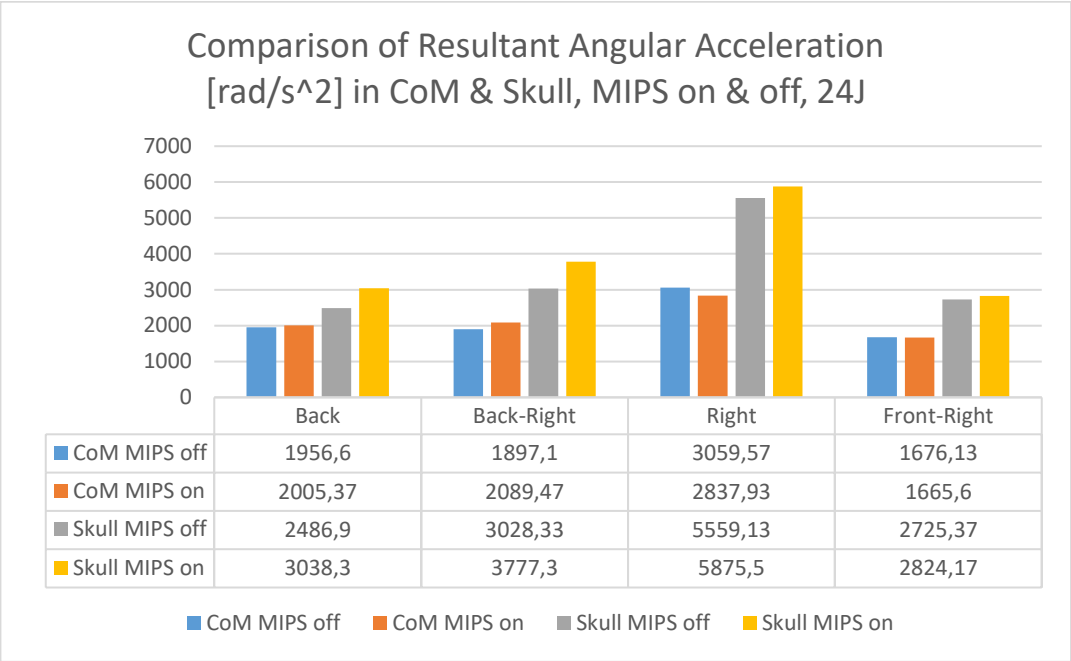


| | Back | Back-Right | Right | Front-Right |
|---|---|---|---|---|
| CoM MIPS off | 1956,6 | 1897,1 | 3059,57 | 1676,13 |
| CoM MIPS on | 2005,37 | 2089,47 | 2837,93 | 1665,6 |
| Skull MIPS off | 2486,9 | 3028,33 | 5559,13 | 2725,37 |
| Skull MIPS on | 3038,3 | 3777,3 | 5875,5 | 2824,17 |

**Figure 6.29** *Comparison of Resultant Angular Accelerations between CoM and Skull and between MIPS on and MIPS off tests.*

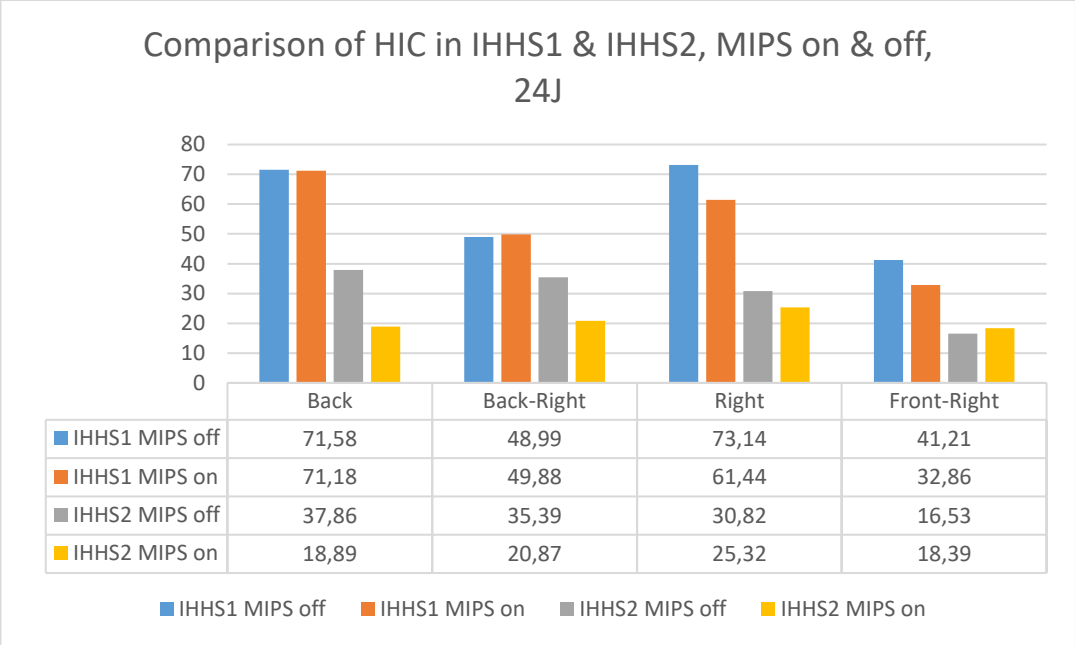


| | Back | Back-Right | Right | Front-Right |
|---|---|---|---|---|
| IHHS1 MIPS off | 71,58 | 48,99 | 73,14 | 41,21 |
| IHHS1 MIPS on | 71,18 | 49,88 | 61,44 | 32,86 |
| IHHS2 MIPS off | 37,86 | 35,39 | 30,82 | 16,53 |
| IHHS2 MIPS on | 18,89 | 20,87 | 25,32 | 18,39 |

**Figure 6.30** *Comparison of HIC in IHHS1 and IHHS2, both for MIPS on and MIPS off tests.*

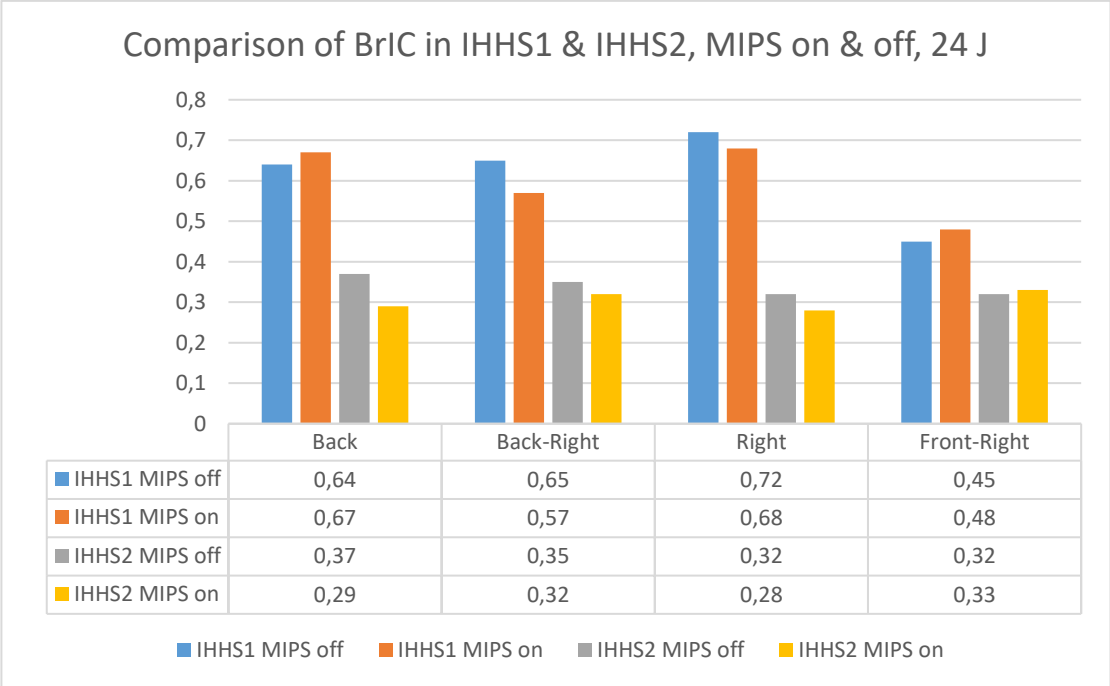


| | Back | Back-Right | Right | Front-Right |
|---|---|---|---|---|
| IHHS1 MIPS off | 0,64 | 0,65 | 0,72 | 0,45 |
| IHHS1 MIPS on | 0,67 | 0,57 | 0,68 | 0,48 |
| IHHS2 MIPS off | 0,37 | 0,35 | 0,32 | 0,32 |
| IHHS2 MIPS on | 0,29 | 0,32 | 0,28 | 0,33 |

**Figure 6.31** *Comparison of BrIC in IHHS1 and IHHS2, both for MIPS on and MIPS off tests*

In *Figures 6.30* and *6.31* a comparison between HIC and BrIC of CoM for IHHS1 and IHHS2 has been assessed. A comparison for what concerns the angular accelerations does not make sense because it is already known the fact that for IHHS1, lacking of cerebrospinal fluid, the angular accelerations can arrive to be from 5 to 10 times the accelerations recorded by IHHS2.

Both for HIC and BrIC it is visible that the values calculated with data recorded from IHHS1 are much higher that the indexes from IHHS2 and it is surely due to the fact that the silicone oil acts as a dumping system in the second model of head. Another thing that is interesting to notice is the fact that IHHS1 is more sensible to the variation of the kind of impact, while for IHHS2 does not matter so much if the impact is Back or Right or any other position, the values of HIC and BrIC will always be similar. Even if IHHS2 does not seem to be susceptible for what concerns the effects of MIPS protection, the results are surely more precise that the ones obtained by IHHS1 because of the silicon oil.

# Chapter 7

# Deformations in the Brain

The latest model of sensorized head developed in the project, called IHHS2, is capable of measuring the accelerations of the helmet, of the skull and of different points of the brain in order to understand the complex motion of the lobes. In addition to the accelerations, a triaxial gyroscope in the center of mass of the brain, a biaxial gyroscope in the center of cerebellum and triaxial gyroscope on the skull are used to detect angular velocities and from it angular accelerations can be calculated. Besides accelerations and angular velocities, there is another thing that would be interesting to measure, and it is the deformations inside the brain. There is no device or hardware in IHHS2 capable to record deformations, in fact the commercial strain gauges can measure only deformations in the range of 5%. Because of the absence of devices that can arrive to deformations range of 20 – 30%, the idea of using accelerometers to find the displacements was born. Double integrating by time the accelerations, the displacements can be detected. However it has to be verified the fact that displacements so calculated are precise or at least realistic. To verify this, a mockup cube in the same material of the brain has been built.

## 7.1 Mockup Cube

To verify if it is possible to detect in a precise way the displacements of different points in the brain, it was decided to build a mockup cube in *Plastil Gel 00-25* with 4 accelerometers inside. The dimension of the edges of the cube is 75 mm and the accelerometers are placed in order to define a reference system inside the cube. To define the reference system inside the cube are needed 4 accelerometers, in fact one is used to simulate the origin of the system, while the other 3 are used to indicate the directions of the axes. This is helpful for testing the cube, in fact if the cube is solicited by a weight falling onto it, the 4 sensors record the accelerations while the silicon rubber is deformed. The signals of the accelerometers are integrated in order to calculate the displacements of the same

devices and the displacements can be used to measure the deformations in three different directions. In the following images the cube will be shown through drawings in order to make it clear the accelerometers position.

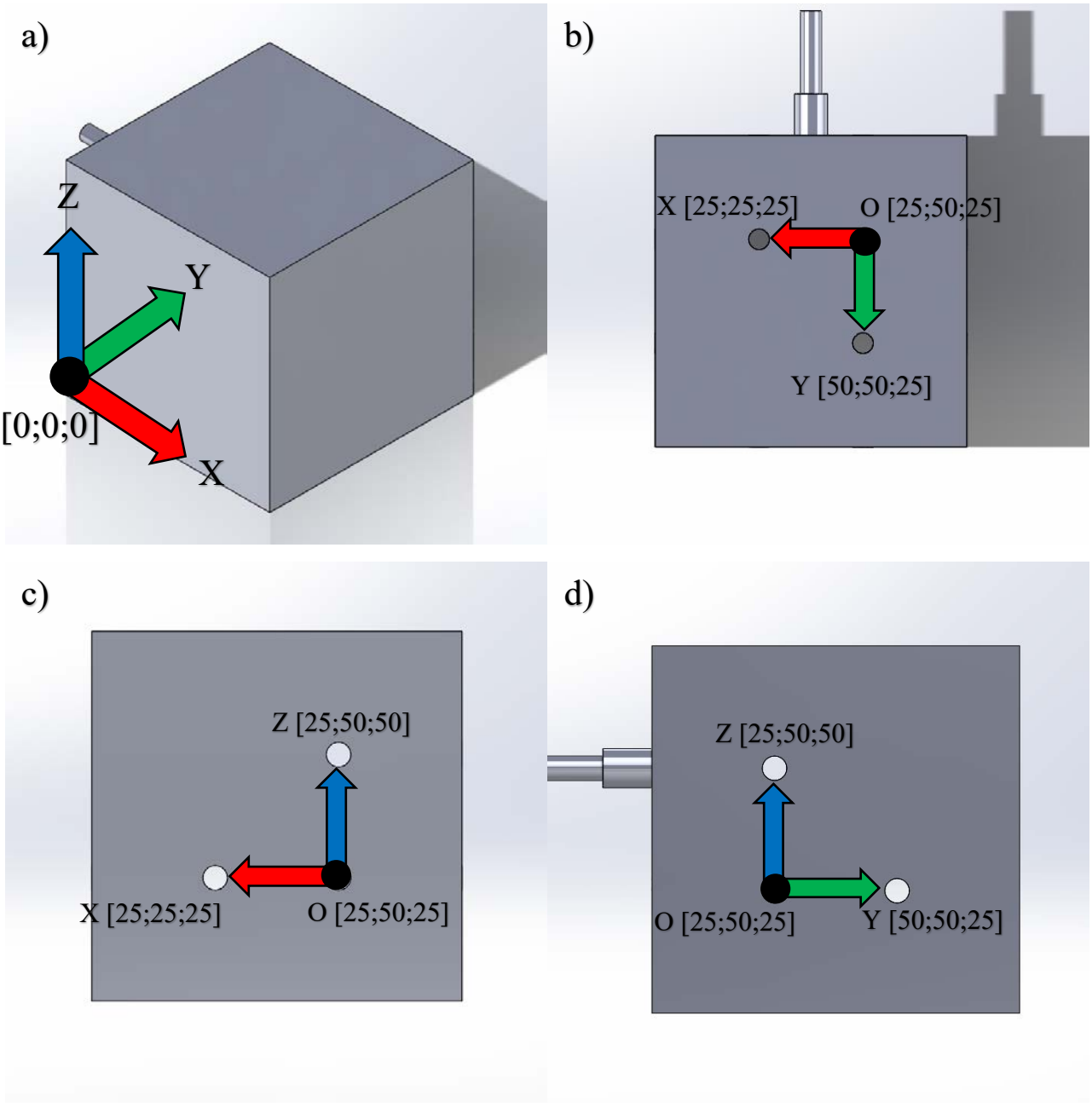


**Figure 7.1** *Definition of accelerometers positions in cube. (a) Definition of a provisional reference system needed to express position of accelerometers defining axes of the principal reference system. (b) Cube seen from above with highlighted X and Y axes of the reference system defined by accelerometers (c) Cube seen from the front with highlighted X and Z axes of the reference system defined by accelerometers (d) Cube seen from right with highlighted Y and Z axes of the reference system defined by accelerometers.*

It is now time to describe the production of the cube. 5 parts were needed to realize the molds. So many pieces were useful to find the right position in which the accelerometers are placed and to extract the cube at the ending of the curing time. The parts were designed in *Solidworks* and 3D printed with the *uPrint SE PLUS* machine. In the following images the step needed to produce the cube are shown and then the cube itself.

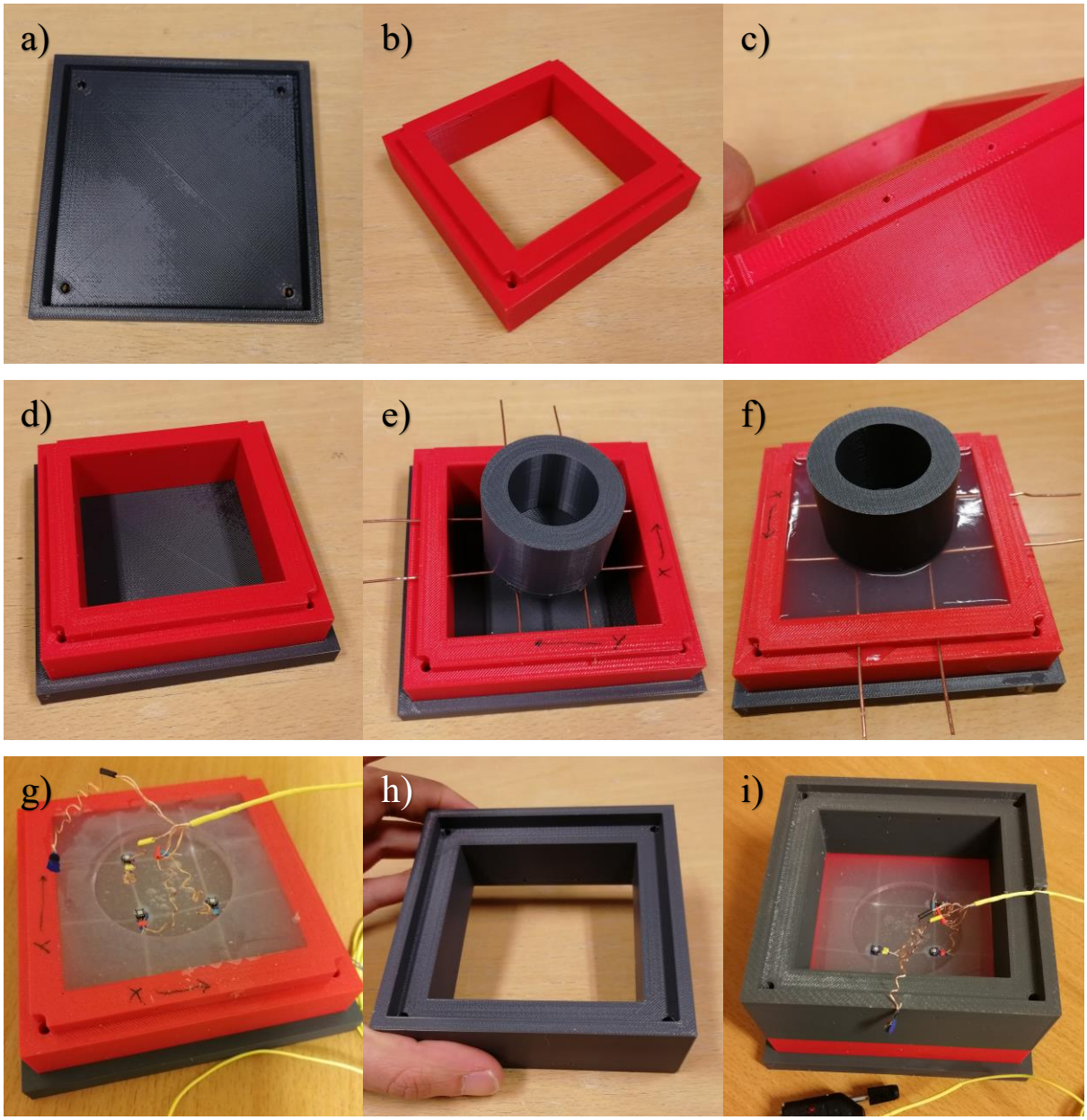

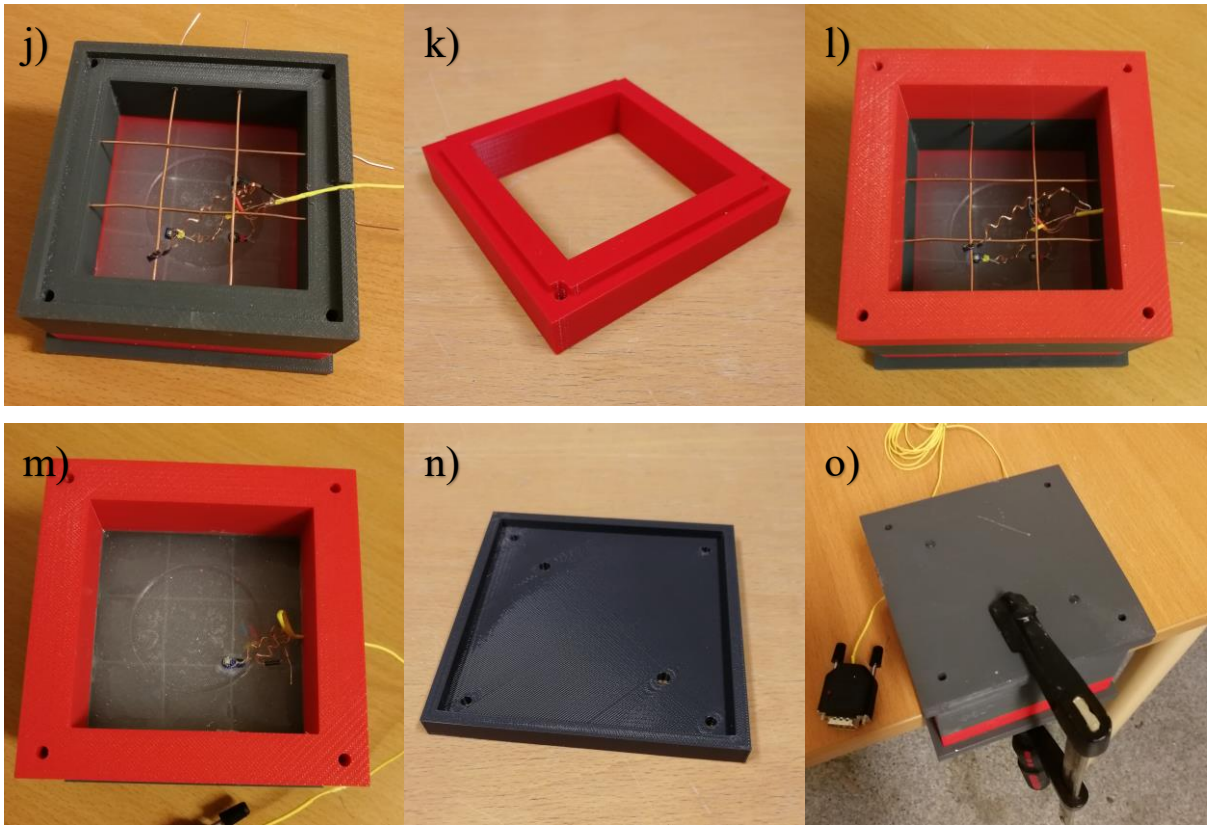


**Figure 7.2** *Parts and steps required to produce the cube. (a) Base of the molds (b) First part of the molds used to define the first layer in which the accelerometers are placed (c) On this part, every face of the inner step, needed to connect the different pieces of the molds, is characterized by 2 monospaced holes. The distance between the holes is 25mm. (d) Connection of the base with the first part of the molds. (e) The monospaced holes on the inner step of the part are needed to insert wires in order to define the level in which the accelerometers are posed. On the wires a cylindrical object is fixed. (f) The first layer of the molds is filled with component A and B of PlastilGel 00-25. The level of the silicon rubber is some mm higher than the wires and the lower face of the fixed cylindrical object. (g) The silicon rubber is left to cure and solidify during night. After the removal of the cylindrical object a flat face is left. After the removal of the wires lighter lines are left in order to find the position of accelerometers. The first 3 accelerometers are placed in the decided crossings of the lines. One accelerometer defines the Origin of the reference system (the one near the left lower corner), one defines the X direction (the right one) and the last one defines the Y direction (the one above Origin in the image). (h) Second part of the molds. This part is also characterized by the holes for inserting the reference wires and one more bigger gap needed to leave the wires of accelerometer outside the molds. (i) Connection of the first and second part of the molds (j) Insertion of the reference wires (k) Third part of the molds. It is a piece very similar to the first one, in fact are both characterized by a step useful for the connection with the second part. (l) Connection of the second*

*and third part of the molds (m) On the reference wires the cylindrical object is fixed, as for the first layer. The silicon rubber is put inside the molds and left to solidify during night. The cylindrical object and the wires are removed in order to obtain the flat surface and the lines needed to find the exact position of the last accelerometer. The last accelerometer defines the Z direction. (n) Top part of the molds. It is useful to have a flat face of the cube. It is characterized by 2 holes in order to leave the surplus of silicon rubber to flow away. (o) It is placed more silicon rubber than needed inside the molds, then the top part is placed to close the molds. It can be seen some surplus silicon rubber from the holes.*

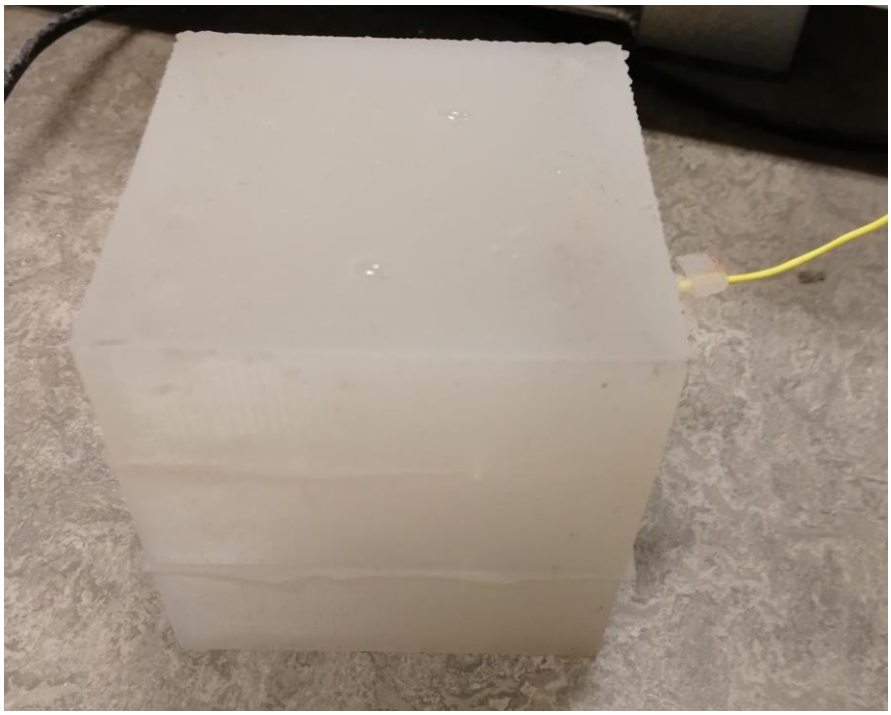

**Figure 7.3** *Mockup cube*

## 7.2 Examples of Tests Performed on the Mockup Cube

Tests on the cube are needed to verify if the calculation of displacements and then deformations between two different points of the silicon rubber is possible and precise by working on the data acquired by accelerometers. During the tests the cube is clenched to the ground and on top of it a weight of 5 kg is left to fall. The weight has an accelerometer placed on it, with the Z axis pointing downward, in order to arrive to calculate the displacement of the weight itself, and so how much the weight during its falling deforms the cube. The deformation calculated on the basis of the

accelerometers of the weight will be compared with the compression calculated by accelerometers inside the cube.

In this section two tests will be shown as example. The first one has the cube positioned in order to have the Z axis of its reference system defined by accelerometers pointing upward, so the weight falls from the positive Z direction, instead the other test has the X direction pointing upward, so the weight falls from the positive X direction. In both tests the distance between the lower face of the weight and the upper face of the cube is 50mm. This distance is important to remember because it is used to see if the double integration of data from accelerometer on weight is correct.

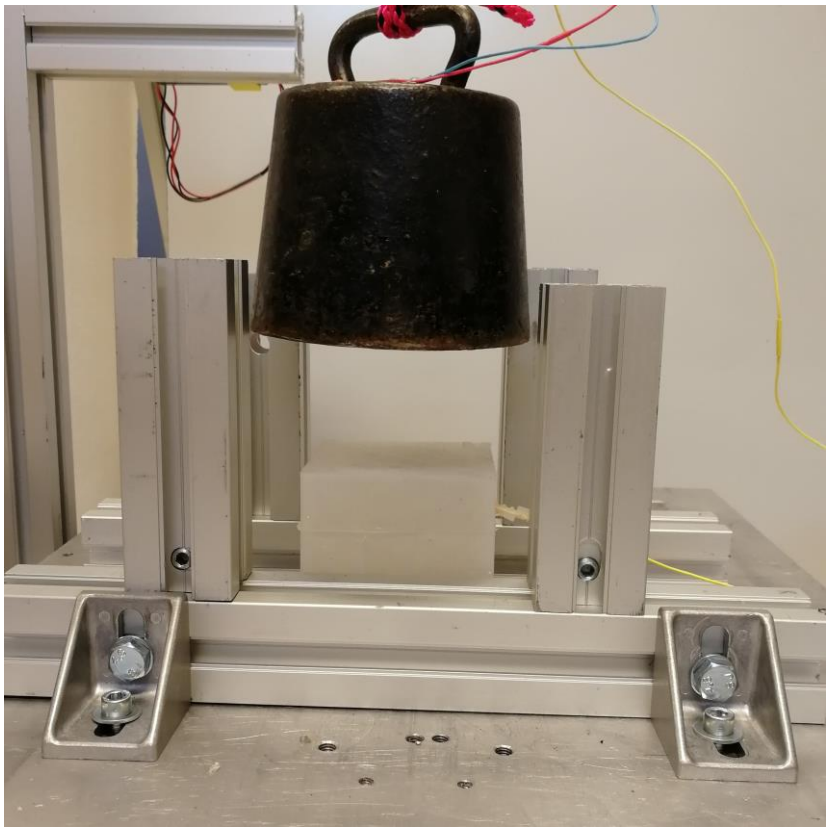

**Figure 7.4** *Setup of tests performed on cube*

### 7.2.1 Test with Z Axis of Cube Reference System Pointing Upward

This test is characterized by the Z axis of the cube pointing upward, so, with the weight falling on it, the Z direction will be characterized by compression, while X and Y direction will be characterized by positive deformation.

In the following figure will be shown the accelerations recorded by sensors inside the silicon rubber of cube.

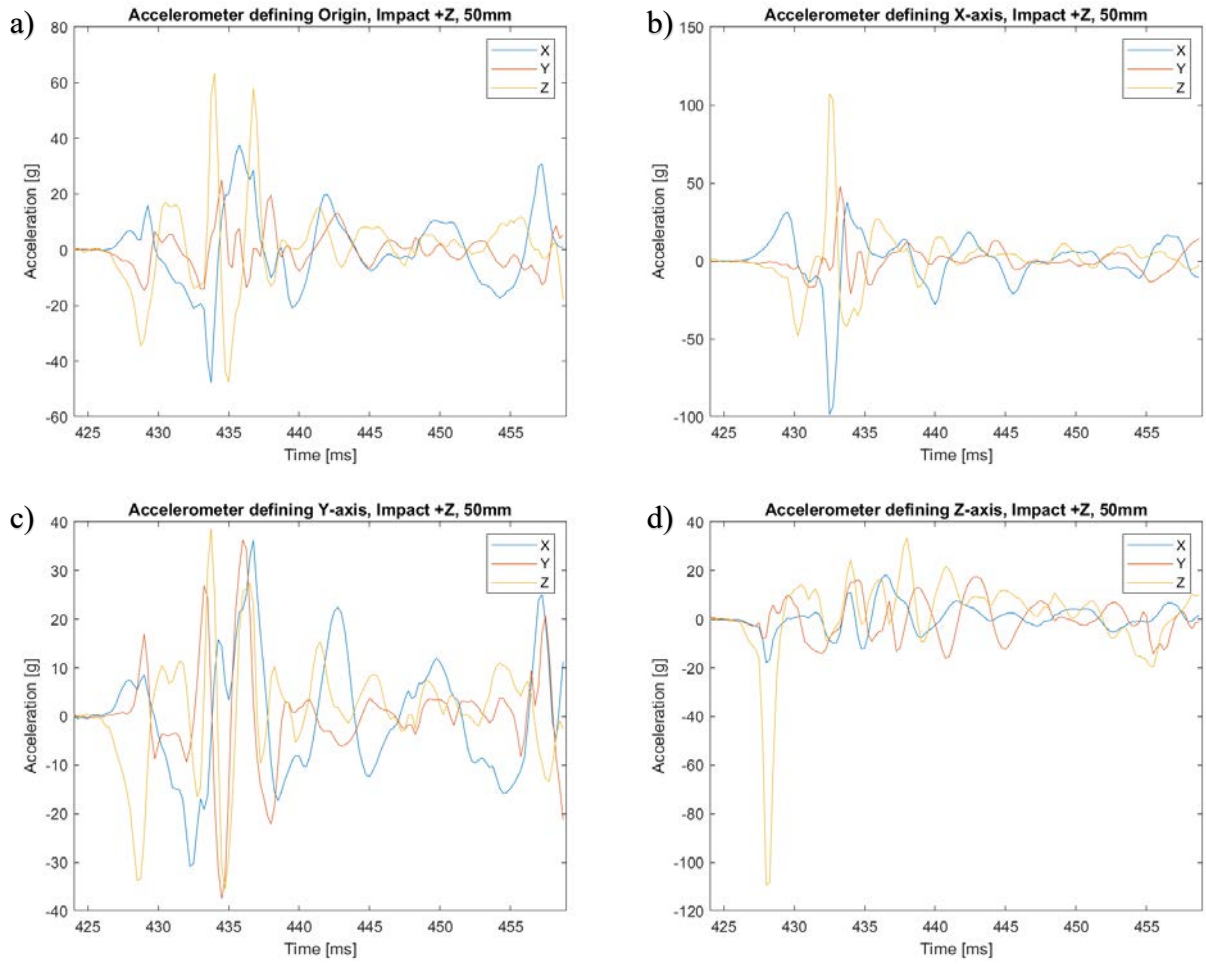


**Figure 7.5** *Accelerations inside the cube (a) Origin (b) accelerometer defining X axis (c) accelerometer defining Y axis (d) accelerometer defining Z axis.*

In the graphs only the first impact of weight with cube is shown. After the first impact the weight is pushed upward by rebound and then falls back a various number of times. The rebound fallings are not described. The Z signal of the accelerometer defining Z direction is characterized by an high and negative peak, in fact this accelerometer is the nearest to the point of impact, while the other 3 accelerometers are 50 mm under the point of impact and 25 mm under the accelerometer.

By using the following formulas the velocity is firstly obtained and lastly the displacement, were *a(t)* is the acceleration in the hypothetical X direction, *v(t)* is the speed and *x(t)* is the displacements.

$$v(t) = \int_{t_1}^{t_2} a(t)dt$$

$$x(t) = \int_{t_1}^{t_2} v(t)dt$$

Now the displacements obtained by the single accelerometers will be shown.

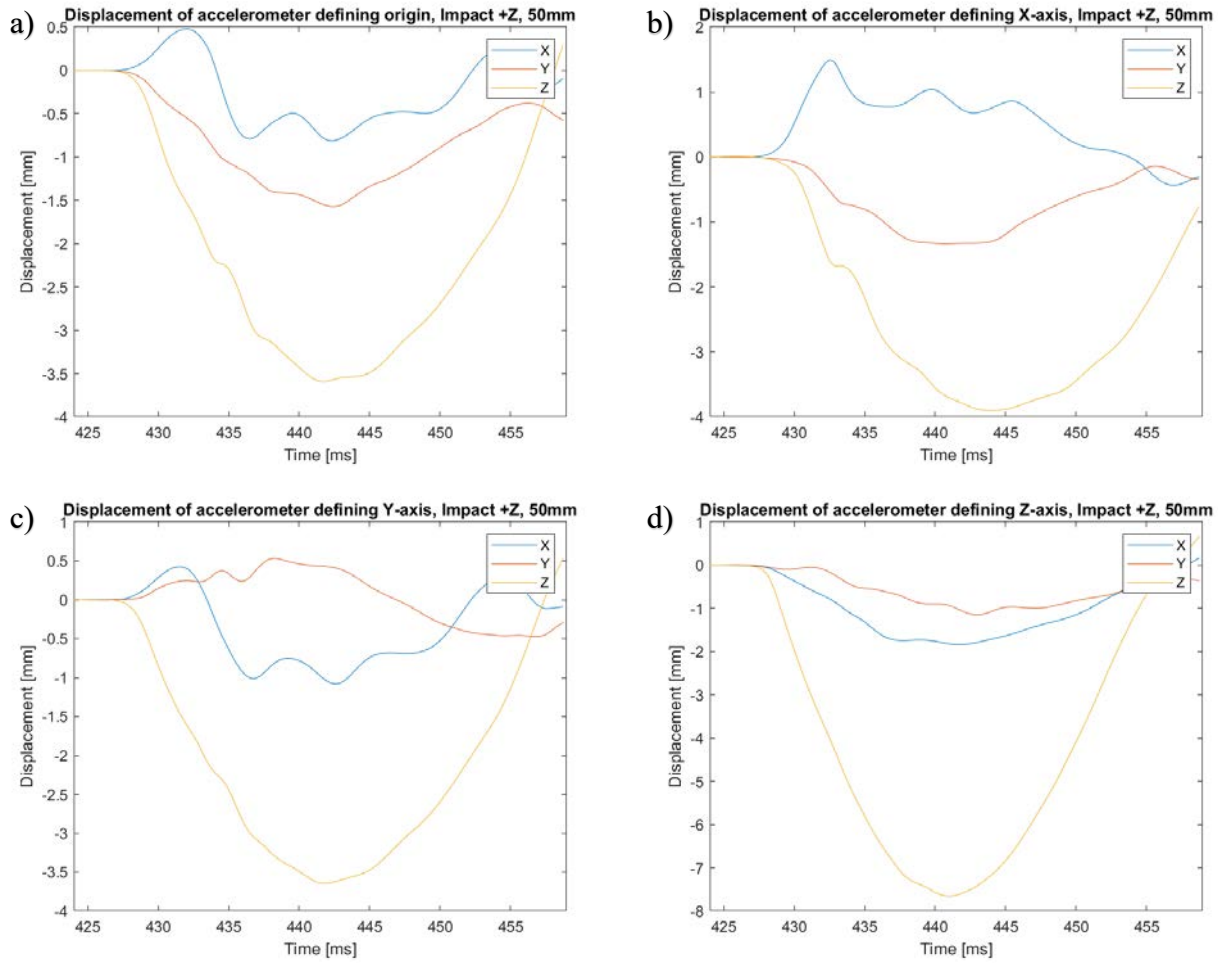


**Figure 7.6** *Displacemets inside the cube (a) Origin (b) accelerometer defining X axis (c) accelerometer defining Y axis (d) accelerometer defining Z axis.*

From all the graph of the previous figure, all the displacements in Z direction are negative.

To calculate the deformations along the axis defined by the accelerometers inside the cube are needed only to elaborate 6 signals of displacements out of 12. They are the X, Y and Z signal of Origin, called $x_0$, $y_0$, $z_0$, the X signal recorded by the accelerometer defining X axis, $x_x$, the Y signal of the accelerometer defining Y axis, $y_y$, and the Z signal of the accelerometer defining Z axis, $z_z$.

The formulas are used to calculate strain. Strain is indicated with ε letter. The initial distance between accelerometers is always 25mm and indicated with $l_0$.

$$\varepsilon_x = \frac{x_x - x_0}{l_0}$$

$$\varepsilon_y = \frac{y_y - y_y}{l_0}$$

$$\varepsilon_z = \frac{z_z - z_0}{l_0}$$

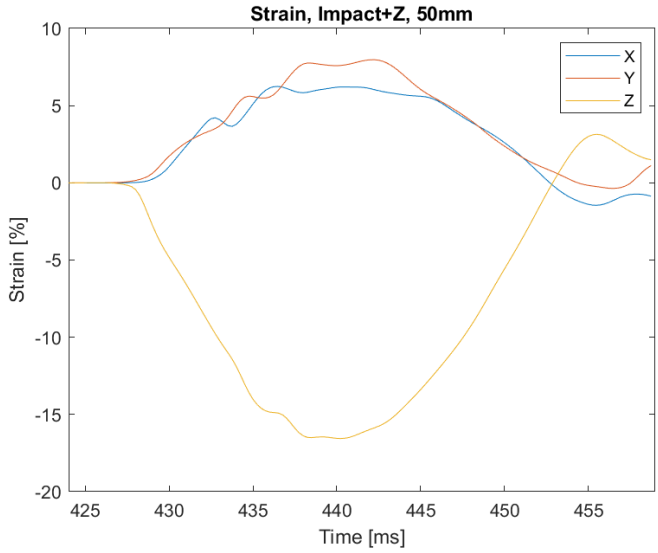


**Figure 7.7** *Strain in X, Y and Z direction*

From the figure can be seen the fact that Z strain is negative as predicted and X and Y strain are positive. It is a good sign because the deformations respect the theory. The Z strain, that is compression, is near 15% while X and Y which are positive deformation are both near 7%.
It is now time to analyse the accelerometer on weight.

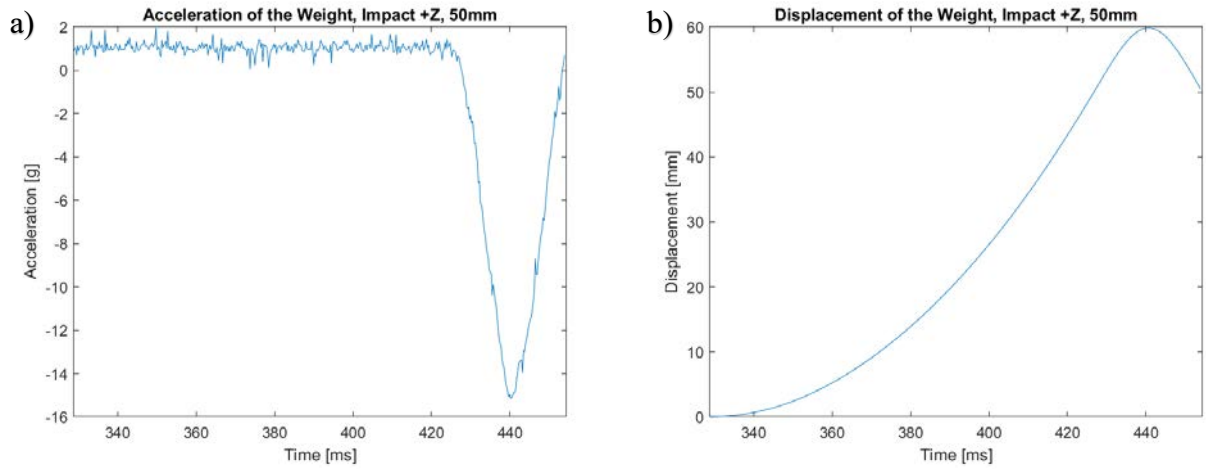


**Figure 7.8** *Data from accelerometer on weight. (a) Acceleration (b) Displacement*

The acceleration used to calculate the displacement is only the part composed by falling of the weight, characterized by the value of 1g, and the negative peak of acceleration. The integration is calculated until the acceleration reaches again the value of 1g, that is when the silicon rubber of the cube finish to push upward the weight, in fact at 1g the weight is free to move in the air without touching anything. If the integration is done this way, the displacement is firstly 0, when the weight is falling,

displacement is increasing, then weight sinks in the silicon rubber and reaches its lowest points corresponding to maximum displacements. After that silicon pushes weight upward and when the weight shows another time the acceleration of 1g means that it is no more in contact with cube and the displacement has to be in value 50 mm, that is the drop height.
In the following table will be shown the informations taken from the weight accelerometer, and then the maximum deformations along the X, Y, Z axis of the cube. The sinking of weight inside the cube is calculated as difference between maximum displacement, $l_{max}$, and displacement at detachment of weight and cube, $l_d$. This sinking is used to calculate the deformation of the whole cube in the vertical direction. The high of cube is 75 mm and is indicated as $L_0$.

$$\varepsilon_{cube} = -\frac{L_0 - (l_{max} - l_d)}{L_0}$$

| | |
|---|---|
| Maximum displacement | 59,85 mm |
| Displacement at detachment of weight and cube | 50,44 mm |
| Drop height | 50,00 mm |
| Sinking of weight inside the cube | 9,42 mm |
| Cube deformation | -12,56% |
| Maximum X deformation | 6,24% |
| Maximum Y deformation | 7,97% |
| Maximum Z deformation | -16,56% |

**Table 7.1** *Sum up of information acquired during test*

From the table it can be seen that the displacement of accelerometer on weight at detachment of weight and cube is very similar to the nominal drop height, with a difference inferior to 0,5 mm. That information suggests that integrating the acceleration to arrive to displacement is a good method. However the compression in Z direction recorded through the accelerometers in the cube is -16,56% and there is a not negligible difference with the deformation estimated on the sinking of weight inside cube. However it is right to remember that the deformation estimated with considering the sinking is calculated on the distance of 75 mm, while the deformation inside the cube is calculated only in the space between two different accelerometers placed at 25 mm distance.

### 7.2.2 Test with X Axis of Cube Reference System Pointing Upward

The only difference with the previous test is the position of the cube, in fact now the cube has the X axis pointing toward, while the drop height instead remains the same. In this case the compression will be found in the X direction, while positive deformations will be detected in Y and Z direction. Now graphs showing the accelerations of the first peak of impact in the cube will be presented.

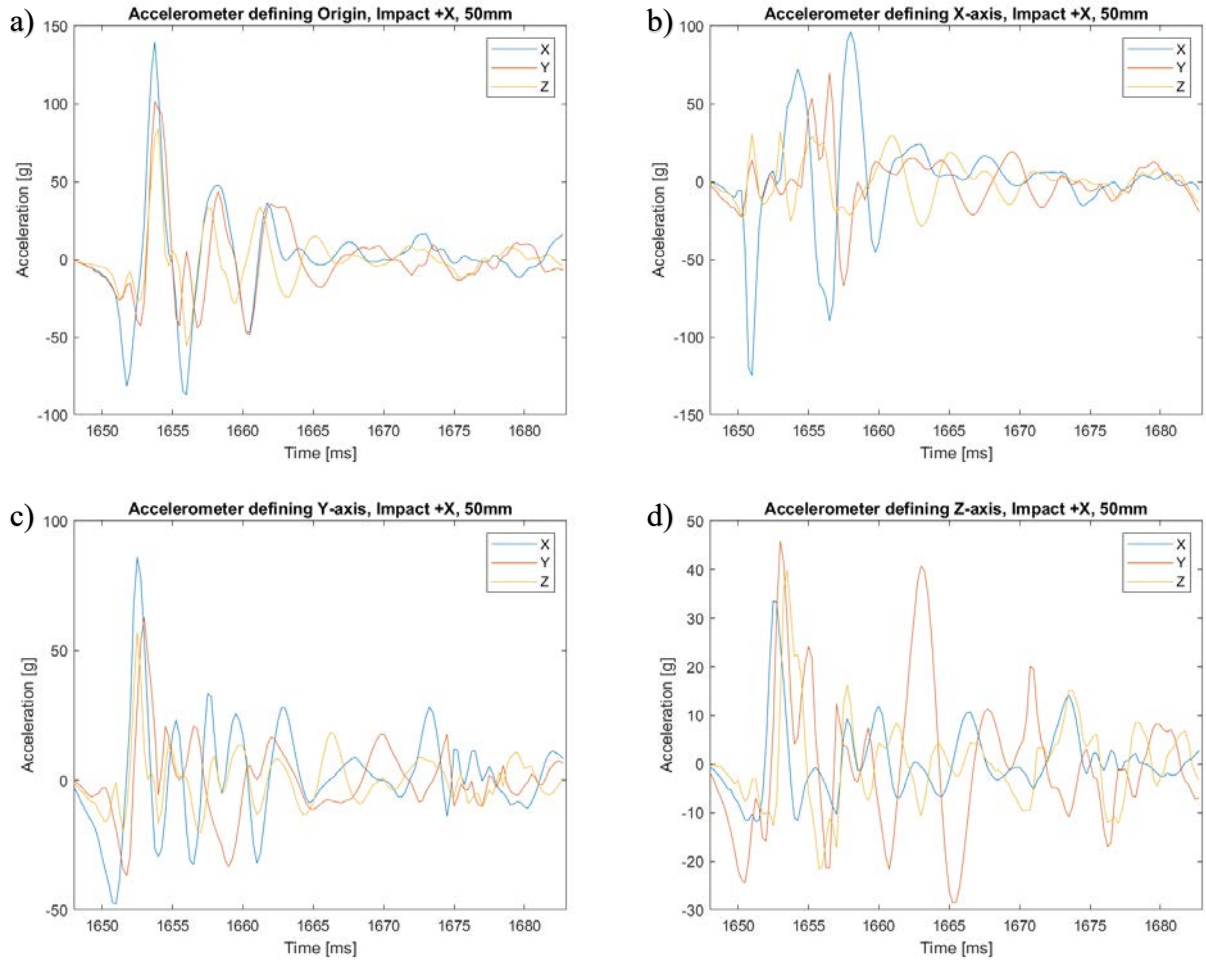


**Figure 7.9** *Accelerations inside the cube (a) Origin (b) accelerometer defining X axis (c) accelerometer defining Y axis (d) accelerometer defining Z axis.*

Now the accelerometer that is near the place of impact is the one defining the X direction, only 25 mm under the top face of cube, while the accelerometers defining Origin, Y and Z direction are 50 mm under the point of impact. That is visible in the differences of signals recorded, in fact the X acceleration of the accelerometer defining X axis has a negative peak surpassing the level of 100 g, while the other accelerometers have not so high peaks.

In the following figure the displacements calculated will be shown.

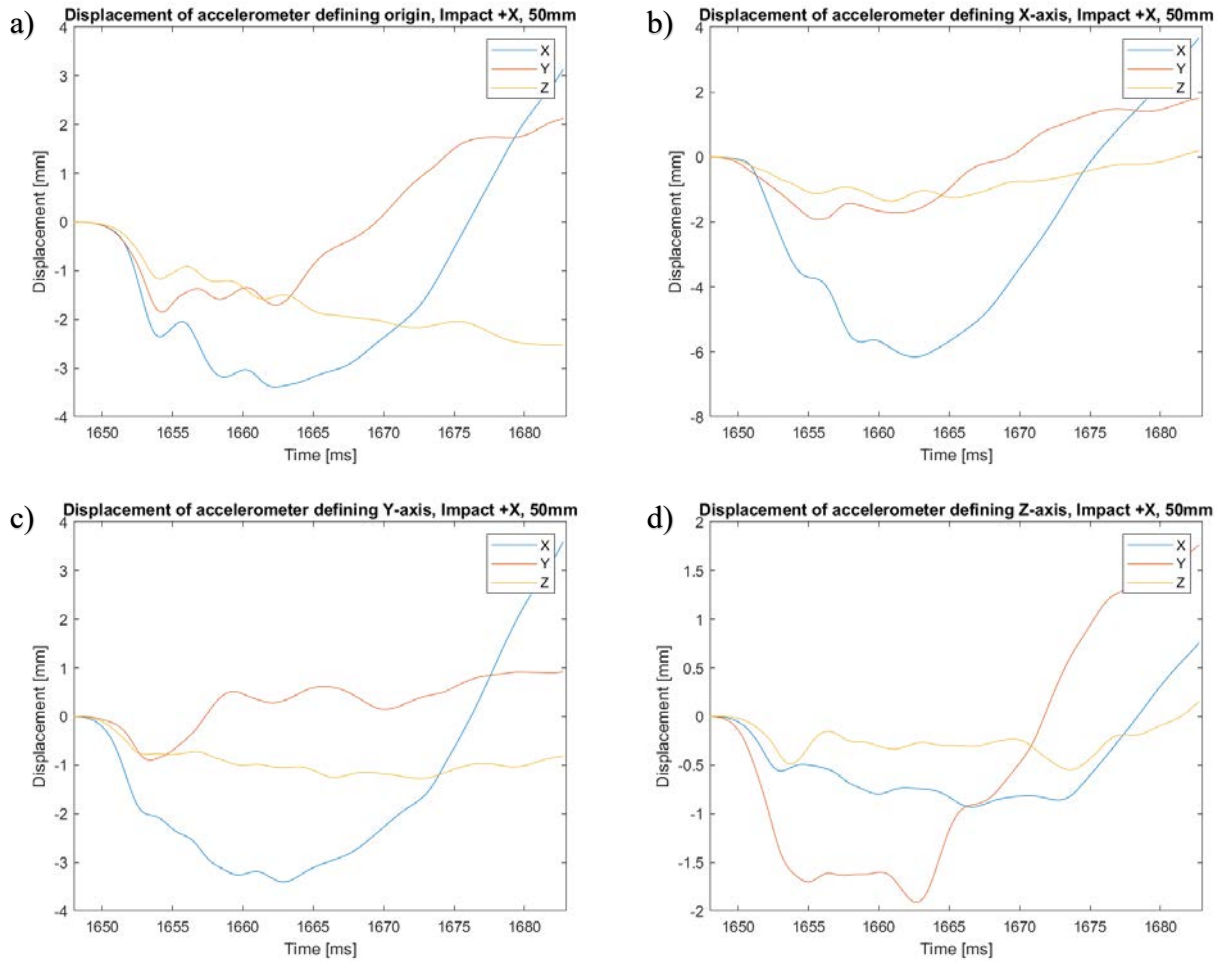


**Figure 7.10** *Displacemets inside the cube (a) Origin (b) accelerometer defining X axis (c) accelerometer defining Y axis (d) accelerometer defining Z axis.*

From the displacements the strain in X, Y and Z direction of the reference system individuated by the accelerometers' position will be calculated. After the strain it is time to present the data acquired by accelerometer on the weight. Of the acceleration recorded will be only shown the portion of the signal characterized by the value of 1g, that is weight falling, until the signals arrive at the value of 1g after the negative peak of acceleration representing impact.

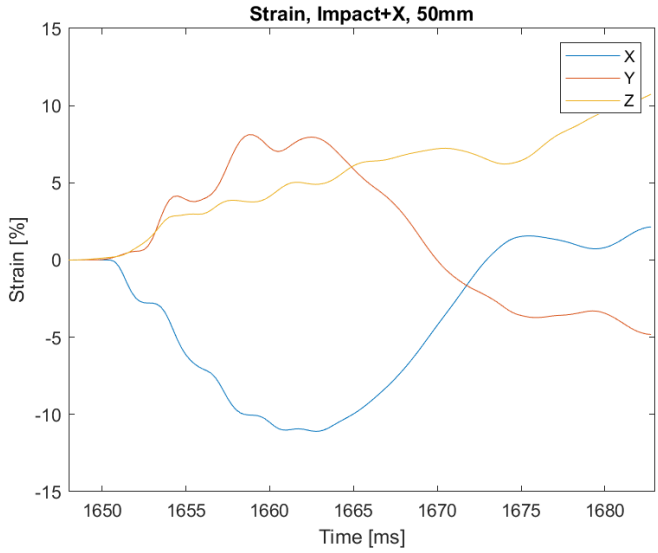


**Figure 7.11** *Strain in X, Y and Z direction*

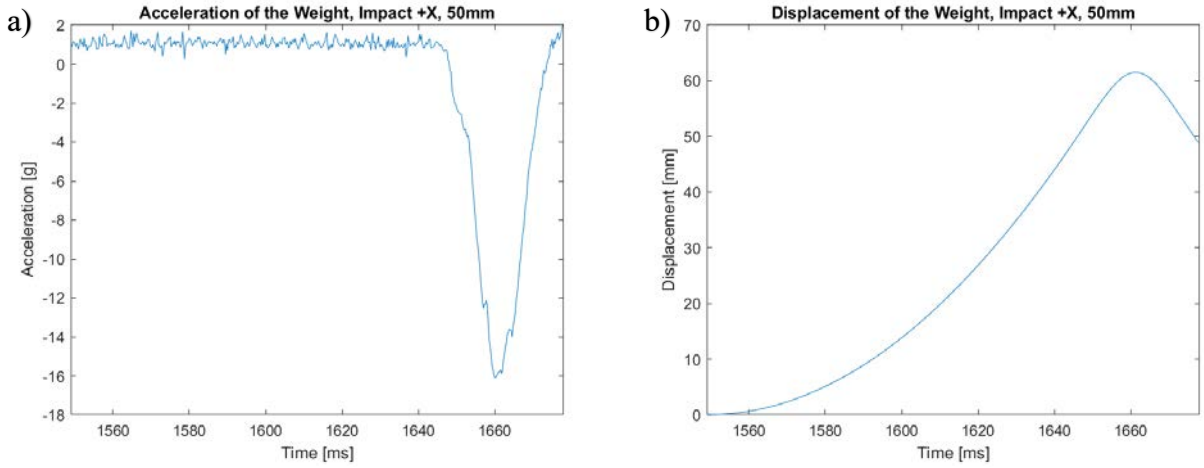


**Figure 7.12** *Data from accelerometer on weight. (a) Acceleration (b) Displacement*

In the table will be summed up the data obtained from the test.

| | |
|---|---|
| Maximum displacement | 61,49 mm |
| Displacement at detachment of weight and cube | 48,86 mm |
| Drop height | 50,00 mm |
| Sinking of weight inside the cube | 12,63 mm |
| Cube deformation | -16,84% |
| Maximum X deformation | -11,10% |
| Maximum Y deformation | 8,12% |
| Maximum Z deformation | 10,74% |

**Table 7.1** *Sum up of information acquired during test*

From both of tests is understandable the fact that integration of the acceleration signal is not perfectly precise but at least can be used to understand the magnitude order of strains inside the silicon rubber. The data presented in this section were cut only in the interesting part of the acquisition and not all of that because of the time required by computer to elaborate vectors in order to obtain displacements and deformations.

## 7.3 Attempts of Calculating Strain inside IHHS1

The tests on cube suggests that it is possible to apply the integration process to the accelerations recorded by IHHS1 or IHHS2 sensors. In this section will be shown the attempts of calculating displacements and strain in IHHS1. It has been decided to calculate strains along the lines connecting ML and MR, posed at 80 mm distance, ML and CoM, MR and CoM, both characterized by sensors distance of 40mm, CL and CR, at 70 mm distance. All of this deformations are along the Y direction. In addition to them also the stains in the line connecting TL with ML and TR with MR. This two lines lie neither in the Y direction nor Z direction. The strain between TL and TR was not possible to be calculated because of the separations of the lobes. Strains in the X direction are not possible to be individuated because all of the sensors are placed in the same coronal plane passing through CoM, besides for the cerebellum sensors, which are on an appendix of the whole brain structure.
In the following figure will be shown only the displacement calculated for an impact Back occurring at 24J.

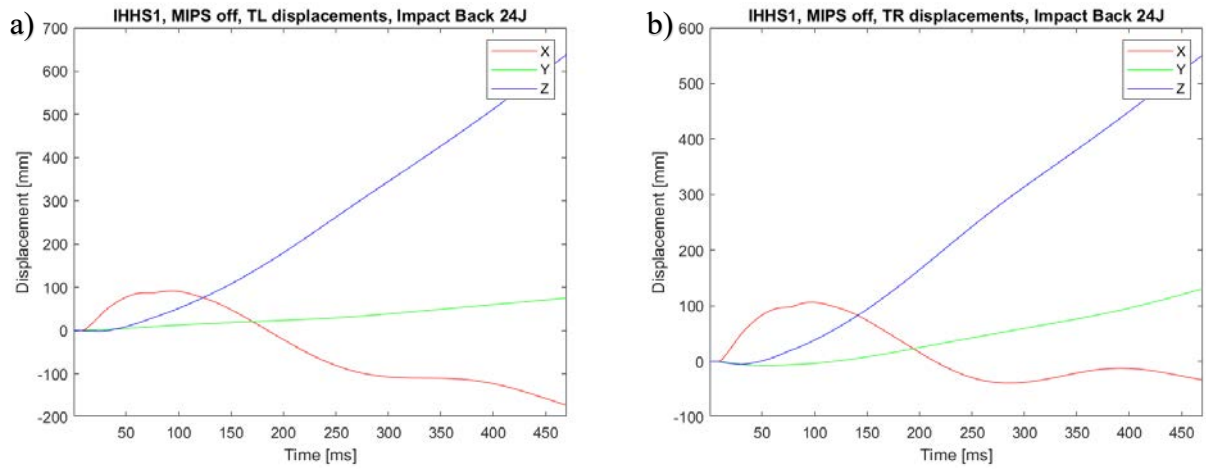

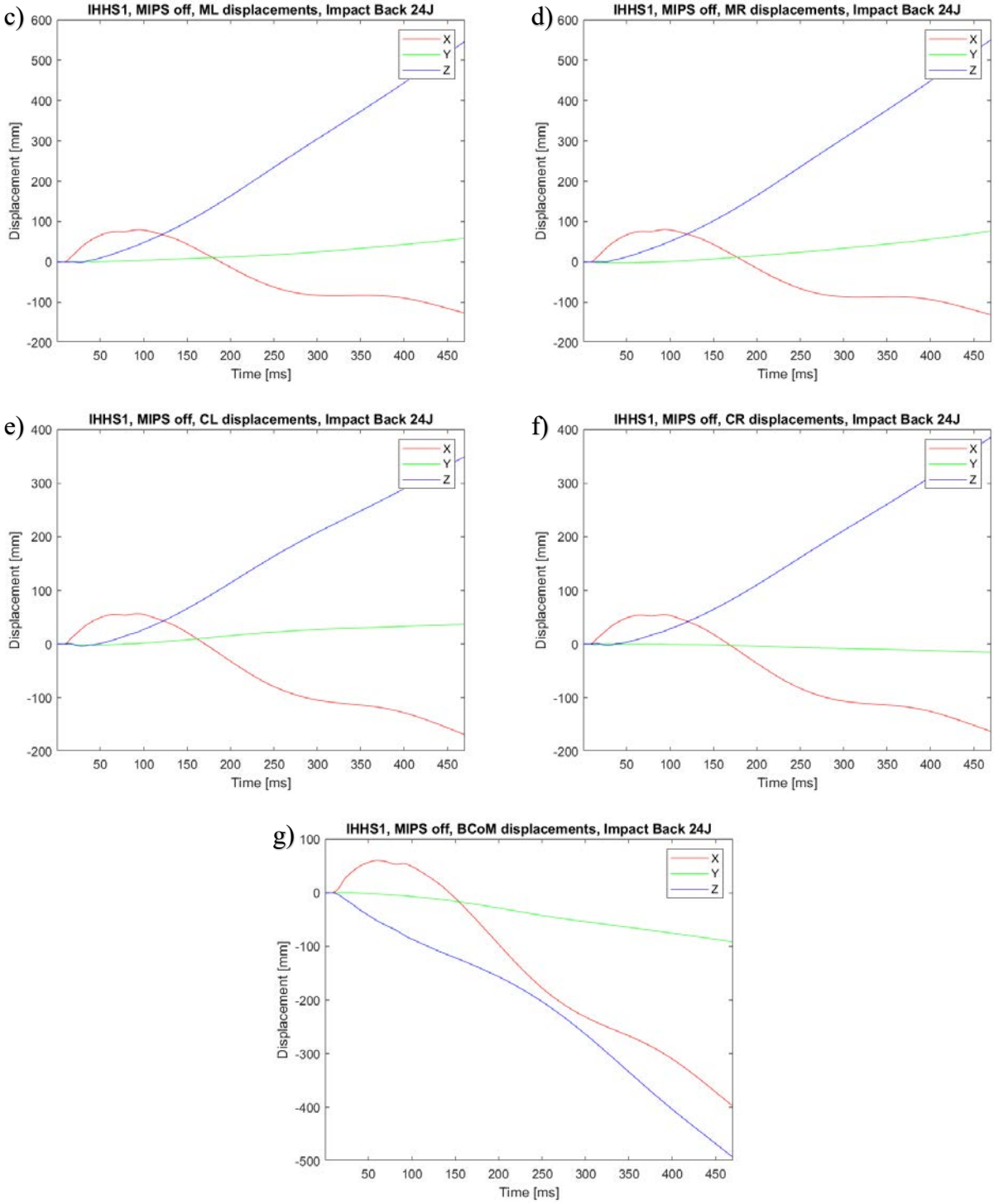


**Figure 7.13** *Calculated displacements of accelerometers. (a) TL (b) TR (c) ML (d) MR (e) CL (f) CR (g) CoM.*

As can be seen from all of the graphs, the displacements show not correct values and behaviour, in fact at the end of acquisition, when the head has finished its motion, the accelerometers should be placed at the initial position or at a position near it, characterized by values near 0mm of displacements. Each signal of the accelerometers instead tends to have the final position with

displacements even surpassing 600 mm. That means that the process of double integration is characterized by an error that continue to increase at the increasing of the temporal window. In the cube tests this phenomenon was not visible because of the short temporal window used, focused only on the first peak of impact between weight and cube. The temporal window used in cube tests was around the value of 0,035 s while in IHHS2 was decided to use the whole acquisition. The acquisition on IHHS1 is 0,5 s long, carried out at 10 ksps. Each signal is represented by a vector of 5000 samples, but the first 300 samples are cut because they contain the electrical trigger signal, so the useful values are 4700, corresponding to the 470 ms shown. However the dimensions of the temporal window are different for an order of magnitude and this lead to results really discordant.

If the values of displacements are terribly wrong, also the strain calculated will show the same error, in fact some of the strain arrive at the final instant of time with strains above 400%.

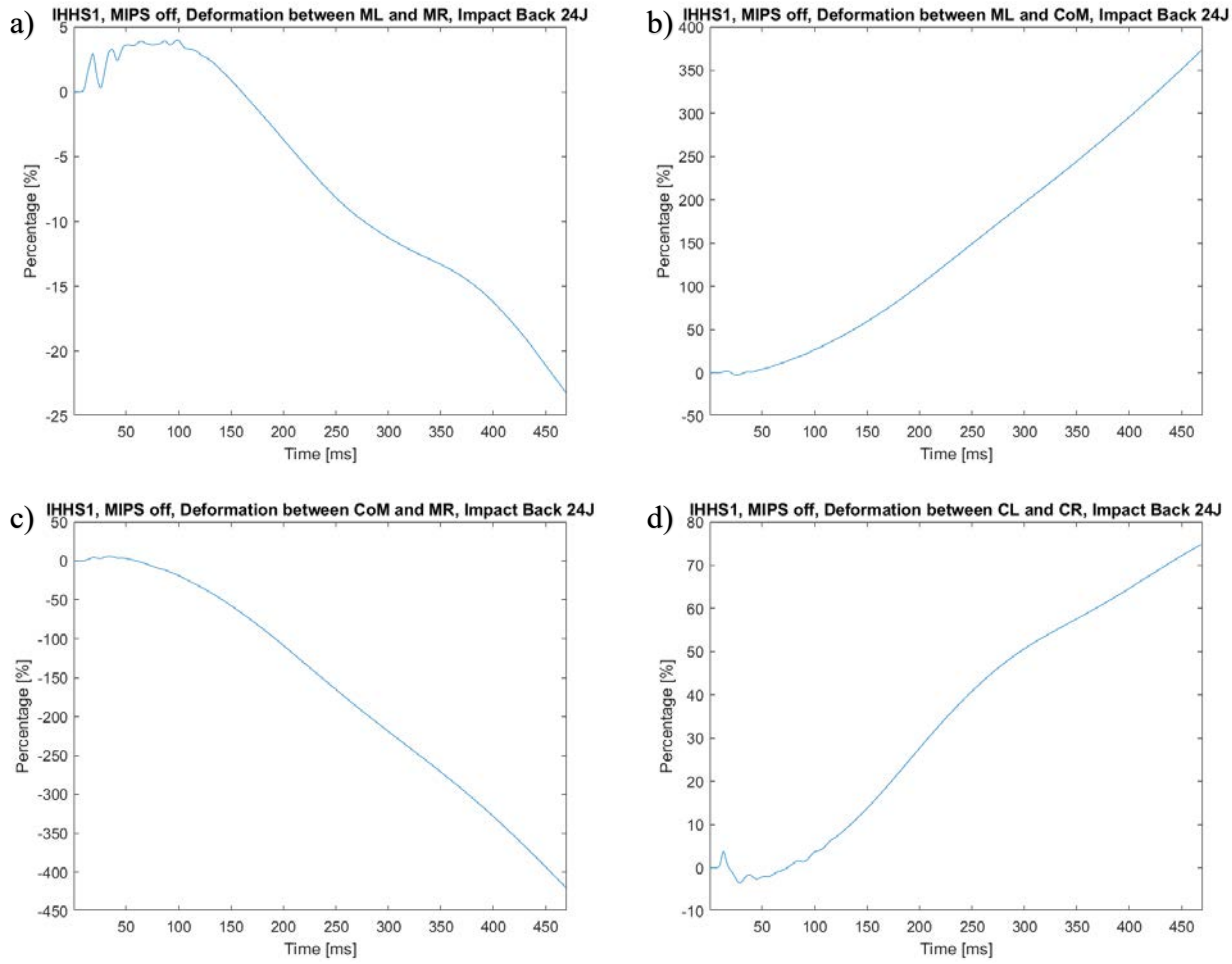

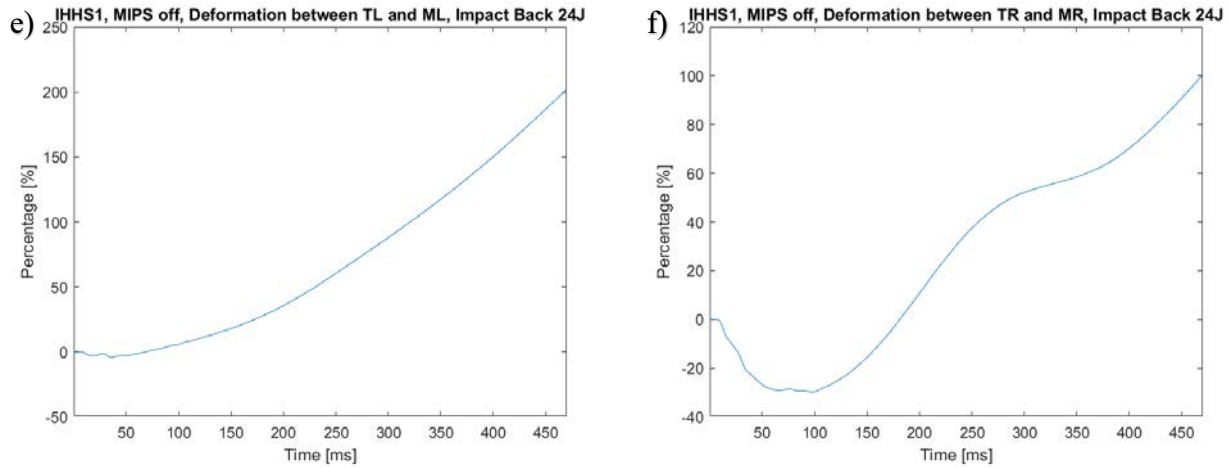


**Figure 7.14** *Strains between different accelerometers (a) between ML and MR (b) between ML and CoM (c) between CoM and MR (d) between CL and CR (e) between TL and ML (f) between TR and MR*

The error that increase with time can be caused by the not perfect waving of signal around the value of 0 g, but around a constant value slightly above or slightly under it. This value maybe cannot be seen from the graphs but if present, can create a linear error pointing toward + or - ∞ integrating one time, so passing from acceleration to speed, and integrating another time the linear error becomes a parabolic error, passing from speed to displacement. Under this hypothetical type of error, a method of correction has been developed. Firstly the acceleration in g is multiplied for 9,80665 in order to obtain the dimension of $m/s^2$. Then the signal is integrated in order to arrive to the speed in m/s. The speed will show an error in fact at the end of the temporal window the value will not be near 0 m/s, and this error should have a linear component. Because of that, through Matlab, a vector representing a line passing for 0 m/s at the first sample (0,0001 s) and for the final point at 0.47 s is built and subtracted from the speed signal. After that the speed signal will pass for 0 m/s both in the initial sample and in the final one. This is a simplification, in fact after 0,47 s the hit is finished but the head probably is slightly and slowly waving around the initial position, so it cannot be certain that in 0.47 the speed is really 0 m/s but it also can't be too wrong. The corrected speed will be integrated another time to pass to displacement expressed in meters and the displacement will show another error. As before it is needed to build a line passing for the initial and final point to subtract from displacement, in order to have a correct displacement passing through the value of 0 m both at the initial and final point. In the following figure will be shown the process in the X direction for CoM. The same process has to be applied to each signal, X, Y and Z, of every accelerometer.

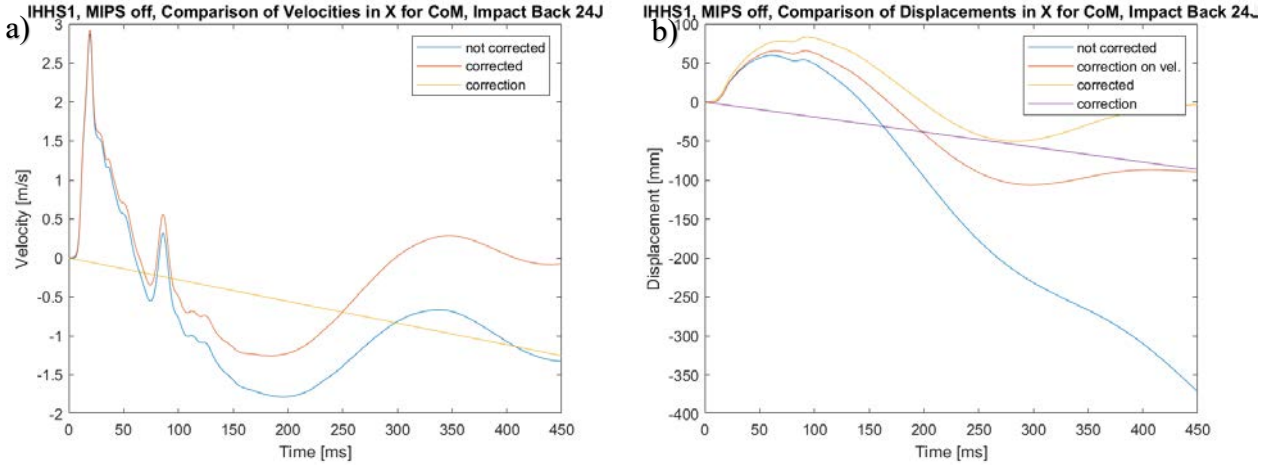


**Figure 7.15** *Process of correction of integrated signals. (a) Comparison of speed corrected and not corrected. In blue there is the signal obtained only by integration of acceleration, in yellow the correction line, while the last signal is the result of subtraction between the integration and aforementioned line. (b) Comparison of displacement corrected and not corrected. In blue there is the integration of speed not corrected, that is the signal without any correction. In green there is the integration of the corrected speed. In purple there is the line to correct the aforementioned signal. In yellow there is the correct displacement.*

It is now time to show the corrected displacements on the Back impact occurring at 24J.

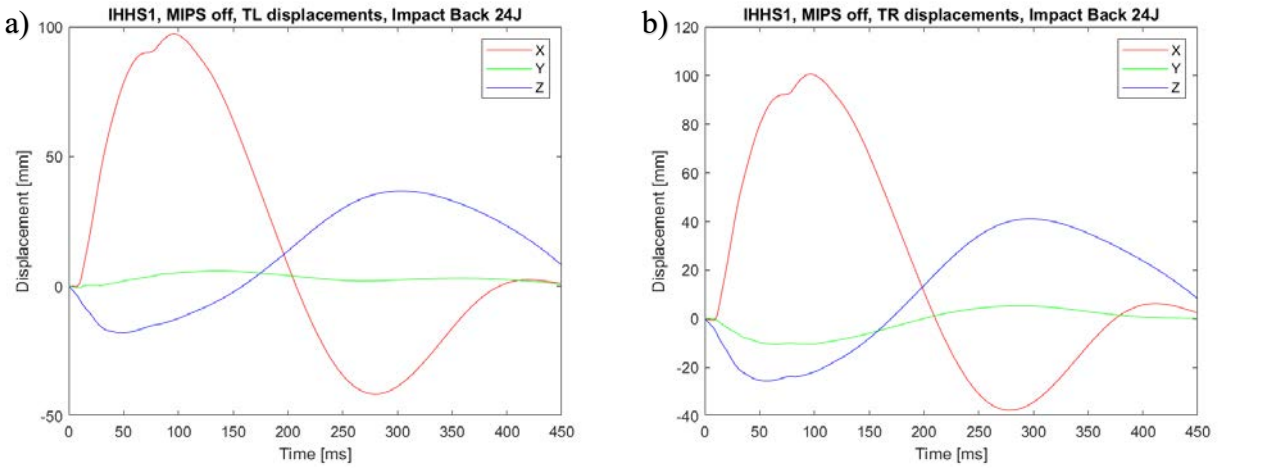

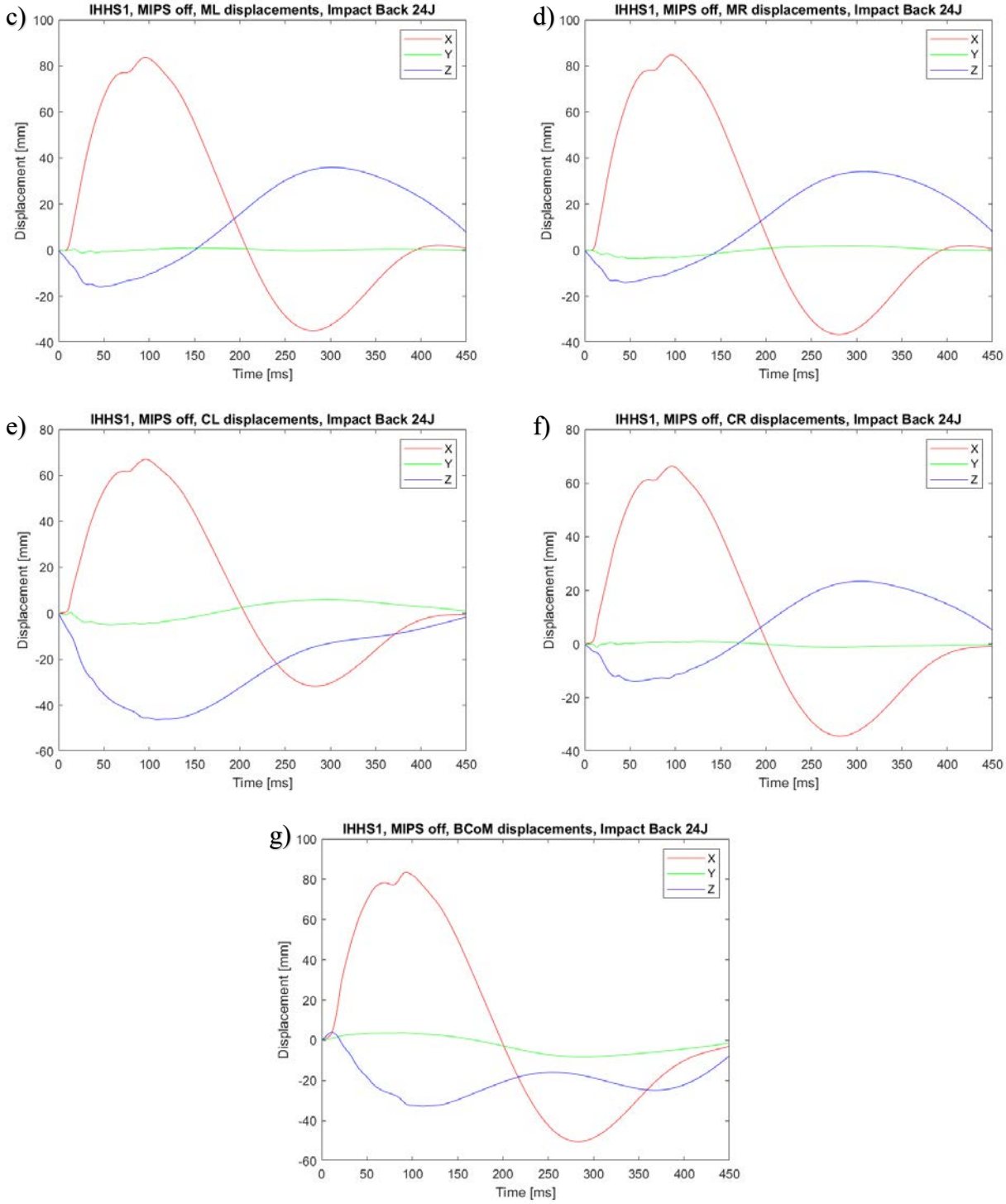


**Figure 7.16** *Corrected displacements of accelerometers. (a) TL (b) TR (c) ML (d) MR (e) CL (f) CR (g) CoM.*

As can be seen form the figure, the displacemet in the top layer are bigger than displacements in middle or cerebellum layer, and that is because TL and TR are in a position far from the center of rotation of the head. TL and TR show a displacement in X that arrive to 100 mm, while ML, MR and CoM in the middle layer arrive to 80 mm. Instead the cerebellum sensors positioned in the lowest

positions can touch 60 mm. In Y direction each accelerometer have really low values, in fact Y is not a principal direction of impact. The Z direction instead is characterized by a waving of 40 mm around. The values found in this graphs are concordant with what can be seen in the video of the test. Now the strain obtained from the corrected displacements will be presented.

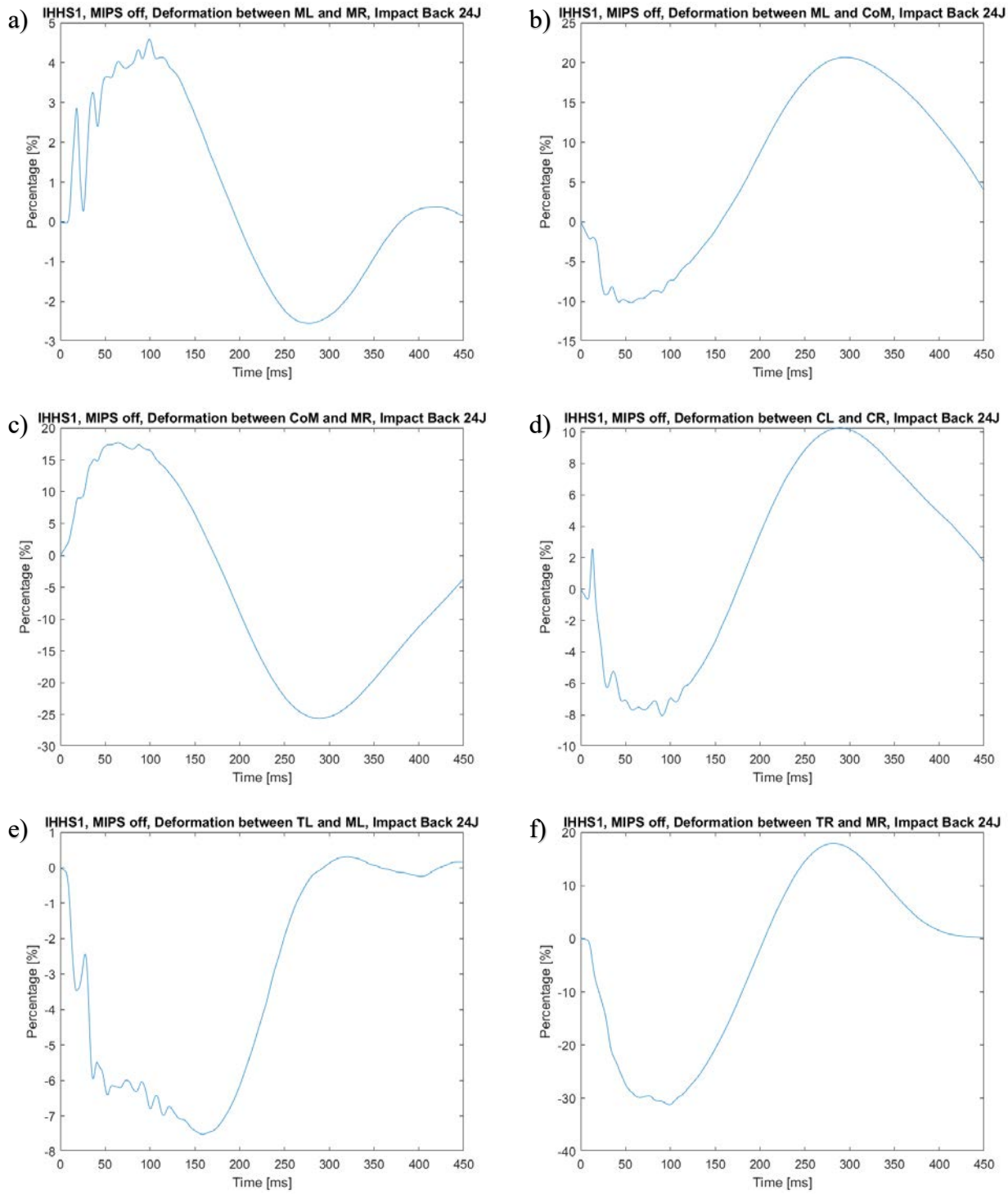


**Figure 7.17** *Strains between different accelerometers (a) between ML and MR (b) between ML and CoM (c) between CoM and MR (d) between CL and CR (e) between TL and ML (f) between TR and MR*

Results presented in *Figure 7.17* are only supposed to be right and have to be taken only as a first attempt to understand and predict them. In fact this method of strain calculation is based on two hypotheses. The first one is that the error has a linear behaviour in speed and a parabolic behaviour in displacement due to the fact that the acceleration signal does not wave around 0 g but a value slightly under or slightly above it. However there is no confirmation to this hypothesis, in fact there is no way to understand if the value around which acceleration waves is the same during all of the acquisition, or if, because of electrical phenomena inside the acquisition system, this component changes. The other hypothesis is that the head is completely still after 0.47s that the acquisition begins. Probably it is not correct because of a slow and slight movement that is not already finished. Another problem that can affect the veracity of the strain calculated with corrections is the fact that the head during the impact changes its inclination because of rotations around different axis, and for a Back impact as the one shown, the main rotation is around Y. That means that the X signal of acceleration recorded also is influenced by a Z component, while the Z signal incorporates a part of acceleration in X.

Even if the aforementioned problems are individuated, there are some details in the displacements graphs and strain graphs that seems suggesting a correct behaviour or at least a realistic one for what concerns the order of magnitude for values. The fact that displacements show higher values in the top layer instead of the middle one and the middle one has higher values than cerebellum sensors in the principal direction of impact is correct. Another thing that is correct is the signs of the strain in middle layer. Only from the accelerations of ML and MR for Back impact occurring at 24 J presented in chapter 5 was understood that the brain in Y direction is firstly characterized by a positive deformation and then compression in an alternate way, and it is confirmed by *Figure 7.14 (a)*. If it is analysed the deformation between CoM and ML, it seems that CoM is moving towards left, meaning that the distance between ML and CoM is decreasing. But if the distance between CoM and ML is decreasing, the distance between CoM and MR has to increase and it is confirmed by *Figure 7.17 (c)*. What is strange and probably not correct is the behaviour shown by *Figure 7.17 (e)* and *(f)* representing respectively the deformation between TL and ML and between TR and MR. In fact from this two pairs of sensors should be expected similar shape of signal and similar values while in the first case there is a compression slightly above 7% and in the second case the compression surpasses the level of 30%.

As previously said these results has to be considered as a first attempt to understand deformations. A validation of these method is needed in order to understand how much is the error that affects the different calculated signals of strain and to understand if the shape of the signal is proper or not.

Further studies have to be carried on in future about strains. It is not understandable yet if the accelerometers can be used to calculate strain. If possible a new disposition of accelerometers inside brain has to be developed. In fact both in IHHS1 and IHHS2, the sensors in the lobes are placed on the same coronal plane of CoM, so it is possible only to calculate deformations in Y and Z directions but not along X axis. If not possible, it is needed a deep study of scientific literature to find a method or proper tools with which high strains could be detected. A feasible way to detect high strains that could be implemented inside a new instrumented human head surrogate is the utilization of graphene-rubber composites as shown in different works [58-60] or carbon nanotube-natural rubber composite [61]. The graphene-rubber composite can be easy to obtain because as rubber can be used *Plastil Gel 00-25*, the same material of IHHS2 brain, and graphene powder is already present in the materials of *Mittuniversitet*.

# Conclusions

The aim of this thesis is to make and compare tests on IHHS1 and IHHS2 and make the first studies and attempts in calculation of strains inside the brain of the surrogate head models. In IHHS1 some problems have been discovered as the interaction between oil resembling cerebrospinal fluid and brain with its swelling and the oil leakage. The analysis of this problems was useful for further improvement of IHHS2. IHHS1 has been however prepared and mounted in order to perform proper impact tests.

IHHS2 has been redesigned to solve the problems encountered in the first prototype. Its dimensions were reduced to 90% of the original ones, the oil needed to fill the space left between brain and skull has been chosen carefully in order to not let happen interaction with silicon rubber of the brain, more attention was given to the sealing of the head because of the oil leakage problem, brain and skin were produced with softer silicon rubber that the kind used in IHHS1. Seven accelerometers has been placed inside the brain in points of interest needed to compare different behaviour of the lobes and cerebellum. In IHHS2, because of the presence of oil inside the head, it was possible to record data also through ten pressure sensors placed in the inner surface of skull. Silicon oil inside IHHS2, with its dumping effect, produced peak values of accelerations, angular velocities and in particular angular accelerations lower than the ones obtained in IHHS1. It is interesting to remember, in fact, that angular accelerations of 10000 or 12000 rad/s$^2$ in IHHS2 corresponded to 2000 or 3000 rad/s$^2$ in IHHS2.

First considerations concerning strain calculation has been given. The method of integrating the signal of accelerations is not feasible for the high error which characterizes it. The method of integration with correction is not validated yet, however the results obtained through it are realistic. If this method will be validated, a new disposition of accelerometers embedded inside silicon rubber of brain has to be designed in order to analyse deformations also in X direction. If the method is incorrect and not validated a new method of calculating strain that does not utilize accelerometers is needed. A good choice can be the design, production and calibration of a new model of strain sensors based on graphene-rubber composites.

In conclusion this project has reached an admirable milestone in the production of a biofidelic human head surrogate, not comparable with the other attempts found in literature, characterized by lack of details as the presence of a brain or the cerebrospinal fluid and so lack of biofidelity.

# Bibliography


[1] G. Carraro, “Development of a Sensorized Human Head Prototype for Studying Traumatic Brain Injury Mechanisms,” 2016, Università degli Studi di Padova.

[2] S. Dal Castello, “New Project of Physical Modeling of the Anatomically Correct Multi Sensors Human Head,” 2016, Università degli Studi di Padova.

[3] L. Broggio, “Development of a Sensorized Human Head Prototype.,” 2017, Università degli Studi di Padova.

[4] F. Uriati, “Development of a Sensorized Physical Model of the Human Head for the Innovation of Helmet Safety Tests.” 2018, Università degli Studi di Padova.

[5] R. C. Gardner and K. Yaffe, “Epidemiology of mild traumatic brain injury and neurodegenerative disease,” *Mol. Cell. Neurosci.*, vol. 66, no. PB, pp. 75–80, 2015.

[6] B. M. Knowles and C. R. Dennison, “Predicting Cumulative and Maximum Brain Strain Measures From HybridIII Head Kinematics: A Combined Laboratory Study and Post-Hoc Regression Analysis,” *Ann. Biomed. Eng.*, vol. 45, no. 9, pp. 2146–2158, 2017.

[7] Center for Disease Control, J. Gilchrist, K. E. Thomas, L. Xu, L. C. McGuire, and V. Coronado, “Nonfatal traumatic brain injuries related to sports and recreation activities among persons aged ≤19 years--United States, 2001-2009.,” *MMWR. Morb. Mortal. Wkly. Rep.*, vol. 60, no. 39, pp. 1337–42, 2011.

[8] B. Chinn *et al.*, “COST 327 Motorcycle Safety Helmets,” *COST 327 Mot. Safty Helmets*, p. 327, 2001.

[9] T. I. Harrison, N. J. Mills, and M. S. Turner, “Jockeys’ Head Injuries and Skull Cap Performance” T.I. Harrison, School of Metallurgy and Materials, University of Birmingham. * The Jockey Club, 42 Portman Square, London,” pp. 49–62.

[10] A. Iwata, “Traumatic Axonal Injury Induces Proteolytic Cleavage of the Voltage-Gated Sodium Channels Modulated by Tetrodotoxin and Protease Inhibitors,” *J. Neurosci.*, vol. 24, no. 19, pp. 4605–4613, 2004.

[11] D. J. Thurman, C. Alverson, K. A. Dunn, J. Guerrero, and J. E. Sniezek, “Traumatic brain injury in the United States: A public health perspective.,” *J. Head Trauma Rehabil.*, vol. 14, pp. 602–615, 1999.

[12] Trauamtic Brain Injury Task Force, “Report to the surgeon general,” no. May 2007, 2008.

[13] A. Becker *et al.*, “Analysis of incidence of traumatic brain injury in blunt trauma patients with Glasgow Coma Scale of 12 or less,” *Chinese J. Traumatol. - English Ed.*, vol. 21, no. 3, pp. 152–155, 2018.

[14] S. M. Green, J. S. Haukoos, and D. L. Schriger, “How to Measure the Glasgow Coma Scale,” *Ann. Emerg. Med.*, vol. 70, no. 2, pp. 158–160, 2017.

[15] D. Hack, J. S. Huff, K. Curley, R. Naunheim, S. Ghosh Dastidar, and L. S. Prichep, “Increased prognostic accuracy of TBI when a brain electrical activity biomarker is added to loss of consciousness (LOC),” *Am. J. Emerg. Med.*, vol. 35, no. 7, pp. 949–952, 2017.

[16] L. A. G. Marshman, D. Jakabek, M. Hennessy, F. Quirk, and E. P. Guazzo, “Post-traumatic amnesia,” *J. Clin. Neurosci.*, vol. 20, no. 11, pp. 1475–1481, 2013.

[17] T. A. Gennarelli, “Mechanisms of brain injury.,” *J. Emerg. Med.*, vol. 11 Suppl 1, pp. 5–11, 1993.

[18] D. H. Smith and D. F. Meaney, “Axonal Damage in Traumatic Brain Injury,” *Neurosci.*, vol. 6, no. 6, pp. 483–495, 2000.

[19] M. Kim *et al.*, “Diffuse axonal injury (DAI) in moderate to severe head injured patients: Pure DAI vs. non-pure DAI,” *Clin. Neurol. Neurosurg.*, vol. 171, no. March, pp. 116–123, 2018.

[20] Y. D. Won *et al.*, “Radiologic Factors Predicting Deterioration of Mental Status in Patients with Acute Traumatic Subdural Hematoma,” *World Neurosurg.*, vol. 111, pp. e120–e134, 2018.

[21] “http://neurosurgery.ucla.edu/acute-subdural-hematomas”

[22] T. Gennarelli and L. Thibault, “Biomechanics of acute subdural hematoma,” *The Journal of Trauma*, vol. 22, no. 8. pp. 680–686, 1982.

[23] “http://neurosurgery.ucla.edu/chronic-subdural-hematomas”

[24] D. Price, “Epidural hematoma in emergency medicine,” *Medscape*, p. 824029, 2014.

[25] M. I. Aguilar and T. G. Brott, “Update in Intracerebral Hemorrhage,” *The Neurohospitalist*, vol. 1, no. 3, pp. 148–159, 2011.

[26] D. Adukauskiene, A. Bivainyte, and E. Radaviciute, “[Cerebral edema and its treatment].,” *Medicina (Kaunas).*, vol. 43, no. 2, pp. 170–176, 2007.

[27] W. Regard, T. O. The, E. Of, P. By, T. H. E. Engine, and U. Nations, “Concerning the Adoption of Uniform Technical Prescriptions for Wheeled Vehicles , Equipment and Parts Which Can Be Fitted and / or Be Used on Wheeled Vehicles and the Conditions for Reciprocal Recognition of,” no. April, pp. 1–194, 2002.

[28] P. Used, “Standard Specification for Helmets Used for Recreational Snow Sports 1,” vol. 15, no. December, pp. 1–4, 2002.

[29] B. R. Donnelly and J. Medige, “Shear properties of human brain tissue.,” *J. Biomech. Eng.*, vol. 119, no. 4, pp. 423–432, Nov. 1997.

[30] M. W. Wojnarowicz, A. M. Fisher, O. Minaeva, and L. E. Goldstein, “Considerations for experimental animal models of concussion, traumatic brain injury, and chronic traumatic encephalopathy-these matters matter,” *Front. Neurol.*, vol. 8, no. JUN, pp. 1–14, 2017.

[31] H. Sun Chan, “Mathematical Model for Closed Head Impact,” 1974. .

[32] V. H. Kenner and W. Goldsmith, “Dynamic loading of a fluid-filled spherical shell,” *Int. J. Mech. Sci.*, vol. 14, no. 9, pp. 557–568, Sep. 1972.

[33] Hatam Samaka and Faris Tarlochan, “Finite Element (FE) Human Head Models: Literature Review,” *Int. J. Sci. Technol. Res.*, vol. 2, no. 7, pp. 17–31, 2013.

[34] “http://www.humaneticsatd.com/crash-test-dummies/frontal-impact/hiii-50m”

[35] “http://www.humaneticsatd.com/crash-test-dummies/frontal-impact/thor-50m”

[36] “http://www.humaneticsatd.com/crash-test-dummies/frontal-impact/worldsid-50m”

[37] J. Zhang, F. A. Pintar, N. Yoganandan, T. A. Gennarelli, and S. F. Son, “Experimental study of blast-induced traumatic brain injury using a physical head model.,” *Stapp Car Crash J.*, vol. 53, pp. 215–227, Nov. 2009.

[38] F. Zhu *et al.*, “Using a gel/plastic surrogate to study the biomechanical response of the head under air shock loading: a combined experimental and numerical investigation.,” *Biomech. Model. Mechanobiol.*, vol. 11, no. 3–4, pp. 341–353, Mar. 2012.

[39] Z. Taha, M. H. A. Hassan, I. Hasanuddin, M. A. Aris, and A. P. P. A. Majeed, “Impact-absorbing Materials in Reducing Brain Vibration Caused by Ball-to-head Impact in Soccer,” *Procedia Eng.*, vol. 72, pp. 515–520, Jan. 2014.

[40] C. J. Freitas, J. T. Mathis, N. Scott, R. P. Bigger, and J. Mackiewicz, “Dynamic response due to behind helmet blunt trauma measured with a human head surrogate.,” *Int. J. Med. Sci.*, vol. 11, no. 5, pp. 409–425, 2014.

[41] J. Versace, “A Review of the Severity Index.” SAE International , 1971.

[42] D. R. Namjoshi *et al.*, “Towards clinical management of traumatic brain injury: a review of models and mechanisms from a biomechanical perspective.,” *Dis. Model. Mech.*, vol. 6, no. 6, pp. 1325–1338, Nov. 2013.

[43] F. Petrella, “Studio e Riformulazione dei Criteri di Lesione della Testa attraverso il Modello di Corpo Umano THUMS” 2012, Politecnico di Milano.

[44] M. Shojaati, “Correlation between injury risk and impact severity index ASI,” *Swiss Transp. Res. Conf.*, pp. 1–10, 2003.

[45] M. R. Begley and F. W. Zok, “Optimal Material Properties for Mitigating Brain Injury During Head Impact,” *J. Appl. Mech.*, vol. 81, no. 3, pp. 31014–31015, Oct. 2013.

[46] B. Mueller, A. MacAlister, J. Nolan, and David Zuby, “Comparison of HIC and BrIC Head Injury Risk in IIHS Frontal Crash Tests to Real-world Head Injuries,” *Enhanc. Saf. Veh.*, pp. 1–18, 2015.

[47] E. G. Takhounts, M. J. Craig, K. Moorhouse, J. McFadden, and V. Hasija, “Development of brain injury criteria (BrIC).,” *Stapp Car Crash J.*, vol. 57, pp. 243–266, Nov. 2013.

[48] “https://www.astm.org/COMMITTEE/F42.htm”

[49] “www.stratasys.com/3d-printers/uprint-se-plus”

[50] “www.arcam.com/technology/products/arcam-q10”

[51] “https://www.kistler.com/?type=669&fid=60702&model=document”

[52] “https://it.shop.gopro.com/EMEA/cameras/hero5-black/CHDHX-502-master.html”

[53] J. Travis and J. Kring, *LabVIEW for Everyone: Graphical Programming Made Easy and Fun (3rd Edition) (National Instruments Virtual Instrumentation Series)*. Upper Saddle River, NJ, USA: Prentice Hall PTR, 2006.

[54] “https://www.kistler.com/en/product/type-2812a/”

[55] “https://it.mathworks.com/help/matlab/learn_matlab/product-description.html”

[56] “https://launch.solidworks.com/it”

[57] P. Halldin, A. Gilchrist, and N. J. Mills, “A new oblique impact test for motorcycle helmets,” *Int. J. Crashworthiness*, vol. 6, no. 1, pp. 53–64, 2001.

[58] C. S. Boland *et al.*, “Sensitive, high-strain, high-rate bodily motion sensors based on graphene-rubber composites,” *ACS Nano*, vol. 8, no. 9, pp. 8819–8830, 2014.

[59] C. Zhou, Z. Zeng, Q. Yu, D. C. Klerk, W. Li, and Y. Yu, “Highly stretchable and sensitive strain sensor based on a simple friction-transfer method,” *Transl. Mater. Res.*, vol. 5, no. 1, p. 015001, 2018.

[60] S. R. Larimi, H. Rezaei Nejad, M. Oyatsi, A. O’Brien, M. Hoorfar, and H. Najjaran, “Low-cost ultra-stretchable strain sensors for monitoring human motion and bio-signals,” *Sensors Actuators, A Phys.*, vol. 271, pp. 182–191, 2018

[61] L. Bokobza, “Multiwall Carbon Nanotube-filled Natural Rubber: Electrical and Mechanical Properties”, *Express Polym. Lett.*, vol. 6, no. 3, pp. 213-223, 2012.

# Appendix

ANALOG DEVICES

# Small, Low Power, 3-Axis ±200 *g* Accelerometer

Data Sheet **ADXL377**

## FEATURES

- 3-axis sensing
- Small, low profile package
  - 3 mm × 3 mm × 1.45 mm LFCSP
- Low power: 300 µA (typical)
- Single-supply operation: 1.8 V to 3.6 V
- 10,000 *g* shock survival
- Excellent temperature stability
- Bandwidth adjustment with a single capacitor per axis
- RoHS/WEEE and lead-free compliant

## APPLICATIONS

- Concussion and head trauma detection
- High force event detection

## GENERAL DESCRIPTION

The ADXL377 is a small, thin, low power, complete 3-axis accelerometer with signal conditioned voltage outputs. The ADXL377 measures acceleration resulting from motion, shock, or vibration with a typical full-scale range of ±200 *g*.

The user selects the bandwidth of the accelerometer using the $C_X$, $C_Y$, and $C_Z$ capacitors at the $X_{OUT}$, $Y_{OUT}$, and $Z_{OUT}$ pins. Bandwidths can be selected to suit the application, with a range of 0.5 Hz to 1300 Hz for the x-axis and y-axis and a range of 0.5 Hz to 1000 Hz for the z-axis.

The ADXL377 is available in a small, low profile, 3 mm × 3 mm × 1.45 mm, 16-lead lead frame chip scale package (LFCSP_LQ).

## FUNCTIONAL BLOCK DIAGRAM

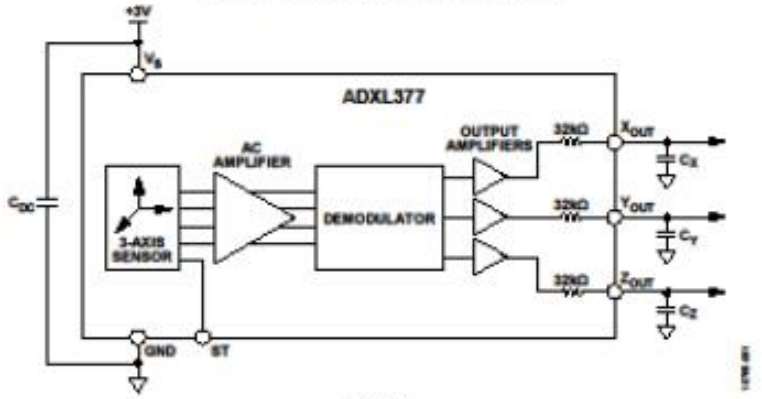


*Figure 1.*

Rev. 0 Document Feedback



One Technology Way, P.O. Box 9106, Norwood, MA 02062-9106, U.S.A.
Tel: 781.329.4700 
Technical Support www.analog.com

# LPR4150AL

## MEMS motion sensor: dual-axis pitch and roll ±1500 dps analog gyroscope

## Features

- 2.7 V to 3.6 V single-supply operation
- Wide operating temperature range (-40 °C to +85 °C)
- High stability over temperature
- Analog absolute angular-rate outputs
- Two separate outputs for each axis (1x and 4x amplified)
- Integrated low-pass filters
- Low power consumption
- Embedded power-down
- Embedded self-test
- Sleep mode
- High shock and vibration survivability
- ECOPACK® RoHS and "Green" compliant (see *Section 6*)

## Applications

- Gaming applications
- Pointing devices, remote and game controllers
- Motion tracking with user interface
- Industial and robotics

## Description

The LPR4150AL is a low-power dual-axis micromachined gyroscope capable of measuring angular rate along pitch and roll axes.

It provides excellent temperature stability and high resolution over an extended operating temperature range (-40 °C to +85 °C).

LGA-28 (4x5x1 mm)

The LPR4150AL has a full scale of ±1500 dps and is capable of detecting rates with a -3 dB bandwidth up to 140 Hz.

The device includes a sensing element composed of a single driving mass, kept in continuous oscillation and capable of reacting, based on the Coriolis principle, when an angular rate is applied.

A CMOS IC provides the measured angular rate to the external world through an analog output voltage, allowing high levels of integration and production trimming to better match sensing element characteristics.

ST's family of gyroscopes leverages on the mature and robust manufacturing process already used for the production of micro-machined accelerometers.

ST is already in the field with several hundred million sensors which have received excellent acceptance from the market in terms of quality, reliability and performance.

The LPR4150AL is available in a plastic land grid array (LGA) package, which ST successfully pioneered for accelerometers. Today ST has the widest manufacturing capability and strongest expertise in the world for production of sensors in plastic LGA packages.

**Table 1. Device summary**

| Order code | Temperature range (°C) | Package | Packing |
|---|---|---|---|
| LPR4150AL | -40 to +85 | LGA-28 (4x5x1) | Tray |
| LPR4150ALTR | -40 to +85 | LGA-28 (4x5x1) | Tape and reel |

# LPY4150AL

## MEMS motion sensor: dual-axis pitch and yaw ±1500 dps analog gyroscope

### Features

- 2.7 V to 3.6 V single-supply operation
- Wide operating temperature range (-40 °C to +85 °C)
- High stability over temperature
- Analog absolute angular-rate outputs
- Two separate outputs for each axis (1x and 4x amplified)
- Integrated low-pass filters
- Low power consumption
- Embedded power-down
- Embedded self-test
- Sleep mode
- High shock and vibration survivability
- ECOPACK® RoHS and "Green" compliant (see *Section 6*)

### Applications

- Gaming applications
- Pointing devices, remote and game controllers
- Motion control with user interface
- Industrial and robotics

### Description

The LPY4150AL is a low-power dual-axis micromachined gyroscope capable of measuring angular rate along pitch and yaw axes.

It provides excellent temperature stability and high resolution over an extended operating temperature range (-40 °C to +85 °C).

LGA-28 (4x5x1 mm)

The LPY4150AL has a full scale of ±1500 dps and is capable of detecting rates with a -3 dB bandwidth up to 140 Hz.

The device includes a sensing element composed of a single driving mass, kept in continuous oscillation and capable of reacting, based on the Coriolis principle, when an angular rate is applied.

A CMOS IC provides the measured angular rate to the external world through an analog output voltage, allowing high levels of integration and production trimming to better match sensing element characteristics.

ST's family of gyroscopes leverages on the mature and robust manufacturing process already used for the production of micro-machined accelerometers.

ST is already in the field with several hundred million sensors which have received excellent acceptance from the market in terms of quality, reliability and performance.

The LPY4150AL is available in a plastic land grid array (LGA) package, which ST successfully pioneered for accelerometers.Today ST has the widest manufacturing capability and strongest expertise in the world for production of sensors in plastic LGA packages.

**Table 1. Device summary**

| Order code | Temperature range (°C) | Package | Packing |
|---|---|---|---|
| LPY4150AL | -40 to +85 | LGA-28 (4x5x1) | Tray |
| LPY4150ALTR | -40 to +85 | LGA-28 (4x5x1) | Tape and reel |

RoHS

# MS54XX

## Miniature SMD Pressure Sensor

### SPECIFICATIONS

- **1, 7, 12, and 70 bar absolute pressure range**
- **Uncompensated**
- **Piezoresistive silicon micromachined sensor**
- **Miniature surface mount**
- **Ceramic carrier**
- **Low noise, high sensitivity, high linearity**

The MS54XX SMD pressure sensor series is designed for pressure sensor systems with highest demands on resolution and accuracy. The device consists of a silicon micromachined pressure sensor die mounted on a 6.2 x 6.4 mm ceramic carrier. The MS54XX can be delivered in a high sensitivity version giving a maximal output voltage or in a high linearity version. Both versions provide an output voltage directly proportional to the applied pressure

| Carrier | Full scale pressure | High Sensitivity Versions | | | High Linearity Versions | | |
|---|---|---|---|---|---|---|---|
| | | Product code | Full scale span | Linearity | Product code | Full scale span | Linearity |
| Ceramic | 1 bar | MS5401-AM | 240 mV | ±0.20 % FS | MS5401-BM | 150 mV | ±0.05 % FS |
| | 7 bar | MS5407-AM | 392 mV | ±0.20 % FS | | | |
| | 12 bar | | | | MS5412-BM | 150 mV | ±0.05 % FS |
| | 70 bar | MS5470-AM | 310 mV | ±0.25 % FS | | | |

# Q8 FORMULA ULTRA V 0W-20

## Descrizione

**Q8 Formula Ultra V 0W-20** è un lubrificante sintetico multigrado Low SAPS (a bassi livelli di Ceneri Solfatate, Fosforo e Zolfo) di nuovissima generazione con spiccate proprietà di Fuel Economy (risparmio di carburante).

## Applicazioni

Si tratta di un prodotto specificamente sviluppato per i motori delle autovetture Volvo Euro 6, che richiedono la Specifica Volvo VCC RBS0-2AE.
Se ne consiglia l'utilizzo laddove viene richiesto l'impiego di un lubrificante con un basso tenore di ceneri solfatate unitamente ad una elevata compatibilità con i sistemi di trattamento dei gas di scarico e, comunque, dove è richiesto un olio con detta Specifica.

## Specifiche

- Volvo VCC RBS0-2AE 0W-20
- ACEA C5

## Proprietà e prestazioni

- Straordinaria fluidità alle bassissime temperature, che consente partenze sicure anche in condizioni ambientali estreme e garantisce una protezione totale del motore fin dall'avviamento.
- Eccellente stabilità alle alte temperature, che assicura una riduzione della formazione di residui e una superiore resistenza all'ossidazione.
- Appositamente formulato per fornire eccezionali riduzioni nel consumo di carburante, nel corso dei test svolti ed in particolare nel test motoristico M111FE, ha dimostrato un miglioramento della Fuel Economy fino al 3,4% di carburante.
- Offre intervalli di carica prolungati, grazie all'impiego di basi sintetiche particolarmente pregiate.
- Allunga la vita del motore per le sue eccezionali proprietà antiusura, antiruggine e antiossidanti.
- Elevatissima compatibilità con i sistemi di trattamento dei gas di scarico.

## Caratteristiche

| Proprietà | Metodologia | Unità | Grandezze |
|---|---|---|---|
| Viscosità | SAE | | 0W-20 |
| Densità a 20 °C | ASTM D 4052 | Kg/m3 | 842 |
| Viscosità a 40 °C | ASTM D 445 | cSt | 48,7 |
| Viscosità a 100 °C | ASTM D 445 | cSt | 9,2 |
| Indice di Viscosità | ASTM D 2270 | | 175 |
| Punto di congelamento | ASTM D 97 | °C | -48 |
| Punto di infiammabilità | ASTM D 92 | °C | 205 |
| Viscosità apparente | ASTM D 5293 | mPa.s | 5700 |
| Viscosità dinamica HTHS | CEC-L-36-A-90 | mPa.s | > 2,6 |

Le caratteristiche sono medio – indicative e non costituiscono specifica – 201703

**Conqord Oil S.r.l.**
Via Volpedo, 2 - 15050 Castellar Guidobono (AL)
Tel. +39 02 90595.1 - q8oils@conqordoil.it - www.Q8Oils.it